Garnet as a monitor for melt–rock interaction: Textural, mineralogical, and compositional evidence of partial melting and melt-driven metasomatism

Philippe Goncalves, Tom Raimondo, Jean-Louis Paquette, Jailma Santos de Souza de Oliveira

Journal of METAMORPHIC GEOLOGY

Garnet as a monitor for melt-rock interaction: textural, mineralogical and compositional evidence of partial melting and melt-driven metasomatism

Journal:	*Journal of Metamorphic Geology*
Manuscript ID	JMG-20-0059.R1
Manuscript Type:	Original Article
Date Submitted by the Author:	n/a
Complete List of Authors:	Goncalves, Philippe; Université de Bourgogne Franche-Comté, Laboratoire Chrono-environnement / CNRS Raimondo, Tom; University of South Australia, UniSA STEM; University of South Australia, Future Industries Institute Paquette, Jean Louis; Université Clermont Auvergne, Laboratoire Magmas et Volcans Santos de Souza, Jailma; Universidade Federal da Bahia, Instituto de Geociências.
Keywords:	garnet zoning, partial melting, chemical potential, diffusion metasomatism, LA-ICP-MS mapping

1

2

3 **Garnet as a monitor for melt-rock interaction: textural, mineralogical and compositional**

4 **evidence of partial melting and melt-driven metasomatism**

5

6 Abridged title : Garnet as a monitor for melt-rock interaction

7

8 Philippe Goncalves[1*], Tom Raimondo[2,3], Jean-Louis Paquette[4], Jailma Santos de Souza[5]

9

10

11 1: Laboratoire Chrono-Environnement, CNRS / Université de Bourgogne-Franche-Comté, 16 route

12 de Gray, 25030 Besançon, France

13 2 : UniSA STEM, University of South Australia, GPO Box 2471, Adelaide SA 5001, Australia

14 3 : Future Industries Institute, University of South Australia, GPO Box 2471, Adelaide SA 5001,

15 Australia

16 4 : Laboratoire Magmas et Volcans, Université Clermont-Auvergne, CNRS, IRD, OPGC, 63000

17 Clermont-Ferrand, France

18 5 : Centro de Pesquisa em Geofisica e Geologia, Universidade Federal da Bahia, Rua Caetano

19 Moura 123, Federaçao Cep 40210-340 Salvador, Bahia, Brazil

20

21

22

23 * corresponding author: philippe.goncalves@univ-fcomte.fr

24

25

26

27

ABSTRACT

In this study, we focus on a partially melted garnet-bearing granulite from the Salvador-Esplanade belt (Salvador da Bahia, Brazil), and examine the behavior of major and trace elements during partial melting and melt-driven metasomatism. Phase equilibria modeling and U-Th-Pb geochronology shows that the sample underwent partial melting during the heating segment of the decompression path from ~ 1.2 GPa and 675-700°C to ~ 0.8 GPa and 790°C at ca. 2.06 Ga. During the last stage of decompression, from 0.8 to ~ 0.5 GPa, physical segregation of melt resulted in the establishment of chemical potential gradients and mass transfer between the host-granulite and the leucosome. Modelling shows that H_2O, CaO, K_2O and Na_2O diffuse from the melt into the host residue, whereas SiO_2 is transferred from the host-granulite into the adjacent leucosome. Opposed senses of diffusional transfer resulted in the formation of a quartz-rich anhydrous leucosome and a quartz-undersaturated selvage in the host-granulite. Compositional maps show that garnets exhibit unusual and contrasting major and trace element distribution depending on their textural position. The largest garnets located in the quartz-undersaturated selvage preserve their original Ca and trace element growth zoning. A transition from bell-shaped profiles for Y and HREEs to bowl-shape profiles for LREEs is consistent with a typical Rayleigh fractionation model, fast intergranular element mobility and rock-wide equilibrium during prograde partial melting. In contrast, smaller garnets away from the leucosome show evidence of prograde growth zoning modified by intragranular diffusion, as evidenced by a network of open channels and healed-cracks that act as connecting pathways between the matrix and garnet core. This results in either subtle modification of both major and trace elements adjacent to the inner core inclusions, or a complete re-equilibration. The recognition that the initial Ca growth zoning, including the inner core compositions, was later modified by intragranular diffusion implies that misleading thermobarometric results and tectonic interpretations would be obtained if the garnet core composition was used to fingerprint the early garnet nucleation stage. This study further demonstrates that at high

55 temperature (> 750°C) and in the presence of melt, REE are not less vulnerable to diffusive
56 resetting than divalent cations like Ca^{2+}.

57 keywords : garnet zoning, partial melting, chemical potential, diffusion metasomatism, LA-ICP-
58 MS

59

1. INTRODUCTION

Partial melting is a fundamental process for differentiating (Brown, 2010) and weakening the deep crust (Piazolo, Daczko, Silva & Raimondo, 2020; Rosenberg & Handy, 2005), which in turn exerts a first-order control on deformation style, lateral redistribution of mass, crustal thickness and surface topography (Beaumont, Jamieson, Nguyen & Medvedev, 2004; Hollister & Crawford, 1986; Jamieson, Unsworth, Harris, Rosenberg & Schulmann, 2011; Rabin, Trap, Carry, Fréville & Cenki-Tok, 2015; Royden et al., 1997; Vanderhaeghe, 2012). Exhumed migmatites preserve, through their mineralogy and structure, a wealth of information that can be used to decipher the thermo-mechanical behavior of orogenic continental crust. With this motivation, the petrological analysis of partially melted feldsic rocks is now commonplace in metamorphic petrology, thanks to extended experimental work (e.g. Clemens, 1984; Grant, 1985; Le Breton, 1988; Thompson, 1982; Vielzeuf & Holloway, 1988; Vielzeuf & Montel, 1994) and thermodynamic phase relation modeling (Holland & Powell, 2001a; Spear, Kohn & Cheney, 1999; Vielzeuf & Schmidt, 2001; White, Powell & Holland, 2001; White & Powell, 2010). Despite this progress, modeling phase relations in migmatites is not trivial because they are subject to redistribution and transfer of the highly mobile melt component at various scales, from grain- to crustal-scale (Etheridge, Daczko, Chapman & Stuart, 2020; Sawyer, 2001). Therefore, phase relation modeling in migmatites requires the consideration of not only changes in environmental variables like pressure and temperature, but also the variation of the equilibrium volume and composition of the system (i.e. open system processes).

Modeling the role of melt transfer (loss and gain) on phase relations has been extensively investigated (Alessio, Hand, Morrissey, Kelsey & Payne, 2017; Bartoli, 2017; Dumond, Goncalves, Williams & Jercinovic, 2015; White et al., 2001; Yakymchuk & Brown, 2014;). Among the many benefits of open system forward modeling is the application of a melt-reintegration approach that consist of recovering the bulk composition prior to any melt transfer. This method allows investigating the prograde evolution of melt-bearing systems that tend to be obliterated by continuous re-equilibration up to peak metamorphic conditions. Another complexity arising from

the segregation of melt from the solid residue is that the system becomes physically and chemically differentiated into melt-rich domains (leucosome) and solid-rich domains (melanosome). The thermodynamic system is therefore composed of two sub-systems that will interact, with changing pressure and temperature conditions, due to the establishment of chemical potential gradients of components at the interface between both sub-systems (White & Powell, 2010). The diffusion of components (H_2O, SiO_2,...) between the two sub-systems produces significant variations in composition, mineral reactions and assemblages (Fitzsimons, 1996; White & Powell, 2010). Despite this conceptual framework being generally accepted, melt-rock interaction in segregated migmatites remains rarely identified via textural, geochemical and/or mineralogical evidence, nor investigated via thermodynamic modeling (Kriegsman & Hensen, 1998; Lin & Sawyer, 2019; White & Powell, 2010).

In migmatites, garnet is very common as a peritectic phase and has the ability to preserve zoning of divalent cations (Fe, Mg, Ca and Mn) that reflects changing P-T conditions and/or bulk rock chemistry, either due to garnet fractionation or mass transfer during melt segregation, transport and interaction with the garnet-bearing residual rock (e.g. Caddick, Konopásek & Thompson, 2010; Konrad-Schmolke, O'Brien, de Capitani & Carswell, 2008). To retrieve the maximum information related to garnet chemical evolution, the characterization of major element zoning can be complemented with trace elements (Hyppolito et al., 2019; Raimondo et al., 2017). Trivalent cations, like rare-earth elements, have lower diffusion coefficients than major divalent cations. They are therefore more resistant to diffusional modification and allow the preservation of prograde and high temperature processes (Carlson, 2012; Gaidies et al., 2020; George & Gaidies, 2017; Moore, Carlson & Hesse, 2013; Rubatto et al., 2020), including those involved during partial meting (Dumond et al., 2015).

The trace element characteristics of garnet can be linked to the evolution of accessory phases used for geochronology (e.g. monazite, zircon and rutile) to better constrain tectonometamorphic histories (Dumond et al., 2015; Hermann & Rubatto, 2003; Mahan, Goncalves, Williams & Jercinovic, 2006; Prent et al., 2019; Pyle & Spear, 2003; Tomkins & Pattison, 2007; Weller, jackson, Miller, St-Onge & Rayner, 2020). They also provide insight into

the mechanisms controlling the uptake (interface- vs diffusion-controlled growth) and mobility of trace element during metamorphism and metasomatism (George, Gaidies & Boucher, 2018; Konrad-Schmolke, Zack, O'Brien & Jacob, 2008; Moore et al., 2013; Raimondo et al., 2017; Skora et al., 2006). With the recent development of in-situ laser ablation - inductively coupled plasma - mass spectrometry (LA-ICP-MS), it is now possible to rapidly and quantitatively map the 2D distribution of trace elements across major and accessory minerals of interest (George et al., 2018; Raimondo et al., 2017; Ubide, McKenna, Chew & Kamber, 2015). Yet, despite the known benefits of analyzing trace elements in garnet for the purposes listed above, there remains a limited number of studies using this approach to understand the grain-scale controls on garnet crystallization (Gaidies et al. 2020; George et al., 2018; Rubatto et al. 2020).

In this contribution, we report the integrated petrological and geochemical characterization of a high-grade rock that preserves evidence of changes in P-T conditions, partial melting and melt-driven metasomatism. The selected sample, from the São Francisco craton in Brazil, is a layered composite rock that consists of a garnet-bearing quartz-saturated host granulite, a quartzo-feldspatic leucosome, that may correspond to crystallized segregated melt or differentiated melt residue (Guernina & Sawyer, 2003), and a quartz-undersaturated garnet-bearing selvage formed at the interface between the host-granulite and leucosome. Petrological analysis and thermodynamic modeling (using P-T-μ-X phase diagrams, where μ = chemical potential and X = composition) shows that the distinct mineralogy of the selvage is the result of mass transfer driven by chemical potential gradients established between the host-granulite and the segregated melt during decompression. In addition, garnets show a consistent change in grain size, morphology, major and trace element composition and zoning patterns across the gneissic layering, as revealed by quantified LA-ICP-MS raster maps. The strong correlation between textural position and zoning pattern in garnet gives insight into the grain-scale petrogenetic processes involved in partially-molten granulites. We distinguish the role of (1) intergranular mobility of elements and accessory phases during metamorphic garnet growth; and (2) post-growth intragranular diffusion of major and trace elements during melt-driven metasomatism.

2. GEOLOGICAL SETTING

2.1. São Francisco craton and the Salvador-Esplanade belt

The São Francisco Craton, located in the east-central part of Brazil, consists of an Archean to Paleoproterozoic crystalline basement mostly overlain by Meso to Neoproterozoic sediments in its western part (Figure S1). The craton is bounded by Neoproterozoic marginal fold belts (Figure S1). The eastern part of the craton, where most of the metamorphic rocks are exposed, is subdivided into four major geological units: three Archean blocks (Gavião, Jequié and Serrinha) and two Paleoproterozoic belts: the Itabuna-Salvador-Curaçá Orogen (ISCO) and the Salvador-Esplanada belt (SEB) (Figure S1) (Barbosa & Sabaté, 2004, see references therein). The southernmost part of the Salvador-Esplanada belt, where this study has been conducted, trends broadly North-East and consists mostly of mafic to felsic granulites and migmatites.

2.2. Farol da Barra: metamorphism and age constraints

In the Salvador da Bahia city, high grade metamorphic and magmatic rocks of the SEB are exposed in a horst that is bound on the western side by the Recôncavo sedimentary basin and on the eastern side by the Atlantic coastal margin. The studied area is located at the Barra lighthouse (Farol da Barra; 13°00'41"S; 38°31'57"W, Figure 1a). Four distinct lithologies are identified (Souza Barbosa & Gomes, 2010; Souza-Oliveira et al., 2014) (Figure 1a): (1) orthopyroxene-bearing granulites that constitute most of the basement of the city of Salvador da Bahia and are interpreted to be derived from late Archean tonalitic magmatic rocks (2) garnet-bearing granulites and sapphirine-bearing Al-Mg granulites interpreted as meta-sediments (3) granulitized ultramafic and mafic rocks that occur as centimeter to meter-scale boudins within the paraderived granulites; and (4) monzonitic to syenitic intrusives dykes, oriented ~N10° (Figure 1a), that are either deformed or undeformed with sharp intrusive contacts.

Metamorphic conditions have been estimated at 0.75-0.9 GPa and 840-900°C in the sapphirine-bearing granulites (Fujimori, 1988). The age of the granulitic metamorphism has been

constrained by SHRIMP U-Pb dating at 2089 ± 11 Ma on zircon overgrowths from the orthopyroxene-bearing granulites (Da Silva, McNaughton, 1997). On the same samples, zircon cores yielded an age of 2561 ± 7 Ma interpreted as the crystallization age of the protolith magmatic rocks. The later syenitic to monzonitic magmatism has been dated by Pb-Pb evaporation on zircon at 2064 ± 6 Ma (Souza et al., 2010).

2.3. Farol da Barra: structural relationships

The Barra lighthouse outcrop is characterized by a complex ductile finite strain pattern that results from the superposition of two main phases of deformation (D_1 and D_2) (Figure 1b). The overall geometry consists of meter to decameter lenses, in which D_1 structures are best preserved, surrounded by D_2 ~East-West striking high strain zones (Figures 1b and S2). The first deformation phase (D_1) is characterized by a gently dipping gneissic foliation (S_1) that strikes NE-SW (Figure 1b and S2). This foliation is associated with isoclinal folds with axial planes parallel to S_1 (Figure 1b). The S_1 foliation bears a sub-horizontal L_1 stretching and mineral lineation plunging 0-20°, marked by the preferred orientation of feldspars, quartz ribbons, mafic mineral and elongated ultramafic to mafic boudins. The second deformation phase (D_2) is characterized by heterogeneous deformation that progressively steepens and transposes the previous D_1 fabric along upright D_2 folds and steeply dipping high strain zones (> 55°) that forms an anastomosing network of conjugated shear zones trending approximately east-west (Figures 1b and S2). An L_2 lineation is defined by stretched quartz, feldspars and by the preferred orientation of biotite with a moderate plunge of 10 to 35° towards the NE.

Kinematic analysis in the low D_2 strain domains show that the two sets of ductile conjugate shear zones consist of a dominant 108/72SSW dextral shear zone and minor sinistral 021/79ESE shear zones (Figure S2). This pattern of D_2 finite strain is consistent with a NNW-SSE shortening and a bulk dextral sense of shear. The NW-SE cross-section from the Santa Maria Forte towards the Cristo hill (Figure 1b) shows that the studied area (the Barra lighthouse) corresponds to a major localized D_2 high strain zone within a preserved D_1 low strain domain characterized by gently dipping foliation. Whereas the D_1 domains (Santa Maria fort, Hispaniola hospital, and

198 Cristo Hill) consist mainly of orthopyroxene-bearing granulites, the Barra lighthouse D_2 high
199 strain zone is characterized by the abundance of garnet-bearing granulite. This apparent
200 relationship between deformation and lithology is beyond the scope of this contribution and will
201 not be
202 discussed further.
203
204

205 **3. TEXTURAL AND MINERALOGICAL CHARACTERISATION**

206 **3.1. Outcrop and sample descriptions**

207 The studied sample is located in a S_2 high strain zone that surrounds a large decametric
208 lense of low strain rocks where an earlier fabric (S_1) is preserved (Figure 1). The S_2 granulite-
209 grade gneissic foliation is steeply dipping (072/80S) and contains a gently plunging mineral
210 lineation (09—>075) defined by the preferred orientation of biotite and sillimanite. The gneissic
211 foliation is marked by a compositional banding with centimer-wide quartzo-feldspathic
212 leucosomes in a garnet-bearing granulite (Figure 2a). Leucosomes are usually less than a three
213 centimeters in width and are systematically surrounded by a centimeter thick dark and coarse-
214 grained quartz-undersaturated selvage developed at the expense of the surrounding garnet-
215 bearing granulite (Figure 2b).
216 The studied sample 06SB06 encompasses the three lithologies described above: the host
217 quartz-saturated granulite, a 1 cm-wide quartz-undersaturated selvage and a thin leucosome
218 (Figure 2b). The peak-metamorphic assemblage of the quartz-saturated granulite consists of
219 garnet, sillimanite, plagioclase, biotite, quartz and K-feldspar (Figure 3a). Garnet is interpreted
220 as a peritectic phase produced during biotite dehydration melting via the reaction:
221 biotite + sillimanite + plagioclase + quartz ± K-feldspar = garnet + melt (1)
222 Spinel is locally observed in the matrix but it is always surrounded by a thin corona of sillimanite
223 and it is never in contact with quartz. The preferred orientation of large sillimanite blades (up
224 to 5 mm), K-feldspar and biotite, that occurs either as small flakes or large resorbed grains,

defines the main S_2 foliation observed at the outcrop scale. Garnet contains numerous quartz inclusions and polyphase aggregates of plagioclase + quartz with minor biotite inclusions that all show a preferred orientation at high angle with respect to the S_2 foliation (Figure 3a). This alignment is interpreted as a relict of the former shallow dipping S_1 foliation. Peak metamorphic garnet in contact with sillimanite is partially resorbed and surrounded by a moat of retrograde cordierite (Figure 3b), consistent with the classic reaction

garnet + sillimanite + quartz = cordierite ± melt ± ilm (2)

which proceeds during decompression and/or cooling.

The selvage, in direct contact with the leucosome, is composed of the same peak metamorphic assemblage, consisting of prismatic sillimanite, plagioclase, garnet, biotite and K-feldspar, except it lacks quartz. Biotite is more abundant than in the quartz-saturated granulite. Garnet cores contain numerous quartz inclusions, in association with plagioclase, suggesting that the onset of partial melting and crystallization of peritectic garnet occurred under quartz-saturated conditions. Garnet porphyroclasts are partially broken-down into cordierite and sillimanite is strongly resorbed and replaced by cordierite + spinel symplectites (Figure 3c) via the reaction

sillimanite + garnet ± melt ± biotite = spinel + cordierite (3)

The leucosome consists mainly of quartz and thin elongated K-feldspar ribbons. Plagioclase is very rare and occurs as late myrmekite intergrowths next to K-feldspar.

Mineral compositions are available in Dataset S1. Biotite has XMg of 0.67-0.69 and 0.71-0.73 for the small flakes and large grains respectively, with a constant Ti content of 0.25 to 0.30 pfu. Plagioclase in the matrix has a variable range in anorthite content from 0.43 to 0.52. Spinel is very homogeneous in composition with a XMg of 0.31. Garnet compositions are described in Section 4.

3.2. Evolution of garnet morphology and inclusions

One of the most conspicuous observations is the evolution of garnet size, distribution of

252 inclusions and composition across the quartz-undersaturated selvage and the granulite
253 perpendicular to the gneissic layering. Although no quantitative textural analysis has been
254 conducted, it appears that garnet grain size decreases and the number of garnet grains increases
255 away from the leucosome, with the biggest garnet grains observed in the quartz-undersaturated
256 selvage (Figures 4 and 5). Furthermore, the amount, shape and composition of inclusions in
257 garnet varies greatly and continuously across the gneissic foliation. To describe this evolution,
258 seven garnets (A to G) were selected (see location in Figure 4).
259 In the quartz-undersaturated selvage, most garnets contain a few rounded inclusions of
260 quartz in their core (garnet A, Figure 5a). Away from the leucosome, but still in the selvage, the
261 largest garnet porphyroblast (b) contains in its core a small polymineralic inclusion, that consists
262 of plagioclase and quartz, surrounded by rounded isolated quartz inclusions (Figure 5b).
263 Inclusion-rich garnet cores are surrounded by a large rim free of inclusions except for numerous
264 and homogeneously distributed crystallized granitic melt inclusions that are less than 20 microns
265 in diameter (Figures 5a-b and 6). The inclusions have been identified as crystallized melt based
266 on the main microstructural criteria summarized in Cesare, Acosta-Vigil, Bartoli & Ferrero (2015)
267 : (1) the development of a perfect negative crystal shape (Figure 6a); (2) its polycrystalline
268 nature that consists of biotite, plagioclase, quartz and apatite for the most common phases
269 (nanogranitoids) (Figure 6b-c); and (3) the development of cracks (decrepitation) during
270 decompression filled with minerals similar to those in the melt inclusion(Figure S6). The
271 presence of these crystallized melt inclusions attest to the growth of the garnet rim in the
272 presence of melt.
273 In the quartz-saturated granulite, the abundance of polymineralic inclusions of
274 plagioclase and quartz observed in garnets increases away from the leucosome (Figures 4 and 5c-
275 g). The garnet core, defined as the garnet containing plagioclase-quartz polymineralic inclusions
276 surrounded by isolated quartz grains can be as large as 1mm and represent up to 50% of the
277 garnet volume. Polymineralic inclusions have rounded (Figure 5c-d-f) to very irregular shapes
278 with straight boundaries (Figure 5e). These facets are inferred to be parallel to crystallographic
279 orientations of the garnet host and result from post-entrapment readjustment of the inclusion

and host by dissolution-reprecipitation processes (e.g. Frezotti, 2001). Plagioclase in the polymineralic inclusions are chemically zoned with a composition varying almost continuously from pure anorthite $An_{95}Ab_{05}$ to $An_{58}Ab_{41}$. Highest amounts of albite are measured in the vicinity of rounded quartz inclusions within plagioclase and the garnet host (Figure S3). All garnets have an inclusion-free rim without any melt-inclusions, as for the garnet located in the quartz-undersaturated selvage (Figure 5). This difference in the ability for garnet rims to entrap melt inclusions may be related to a slowdown of radial growth rate as garnet continuously grows.

X-ray computed microtomography and sequential cuts through a single garnet crystal has been performed to highlight the volume, shape and potential connectivity of the polyphased inclusions with the matrix. The selected garnet is located in the quartz-saturated granulite where the amount of polyphase quartz-plagioclase is most abundant. The X-ray tomography reveals the very irregular shape of the polyphased inclusions as well as the “spongy” texture of the garnet core (Figure 7). Although all thin-section photomicrographs of garnet presented in Figure 5 suggest that polyphase inclusions are completely enclosed in the garnet, the 2D cuts rather suggest that they are connected to the matrix through small pathways (Figure 7d-f and Movie S1).

3.3. Microtextures in the quartz-undersaturated selvage

Microtextures in the quartz-undersaturated selvage have been revealed using a cold cathode cathodoluminescence detector on an optical microscope. The matrix consists mainly of K-feldspar grains (in blue in the CL images) that form a fine-grained mosaic texture with straight boundaries and triple junctions at 120° (Figure 8a-b). K-feldspar is characterized by a core with fine-grained perthite textures surrounded by a K-feldspar rim (Figure 8a). These boundaries are coated with thin plagioclase films or elongated grains (brown color in Figure 8a-b) that can be connected to form a branching array. Terminations of the films and elongated grains are characterized by small dihedral angles (< 20°). The connection of these films also leads to the formation of plagioclase pools along grain boundaries (Figure 8a-b) or at K-feldspar triple

junctions. Where plagioclase films are abundant, K-feldspar grains show very irregular resorbed grain boundaries (Figure 8b) and plagioclase films are connected to myrmekites pools (Figure 8a-b). Finally, a large plagioclase (± quartz) moat surrounds sillimanite and garnet porphyroblasts (Figure 8b).

4. GARNET COMPOSITION

To investigate the link between the textural and mineralogical features of melt-rock interaction and their compositional characteristics, major element data from multiple garnet grains were obtained by EMPA, and trace element data by LA-ICP-MS. X-ray maps and linear spot traverses were acquired to reveal the evolution of major element zoning patterns across the quartz-undersaturated selvage and granulite. Trace element mapping was performed to better inform the paragenetic context, particularly with regard to accessory minerals, and evaluate the record of geochemical mobility during garnet growth and dissolution. Major and trace element data are provided in Datasets S1 and S2, respectively, and presented in Figures 9, 10, 11, 12 and 13. . Raw trace element maps from which the profiles were extracted are available as ".csv" text file images (Dataset S3-S5). LA-ICP-MS analytical methods are provided in Appendix S1.

4.1. Major element zoning

Garnets are almandine – pyrope – grossular solid solutions with minor amounts of spessartine (< 0.015) (Dataset S1). All garnets are zoned and their composition varies with respect to their location and distance from the leucosome. In the quartz-undersaturated selvage, a polymineralic inclusion-free garnet porphyroblast in direct contact with the leucosome (Garnet A; Figure 5a) is characterized by bell-shaped zoning in grossular, with a maximum content of 0.12 in the core that decreases continuously towards the rims down to 0.03 (Figure 9a). Almandine and pyrope content increase towards the rim from 0.56 to 0.61 and 0.30 to 0.35, respectively, which results in a constant XMg [=Mg/(Fe+Mg)] of 0.34-0.35. Garnet B has equivalent zoning, except that close to the polymineralic inclusions, grossular content decreases

from a 700 μm wide and uniform plateau at 0.12 down to 0.08 (Figure 9b). This decrease in grossular content is mimicked by an increase of XMg from 0.35 to 0.38. It is noteworthy that the depleted grossular core also corresponds to the domain containing smoothed and rounded inclusions of quartz (light gray area in Figure 9b). The outer rim of Garnet B is characterized by grossular content and XMg value of 0.03 and ~0.35-0.36, respectively (Figure 9b). The resorbed outer left rim, in contact with cordierite and biotite, shows a sharp decrease in XMg down to 0.28 over a distance not greater than 100 μm (Figure 5b and 9b).

Garnets from the quartz-saturated granulite (Garnets C-G) show zoning profiles comparable in shape to Garnet B from the quartz-undersaturated selvage, except that the endmember modal abundances are significantly different (compare Figure 9b and Figure 9c-g). Garnet cores in direct contact with the polymineralic inclusions are characterized by low grossular values (0.03-0.04) that are similar in composition to garnet rims in contact with the matrix. Grossular content then increases towards the rim to a maximum value that is systematically located at the transition between the inclusion-bearing and inclusion-free garnet (Figure 9c-g). The maximum grossular content varies from grain to grain, from 0.095 (Garnet E) down to 0.045 (Garnet F). Finally, the inclusion-free rims show a decrease in grossular content towards the matrix to a minimum value of 0.03, equivalent to the core compositions. XMg ratio profiles for all samples are relatively flat, with values evolving from 0.36-0.37 (Garnet C) to 0.41-0.44 (Garnet G) with increasing distance from the leucosome. The smallest garnet grain analyzed (Garnet F) does not follow this trend, showing a lower XMg value of 0.36 and a near-constant grossular content of 0.03-0.04. Garnet E profile shows on its left side a sharp decrease in XMg from 0.40 to 0.36, over a distance less than 100 μm, that is interpreted as late Fe-Mg exchange during partial garnet breakdown into cordierite, comparable to Garnet B.

4.2. Trace element zoning

Similar to their major element characteristics, the analyzed garnets show significant

variations in trace element composition and zoning patterns depending on their location with respect to the leucosome. We will focus on Garnets A and B, located in the quartz-undersaturated selvage, and Garnet G, located in the quartz-present host granulite.

Garnet A is located directly adjacent to the leucosome, and contains the least inclusions in its core except for a few rounded quartz grains. Figures 10a, 11 and Figure S4 illustrate the key features of the trace element zoning. Y, Zr, V and heavy rare-earth elements (HREEs), from Dy to Lu, show a symmetrical bell-shaped profile without sharp discontinuities except for an abrupt increase at the rim. In contrast, light rare-earth elements (LREEs), from La to Gd, show a bowl-shaped zoning profile with a broad flat core that is mimicked by Li, P and Sc. Notably, the radial positions of broad peaks along the zoning profile are correlated for all REEs and Y (Figure 11), and there is no difference in gradient with decreasing atomic number.

Garnet B is the largest analyzed grain, with a small polyphase plagioclase + quartz inclusion in its core. It is located a few millimeters from Garnet A within the quartz-undersaturated selvage but further displaced from the leucosome. Trace element map and profile are shown in Figure 10b, 12 and S4. Its zoning pattern shows the same symmetrical bell-shape profile for Y, Zr and the heaviest HREE (from Yb to Er), but with elevated concentrations compared to Garnet A (e.g. Y ~360 vs 270 ppm; Yb ~75 vs 45 and Lu ~15 vs 6 ppm). In contrast, rim compositions are strictly identical for all elements in both samples (compare Figures 11 and 12 and S4). Because Garnets A and B are located in the same petrographic setting, we suggest that the difference in absolute concentrations reflects a sectioning effect (i.e. Garnet A is not sectioned through its core) rather than a geological process. The outer rim of Garnet B is characterized by a sharp increase in Y, Zr and HREEs, and LREEs and P have the same overall bowl-shaped zoning as Garnet A despite a more irregular profile that includes several narrow peaks. Concentrations in La, Ce and P are significantly enriched next to the polyphase inclusion and the matrix on the left side of the profile (Figure 12). The major difference in comparison to Garnet A corresponds to a broad depletion in Dy, Ho and Tb adjacent to the polyphase inclusion located at the garnet core. This feature closely matches the grossular zoning profile (Figure 9b),

and corresponds to the domain containing rounded inclusions of quartz.

Garnet G is derived from the quartz-present host granulite and is located furthest from the leucosome (Figures 4 and 5). It is the smallest analyzed grain and contains a large irregular polyphase inclusion in its core. Trace element map and profile are shown in Figure 10c, 13 and S4. Y and HREEs, from Lu to Tb, show a broad bell-shaped profile, but with maximum concentrations on average two to three times lower than the larger Garnets A and B (Figure 13). In contrast, rim compositions for all elements are once again similar for all samples. La, Ce and P show bowl-shaped profiles with a large flat core surrounded by an enriched rim. Sm (and to a lesser extent Gd) are no longer characterized by a typical bowl-shaped profile but rather mimic the grossular zoning, with a depleted core next to the polyphase inclusion (Figure 13). This similarity continues along the profile, with an identical location for the maximum Sm concentration and a core composition adjacent to the polyphase inclusion that is equivalent to the rim composition (2 to 3 ppm on average; Figure 13).

5. PETROLOGICAL MODELING

We use computed phase diagram sections to constrain (1) the pressure and temperature of garnet nucleation and growth, partial melting, and retrogression; and (2) the most likely processes responsible for the formation of the quartz-undersaturated selvage. For this purpose, the model system Na_2O-CaO-K_2O-FeO-MgO-Al_2O_3-SiO_2-H_2O was chosen to calculate phase relationships using Perple_X 6.6.6 software (Connolly, 2005), with the thermodynamic database of (Holland & Powell (1998), as revised in 2002). TiO_2 and Fe_2O_3 where not considered in the modeling because (1) the bulk rock content of TiO_2 is less than 0.6 wt%; and (2) there is no Fe^{3+}-bearing phase like hematite or magnetite and the amount of Fe^{3+} in garnet based on structural formulae is negligible. Solution models and end-member phases considered in the modeling are listed in Table S1.

413 **5.1. P-T conditions of garnet nucleation and growth**

414 Deciphering the P-T conditions of the early garnet growth and prograde path relies
415 essentially on the observation of garnet inclusions and the valid interpretation of garnet
416 composition and zoning. Garnet cores are characterized by the occurrence of quartz and
417 polyphase plagioclase-quartz inclusions, whereas the inner rim of the largest garnet grains show
418 abundant crystallized melt inclusions. We therefore suggest that the onset of garnet growth may
419 have occurred under sub-solidus conditions.

420 Garnet core compositions are typically used to retrieve the approximate P-T conditions of
421 garnet nucleation. However we will show later that major and trace element zoning patterns
422 and more particularly garnet core compositions have been modified, most likely as a result of
423 post-growth re-equilbration during partial melting and retrogression. The biggest garnets located
424 in the quartz under-saturated selvage (garnet A and B, Figure 4-5) show the least modified
425 zoning profile, with typical bell-shape zoning in grossular (Figure 9a,b) and trace elements
426 (Figure 11-12). Although these large garnets A and B are located in the quartz-undersaturated
427 selvage, the presence of quartz inclusions within their cores suggests that the onset of garnet
428 growth occurred under quartz-saturated conditions. We therefore suggest that the loss of SiO_2
429 and the formation of the quartz-undersaturated layer is a post-garnet growth process. Hence, to
430 retrieve the P-T conditions of early garnet growth and constrain the prograde path, we have
431 computed a P-T phase diagram section with a XRF bulk composition corresponding to the quartz-
432 saturated domain composition (Table 1 and Figure 14). The phase diagram section has been
433 contoured for grossular content, XMg (= MgO/MgO+FeO) in garnet and garnet modes (Figure 14).

434 The amount of water is known to be a critical variable when modeling phase relations in
435 melt-bearing systems (e.g. White et al., 2001). A classic strategy to estimate the amount of
436 water in melt-bearing systems consists of adding enough water to the system such that the
437 solidus is water-saturated. However, if we follow this approach, high-grossular garnet core
438 compositions cannot be reproduced. Therefore, the system was kept water-undersaturated, such
439 that measured garnet core compositions (i.e. the highest grossular values) are predictable, and

the amount of major rock-forming phases are consistent with observed mineral modes. The amount of water was adjusted and fixed at 1.67 mol% (0.025 mol or 0.46 wt%). With this low water condition, partial melting was restricted to temperatures higher than ~750°C (Figure 14)

The maximum grossular content of ~0.12, coupled with the corresponding XMg (0.35-0.38), allow estimating the minimum P-T conditions of garnet growth at ~1.2 GPa, 675°C (black circles with letters in Figure 14). This corresponds to sub-solidus conditions where garnet is in equilibrium with plagioclase, biotite, kyanite and muscovite. Although these last two phases have never been observed as inclusions in garnet, the predicted plagioclase composition (An_{76}-Ab_{23}) is consistent with the high anorthite compositions measured in plagioclase inclusions. Furthermore, melt-inclusions are absent in the high grossular cores (Figure 5), whereas they are abundant in the low-grossular rims. This observation is consistent with an early garnet nucleation and growth under sub-solidus conditions with peak metamorphism and garnet rim crystallization occurring in melt-present conditions.

In Figure 14, we report the composition of Garnet C to G, located in the quartz-saturated domain, with the highest grossular content and corresponding XMg values (grey circles with letters in Figure 14). The maximum grossular content, preserved in the inner rim at the transition between the inclusion-bearing and inclusion-free domains, varies from grain to grain from 0.095 (Garnet E) down to 0.04 (Garnet F) and XMg from 0.36 (Garnet C) to 0.43 (Garnet G) (Figure 9). The inferred P-T conditions vary from ~1.3 GPa and 720°C to 0.85 GPa and 780°C corresponding approximately to the P-T conditions of garnet nucleation and peak metamorphism / partial melting , respectively (see Section 5.2 below). We suggest that this could reflect the progressive and incomplete re-equilibration of garnet during a prograde (heating/decompression) path from ~1.2 GPa and 675°C down to 0.8 GPa and 790°C. During this P-T evolution minor garnet growth is expected (volume % = 14-16, Figure 14).

465 **5.2. P-T conditions of peak metamorphism, partial melting and retrogression**

466 The computed P-T phase diagram in Figure 14 shows the classic phase relations for
467 partially melted aluminous-rich pelites (e.g. White et al., 2001), with the divariant muscovite-
468 dehydration melting equilibrium at high pressure (1.2 > P > 0.9 GPa) and the biotite-dehydration
469 melting equilibrium that produces garnet and cordierite at lower pressure (0.8 > P > 0.6 GPa).
470 Between these two divariant narrow fields lies a trivariant assemblage with garnet, biotite,
471 sillimanite, K-feldspar, quartz and melt in equilibrium, between 770 and 820°C (Figure 14). This
472 calculated assemblage is consistent with the observed assemblage in the quartz-saturated
473 granulite. Garnet core and rim compositions in direct contact with the polyphased plagioclase-
474 quartz inclusions (ca. 3% grossular and XMg = 0.36-0.44) give consistent P-T conditions of 0.8 ±
475 0.05 GPa and 790 ± 20 °C (white circles with letters in Figure 14), with the predicted XMg of
476 biotite (0.70) consistent with the measured biotite composition. We interpret these estimates to
477 reflect partial melting during the development of the steeply dipping S_2 granulite-grade gneissic
478 foliation. As discussed in Section 7.2, however, the garnet trace element distribution indicates
479 that core compositions may have been affected by post-growth re-equilibration.
480 Retrogression in the quartz-saturated domain is characterized by the local development
481 of cordierite at the expense of garnet and sillimanite (Figure 4b), through reaction (1). This local
482 and partial retrogression is also evidenced by the sharp decrease in XMg from 0.40 to 0.36, at
483 constant grossular content (~0.30) (Figure 9e, outer rim of Garnet E). Figure 14 shows that the
484 development of cordierite and the decrease in XMg, at almost constant grossular content, would
485 require further isothermal decompression at or below 0.7 GPa in the garnet + cordierite +
486 sillimanite + K-feldspar + plagioclase + quartz stability field.
487

488 **5.3 Formation of the quartz-undersaturated selvage via melt-driven metasomatism**

489 In migmatites, the formation of quartz-undersaturated assemblages has been interpreted
490 as characteristics of advance quartz-consuming reactions during partial melting coupled with
491 local melt extraction (Fitzsimons, 1996; Owen, 1991). Alternative models consist of producing

492 the quartz-depleted selvage by small-scale silica metasomatism between the host rock and a
493 quartz vein (Penniston-Dorland & Ferry, 2008) or a silica-rich leucosome formed after melt
494 segregation and transport (Dunkley, Clarke & Harley, 1999). In the later case, selvage formation
495 is a post-anatectic process rather than being directly related to partial melting of the host-rock
496 (Lin & Sawyer, 2019). In the following section, we model and show that element exchange
497 (diffusion-metasomatism) between the segregated melt (leucosome) and the host granulite is
498 likely to be responsible for the formation of the quartz-depleted selvage during post-peak
499 decompression.

500 Following the approach of White and Powell (2010), we investigate through phase
501 equilibria modeling the melt-driven metasomatism and more particularly the role of diffusion,
502 between melt-rich domains (leucosome) and the host granulite, on the formation of the selvage.
503 Our conceptual model is similar to Lin & Sawyer (2019) and requires a first stage of partial
504 melting and melt segregation to produce two subsystems corresponding to the quartz-saturated
505 domain (~residue) and the melt domain. At the P-T conditions of partial melting and melt
506 segregation (i.e. 0.8 GPa and 790°C), chemical potentials are the same in the solid phases and
507 the melt of both domains, if thermodynamic equilibrium is maintained. The second stage
508 corresponds to decompression into the cordierite-bearing stability field below 0.7 GPa. As
509 pressure decreases, chemical potential evolve independently in both subsystems. Therefore,
510 diffusion of components is driven by the chemical potential gradient established at the interface
511 between the quartz-saturated residue and the leucosome.

512 In order to determine the direction of diffusion, we have computed the chemical
513 potentials of H_2O, SiO_2, CaO and K_2O for the quartz-saturated and melt domains along an
514 isothermal decompression path from 0.8 to 0.5 GPa at 790°C (Figure 15). The chemical
515 potentials in the melt domain were determined using the chemical composition of melt
516 produced at 0.8 GPa and 790°C (Table 1). Chemical potential of the selected components were
517 computed separately for each sub-systems (segregated melt and residue) by assuming that
518 during decompression these two sub-systems are closed and chemically isolated from each other
519 (Figure 15). This implies that there is no interaction or mass transfer between the two

subsystems. This ideal chemical isolation model is in a strict sense impossible because the two sub-systems are physically in contact and therefore chemical interactions are expected at some scale and chemical potential will continuously evolve with ongoing decompression due to diffusive mass transfer (White & Powell, 2010). However, our approach can be used at first order to determine the direction of transport of the four selected species if chemical interaction at the interface is permitted. During decompression, the chemical potentials of H_2O, CaO, K_2O and Na_2O (Na_2O not shown in Figure 15) become higher in the melt segregated domain (leucosome) than in the residue. In contrast, the chemical potential of SiO_2 is lower in the melt than in the residue. This suggests that species such as H_2O, CaO, K_2O and Na_2O will diffuse from the melt into the host residue whereas SiO_2 is transferred from the host residue into the adjacent melt domain.

To model the effect of metasomatism and pressure on phase relations, a P-X phase diagram section was computed at 790°C (Figure 16). The initial amounts of CaO and Na_2O are very low (< 1.3 and 0.6 wt%, respectively) and do not significantly influence the phase relations. Therefore, variations in Na_2O and CaO content are not considered. The bulk composition for X = 0 corresponds the quartz-saturated host-rock composition prior to any mass transfer. The bulk composition for X=1 is obtained assuming a gain in H_2O of 200% (H_2O = 0.075 mol) and a SiO_2 loss of 55% (SiO_2 = 0.342 mol). These values are arbitrary. Bulk compositions used are provided in Table 1.

Figure 16 shows the location of the two main low variance (V=2) retrogression equilibria that have been observed in the quartz-saturated domain and quartz-absent selvage: Grt + Sil + Qz ± Bt = Crd + L (2) and Grt + Sil ± Bt = Crd + Spl + L (3) at 0.72 GPa and 0.55 GPa respectively. These divariant equilibria together with their related trivariant assemblage are used to locate the quartz-out, cordierite-in and spinel-in boundaries (Figure 16). The formation of selvage assemblage (Crd + Spl + Sil + L ± Grt/Bt) requires a decompression below 0.55 GPa and a bulk composition with X ranging from ~0.65 to 0.8. Taking a value of X = 0.7, mass transfer required to produce the selvage from the host quartz-saturated granulite corresponds to a relative gain of

about 140 % of H_2O coupled with a relative loss of 47% of SiO_2. The P-X phase diagram is also contoured for garnet mode (Figure 16). As expected, decompression is associated with garnet breakdown, but at pressures above the cordierite-in boundary (P > 0.72 GPa), mass transfer (SiO_2 loss coupled with H_2O gain) induces a slight increase in garnet mode, from 12 to 17 vol%. This mineralogical evolution is consistent with the observation of a higher modal abundance of garnet in the metasomatic selvage with respect to the host granulite.

Based on the estimation of mass transfer required to produce the quartz-undersaturated selvage, a P-T phase diagram section has been computed with an estimated selvage composition (Figure 17 and table 1). This composition corresponds to X = 0.70 in Figure 16. Figure 17 shows the location in a P-T space of the two main low-variance retrogression reactions (2) and (3) and the position of the quartz-out, cordierite-in and spinel-in lines. Once again, the selvage formation is consistent with a decompression from about 0.8 GPa down to 0.5 GPa at temperatures greater than 750°C.

6. U-TH-PB MONAZITE AND ZIRCON GEOCHRONOLOGY

Monazite and zircon geochronology were acquired to establish a temporal framework for melt-rock interactions and the relationship of garnet growth and dissolution to the accessory mineral evolution. Chemical zoning in monazite and zircon were first characterised via X-ray mapping and cathodoluminescence respectively. In situ U–Th-Pb monazite and zircon ages were then acquired by laser ablation inductively coupled plasma-mass spectrometry (LA-ICP-MS). Sample preparation and operational procedures for all techniques are described in Hurai, Paquette, Huraiová & Kronečný (2010) and Paquette et al. (2014) and presented in Appendix S2. U-Th-Pb geochronological data are provided in Dataset S6.

572 **6.1. Textural features and dates**

573 Monazite is abundant in both quartz saturated and undersaturated domains but is totally
574 absent in the leucosome. The analyzed monazites range in size from 50 to 250 μm and occur in
575 the matrix, at grain boundaries and included in sillimanite and plagioclase (M1-2-13), in the
576 vicinity of garnet and within the retrograde cordierite moat (M3-6-4-8-9-10-11-12) (Figure 18a).
577 Monazite grains M3, M6 and M12, located in cordierite moats, have an unusual worm-like shape
578 that mimics the embayed garnet rim (Figure 18c). Only one grain (M7) was found included in a
579 garnet rim.

580 All monazite grains are chemically homogeneous (Y-poor) (Figure 18b,c) except for two
581 grains (M9 and M10) that show a subtle zoning with high Th domains. Grains located in the
582 cordierite moat show discrete and discontinuous micron-scale Y-rich rims (Figure 18c) whereas
583 those included in other phases are devoid of such overgrowths (Figure 18b). These observations
584 suggest that the crystallization of the low Y grains might precede or be coeval with the peak
585 assemblage garnet (rim), sillimanite, biotite, plagioclase, K-feldspar ± quartz. The crystallization
586 of discrete Y-rich monazite overgrowths in the vicinity of garnet porphyroblasts partially
587 retrogressed into cordierite has been previously interpreted as an indicator of accessory phase
588 growth during garnet breakdown (Mahan et al., 2006). We suggest that Y overgrowths are also
589 contemporaneous with cordierite crystallization and selvage formation.

590 Ten homogeneous Y-poor grains were analyzed for a total of 39 analyses (Dataset S6). The
591 Y-rich overgrowths were not analyzed due to their small size in order to avoid mixing during
592 ablation. In a $^{206}Pb/^{238}U$ versus $^{208}Pb/^{232}Th$ diagram all analyses are concordant or sub-concordant
593 (Figure 19a). Excluding six analyses (see Dataset S6) gives a concordia age of 2061± 6 Ma
594 (MSWD(C+E) = 1.3). The weighted mean of $^{208}Pb/^{232}Th$ dates gives an age of 2069 ± 8 Ma (MSWD =
595 1.6) (Figure 19b). The $^{208}Pb/^{232}Th$ dates show no systematic variation with textural location (see
596 Figure 18a and Dataset S6), and more specifically, monazite included in garnet (M7) is not
597 statistically different from matrix grains (Figure 19). The date of 2.06 Ga is interpreted as the
598 age of partial melting at 0.8 ± 0.05 GPa and 790 ± 20 °C, before decompression responsible for

599 partial garnet breakdown and crystallization of small Y-rich overgrowths.

600 Zircons are rare and do not exceed 50 µm in diameter. They are translucent with a
601 rounded shape typical of zircons recrystallized under granulite facies conditions. Fourteen
602 analyses were performed on fourteen grains (Dataset S6). They do not show significant zoning in
603 cathodoluminescence. A first group of 7 analyses are concordant and gives a concordia age of
604 2072 ± 7 Ma (MSWD(C+E) = 2.3) (Figure 19c). A second group of 4 analysis are discordant and
605 when plotted together with the previous 7 analysis, it defines a discordia with an upper
606 intercept at 2073 ± 11 Ma (MSWD = 2.0). The last group, consists of 4 analyses that do not match
607 the previous tow identified clusters (white ellipses in Figure 19), with $^{207}Pb/^{206}Pb$ dates that
608 range from 2.07 to 2.33 Ga and one concordant analysis at 2192 ± 15 Ma. The 2.07 Ga date is
609 similar to that obtained for monazite and is interpreted as the age of partial melting. The
610 remaining three analyses are interpreted as inherited ages.

611

612 **7. DISCUSSION**

613 Petrological and micro-textural analysis carried out across the interface between the
614 leucosome and the host-granulite shows a systematic and consistent evolution in mineral
615 paragenesis, micro-textures, garnet grain size and composition (major and trace element) with
616 the distance from the leucosome. The studied sample is therefore used to discuss small-scale
617 melt-rock interaction processes. In this section, we will first summarize the petrological model
618 of formation of the migmatite and more particularly the quartz-undersaturated selvage at the
619 interface between the segregated melt (leucosome) and the partially melted host granulite.
620 Based on this petrological evolution, we will discuss the significance of major and trace element
621 zonation observed in garnet.

622

623 **7.1. Petrological model of migmatite and quartz-undersaturated selvage formation through**
624 **diffusion metasomatism**

625 The phase relation modeling performed suggests that the onset of garnet crystallization
626 occurred under subsolidus conditions at high pressure (P~ 1.2 GPa) and temperatures of 675 to
627 700°C. These P-T conditions, that were estimated using the maximum grossular content of
628 garnet cores and anorthite content of plagioclase inclusions, are consistent with a steady state
629 geotherm considering average crustal thermal parameters (thermal conductivity k = 3 $W.m^{-1}.K^{-1}$,
630 heat production A = 0.75 $\mu W.m^{-3}$, a mantle heat flow Q = 30 mW^{-2}, a density ρ = 2.7 $kg.m^{-3}$) at a
631 depth of 45 km (1.2 GPa). We suggest that the gently dipping gneissic foliation (S_1) that trends
632 NE-SW (Figures 2b and S1) may be occurred at to these conditions and may correspond to a
633 crustal thickening event. This interpretation is also supported by the observation of quartz and
634 plagioclase inclusions trails, defining a S1 foliation, in the high-grossular garnet cores (Figure
635 3a).

636 Partial melting occurred at 0.8 GPa and 790°C at ~2.06-2.07 Ga. The former presence of
637 melt at peak metamorphic conditions can reliably be inferred from the occurrence of peritectic
638 garnet, produced by biotite-dehydration melting (1) (Figures 4-5) and the presence of
639 crystallized melt inclusions within the garnet (Figure 6). Interstitial elongated films along grains
640 boundaries and pools at the triple junction (Figure 8) are alternative criteria diagnostic of the
641 former presence of melt and melt movement at the grain scale (Holness & Sawyer, 2008; Sawyer,
642 2001; Stuart, Piazolo & Daczko, 2018; Vernon, 2011). The interstitial plagioclase may represent
643 the plagioclase component crystallized from the melt (Hasalová, Schulmann, Lexa, Štípská &
644 Hroda, 2008; Stuart et al., 2018). The corroded K-feldspar grains and the crystallization of
645 plagioclase and myrmekite (figure 8) are interpreted as the result of K-feldspar dissolution
646 during the interaction between the host rock and a migrating melt (Hasalová et al., 2008). We
647 suggest that the connection between the leucosome and the host-granulite via the grain
648 boundary melt array favored efficient small-scale mass transfer in and out of the host-granulite
649 to produce the quartz-undersaturated selvage.

Thermodynamic modeling shows that decompression from 0.8 to 0.5 GPa at 790°C coupled with melt segregation are responsible for the establishment of chemical potential gradients between the leucosome and the host-granulite. Chemical potential gradients drive diffusive metasomatism of species between the two reservoirs and the formation of the quartz-undersaturated selvage at the interface. The modeling suggests that, during post-peak decompression from 0.8 to ~0.5 GPa at 790°C, species like H_2O, CaO and Na_2O will be transferred from the leucosome to the host-rock while SiO_2 had an opposite diffusion direction, going from the host-rock to the leucosome. Phase diagrams in figure 16 and 17 show that mass transfer coupled with decompression resulted in the partial transformation of the quartz-saturated peak metamorphic assemblages (Grt, Bt, Sil, Qz + L) into a quartz-undersaturated assemblage with cordierite and spinel (see location of Qz-out, Crd-in and Spl in Figure 16). Formation of the quartz-undersaturated selvage via melt-driven metasomatism (ie. SiO_2 loss), is well supported by the absence of quartz in the matrix and the observation of quartz only as inclusions in garnet cores. This observation rules out the possibility that the gneissic layering and more particularly the quartz-absent selvage is inherited from the sedimentary protolith. The phase diagram shows that further mass transfer and decompression below 0.5 GPa could result in the formation of corundum-bearing assemblage.

Several other petrological and micro-textural observations provide support for the modeled mass transfer direction and the formation of the selvage:

(1) The quartz-undersaturated selvage, where local mass-transfer is inferred as the dominant process, is characterized by larger garnet grain sizes. This is consistent with modeled garnet modes in Figure 16, that show an isobaric and isothermal increase in garnet abundance at 0.8 GPa, only due to mass transfer (SiO_2 gain and H_2O loss).

(2) Diffusion of water from the melt into the host-granulite will favor the crystallization of anhydrous products in the melt, producing almost an anhydrous leucosome, while the adjacent host granulite is hydrated, as demonstrated by the slight enrichment of the selvage in hydrous-phases like biotite and cordierite. This observation is very consistent with results from

White and Powell (2010) who also predicted that the diffusion of H_2O into the residue will be responsible for the formation of anhydrous leucosomes during an isobaric cooling under granulite facies conditions.

(3) Diffusion of other mobile species like CaO, Na_2O and K_2O, from the leucosome into the selvage is indirectly supported by the mineralogical composition of the leucosome that consists mostly of quartz with very minor K-feldspar and almost no plagioclase. It is well known that leucosomes in migmatites do not have the expected minimum granitic composition (Ashworth & McLellan, 1985) due to post-anatectic magmatic differentiation processes. However, following Olsen and Grant (1991), who performed a mass-balance (isocon) analysis on leucosomes, we suggest that the quartz-rich and K-feldspar and plagioclase-poor leucosomes most likely formed by loss of Na_2O and CaO by diffusion.

(4) Diffusion of K_2O into the host-rock is likely to be responsible for the formation of the distinct inclusion-free outer-rim of K-feldspar located in the selvage (Figure 8).

(5) The introduction of a Na_2O/CaO-rich fluid or melt into the selvage, is consistent with the observation of plagioclase films and pools along K-feldspar grain boundaries (Figure 8). The formation of myrmekite in the selvage is also consistent with a fluid or melt mediated Na-Ca replacement of K-feldspar by plagioclase (Yuguchi & Nishiyama, 2008).

Melt segregation and the development of the selvage defines a steeply deeping S_2 gneissic layering that transposes the previous S_1 fabric (Figure 3 and Figure S1). Kinematic analysis of the D_2 high strain is consistent with NNW-SSE shortening and a bulk dextral sense of shear. We conclude that melt transfer and metasomatism may have been enhanced by D2 transpressive deformation.

7.2. Major and trace element behavior during partial melting and retrograde melt-rock interaction

The studied sample preserves mineralogical and textural evidence of prograde partial melting and melt segregation, near-isothermal decompression and melt-driven metasomatism. With respect to other phases, garnet has the tremendous advantage to preserve records of these

various processes via its chemical zoning in major and trace elements, because of the slow rates of intracrystalline diffusion (e.g. Carlson, 2006). However, in order to interpret accurately these zoning patterns in terms of large-scale and long-term geological/geodynamic processes, we have to understand the small-scale processes that control the behavior of major and trace elements during garnet nucleation, growth, breakdown and re-equilibration (George & Gaidies, 2017 and references therein). Although the zoning features varies from garnet to garnet, they show systematic variations and similarities that can be correlated with the P-T-X evolution and petrographic setting. Via a qualitative analysis of zoning profiles, and previous work by others cited below, we suggest these features reflect the superposition of at least three grain-scale processes that control the intra- and intergranular mobility of chemical components (major and trace elements).

Evidence of fast intergranular mobility of elements, including REE, and rock-wide equilibrium

The P-T evolution of the studied sample occurred at high temperature (> 650°C) and in the presence of melt, from peak-metamorphic conditions (0.8 GPa; 790°C) to the conditions of selvage formation (~0.5 GPa; 800°C). Therefore, the high mobility of major and to a lesser extent trace elements is expected. We report below evidence of fast intergranular mobility of elements, including REE, and rock-wide equilibrium.

Rock-wide equilibrium and by extension fast inter-granular transport of major and trace elements during peak metamorphic conditions and subsequent melt-driven metasomatism is best demonstrated using garnet rim compositions. Although the analyzed garnets are located in different petrographic settings (within the quartz-undersaturated selvage or in the host-granulite displaced from the leucosome) and vary markedly in grain size and morphology, their outermost rims share consistent major element (grossular content = 3%; Figure 9) and trace element compositions (Y and REEs; Figure 11-13). This consistency in major element composition of the rims permits an accurate estimation of peak metamorphic conditions at 0.8 GPa and 790°C (Figure 14).

732 The length scale of equilibration during garnet growth, which is related to the degree of
733 mobility of major and trace elements through the intergranular matrix, can be evaluated using
734 the REE zoning pattern (Moore et al., 2013; Skora et al., 2006). In both studies, these authors
735 have shown a dependency of REE distribution on atomic number in large and early nucleating
736 garnets. Such garnets are characterized by pronounced central peaks for Y and HREEs (Lu to Er),
737 central peaks and annular maxima for MREEs (Ho, Dy), and well defined annular maxima for
738 LREEs (Tb to Nd). This distribution is driven by diffusion-limited uptake that evolves during
739 garnet growth. With increasing temperature, intergranular diffusivities increase progressively as
740 garnet grows, but with more rapid diffusion for HREEs compared to LREEs (Moore et al., 2013;
741 Skora et al., 2006). However, this dependency of REE distribution with atomic number is less
742 valid at high temperature. Numerical modeling of garnet zoning along a temperature-time path
743 performed by Moore et al. (2013) demonstrates that a uniform bell-shaped distribution for all
744 REEs is consistent with garnet nucleation and growth at high temperature, whereas at lower
745 temperature a sharp central peak with an annular maximum would be expected (see Figure 19
746 and Figure 20b in Moore et al. (2013)). From these previous studies, we can conclude that a
747 uniform distribution for all REEs is the result of rapid intergranular diffusion that strongly
748 minimizes the development of concentration gradients in the matrix surrounding the growing
749 garnet.

750 All studied garnets are characterized by a bell-shape distribution for Y and REEs, ranging
751 from Lu to Dy (± Tb), with a strong correlation between the radial positions of all peaks. This
752 distribution is consistent with a progressive depletion of the matrix in Y and REEs (Lu-Dy) due to
753 Rayleigh fractionation with an unchanging mineral assemblage (Moore et al., 2013; Otamendi et
754 al., 2002). Although the inferred P-T path in Figure 14 suggests that the onset of garnet growth
755 may have occurred under sub-solidus conditions prior to muscovite dehydration, we instead
756 suggest that the majority of garnet growth occurred via biotite dehydration melting in the
757 trivariant NaCaKFMASH stability field Bio – L – Gt – Kf – sill – pl – q at a temperature greater than
758 ~760°C. The uniform bell-shaped distribution for REEs, ranging from Lu to Dy, is consistent with

759 rapid intergranular diffusivities.

760 All garnet grains are characterized by (1) the absence of progressive outwards migration
761 of REE peak locations with decreasing atomic number; and (2) the lack of a central peak for
762 LREEs between La and Gd. Instead, they show a large LREE-depleted core of constant
763 composition surrounded by an enriched rim. This transition from bell- to bowl-shaped profiles
764 with decreasing atomic number is similar to an example reported by Raimondo et al. (2017) from
765 a metasomatic shear zone in central Australia. Both observations (1) and (2) are once again
766 indicative of fast intergranular mobility and rock-wide equilibrium during garnet growth, without
767 significant differences in diffusivity between HREEs and LREEs. However, we will see below that
768 the bowl-shaped profile could also be related, or at least accentuated, by a post-growth
769 modification.

770 Following Raimondo et al. (2017) and Konrad-Schmolke et al. (2008), we suggest that the
771 REE zoning reflects a typical Rayleigh fractionation model. As garnet nucleates and grows at high
772 temperature (T>750°C), the matrix is progressively depleted in HREEs on a large scale due to the
773 presence of melt along grain boundaries that favor fast element mobility and rock-wide
774 equilibration. Simultaneously, the matrix is passively enriched in LREE on a rock-wide scale due
775 to the low garnet/matrix partition coefficients for LREEs (Moore et al., 2013). The rapid
776 intergranular mobility for all REEs with respect to garnet growth, without any dependence on
777 atomic number, precludes the establishment of diffusion gradients in the matrix, resulting in
778 smooth core-to-rim zoning and a transition from bell-shaped HREE to bowl-shaped LREE profiles.

779 Small garnets located in the quartz-saturated host granulite (e.g. Garnet G) are
780 characterized by a significantly HREE-depleted composition compared to large garnets located in
781 the quartz-undersaturated selvage adjacent to the leucosome (Garnets A and B), whereas their
782 LREE content remains similar. This discrepancy in REE concentrations could be related to a later
783 nucleation of garnets located in the quartz-present host granulite. Assuming a rapid
784 intergranular mobility and rock-wide equilibration for REEs, the early nucleation and enhanced
785 growth of garnet in proximity to the leucosome may have induced a bulk-rock HREE depletion at

the scale of the distance between Garnet A and Garnet G (~7 cm). In contrast, the small garnet/matrix LREE partitioning coefficient has a negligible effect on the bulk rock composition, resulting in an approximately constant LREE concentration for garnet regardless its nucleation and growth history.

Post-growth intragranular diffusion of major and trace elements

Calcium maps and profiles from Garnets B-G reveal that their prograde growth zoning is modified bear the inner core inclusions. This post-growth modification resulted in chemical re-equilibration of the grossular content to varying degrees, depending on the location of the garnet with respect to the quartz-undersaturated selvage and the host granulite. In the quartz-saturated host granulite, the smallest garnets (which also contain the biggest polyphase inclusions) show a complete (Garnet F) or partial re-equilibration (Garnets C, D, E, G) of the garnet core in contact with the inclusions, with grossular content decreasing to 3%, corresponding to the rim composition. This suggests that post-growth modification occurred near peak P-T conditions (0.8 GPa; 790°C). Located in the quartz-undersaturated selvage, the largest analyzed grain (Garnet B) also shows post-growth modification of bell-shaped Ca zoning, but chemical re-equilibration at peak-metamorphic conditions was only partial, with a minimum grossular content of 8% in the garnet core.

The modification of garnet cores in contact with polyphase inclusions and their strong similarity with matrix compositions requires a pervasive connectivity to permit such rock-wide re-equilibration to proceed. Both X-ray tomography (Figure 7) and LA-ICP-MS mapping (e.g. linear features highlighted in Li map; Figure 10) reveal the presence of a network of open channels and re-healed cracks that may have acted as potential connecting pathways. These features confirm that the garnet core was not isolated or armored from the matrix, but was rather freely accessible to the extent that fluid access along these discrete open fractures or larger conduits (Figure 7) may favor cation transport and garnet re-equilibration.

Furthermore, we suggest that REEs are also susceptible to the post-growth re-equilibration process. In contact with the polyphase inclusions in Garnet B, the bell-shaped HREE profile is modified with a decrease in Ho, Dy and Tb that correlates with the Ca zoning (Figure 12). The remaining HREEs are apparently unaffected by this modification, whereas the modification of LREEs such as Sm, Gd, La and Ce is more challenging to interpret. This is largely because the bowl-shaped profile for Sm and Gd, as described above, could also be enhanced by a depletion in LREEs next to the inner core inclusions. However, Grain G does show a pronounced depletion in LREEs at the garnet core, resulting in zoning that closely mimics the Ca distribution (compare Figs 9g and 13). Unlike Grain B, the absence of significant depletion in Ho, Dy and Tb, coupled with its lower HREE content and well-preserved bell-shaped HREE profile, may support the interpretation that Grain G represents a late nucleating garnet in the host granulite at peak metamorphic condition. Post-growth modification proceeded at a lower temperature where only LREE remained mobile, in the presence of F, Cl and/or P complexes (Ague, 2017; Migdisov, Williams-Jones & Wagner, 2009; Williams-Jones, Migdisov & Samson, 2012). Alternatively, it may suggest that selective REE mobility is coupled to Ca substitution via retrograde garnet-plagioclase exchange that favors LREE over HREE according to kinetic controls and element compatibility.

Role of changes in accessory phases and major rock-forming minerals

In the studied sample, the LREE + P whole rock budget is largely controlled by the stability of monazite. As such, an approximately constant LREE concentration for garnet whatever its nucleation and growth history, coupled with a smooth bowl-shaped LREE + P profile prior to post-growth modification (i.e. Garnet A; Figure 13), suggests that monazite did not grow on the prograde path. Bulk rock fractionation of this kind is incompatible with garnet-monazite partitioning relationships if their growth was coeval (Warren et al., 2019). Rather, the apparent lack of monazite competition for LREE + P throughout the garnet growth history necessitates that monazite first appeared at peak conditions, consistent with the U-Pb age interpretation

839 documented previously and further explained below.

840 Superimposed on the bowl-shaped LREE profile, the rims of Garnets B and G show a
841 sharp coincident enrichment in Ce, La and P where garnet is in contact with the matrix
842 assemblage consisting of plagioclase and biotite. The same sharp enrichment is observed next to
843 polyphase plagioclase and quartz inclusions located in garnet cores. There are two possibilities
844 for explaining LREE enrichment. We suggest that these sharp enrichments may reflect
845 modification of garnet zoning during post-peak breakdown of monazite. This interpretation is
846 consistent with the pervasive occurrence of thin Y-rich overgrowths on monazite located in the
847 matrix (Figure 18c), which may represent dissolution-precipitation events during the retrograde
848 evolution. Plagioclase breakdown may also contribute to the LREE enrichment since garnet rims
849 are locally enriched in large ion lithophile elements (LILEs) such as Ba and Sr, further suggesting
850 that post-peak garnet-plagioclase exchange is responsible for the modified grossular zoning and
851 that monazite ages reflect the timing of partial melting prior to breakdown on the retrograde
852 path.

853 The outermost rims of garnets are characterized by a sharp increase in Y and HREEs along
854 grain boundaries (Figures 10-13). This local enrichment is interpreted to be the result of partial
855 garnet breakdown during decompression via reactions (2) and (3) and back-diffusion of elements
856 that strongly partition into garnet with respect to the matrix. Notably, the absence of sharp
857 HREE and Y enrichment in core domains, despite an apparently pervasive matrix connectivity
858 during post-growth re-equilibration and simultaneous monazite replacement, confirms that
859 garnet resorption must have post-dated these events.

860 Similar to the HREEs, Zr zoning is radial in all garnets except for sharp spikes adjacent to
861 grain boundaries (figure S4). There are no satellite peaks or annular maxima indicative of zircon
862 breakdown, nor are there any pronounced depletions indicative of sudden zircon crystallization.
863 This suggests that zircon grew on the prograde P-T path, with the bulk rock Zr budget
864 progressively depleted as zircon and garnet grew under rock-wide equilibrium. The distribution
865 of U-Pb dates supports this interpretation, with concordant zircon analyses at 2.07 Ga being

similar to the 2.06 Ga monazite age inferred to represent peak metamorphism and partial melting. Rimward spikes in Zr are coincident with the HREE and Y enrichment noted above and slope away from the grain boundary, thus most likely due to garnet resorption rather than zircon breakdown.

CONCLUSIONS

The petrological and geochemical investigations of this partially melted granulite highlight the complexity of processes involved during partial melting at a scale ranging from a few microns to centimeters. This study confirms and shows that partially melted rocks are open systems in which changes in P-T conditions, deformation and mass transfer, that we have defined as melt-driven metasomatism, are preserved in the mineralogical assemblage and the major and trace element distribution revealed by X-ray microprobe and LA-ICPMS mapping respectively. One of the main challenges is to be able to distinguish the mineralogical records of a process like metasomatism from those related to changes in P-T conditions.

A first key observation and interpretation is that melt segregation and extraction coupled with changes in P-T conditions (due to decompression in this example) induce local disequilibrium between the segregated melt and the residual host-rock. The establishment of chemical potential gradients at the interface of these two sub-systems drives diffusive mass transfer. Our thermodynamic modeling shows that while H_2O, Na_2O, CaO and K_2O are transferred from the melt to the host rock, SiO_2 diffuses in the opposite direction. This combined mass transfer results in the formation of a quartz-rich and almost anhydrous leucosome and a quartz-undersaturated selvage at the expense of the host-granulite. Depending on the initial bulk-rock composition, P-T conditions of melt extraction and shape of the P-T path, the element that will diffusive (or not) in or out the melt domain and the residue will vary. We suggest that the variety of mineralogical compositions encountered in selvages surrounding leucosomes in migmatites

892 relates directly to these environmental variables and the induced melt-driven metasomatism.

893 Garnets show a complex major and trace element distribution that varies consistently with the
894 petrographic setting. We suggest that preserved chemical zoning reflects the superposition of
895 changes in P-T conditions and melt-driven metasomatism. Major and trace element zoning was
896 first acquired during prograde and peak metamorphism garnet growth in a temperature range of
897 675 and 790°C. Garnet grew mostly as a peritectic phase during biotite-dehydration melting
898 reaction. Calcium, Y and HREEs (from Lu to Dy), are characterized by a bell-shape distribution
899 and LREEs (from La to Gd) show a bowl-shape. The chemical zoning is consistent with a typical
900 Rayleigh fractionation model with fast intergranular element mobility of all elements, including
901 REEs, and rock-wide equilibration. The fast mobility is enhanced by the presence of melt along
902 grain boundaries.

903 The post-peak melt-driven metasomatism event is responsible for the modification of the
904 prograde zoning growth. Both Calcium and REE's are susceptible to the post-growth alteration
905 and results in a complete or partial re-equilibration through diffusion of garnet composition at
906 the P-T-X conditions of metasomatism (0.8 to 0.5 GPa; 790°C). Garnet cores in contact with
907 polyphased inclusions were affected by the post-growth modification due to the presence of a
908 network of open channels and cracks that act as connecting pathways between the matrix and
909 garnet core. Once again, at these high temperature conditions and in the presence of melt (and
910 fluid), divalent cation (Ca^{2+}) and REE are characterized by fast inter-granular and intragranular
911 element mobility and rock-wide equilibration. We conclude that in this peculiar case (high
912 temperature and melt/fluid-bearing open system), REE are not less vulnerable to diffusive
913 resetting than divalent cations.

914 Besides the interpretations regarding the formation of the quartz-undersaturated selvage and
915 the mobility of major and trace elements at high temperature conditions, this contribution
916 shows that an inaccurate interpretation of chemical zoning in garnet could result in misleading
917 thermobarometric results. Indeed, if the modified garnet core compositions (i.e. low calcium
918 content) were used as the chemical fingerprint of the early garnet nucleation stage it would

have resulted in erroneous low-pressure condition estimates for garnet nucleation.

ACKNOWLEDGEMENTS

This work was partially supported by the program CAPES-COFECUB n°624/09. We greatly acknowledge Johildo Barabosa and Hervé Martin, the main investigators of the program. We thank Johildo Barbosa for introducing the Farol da Barra outcrop and for the fruitful discussions. The structural analysis is part of the PhD dissertation of JSS funded by the program CAPES-COFECUB n°624/09. Jean-Luc Devidal is acknowledge for the assistance during EMP analysis at the Laboratoire Magmags et Volcans, Université Clermont-Auvergne and David Floess for the X-ray microtomography at the Institute of Earth Sciences, Univeristy of Lausanne. PG is very grateful to Marylène Monnot and Hugo Bourque that contributed to the petrological study of this sample while they were undergraduate students at the University of Franche-Comté. We would like to acknowledge Gregory Dumond and an anonymous reviewer for their constructive and helpful comments that helped improve this manuscript. Bernardo Cesare is acknowledge for his useful suggestions and the editorial handling.

REFERENCES

Ague, J. J. (2017). Element mobility during regional metamorphism in crustal and subduction zone environments with a focus on the rare earth elements (REE). *American Mineralogist*, *102*(9), 1796-1821. https://doi.org/10.2138/am-2017-6130

Alessio, K. L., Hand, M., Morrissey, L. J., Kelsey, D. E., & Payne, J. L. (2017). Melt Reintegration Modelling : Testing against a Subsolidus Reference Assemblage. *Geosciences*, *7*(3), 75. https://doi.org/10.3390/geosciences7030075

Ashworth, J. R., & McLellan, E. L. (1985). Textures. In J. R. Ashworth (Éd.), *Migmatites* (p. 180-203). Springer US. https://doi.org/10.1007/978-1-4613-2347-1_5

Barbosa, J. S. F., & Sabaté, P. (2004). Archean and Paleoproterozoic crust of the São Francisco Craton, Bahia, Brazil: Geodynamic features. *Precambrian Research*, *133*(1), 1-27. https://doi.org/10.1016/j.precamres.2004.03.001

Bartoli, O. (2017). Phase equilibria modelling of residual migmatites and granulites : An evaluation of the melt-reintegration approach. *Journal of Metamorphic Geology*, *35*(8), 919-942. https://doi.org/10.1111/jmg.12261

Beaumont, C., Jamieson, R. A., Nguyen, M. H., & Medvedev, S. (2004). Crustal channel flows: 1. Numerical models with applications to the tectonics of the Himalayan-Tibetan orogen. *Journal of Geophysical Research: Solid Earth*, *109*(B6), B06406. https://doi.org/10.1029/2003JB002809

Brown, M. (2010). Melting of the continental crust during orogenesis : The thermal, rheological, and compositional consequences of melt transport from lower to upper continental crust. *Canadian Journal of Earth Sciences*, *47*(5), 655-694. https://doi.org/10.1139/E09-057

Caddick, M. J., Konopásek, J., & Thompson, A. B. (2010). Preservation of Garnet Growth Zoning and the Duration of Prograde Metamorphism. *Journal of Petrology*, *51*(11), 2327-2347. https://doi.org/10.1093/petrology/egq059

Carlson, W. D. (2006). Rates of Fe, Mg, Mn, and Ca diffusion in garnet. *American Mineralogist*, *91*(1), 1-11. https://doi.org/10.2138/am.2006.2043

Carlson, W. D. (2012). Rates and mechanism of Y, REE, and Cr diffusion in garnet. *American Mineralogist*, *97*(10), 1598-1618. https://doi.org/10.2138/am.2012.4108

Clemens, J. D. (1984). Water contents of silicic to intermediate magmas. *Lithos*, *17*, 273-287. https://doi.org/10.1016/0024-4937(84)90025-2

Connolly, J. A. D. (2005). Computation of phase equilibria by linear programming: A tool for geodynamic modeling and its application to subduction zone decarbonation. *Earth and Planetary Science Letters*, *236*(1–2), 524-541. https://doi.org/10.1016/j.epsl.2005.04.033

Da Silva, L. C., McNaughton, N. J., Melo, R. C., & Fletcher, I. R. (1997). U-Pb SHRIMP ages in the Itabuna-Caraíba TTG high-grade complex: The first window beyond the Paleoproterozoic overprinting of the eastern Jequié craton, NE Brazil. *ResearchGate*, 282.

https://www.researchgate.net/publication/284106273_U-Pb_SHRIMP_ages_in_the_Itabuna-Caraiba_TTG_high-grade_complex_The_first_window_beyond_the_Paleoproterozoic_overprinting_of_the_eastern_Jequie_craton_NE_Brazil

Dumond, G., Goncalves, P., Williams, M. L., & Jercinovic, M. J. (2015). Monazite as a monitor of melting, garnet growth and feldspar recrystallization in continental lower crust. *Journal of Metamorphic Geology*, *33*(7), 735-762. https://doi.org/10.1111/jmg.12150

Dunkley, D. J., Clarke, G. L., & Harley, S. L. (1999). Diffusion metasomatism in silica-undersaturated sapphirine-bearing granulite from Rumdoodle Peak, Framnes Mountains, east Antarctica. *Contributions to Mineralogy and Petrology*, *134*(2), 264-276. https://doi.org/10.1007/s004100050483

Etheridge, M. A., Daczko, N. R., Chapman, T., & Stuart, C. A. (2020). Mechanisms of melt extraction during lower crustal partial melting. *Journal of Metamorphic Geology*, . https://doi.org/10.1111/jmg.12561

Fitzsimons, I. C. W. (1996). Metapelitic Migmatites from Brattstrand Bluffs, East Antarctica—Metamorphism, Melting and Exhumation of the Mid Crust. *Journal of Petrology*, *37*(2), 395-414. https://doi.org/10.1093/petrology/37.2.395

Fujimori, S. (1988). Condições de P-T de formação dos granulitos do Farol da Barra, Salvador, Bahia, Brasil. *Revista Brasileira de Geociências*, *18*(3), 339-344.

Gaidies, F., Morneau, Y. E., Petts, D. C., Jackson, S. E., Zagorevski, A., & Ryan, J. J. (s. d.). Major and trace element mapping of garnet : Unravelling the conditions, timing and rates of metamorphism of the Snowcap assemblage, west-central Yukon. *Journal of Metamorphic Geology*, *n/a*(n/a). https://doi.org/10.1111/jmg.12562

George, F. R., & Gaidies, F. (2017). Characterisation of a garnet population from the Sikkim Himalaya: Insights into the rates and mechanisms of porphyroblast crystallisation. *Contributions to Mineralogy and Petrology*, *172*(7), 57. https://doi.org/10.1007/s00410-017-1372-y

George, F. R., Gaidies, F., & Boucher, B. (2018). Population-wide garnet growth zoning revealed

by LA-ICP-MS mapping : Implications for trace element equilibration and syn-kinematic deformation during crystallisation. *Contributions to Mineralogy and Petrology*, *173*(9), 74. https://doi.org/10.1007/s00410-018-1503-0

Grant, J. A. (1985). Phase equilibria in partial melting of pelitic rocks. In *Migmatites* (p. 86-144). Springer, Boston, MA. https://doi.org/10.1007/978-1-4613-2347-1_3

Guernina, S., & Sawyer, E. W. (2003). Large-scale melt-depletion in granulite terranes : An example from the Archean Ashuanipi Subprovince of Quebec. Journal of Metamorphic Geology, 21(2), 181-201. https://doi.org/10.1046/j.1525-1314.2003.00436.x

Hasalová, P., Schulmann, K., Lexa, O., Štípská, P., Hrouda, F., Ulrich, S., Haloda, J., & Týcová, P. (2008). Origin of migmatites by deformation-enhanced melt infiltration of orthogneiss : A new model based on quantitative microstructural analysis. *Journal of Metamorphic Geology*, *26*(1), 29-53. https://doi.org/10.1111/j.1525-1314.2007.00743.x

Hermann, J., & Rubatto, D. (2003). Relating zircon and monazite domains to garnet growth zones : Age and duration of granulite facies metamorphism in the Val Malenco lower crust. *Journal of Metamorphic Geology*, *21*(9), 833-852. https://doi.org/10.1046/j.1525-1314.2003.00484.x

Holland, T. J. B., & Powell, R. (1998). An internally consistent thermodynamic data set for phases of petrological interest. *Journal of Metamorphic Geology*, *16*(3), 309-343. https://doi.org/10.1111/j.1525-1314.1998.00140.x

Holland, T., & Powell, R. (2001). Calculation of Phase Relations Involving Haplogranitic Melts Using an Internally Consistent Thermodynamic Dataset. *Journal of Petrology*, *42*(4), 673-683. https://doi.org/10.1093/petrology/42.4.673

Hollister, L. S., & Crawford, M. L. (1986). Melt-enhanced deformation : A major tectonic process. *Geology*, *14*(7), 558-561. https://doi.org/10.1130/0091-7613(1986)14<558:MDAMTP>2.0.CO;2

Holness, M. B., & Sawyer, E. W. (2008). On the Pseudomorphing of Melt-filled Pores During the Crystallization of Migmatites. *Journal of Petrology*, *49*(7), 1343-1363. https://doi.org/10.1093/petrology/egn028

Hurai, V., Paquette, J.-L., Huraiová, M., & Konečný, P. (2010). U–Th–Pb geochronology of zircon and monazite from syenite and pincinite xenoliths in Pliocene alkali basalts of the intra-Carpathian back-arc basin. *Journal of Volcanology and Geothermal Research*, *198*(3), 275-287. https://doi.org/10.1016/j.jvolgeores.2010.09.012

Hyppolito, T., Cambeses, A., Angiboust, S., Raimondo, T., García-Casco, A., & Juliani, C. (2019). Rehydration of eclogites and garnet-replacement processes during exhumation in the amphibolite facies. *Geological Society, London, Special Publications*, *478*(1), 217-239. https://doi.org/10.1144/SP478.3

Jamieson, R. A., Unsworth, M. J., Harris, N. B. W., Rosenberg, C. L., & Schulmann, K. (2011). Crustal Melting and the Flow of Mountains. *Elements*, *7*(4), 253-260. https://doi.org/10.2113/gselements.7.4.253

Konrad-Schmolke, M., O'Brien, P. J., de Capitani, C., & Carswell, D. A. (2008). Garnet growth at high- and ultra-high pressure conditions and the effect of element fractionation on mineral modes and composition. *Lithos*, *103*(3), 309-332. https://doi.org/10.1016/j.lithos.2007.10.007

Konrad-Schmolke, M., Zack, T., O'Brien, P. J., & Jacob, D. E. (2008). Combined thermodynamic and rare earth element modelling of garnet growth during subduction : Examples from ultrahigh-pressure eclogite of the Western Gneiss Region, Norway. *Earth and Planetary Science Letters*, *272*(1-2), 488-498. https://doi.org/10.1016/j.epsl.2008.05.018

Kriegsman, L. M., & Hensen, B. J. (1998). Back reaction between restite and melt : Implications for geothermobarometry and pressure-temperature paths. *Geology*, *26*(12), 1111-1114. https://doi.org/10.1130/0091-7613(1998)026<1111:BRBRAM>2.3.CO;2

Le Breton, N. (1988). Fluid-absent (dehydration) melting of biotite in metapelites in the early stages of crustal anatexis. *Contributions to Mineralogy and Petrology*, *99*(2), 226-237. https://doi.org/10.1007/BF00371463

Lin, L., & Sawyer, E. W. (2019). Microstructure and compositional changes across biotite-rich reaction selvedges around mafic schollen in a semipelitic diatexite migmatite. *Journal of Metamorphic Geology*, *37*(4), 539-566. https://doi.org/10.1111/jmg.12475

Mahan, K. H., Goncalves, P., Williams, M. L., & Jercinovic, M. J. (2006). Dating metamorphic reactions and fluid flow : Application to exhumation of high-P granulites in a crustal-scale shear zone, western Canadian Shield. *Journal of Metamorphic Geology*, *24*(3), 193-217. https://doi.org/10.1111/j.1525-1314.2006.00633.x

Migdisov, Art. A., Williams-Jones, A. E., & Wagner, T. (2009). An experimental study of the solubility and speciation of the Rare Earth Elements (III) in fluoride- and chloride-bearing aqueous solutions at temperatures up to 300°C. *Geochimica et Cosmochimica Acta*, *73*(23), 7087-7109. https://doi.org/10.1016/j.gca.2009.08.023

Moore, S. J., Carlson, W. D., & Hesse, M. A. (2013). Origins of yttrium and rare earth element distributions in metamorphic garnet. *Journal of Metamorphic Geology*, *31*(6), 663-689. https://doi.org/10.1111/jmg.12039

Olsen, S. N., & Grant, J. A. (1991). Isocon analysis of migmatization in the Front Range, Colorado, USA. *Journal of Metamorphic Geology*, *9*(2), 151-164. https://doi.org/10.1111/j.1525-1314.1991.tb00511.x

Otamendi, J. E., Rosa, J. D. de la, Douce, A. E. P., & Castro, A. (2002). Rayleigh fractionation of heavy rare earths and yttrium during metamorphic garnet growth. *Geology*, *30*(2), 159-162. https://doi.org/10.1130/0091-7613(2002)030<0159:RFOHRE>2.0.CO;2

Owen, J. V. (1991). Cordierite + spinel parageneses in pelitic gneiss from the contact aureoles of the Mistastin batholith (Quebec) and the Taylor Brook gabbro complex (Newfoundland). *Canadian Journal of Earth Sciences*, *28*(3), 372-381. https://doi.org/10.1139/e91-034

Paquette, J.-L., Piro, J.-L., Devidal, J.-L., Bosse, V., Didier, A., Sannac, S., & Abdelnour, Y. (2014). Sensitivity Enhancement in LA-ICP-MS by N2 Addition to Carrier Gas : Application to Radiometric Dating of U-Th-Bearing Minerals. *Agilent ICP-MS Journal*, *58*, 4-5.

Penniston-Dorland, S. C., & Ferry, J. M. (2008). Element mobility and scale of mass transport in the formation of quartz veins during regional metamorphism of the Waits River Formation, east-central Vermont. *American Mineralogist*, *93*(1), 7-21. https://doi.org/10.2138/am.2008.2461

Piazolo, S., Daczko, N. R., Silva, D., & Raimondo, T. (2020). Melt-present shear zones enable

intracontinental orogenesis. *Geology*, *48*. https://doi.org/10.1130/G47126.1

Prent, A. M., Beinlich, A., Morrissey, L. J., Raimondo, T., Clark, C., & Putnis, A. (2019). Monazite as a monitor for melt-rock interaction during cooling and exhumation. *Journal of Metamorphic Geology*, *37*(3), 415-438. https://doi.org/10.1111/jmg.12471

Pyle, J. M., & Spear, F. S. (2003). Yttrium zoning in garnet : Coupling of major and accessory phases during metamorphic reactions. *American Mineralogist*, *88*(4), 708-708.

Pyle, J., & Spear, F. (2003). Four generations of accessory-phase growth in low-pressure migmatites from SW New Hampshire. *American Mineralogist*, *88*, 338-351. https://doi.org/10.2138/am-2003-2-311

Rabin, M., Trap, P., Carry, N., Fréville, K., Cenki-Tok, B., Lobjoie, C., Goncalves, P., & Marquer, D. (2015). Strain partitioning along the anatectic front in the Variscan Montagne Noire massif (southern French Massif Central). *Tectonics*, *34*(8), 1709-1735. https://doi.org/10.1002/2014TC003790

Raimondo, T., Payne, J., Wade, B., Lanari, P., Clark, C., & Hand, M. (2017). Trace element mapping by LA-ICP-MS : Assessing geochemical mobility in garnet. *Contributions to Mineralogy and Petrology*, *172*(4), 17. https://doi.org/10.1007/s00410-017-1339-z

Rosenberg, C. L., & Handy, M. R. (2005). Experimental deformation of partially melted granite revisited : Implications for the continental crust. *Journal of Metamorphic Geology*, *23*(1), 19-28. https://doi.org/10.1111/j.1525-1314.2005.00555.x

Rubatto, D., Burger, M., Lanari, P., Hattendorf, B., Schwarz, G., Neff, C., Keresztes Schmidt, P., Hermann, J., Vho, A., & Günther, D. (2020). Identification of growth mechanisms in metamorphic garnet by high-resolution trace element mapping with LA-ICP-TOFMS. *Contributions to Mineralogy and Petrology*, *175*(7), 61. https://doi.org/10.1007/s00410-020-01700-5

Royden, L. H., Burchfiel, B. C., King, R. W., Wang, E., Chen, Z., Shen, F., & Liu, Y. (1997). Surface Deformation and Lower Crustal Flow in Eastern Tibet. *Science*, *276*(5313), 788-790. https://doi.org/10.1126/science.276.5313.788

Sawyer, E. W. (2001). Melt segregation in the continental crust : Distribution and movement of

melt in anatectic rocks. *Journal of Metamorphic Geology*, *19*(3), 291-309. https://doi.org/10.1046/j.0263-4929.2000.00312.x

Skora, S., Baumgartner, L. P., Mahlen, N. J., Johnson, C. M., Pilet, S., & Hellebrand, E. (2006). Diffusion-limited REE uptake by eclogite garnets and its consequences for Lu–Hf and Sm–Nd geochronology. *Contributions to Mineralogy and Petrology*, *152*(6), 703-720. https://doi.org/10.1007/s00410-006-0128-x

Souza, J. S. de, Barbosa, J. S. F., & Gomes, L. C. C. (2010). Litogeoquímica dos granulitos ortoderivados da cidade de Salvador, Bahia. *Revista Brasileira de Geociências*, *40*(3), 339-354.

Souza-Oliveira, J. S. de, Peucat, J.-J., Barbosa, J. S. F., Correa-Gomes, L. C., Cruz, S. C. P., Leal, Â. B. M., & Paquette, J.-L. (2014). Lithogeochemistry and geochronology of the subalkaline felsic plutonism that marks the end of the Paleoproterozoic orogeny in the Salvador-Esplanada belt, São Francisco craton (Salvador, state of Bahia, Brazil). *Brazilian Journal of Geology*, *44*(2), 221-234. https://doi.org/10.5327/Z2317-4889201400020004

Spear, F. S., Kohn, M. J., & Cheney, J. T. (1999). <Emphasis Type="Italic">P </Emphasis>-<Emphasis Type="Italic">T</Emphasis> paths from anatectic pelites. *Contributions to Mineralogy and Petrology*, *134*(1), 17-32. https://doi.org/10.1007/s004100050466

Stuart, C. A., Piazolo, S., & Daczko, N. R. (2018). The recognition of former melt flux through high-strain zones. *Journal of Metamorphic Geology*, *36*(8), 1049-1069. https://doi.org/10.1111/jmg.12427

Thompson, A. B. (1982). Dehydration melting of pelitic rocks and the generation of H2O-undersaturated granitic liquids. *American Journal of Science*, *282*(10), 1567-1595. https://doi.org/10.2475/ajs.282.10.1567

Tomkins, H. S., & Pattison, D. R. M. (2007). Accessory phase petrogenesis in relation to major phase assemblages in pelites from the Nelson contact aureole, southern British Columbia. *Journal of Metamorphic Geology*, *25*(4), 401-421. https://doi.org/10.1111/j.1525-1314.2007.00702.x

Ubide, T., McKenna, C. A., Chew, D. M., & Kamber, B. S. (2015). High-resolution LA-ICP-MS trace

element mapping of igneous minerals : In search of magma histories. *Chemical Geology*, *409*, 157-168. https://doi.org/10.1016/j.chemgeo.2015.05.020

Vanderhaeghe, O. (2012). The thermal–mechanical evolution of crustal orogenic belts at convergent plate boundaries : A reappraisal of the orogenic cycle. *Journal of Geodynamics*, *56-57*, 124-145. https://doi.org/10.1016/j.jog.2011.10.004

Vernon, R. H. (2011). Microstructures of melt-bearing regional metamorphic rocks. In D. D. van Reenen, J. D. Kramers, S. McCourt, & L. L. Perchuk, *Origin and Evolution of Precambrian High-Grade Gneiss Terranes, with Special Emphasis on the Limpopo Complex of Southern Africa*. Geological Society of America. https://doi.org/10.1130/2011.1207(01)

Vielzeuf, D., & Schmidt, M. (2001). Melting relations in hydrous systems revisited : Application to metapelites, metagreywackes and metabasalts. *Contributions to Mineralogy and Petrology*, *141*, 251-267. https://doi.org/10.1007/s004100100237

Vielzeuf, Daniel, & Holloway, J. R. (1988). Experimental determination of the fluid-absent melting relations in the pelitic system. *Contributions to Mineralogy and Petrology*, *98*(3), 257-276. https://doi.org/10.1007/BF00375178

Vielzeuf, Daniel, & Montel, J. M. (1994). Partial melting of metagreywackes. Part I. Fluid-absent experiments and phase relationships. *Contributions to Mineralogy and Petrology*, *117*(4), 375-393. https://doi.org/10.1007/BF00307272

Warren, C. J., Greenwood, L. V., Argles, T. W., Roberts, N. M. W., Parrish, R. R., & Harris, N. B. W. (2019). Garnet–monazite rare earth element relationships in sub-solidus metapelites : A case study from Bhutan. *Geological Society, London, Special Publications*, *478*(1), 145-166. https://doi.org/10.1144/SP478.1

Weller, O. M., Jackson, S., Miller, W. G. R., St-Onge, M. R., & Rayner, N. (2020). Quantitative elemental mapping of granulite-facies monazite : Textural insights and implications for petrochronology. *Journal of Metamorphic Geology*, *38*(8), 853-880. https://doi.org/10.1111/jmg.12552

White, R. W., & Powell, R. (2010). Retrograde melt–residue interaction and the formation of near-anhydrous leucosomes in migmatites. *Journal of Metamorphic Geology*, *28*(6),

579-597. https://doi.org/10.1111/j.1525-1314.2010.00881.x

White, R. W., Powell, R., & Holland, T. J. B. (2001). Calculation of partial melting equilibria in the system Na2O–CaO–K2O–FeO–MgO–Al2O3–SiO2–H2O (NCKFMASH). *Journal of Metamorphic Geology*, *19*(2), 139-153. https://doi.org/10.1046/j.0263-4929.2000.00303.x

Williams-Jones, A. E., Migdisov, A. A., & Samson, I. M. (2012). Hydrothermal Mobilisation of the Rare Earth Elements – a Tale of "Ceria" and "Yttria". *Elements*, *8*(5), 355-360. https://doi.org/10.2113/gselements.8.5.355

Yakymchuk, C., & Brown, M. (2014). Consequences of open-system melting in tectonics. Journal of the Geological Society, 171(1), 21-40. https://doi.org/10.1144/jgs2013-039

Yuguchi, T., & Nishiyama, T. (2008). The mechanism of myrmekite formation deduced from steady-diffusion modeling based on petrography : Case study of the Okueyama granitic body, Kyushu, Japan. *Lithos*, *106*(3), 237-260. https://doi.org/10.1016/j.lithos.2008.07.017

937

938

939 **FIGURE CAPTIONS**

940

941

942 Figure 1. (a) Aerial photograph of the Farol da Barra outcrop in the city of Salvador da Bahia,
943 with a corresponding structural and geological map (right-hand side). (b) Simplified structural
944 cross section including the studied area, showing the finite strain pattern consisting of a gently
945 dipping S1 fabric and steeply dipping D2 high strain zones. On both figures, the location of the
946 studied sample 06SB06 is shown as a red star.

947

948 Figure 2. (a) Photograph of the studied outcrop showing the steeply dipping S2 gneissic foliation.
949 The leucosome is surrounded by a melanocratic quartz-undersaturated selvage. (b) Polished slice

950 of the studied sample 06SB06 showing the location of the three thin sections.

951

952 Figure 3. (a) Photomicrograph of the metamorphic assemblage in the quartz-saturated granulite.
953 (b) Cordierite development at the contact between garnet and sillimanite in the quartz-
954 saturated granulite. (c) Spinel and cordierite symplectite developed at the expense of garnet
955 and sillimanite in the quartz-undersaturated selvage.

956

957 Figure 4. Thin-section scans under crossed-polarized light showing the location of the seven
958 analyzed garnets (A to G). Garnets A and B are located in the quartz-undersaturated selvage.
959 Notice the change in grain size and proportion of inclusions with increasing distance from the
960 leucosome.

961

962 Figure 5. Photomicrographs of the seven analyzed garnets. (a) Garnet A; (b) Garnet B; (c) Garnet
963 C; (d) Garnet D; (e) Garnet E; (f) Garnet F; (g) Garnet G. The size of the scale bar shown is 50
964 μm for all cases, and dashed lines correspond to the location of major element profiles shown in
965 Figure 9.

966

967 Figure 6. Backscattered electron images of crystallized melt inclusions in the outer rim of Garnet
968 B located in the quartz-undersaturated selvage. (a), garnet negative crystal shape crystallized
969 melt inclusion; (b) polyphase xenomorph crystallized melt inclusion; and (c) radial crack
970 attesting to melt inclusion decrepitation

971

972 Figure 7. (a) Backscattered electron image of a representative garnet in the quartz-saturated
973 granulite. (b) 3D reconstruction from a computed X-ray microtomography of garnet. (c-f)
974 sequential slices of the 3D reconstructed garnet (in red) showing the channels (white arrows)

975 connecting the irregular inclusions (transparent) to the outside matrix.

976

977 Figure 8. (a) Cathodoluminescence images of K-feldspar texture (blue) with plagioclase films and
978 pool (brown) along grain boundaries. Plagioclase films are connected to myrmekite pools (m).
979 (b) Extensive replacement of K-feldspar by plagioclase and myrmekites.

980

981 Figure 9. Garnet composition (black square = molar amount of grossular and white square =
982 XMg). The location of each line profile is shown in figure 5. The dark and light gray stripes
983 correspond to plagioclase-quartz inclusions and domains with minute inclusions of quartz,
984 respectively.

985

986 Figure 10. LA-ICP-MS trace element maps of (a) garnet A; (b) Garnet B; (c) Garnet G.
987 Concentrations values are in ppm. The line profiles shown in Figure 11-13 are located in each
988 case on the Phosphorus (P) map.

989

990 Figure 11. LA-ICP-MS trace element line profile of Garnet A. . See Figure 10a for traverse
991 location.

992

993 Figure 12. LA-ICP-MS trace element line profile of Garnet B. See Figure 10b for traverse
994 location.

995

996 Figure 13. LA-ICP-MS trace element line profile of Garnet G. See Figure 10c for traverse
997 location.

998

Figure 14. P-T phase diagram section computed for with quartz-saturated granulite composition (see Table 1). Circles with letters indicate the P-T conditions corresponding to measured garnet compositions. The letters refer to garnet grain labels in Figure 5.

Figure 15. Evolution of chemical potential of H_2O, SiO_2, CaO and K_2O for the quartz-saturated domain (black line) and melt (dashed line) along a decompression path from 0.8 to 0.5 GPa at 790°C.

Figure 16. P-X phase diagram section computed at 790°C with X=0 corresponding to the quartz-saturated domain and X=1 corresponding to a 55% loss of SiO_2 and 200% gain of H_2O. See Table 1 for compositions.

Figure 17. P-T phase diagram section computed with a modeled quartz-undersaturated selvage composition produced after a 47% loss of SiO_2 and 140% gain of H_2O. See Table 1 for compositions.

Figure 18. (a) Full thin-section X-ray Al map of sample 06SB06a showing the petrographic setting of dated monazites. (b) Y map of monazite included in garnet and plagioclase. (c) Y map of monazite in the cordierite-bearing matrix. Note the presence of thin Y-rich overgrowths.

Figure 19. (a) Monazite U-Th-Pb concordia diagram. (b) Monazite Th-Pb ages. (c) Zircon U-Pb concordia diagram

TABLE CAPTIONS

1023 Table 1. Bulk geochemical compositions used in phase diagrams shown in figures 14-17

1024

1025 **DATASETS AND SUPPORTING INFORMATION**

1026 Figure S1. Simplified geological map of the São Francisco Craton modified after Barbosa et al.
1027 (2003).

1028

1029 Figure S2. (a) Simplified structural map of the southwestern part of the city of Salvador da
1030 Bahia. (b) Simplified structural cross-section. (c) Equal-area Schmidt lower hemisphere
1031 projection of poles to S_1 and S_2 foliations (dashed lines = conjugated shear zones associated the
1032 S_2 mylonitic foliation).

1033

1034

1035

1036 Figure S3. (a) Backscattered image of a polyphased plagioclase and quartz inclusion in a garnet.
1037 (b) anorthite vs albite content in mole of plagioclase. Grey and black diamonds are plagioclase
1038 composition in contact with quartz and garnet respectively. (c) Profile showing the evolution of
1039 plagioclase composition in contact with quartz and garnet. See location of the profile in figure a.

1040

1041 Figure S4. LA-ICP-MS Zr line profile of garnet A, B and G

1042

1043

1044

1045

1046 Movie S1. 3D reconstruction from computed X-ray microtomography of garnet (see Figure 7).

1047

1048 Table S1. Solid solution models used in Figures 14-17

1049

1050 Dataset S1. Electron microprobe analysis of biotite, plagioclase, spinel and garnet. Garnet
1051 compositions include the seven profiles collected from Garnets A-G in Figure 9 (see Figure 5 for
1052 the line profile locations).

1053

1054 Dataset S2. LA-ICP-MS trace element data of line profiles collected from Garnets A, B and G (see
1055 Figures 11-13).

1056

1057 Dataset S3. Raw LA-ICPMS trace element data of garnet A (see map in Figure 10a)

1058

1059 Dataset S4. Raw LA-ICPMS trace element data of garnet B (see map in Figure 10b)

1060

1061 Dataset S5. Raw LA-ICPMS trace element data of garnet A (see map in Figure 10c)

1062

1063 Dataset S6. LA-ICP-MS isotopic U-Th-Pb data of monazite and zircon

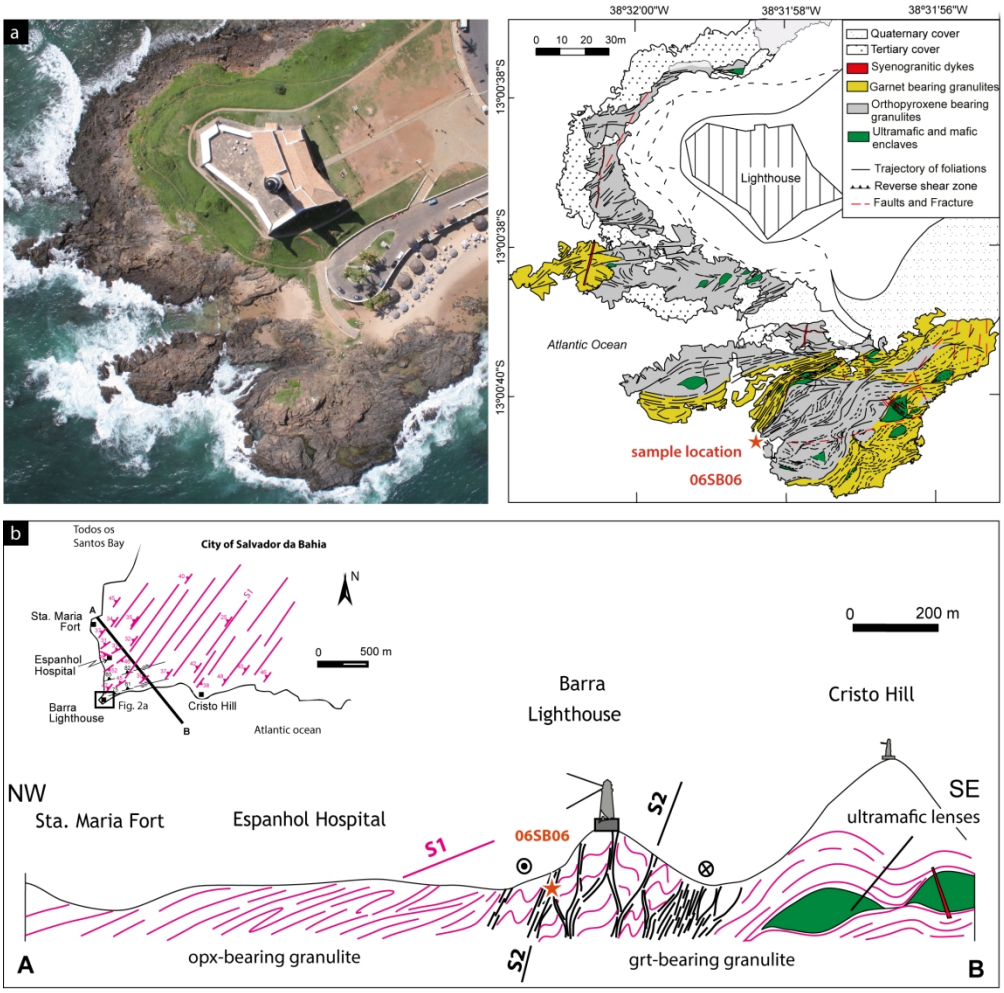

Figure 1

igure 1. (a) Aerial photograph of the Farol da Barra outcrop in the city of Salvador da Bahia, with a corresponding structural and geological map (right-hand side). (b) Simplified structural cross section including the studied area

180x188mm (300 x 300 DPI)

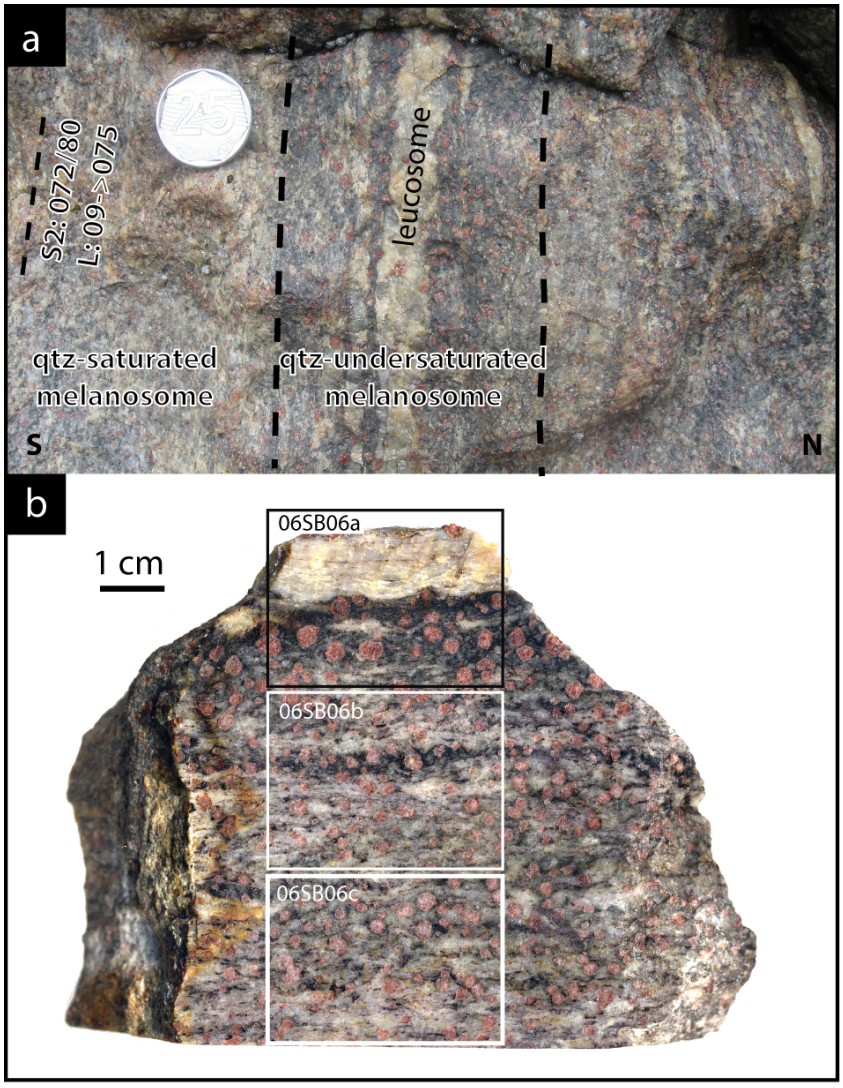

figure 2

Figure 2. (a) Photograph of the studied outcrop showing the steeply dipping S2 gneissic foliation. The leucosome is surrounded by a melanocratic quartz-undersaturated selvage. (b) Polished slice of the studied sample 06SB06 showing the location of the three thin sections.

80x115mm (300 x 300 DPI)

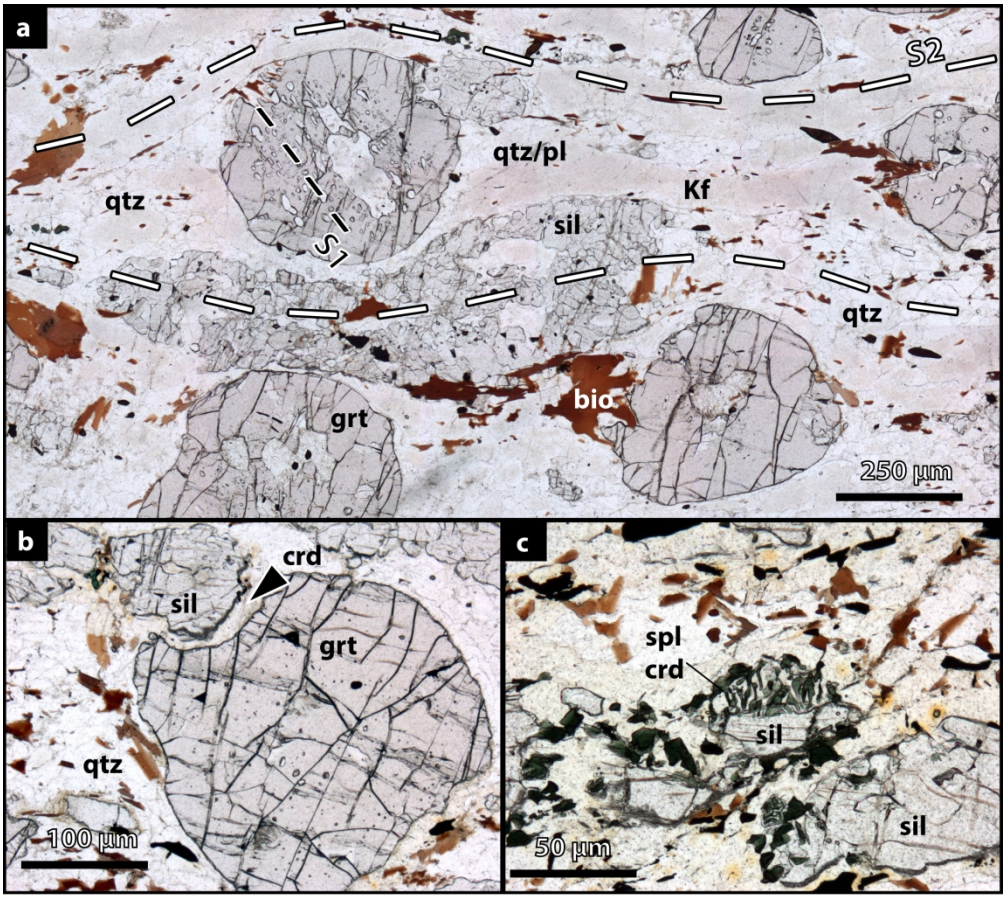

Figure 3

Figure 3. (a) Photomicrograph of the metamorphic assemblage in the quartz-saturated granulite. (b) Cordierite development at the contact between garnet and sillimanite in the quartz-saturated granulite. (c) Spinel and cordierite symplectite developed at the expense of garnet and sillimanite in the quartz-undersaturated selvage.

180x173mm (300 x 300 DPI)

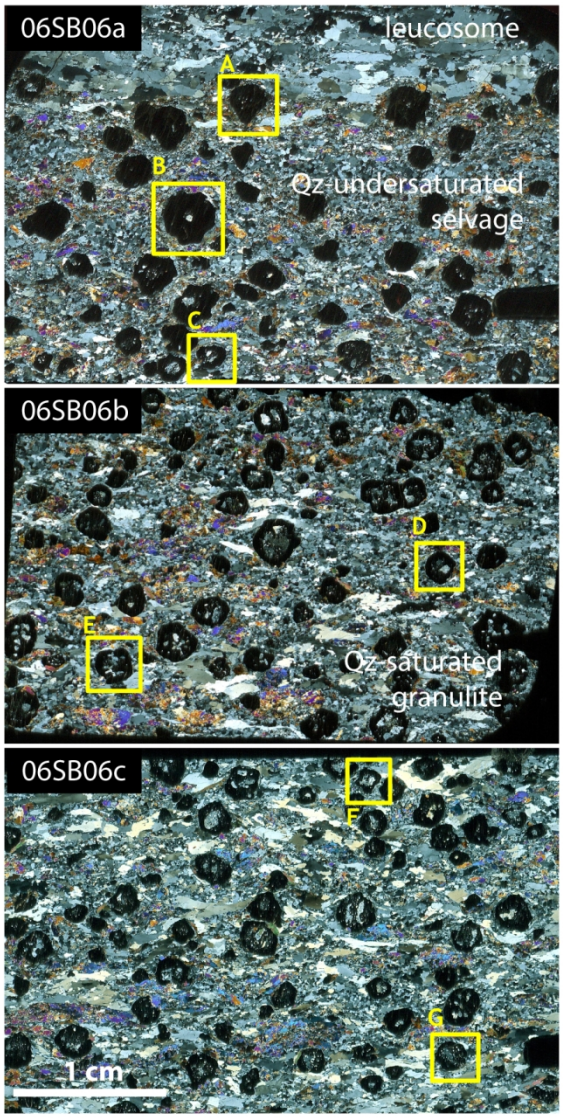

Figure 4

Figure 4. Thin-section scans under crossed-polarized light showing the location of the seven analyzed garnets (A to G).

85x160mm (300 x 300 DPI)

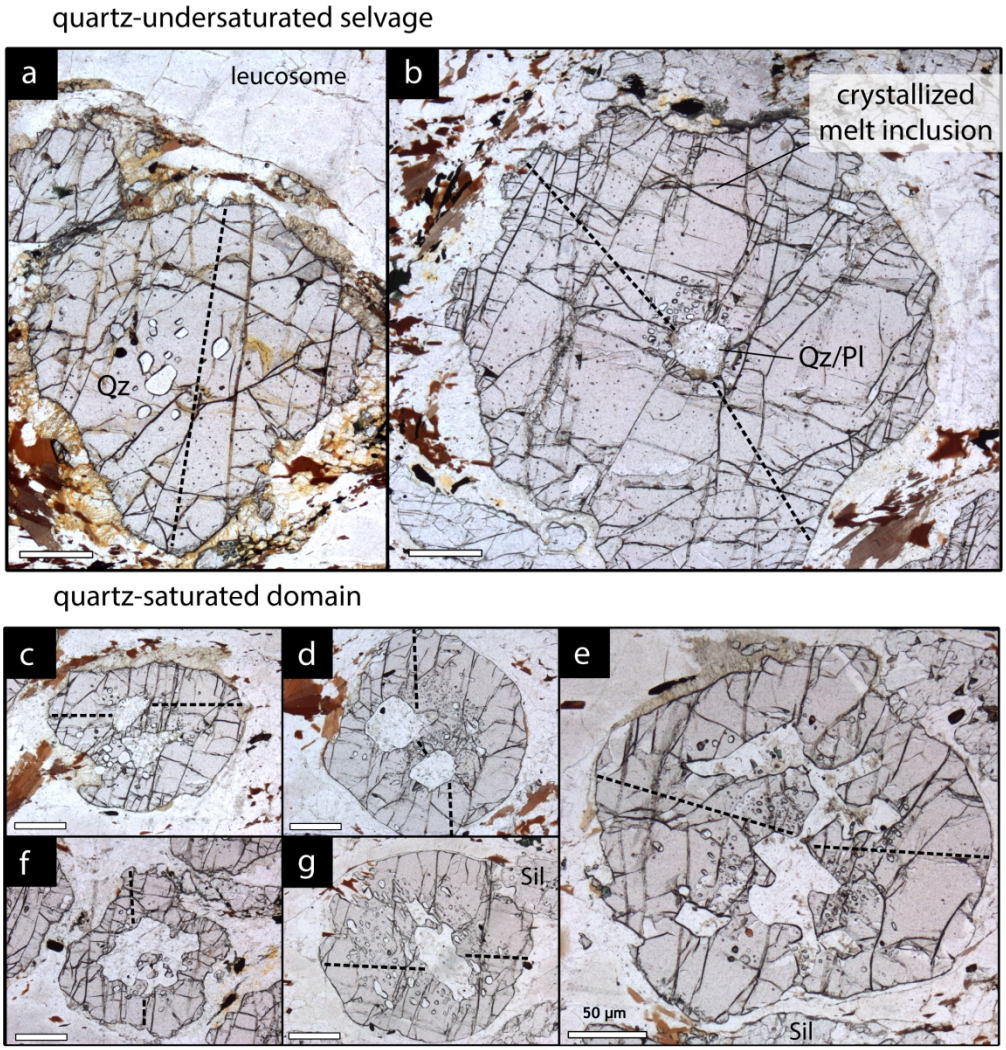

Figure 5

Figure 5. Photomicrographs of the seven analyzed garnets. (a) Garnet A; (b) Garnet B; (c) Garnet C; (d) Garnet D; (e) Garnet E; (f) Garnet F; (g) Garnet G. The size of the scale bar shown is 50 µm for all cases, and dashed lines correspond to the location of major element profiles shown in Figure 9.

180x206mm (300 x 300 DPI)

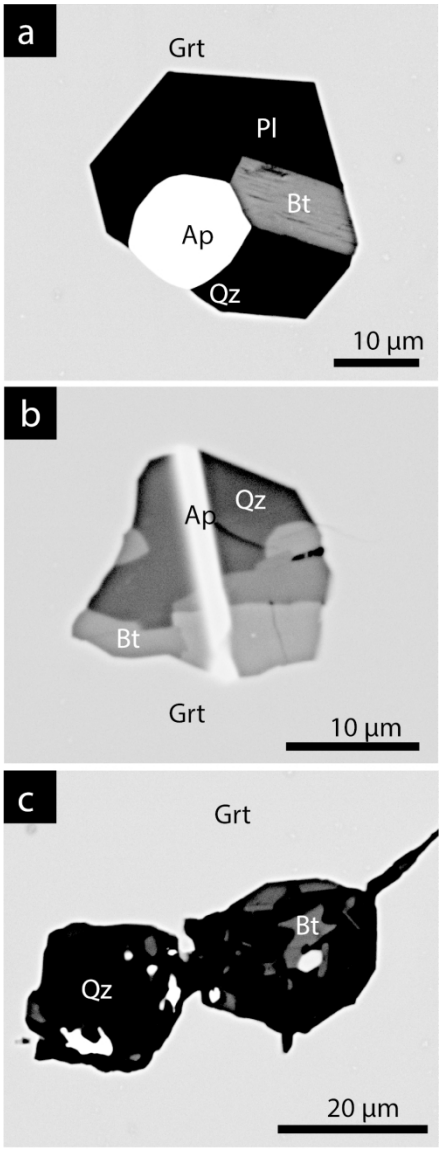

Figure 6

Figure 6. Backscattered electron images of crystallized melt inclusions in the outer rim of Garnet B located in the quartz-undersaturated selvage. (a), garnet negative crystal shape crystallized melt inclusion; (b) polyphase xenomorph crystallized melt inclusion; and (c) radial crack attesting to melt inclusion decrepitation

80x220mm (300 x 300 DPI)

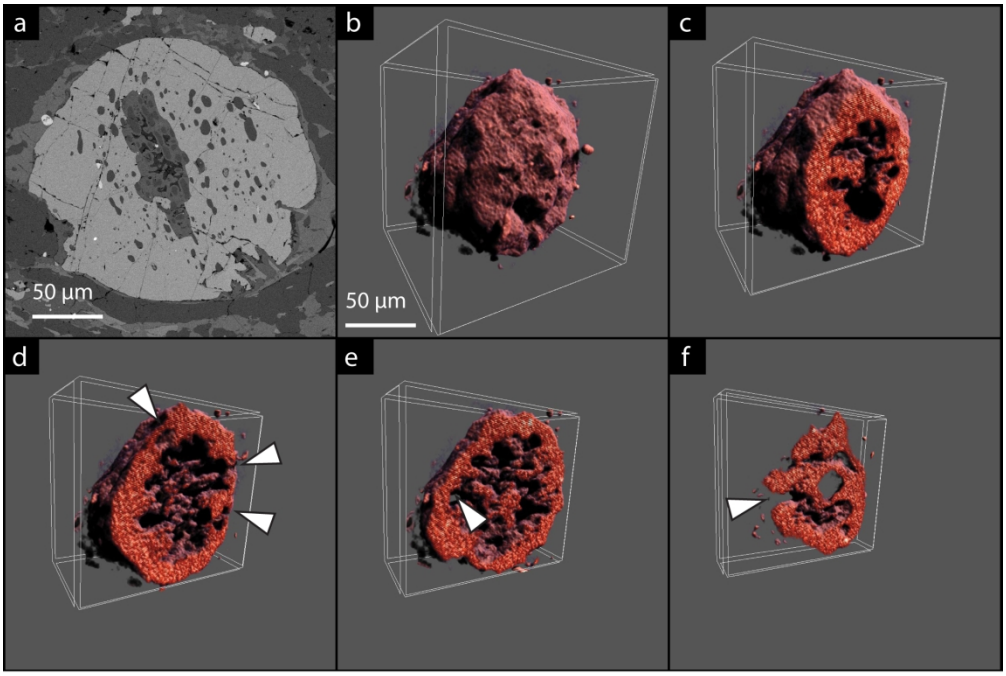

Figure 7

Figure 7. (a) Backscattered electron image of a representative garnet in the quartz-saturated granulite. (b) 3D reconstruction from a computed X-ray microtomography of garnet. (c-f) sequential slices of the 3D reconstructed garnet (in red) showing the channels (white arrows) connecting the irregular inclusions (transparent) to the outside matrix.

180x140mm (300 x 300 DPI)

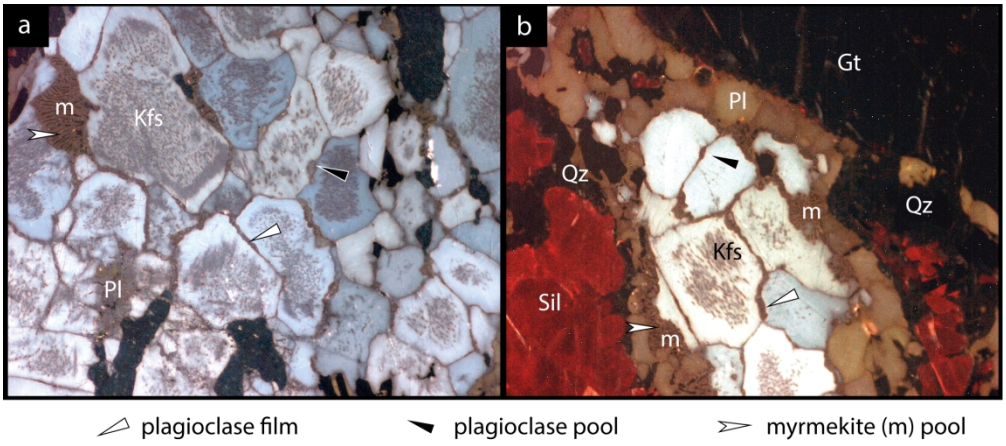

Figure 8

Figure 8. (a) Cathodoluminescence images of K-feldspar texture (blue) with plagioclase films and pool (brown) along grain boundaries. Plagioclase films are connected to myrmékite pools (m). (b) Extensive replacement of K-feldspar by plagioclase and myrmekites.

180x92mm (300 x 300 DPI)

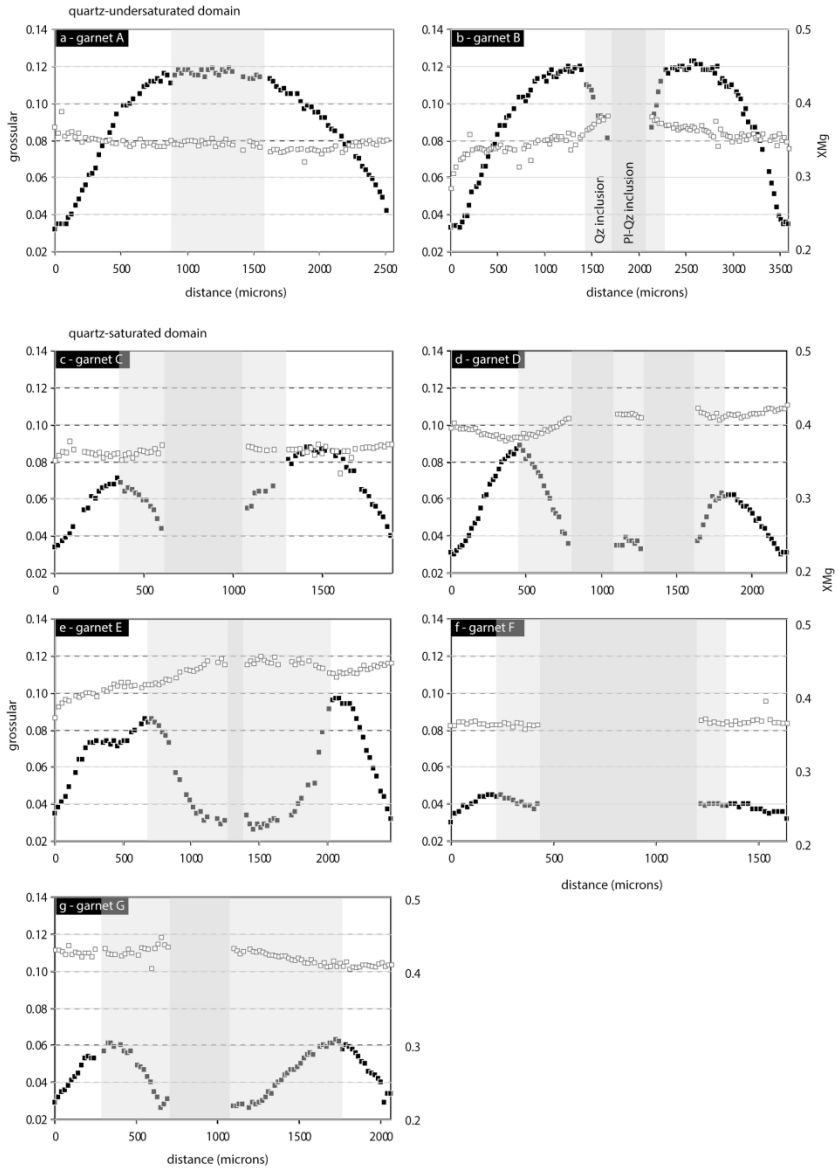

Figure 9

Figure 9. Garnet composition (black square = molar amount of grossular and white square = XMg). The location of each line profile is shown in figure 5. The dark and light gray stripes correspond to plagioclase-quartz inclusions and domains with minute inclusions of quartz, respectively.

180x260mm (300 x 300 DPI)

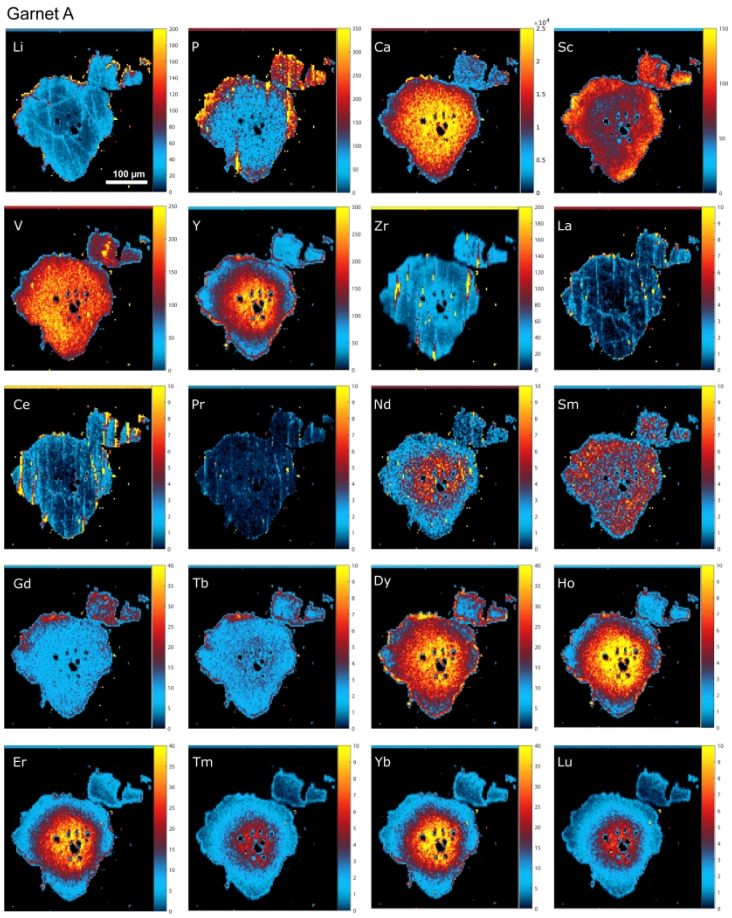

figure 10a

Figure 10. LA-ICP-MS trace element maps of (a) garnet A; (b) Garnet B; (c) Garnet G. Concentrations values are in ppm. The line profiles shown in Figure 11-13 are located in each case on the Phosphorus (P) map.

210x297mm (300 x 300 DPI)

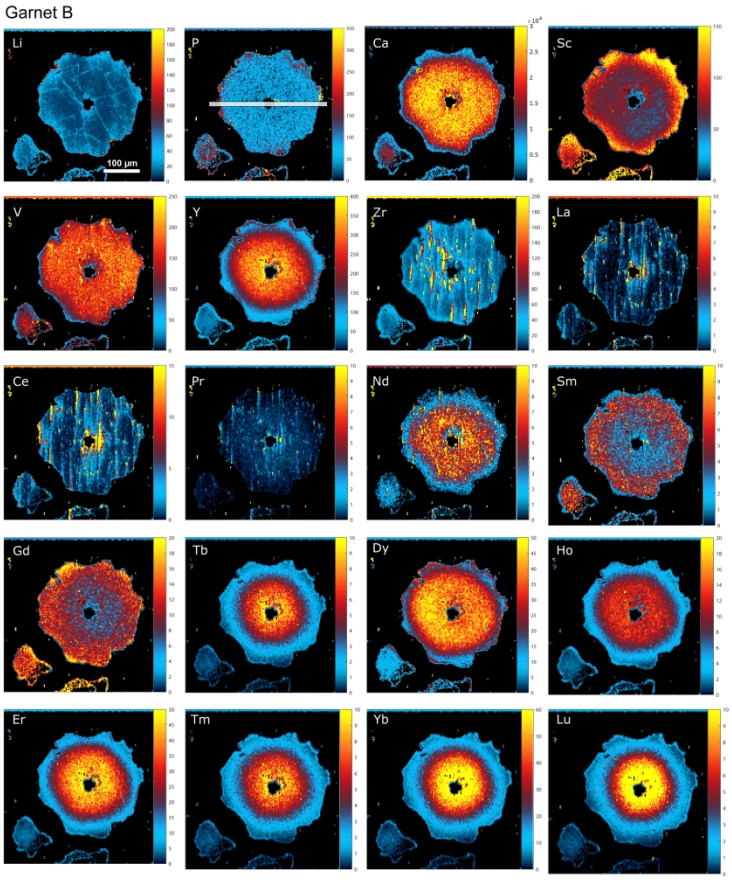

Figure 10b

Figure 10. LA-ICP-MS trace element maps of (a) garnet A; (b) Garnet B; (c) Garnet G. Concentrations values are in ppm. The line profiles shown in Figure 11-13 are located in each case on the Phosphorus (P) map.

210x297mm (300 x 300 DPI)

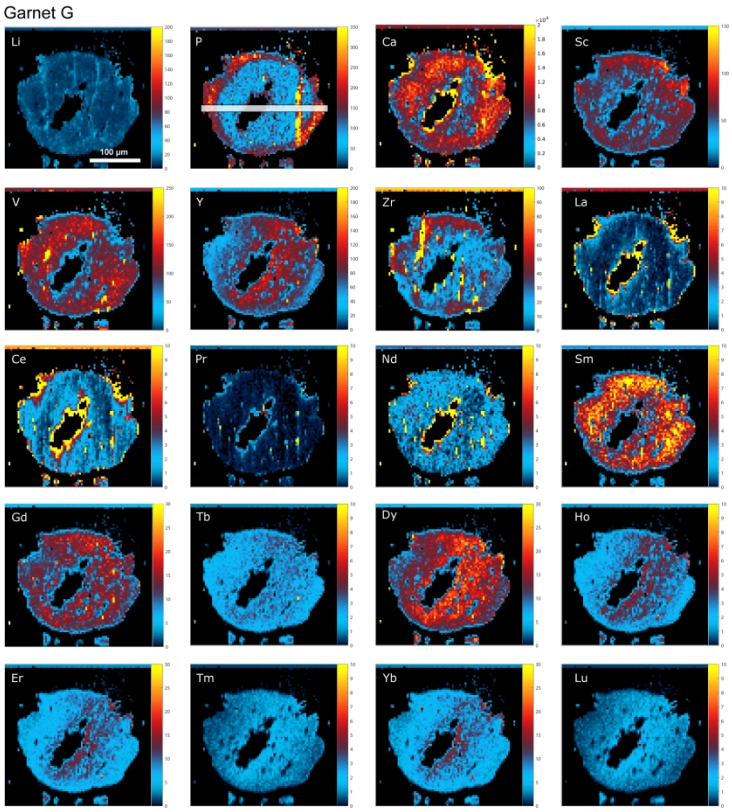

Figure 10c

Figure 10. LA-ICP-MS trace element maps of (a) garnet A; (b) Garnet B; (c) Garnet G. Concentrations values are in ppm. The line profiles shown in Figure 11-13 are located in each case on the Phosphorus (P) map.

210x297mm (300 x 300 DPI)

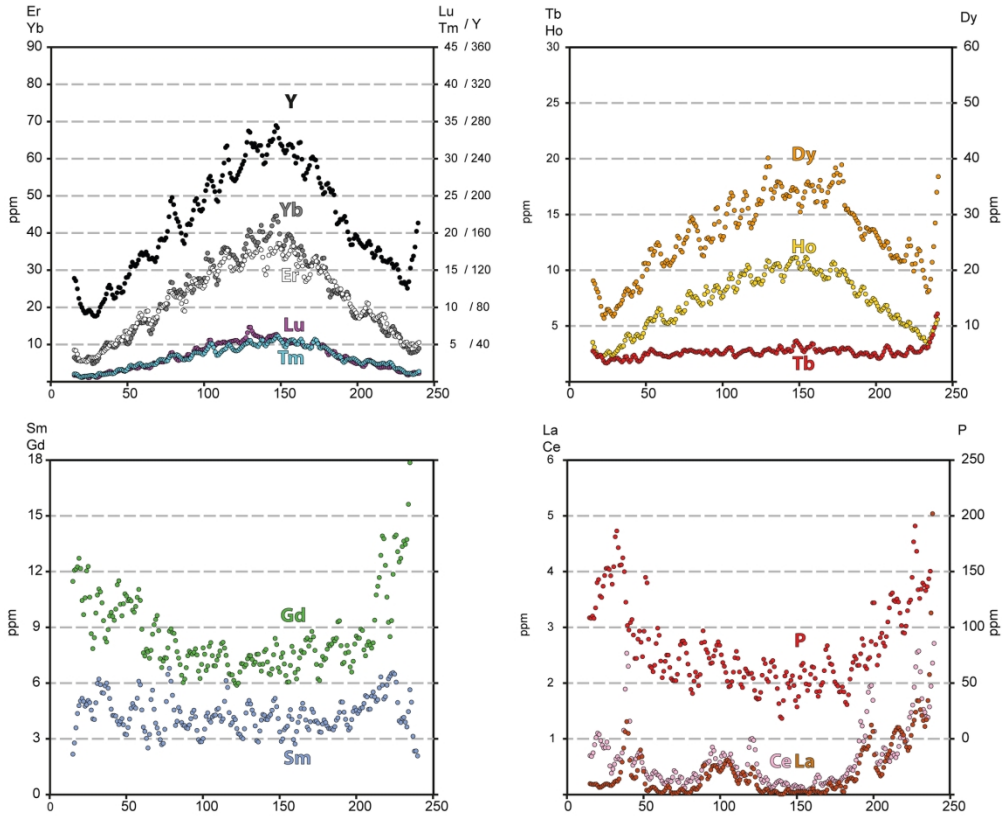

Figure 11

Figure 11. LA-ICP-MS trace element line profile of Garnet A. . See Figure 10a for traverse location.

176x158mm (300 x 300 DPI)

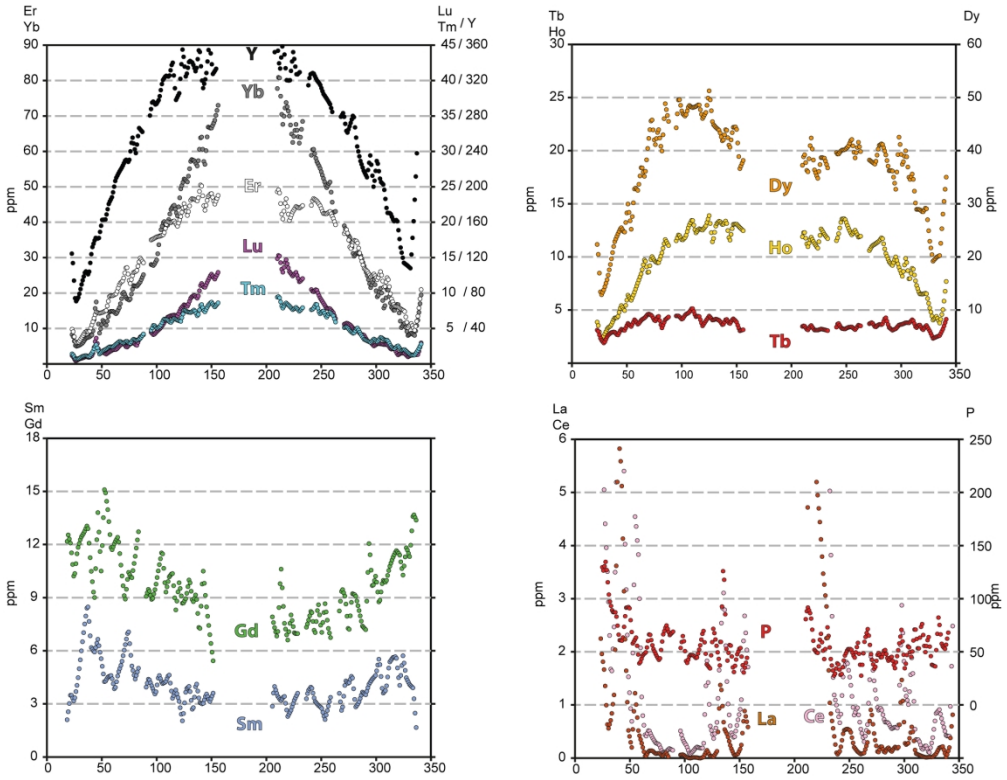

Figure 12

Figure 12. LA-ICP-MS trace element line profile of Garnet B. See Figure 10b for traverse location.

185x165mm (300 x 300 DPI)

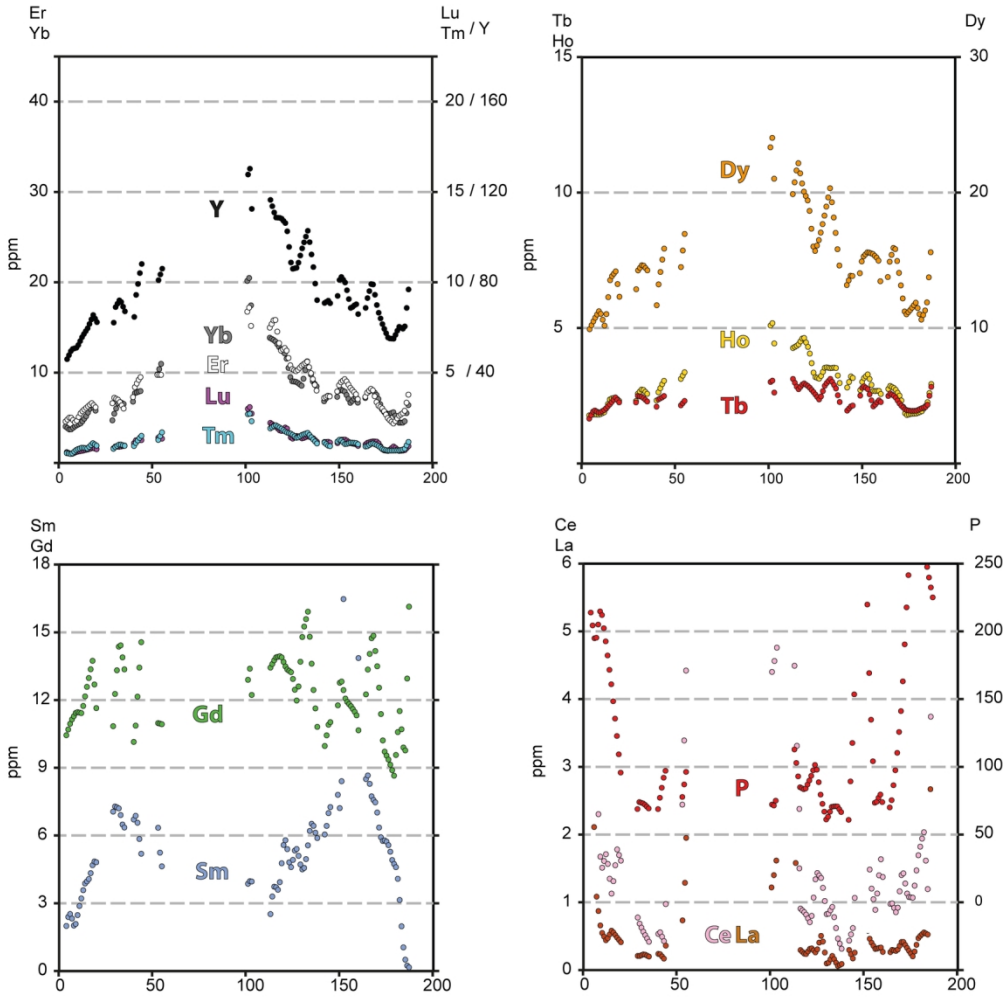

Figure 13

Figure 13. LA-ICP-MS trace element line profile of Garnet G. See Figure 10c for traverse location.

145x161mm (300 x 300 DPI)

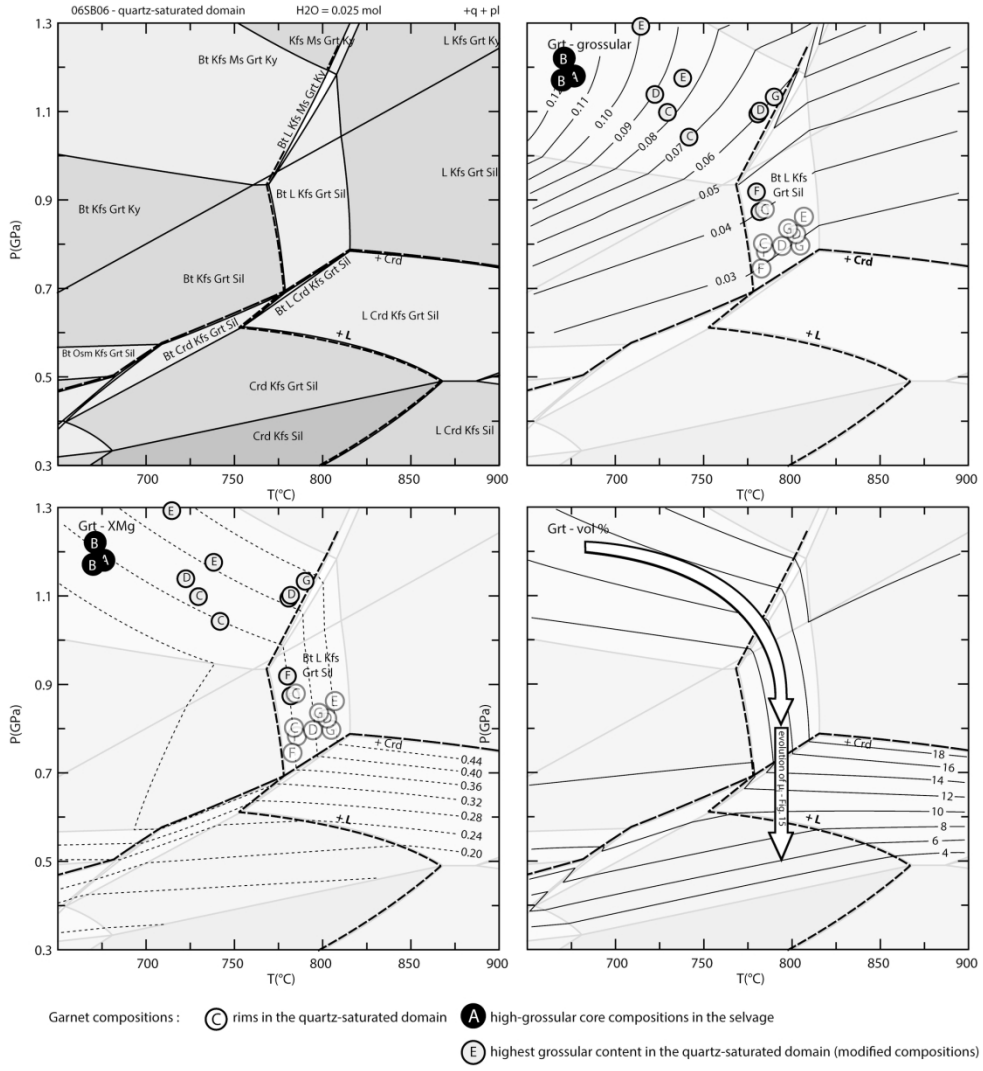

Figure 14

Figure 14. P-T phase diagram section computed for with quartz-saturated granulite composition (see Table 1). Circles with letters indicate the P-T conditions corresponding to measured garnet compositions. The letters refer to garnet grain labels in Figure 5.

180x204mm (300 x 300 DPI)

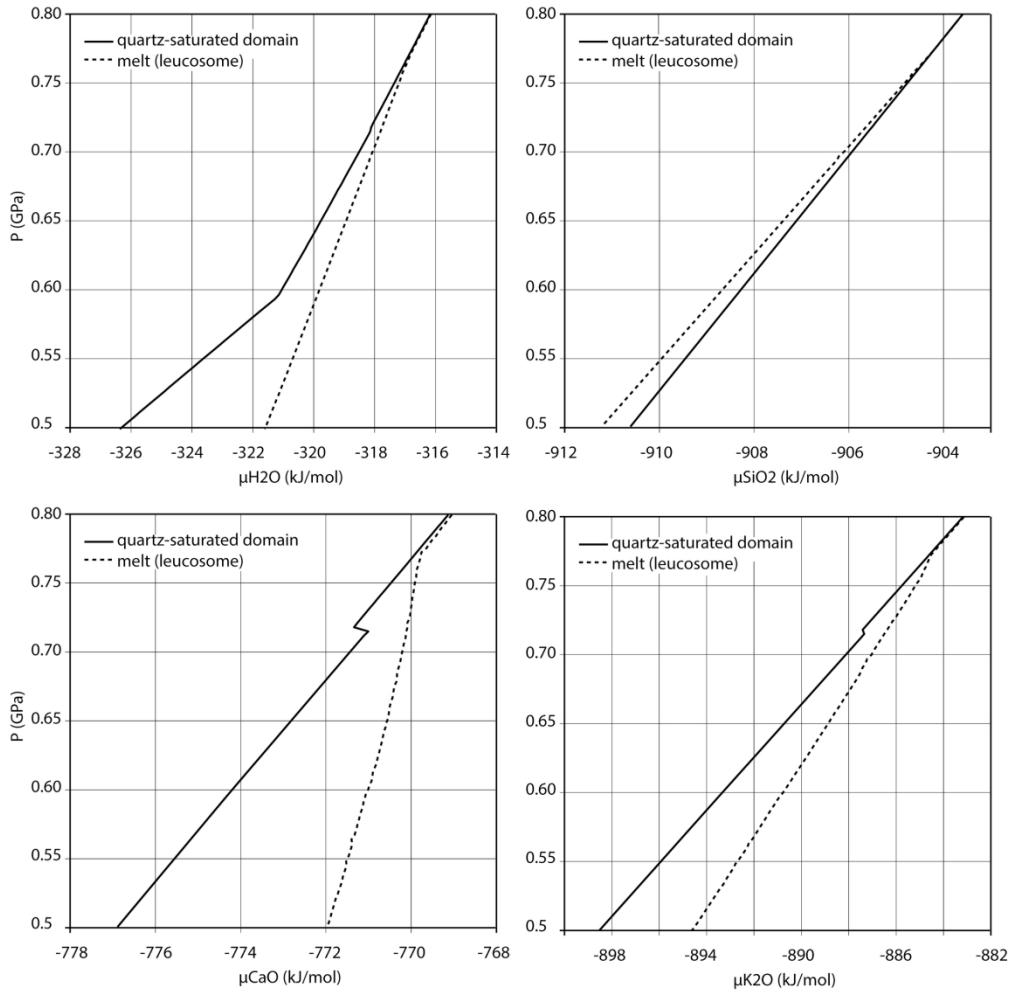

Figure 15

Figure 15. Evolution of chemical potential of H2O, SiO2, CaO and K2O for the quartz-saturated domain (black line) and melt (dashed line) along a decompression path from 0.8 to 0.5 GPa at 790°C.

180x191mm (300 x 300 DPI)

Figure 17

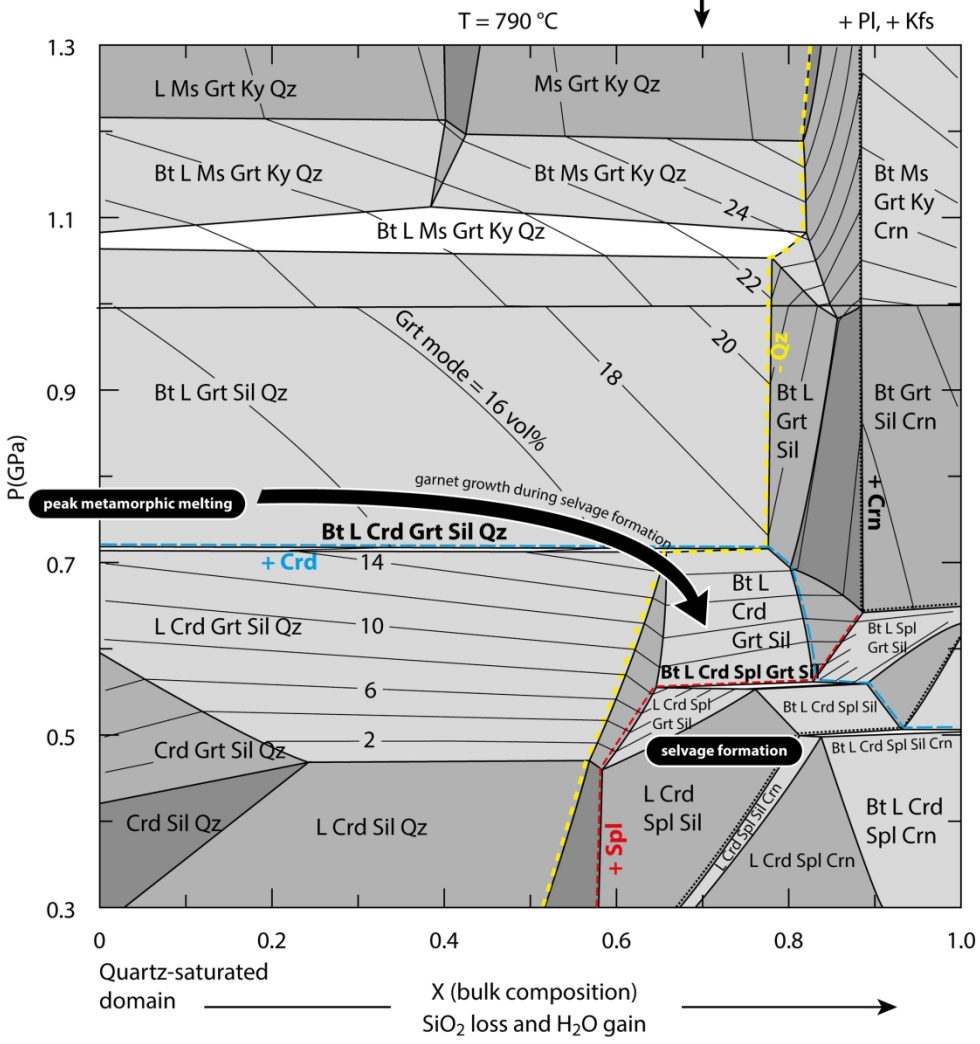

Figure 16

Figure 16. P-X phase diagram section computed at 790°C with X=0 corresponding to the quartz-saturated domain and X=1 corresponding to a 55% loss of SiO2 and 200% gain of H2O. See Table 1 for compositions.

171x212mm (300 x 300 DPI)

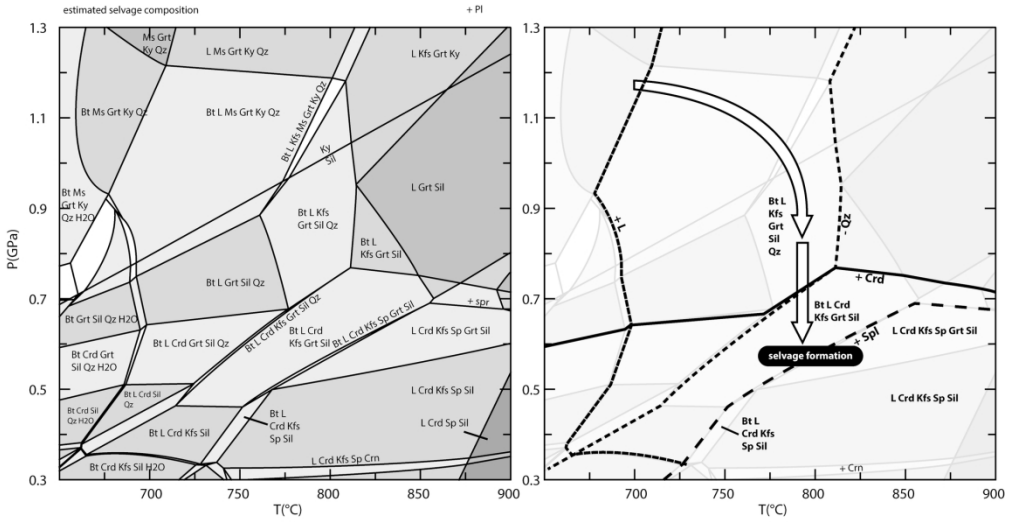

Figure 17

Figure 17. P-T phase diagram section computed with a modeled quartz-undersaturated selvage composition produced after a 47% loss of SiO2 and 140% gain of H2O. See Table 1 for compositions.

179x103mm (300 x 300 DPI)

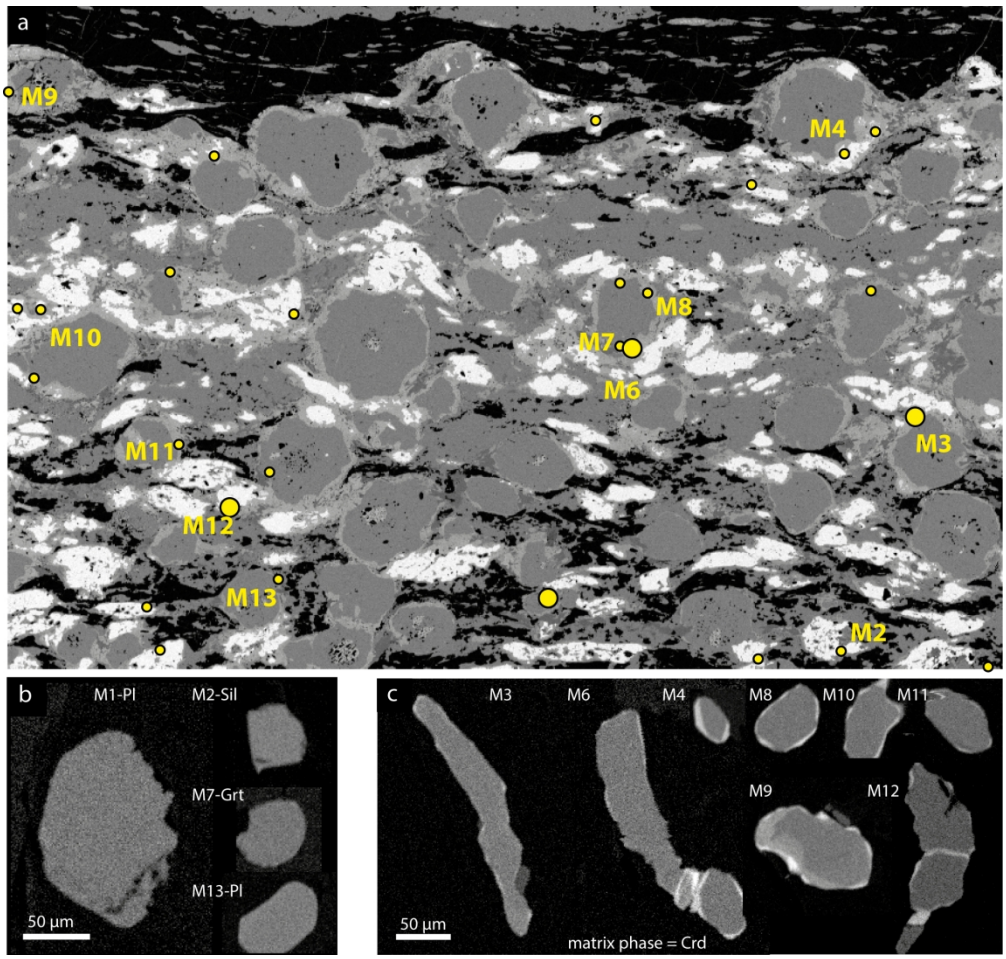

Figure 18. (a) Full thin-section X-ray Al map of sample 06SB06a showing the petrographic setting of dated monazites. (b) Y map of monazite included in garnet and plagioclase. (c) Y map of monazite in the cordierite-bearing matrix. Note the presence of thin Y-rich overgrowths.

180x171mm (300 x 300 DPI)

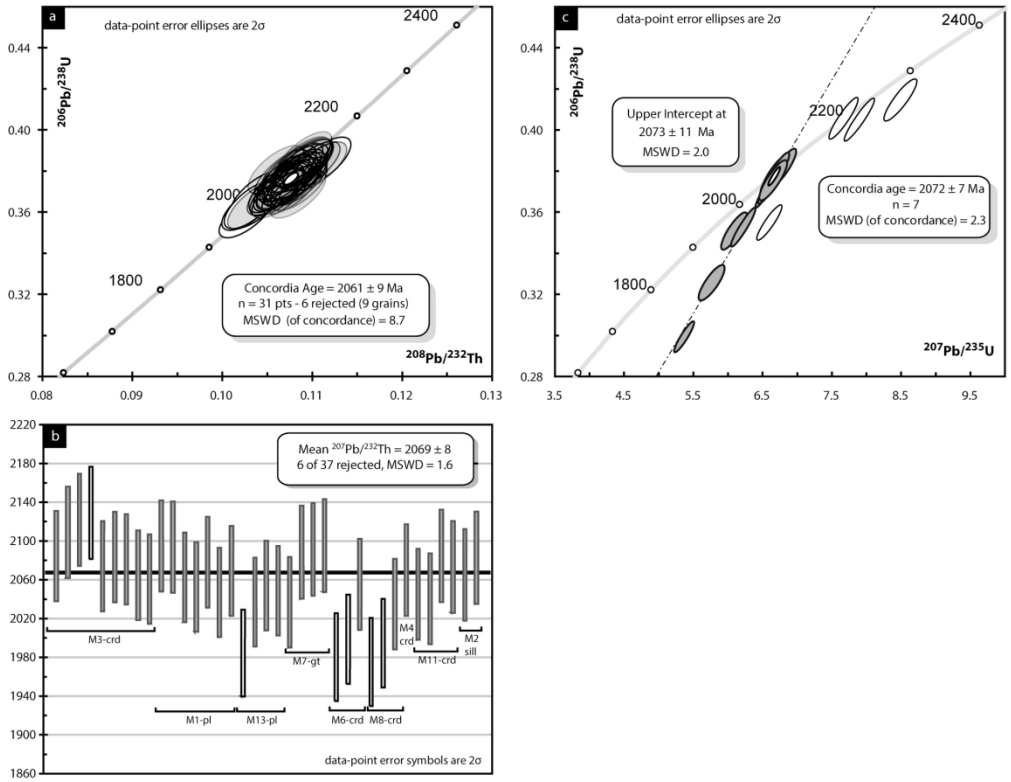

Figure 19. (a) Monazite U-Th-Pb concordia diagram. (b) Monazite Th-Pb ages. (c) Zircon U-Pb concordia diagram

180x139mm (300 x 300 DPI)

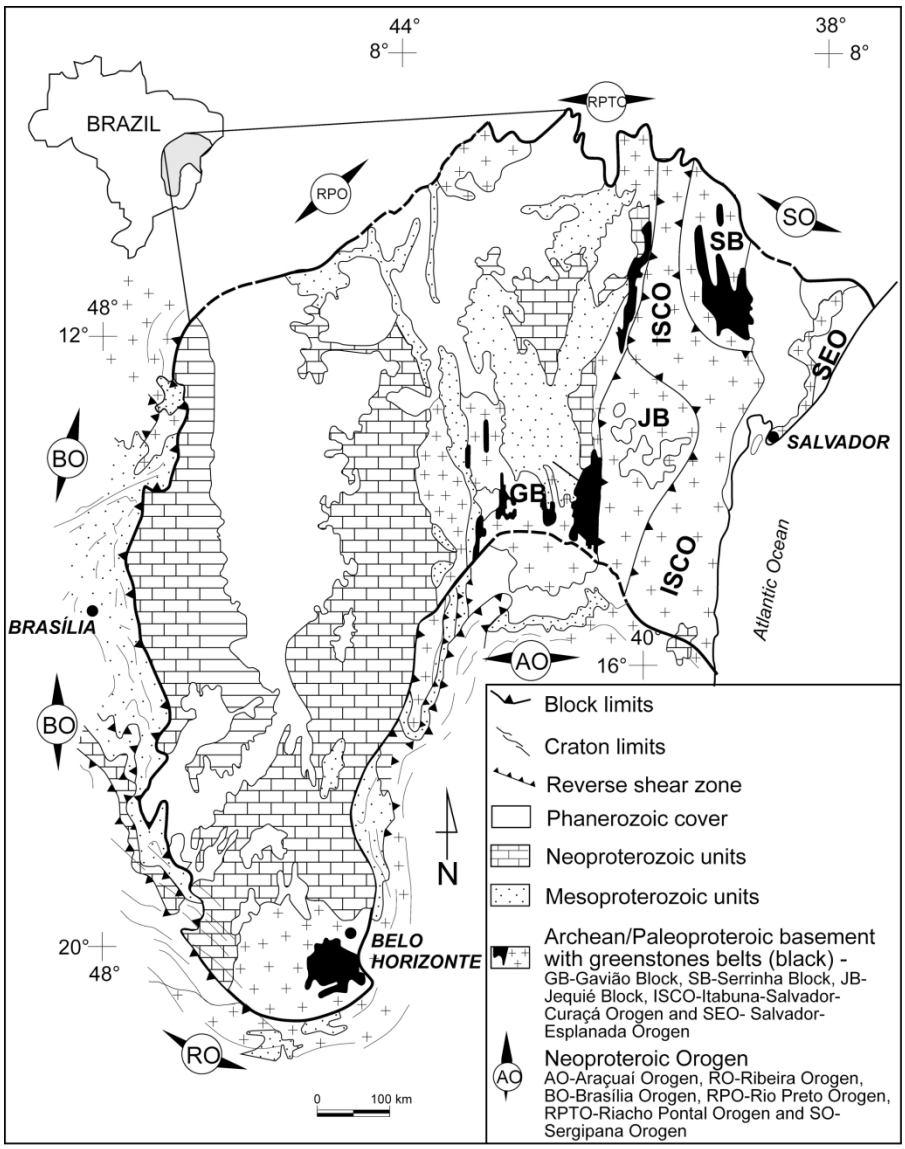

Figure 1

Figure S1. Simplified geological map of the São Francisco Craton modified after Barbosa et al. (2003).

180x240mm (300 x 300 DPI)

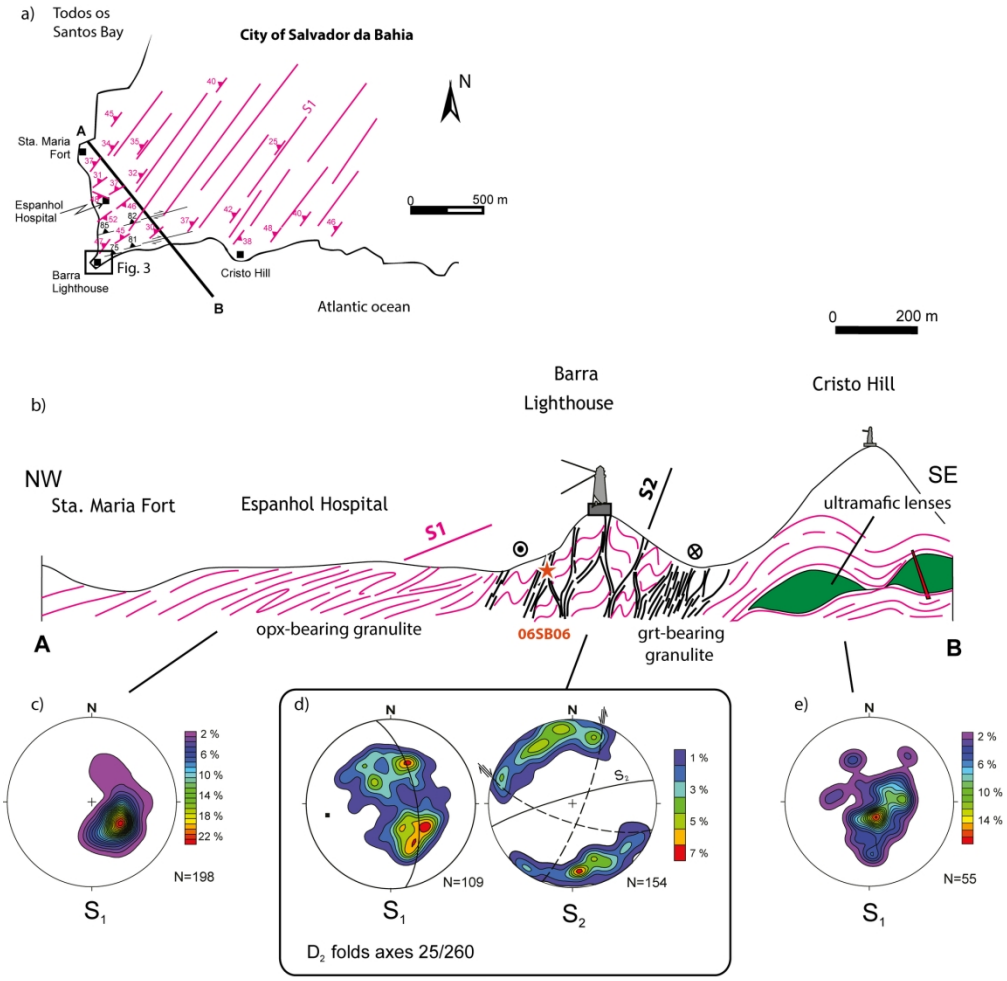

Figure S1

Figure S2. (a) Simplified structural map of the southwestern part of the city of Salvador da Bahia. (b) Simplified structural cross-section. (c) Equal-area Schmidt lower hemisphere projection of poles to S1 and S2 foliations (dashed lines = conjugated shear zones associated the S2 mylonitic foliation).

180x197mm (300 x 300 DPI)

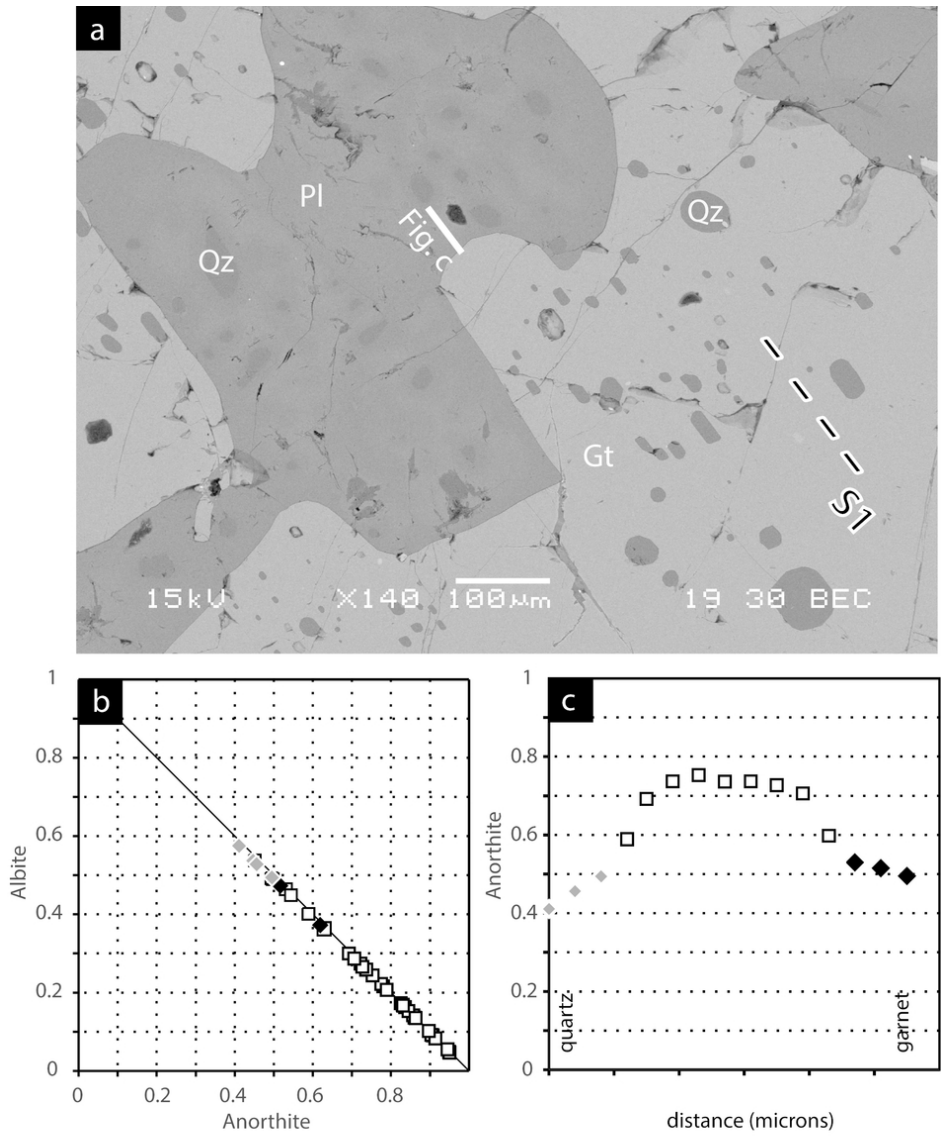

Figure S3

Figure S3. (a) Backscattered image of a polyphased plagioclase and quartz inclusion in a garnet. (b) anorthite vs albite content in mole of plagioclase. Grey and black diamonds are plagioclase composition in contact with quartz and garnet respectively. (c) Profile showing the evolution of plagioclase composition in contact with quartz and garnet. See location of the profile in figure a.

80x102mm (300 x 300 DPI)

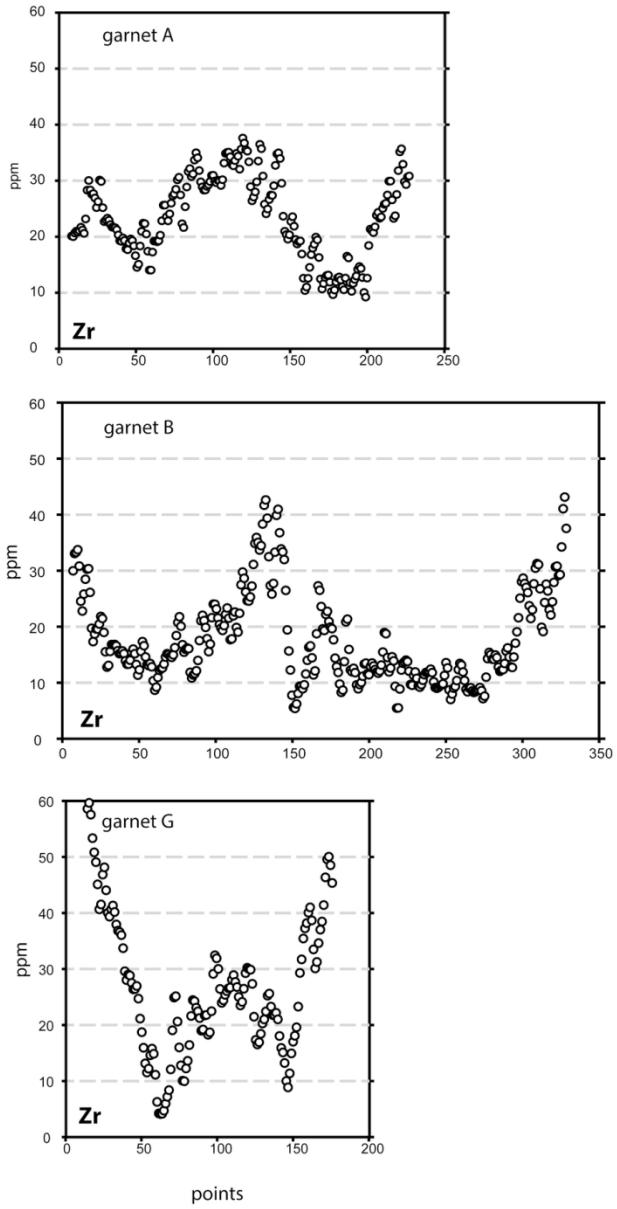

Figure S4. LA-ICP-MS Zr line profile of garnet A, B and G

80x156mm (300 x 300 DPI)

Table 1

	P-T pseudosection Figure 14	P-μ diagrams in Figure 15	P-X diagram in Figure 16		P-T pseudosection in Figure 17
	06SB06 – qtz-saturated granulite	melt produced @ 0.8 GPa and 790°C	X = 0	X = 1	selvage composition after H_2O and SiO_2 transfer (X=0.70)
	wt%	wt%	wt%	wt%	wt%
SiO_2	64.22	69.12	64.22	36.25	48.21
Al_2O_3	22.93	13.94	22.93	39.84	32.61
FeO	5.76	0.42	5.76	10	8.19
MgO	2.89	0.15	2.89	5.02	4.11
CaO	1.25	0.74	1.25	2.17	1.77
K_2O	1.86	6.51	1.86	3.23	2.64
Na_2O	0.64	2.28	0.64	1.11	0.91
H_2O	0.46	6.85	0.46	2.38	1.56
	mol	mol	mol	mol	mol
SiO_2	1.053	1.565	1.053	0.342	0.556
Al_2O_3	0.222	0.186	0.222	0.222	0.222
FeO	0.079	0.008	0.079	0.079	0.079
MgO	0.071	0.005	0.071	0.071	0.071
CaO	0.022	0.018	0.022	0.022	0.022
K_2O	0.019	0.094	0.019	0.019	0.019
Na_2O	0.010	0.050	0.010	0.010	0.010
H_2O	0.025	0.517	0.025	0.075	0.060

Table S1

solid solution models	abbreviation in Perple_X	abbreviation used	references
Biotite	Bio(TCC)	Bio	Tajcmanova et al. (2009)
Orthopyrexene	Opx(HP)	Opx	Powell & Holland (1999)
Melt	melt(HP)	L	White et al. (2001)
K-feldspar	San	Kf	Waldbaum & Thompson (1968)
Plagioclase	Pl(h)	pl	Newton et al. (1981)
Garnet	Gt(WPH)	Gt	White et al. (2007)
Spinel	Sp(HP)	Sp	
Sapphirine	Sapp(KWP)	Spr	Kelsey et al. (2014)
White mica	Mica(CHA)	Mu	Auzanneau et al. (2009)
Cordierite	hCrd	Crd	Holland et al. (1996)

REFERENCES

Auzanneau, E., Schmidt, M. W., Vielzeuf, D., & D Connolly, J. A. (2009). Titanium in phengite : A geobarometer for high temperature eclogites. *Contributions to Mineralogy and Petrology*, *159*(1), 1. https://doi.org/10.1007/s00410-009-0412-7

Holland, T. J. B., Babu, E. V. S. S. K., & Waters, D. J. (1996). Phase relations of osumilite and dehydration melting in pelitic rocks : A simple thermodynamic model for the KFMASH system. *Contributions to Mineralogy and Petrology*, *124*(3), 383-394. https://doi.org/10.1007/s004100050198

Kelsey, D. E., White, R. W., Holland, T. J. B., & Powell, R. (2004). Calculated phase equilibria in K2O-FeO-MgO-Al2O3-SiO2-H2O for sapphirine-quartz-bearing mineral assemblages. *Journal of Metamorphic Geology*, *22*(6), 559-578. https://doi.org/10.1111/j.1525-1314.2004.00533.x

Newton, R. C., Charlu, T. V., & Kleppa, O. J. (1980). Thermochemistry of the high structural state plagioclases. *Geochimica et Cosmochimica Acta*, *44*(7), 933-941. https://doi.org/10.1016/0016-7037(80)90283-5

Powell, R., & Holland, T. (1999). Relating formulations of the thermodynamics of mineral solid solutions; activity modeling of pyroxenes, amphiboles, and micas. *American Mineralogist*, *84*(1-2), 1-14. https://doi.org/10.2138/am-1999-1-201

Tajčmanová, L., Connolly, J. a. D., & Cesare, B. (2009). A thermodynamic model for titanium and ferric iron solution in biotite. *Journal of Metamorphic Geology*, *27*(2), 153-165. https://doi.org/10.1111/j.1525-1314.2009.00812.x

Waldbaum, D. R., & Thompson, J. B. (1968). Mixing Properties Of Sanidine Crystalline Solutions .2. Calculations Based On Volume Data. *American Mineralogist*, 2000-2017.

White, R. W., Powell, R., & Holland, T. J. B. (2001). Calculation of partial melting equilibria in the system Na2O–CaO–K2O–FeO–MgO–Al2O3–SiO2–H2O (NCKFMASH). *Journal of Metamorphic Geology*, *19*(2), 139-153. https://doi.org/10.1046/j.0263-4929.2000.00303.x

White, R. W., Powell, R., & Holland, T. J. B. (2007). Progress relating to calculation of partial melting equilibria for metapelites. *Journal of Metamorphic Geology*, *25*(5), 511-527. https://doi.org/10.1111/j.1525-1314.2007.00711.x

profil garnet A

analysis	1	2	3	4	5	6	7	8	9	10	11	12	13	14	15	16	17	18	19	21	22	23	24	26	27	28	29	30	31	32	33	34	35	36
dist. µm	0	26	52	77	103	129	155	181	207	233	259	284	310	336	362	388	414	439	465	517	543	569	595	646	672	698	724	750	775	801	827	853	879	905
SiO2	38.96	38.96	37.70	39.18	38.89	38.98	38.93	39.02	39.82	38.81	39.10	38.93	38.53	38.74	38.79	38.80	38.62	38.82	38.86	39.36	39.03	39.09	38.44	38.90	39.20	38.76	38.91	38.79	38.64	38.75	38.85	38.99	38.70	38.59
Al2O3	21.92	21.96	22.14	22,05	21.97	22.00	21.91	21.97	22,07	21.84	22.00	21.88	21.90	21.85	21.91	21.73	21.98	21.52	21.74	21.89	21.66	21.93	21.63	21.69	21.85	21.90	21.79	21.97	21.64	21.66	21.84	21.80	21.73	21.72
FeO	27.89	28.47	24.91	28.57	28.55	28.17	28.76	28.53	28.31	28.32	28,11	28.00	28.27	27.93	27.94	27.67	27.43	27.47	27.48	27,08	27.37	27.34	27,04	27,03	26.81	26.91	27,04	27,12	27.19	27,12	26.87	26.84	26.78	26.87
MgO	9,09	8,97	8,90	8,85	9,01	8,97	8,88	8,99	8,49	8,71	8,53	8,58	8,60	8,48	8,39	8,33	8,32	8,20	8,14	8,17	8,08	7,98	7,98	8,25	7,86	8,02	8,05	7,97	7,94	7,90	7,83	8,00	8,10	7,95
MnO	0.74	0.79	0.59	0.70	0.69	0.68	0.69	0.70	0.67	0.67	0.86	0.63	0.71	0.69	0.80	0.67	0.76	0.75	0.73	0.73	0.59	0.76	0.67	0.72	0.66	0.71	0.65	0.59	0.57	0.71	0.71	0.76	0.65	0.62
CaO	1,15	1,26	1,19	1,27	1,40	1,44	1,66	1,79	1,92	2,04	2,24	2,27	2,39	2,65	2,84	2,93	3,09	3,23	3,45	3,64	3,62	3,67	3,70	3,88	3,95	4,04	4,15	4,11	4,15	4,15	4,23	4,23	4,09	4,24
Total	99.74	100.41	95.41	100.61	100.51	100.25	100.82	101.00	101.29	100.40	100.84	100.29	100.40	100.34	100.68	100.13	100.21	99.98	100.40	100.87	100.36	100.78	99.47	100.46	100.32	100.34	100.60	100.55	100.14	100.28	100.33	100.62	100.05	99.98
Si	3,008	2,998	3,008	3,006	2,992	3,000	2,990	2,989	3,032	2,992	2,999	3,000	2,975	2,989	2,986	2,998	2,982	3,006	2,997	3,013	3,009	3,001	2,992	2,996	3,017	2,989	2,994	2,986	2,991	2,994	2,996	2,998	2,992	2,988
Al	1,995	1,992	2,082	1,995	1,991	1,996	1,983	1,984	1,980	1,984	1,989	1,988	1,994	1,987	1,987	1,980	2,001	1,964	1,976	1,975	1,968	1,985	1,984	1,969	1,981	1,990	1,976	1,993	1,974	1,973	1,986	1,976	1,980	1,982
Fe	1,801	1,832	1,662	1,833	1,837	1,813	1,847	1,828	1,803	1,826	1,803	1,804	1,825	1,802	1,798	1,789	1,772	1,779	1,773	1,734	1,764	1,755	1,760	1,741	1,725	1,735	1,740	1,746	1,760	1,753	1,733	1,726	1,732	1,740
Mg	1,047	1,029	1,058	1,012	1,032	1,029	1,017	1,027	0.964	1,001	0.976	0.986	0.99	0.975	0.963	0.959	0.957	0.946	0.936	0.932	0.928	0.913	0.926	0.947	0.901	0.922	0.923	0.914	0.915	0.91	0.9	0.917	0.933	0.917
Mn	0.048	0.051	0.04	0.046	0.045	0.045	0.045	0.045	0.043	0.044	0.056	0.041	0.046	0.045	0.052	0.044	0.05	0.049	0.048	0.048	0.039	0.05	0.044	0.047	0.043	0.046	0.043	0.038	0.038	0.047	0.046	0.049	0.042	0.041
Ca	0.095	0.104	0.101	0.105	0.116	0.119	0.136	0.147	0.157	0.169	0.184	0.188	0.198	0.219	0.234	0.243	0.256	0.268	0.285	0.298	0.299	0.302	0.309	0.32	0.326	0.334	0.342	0.339	0.344	0.343	0.35	0.349	0.339	0.352
XMg	0.37	0.36	0.39	0.36	0.36	0.36	0.36	0.36	0.35	0.35	0.35	0.35	0.35	0.35	0.35	0.35	0.35	0.35	0.35	0.35	0.35	0.34	0.35	0.35	0.34	0.35	0.35	0.34	0.34	0.34	0.34	0.35	0.35	0.35
Alm	0.60	0.61	0.58	0.61	0.61	0.60	0.61	0.60	0.61	0.60	0.60	0.60	0.60	0.59	0.59	0.59	0.58	0.59	0.58	0.58	0.58	0.58	0.58	0.57	0.58	0.57	0.57	0.58	0.58	0.57	0.57	0.57	0.57	0.57
Pyr	0.35	0.34	0.37	0.34	0.34	0.34	0.33	0.34	0.33	0.33	0.32	0.33	0.32	0.32	0.32	0.32	0.32	0.31	0.31	0.31	0.31	0.30	0.31	0.31	0.30	0.30	0.30	0.30	0.30	0.30	0.30	0.30	0.31	0.30
Sps	0.02	0.02	0.01	0.02	0.02	0.02	0.02	0.02	0.02	0.01	0.02	0.01	0.02	0.02	0.02	0.02	0.02	0.02	0.02	0.02	0.01	0.02	0.02	0.02	0.01	0.02	0.01	0.01	0.01	0.02	0.02	0.02	0.01	0.01
Grs	0.03	0.04	0.04	0.04	0.04	0.04	0.05	0.05	0.05	0.06	0.06	0.06	0.07	0.07	0.08	0.08	0.08	0.09	0.09	0.10	0.10	0.10	0.10	0.11	0.11	0.11	0.11	0.11	0.11	0.11	0.12	0.12	0.11	0.12

profil garnet B

Pt	1	2	3	5	6	7	8	9	10	12	13	14	15	16	17	18	19	20	21	22	24	25	26	28	30	32	33	34	35	37	38	41	42	43
Dist	0	25	50	99	124	149	174	199	224	274	299	324	349	374	399	423	448	473	498	523	572	597	622	672	722	771	796	821	846	896	921	996	1021	1046
SiO2	38.05	37.84	38.28	38.17	38.00	37.96	37.64	38.73	37.82	38.29	38.44	38.10	37.98	38.09	37.54	37.91	38.45	38.43	38.08	38.24	38.62	38.16	37.79	38.34	38.09	38.86	38.44	38.24	39.92	38.41	37.17	39.16	38.62	39.67
Al2O3	21.63	21.52	21.75	21.59	21.67	21.58	21.69	21.41	21.90	21.67	21.56	21.56	21.49	21.35	21.29	21.70	21.25	21.54	21.38	21.41	21.77	21.34	21.16	21.79	21.42	21.68	21.41	21.85	22.58	21.53	21,07	21.71	21.84	22.36
FeO	31.22	30.84	30.48	30.42	30.02	29.49	29.99	29,12	27.26	28.95	28.85	28.68	28.76	29,05	28.61	28.66	28.28	28.44	28.16	27.83	28.45	28,04	28.26	27.95	27.41	27.62	27.66	27.51	27.23	27.21	26.87	26.85	26.96	27,04
MgO	7,00	7,58	7,82	8,18	8,15	8,24	8,33	9,11	7,78	8,32	8,35	8,27	8,19	8,16	8,15	8,23	8,18	8,20	8,19	8,20	8,03	8,10	8,14	7,98	7,03	7,96	8,13	8,03	7,30	8,10	8,11	8,12	8,17	7,98
MnO	0.73	0.68	0.68	0.66	0.73	0.63	0.64	0.62	0.54	0.70	0.61	0.65	0.64	0.64	0.69	0.62	0.65	0.75	0.71	0.64	0.57	0.61	0.58	0.59	0.63	0.65	0.61	0.55	0.53	0.48	0.59	0.50	0.50	0.46
CaO	1,17	1,25	1,25	1,23	1,33	1,43	1,46	1,67	1,77	2,01	2,08	2,22	2,44	2,45	2,62	2,78	2,85	2,87	3,07	3,26	3,26	3,42	3,47	3,57	3,63	3,81	3,74	3,85	3,83	4,14	4,19	4,19	4,14	4,26
Total	99.81	99.70	100.26	100.25	99.91	99.33	99.75	100.67	97.07	99.93	99.90	99.48	99.49	99.74	98.90	99.89	99.66	100.23	99.59	99.58	100.70	99.67	99.40	100.22	98.20	100.57	99.98	100.03	101.39	99.87	98.00	100.53	100.23	101.77
Si	2,989	2,973	2,981	2,974	2,969	2,976	2,948	2,988	3,004	2,979	2,989	2,978	2,972	2,977	2,960	2,955	2,998	2,982	2,975	2,982	2,981	2,978	2,964	2,972	3,010	2,996	2,986	2,967	3,033	2,983	2,951	3,009	2,982	3,006
Al	2,002	1,993	1,997	1,983	1,995	1,994	2,002	1,947	2,049	1,987	1,976	1,985	1,982	1,966	1,978	1,994	1,953	1,970	1,968	1,968	1,981	1,963	1,957	1,991	1,994	1,970	1,960	1,998	2,022	1,970	1,972	1,966	1,987	1,997
Fe	2,051	2,027	1,985	1,982	1,961	1,933	1,964	1,878	1,811	1,883	1,876	1,874	1,882	1,899	1,887	1,869	1,844	1,846	1,840	1,815	1,837	1,830	1,854	1,812	1,811	1,781	1,797	1,785	1,730	1,767	1,784	1,725	1,741	1,714
Mg	0.819	0.887	0.908	0.949	0.949	0.963	0.973	1,047	0.92	0.965	0.968	0.963	0.955	0.95	0.957	0.957	0.951	0.948	0.954	0.953	0.924	0.943	0.952	0.922	0.829	0.915	0.941	0.928	0.826	0.938	0.96	0.93	0.94	0.902
Mn	0.049	0.045	0.045	0.043	0.049	0.042	0.042	0.041	0.037	0.046	0.04	0.043	0.042	0.042	0.046	0.041	0.043	0.049	0.047	0.042	0.037	0.04	0.039	0.039	0.042	0.043	0.04	0.036	0.034	0.032	0.04	0.032	0.033	0.03
Ca	0.099	0.105	0.104	0.103	0.112	0.12	0.122	0.138	0.15	0.168	0.173	0.186	0.205	0.205	0.221	0.232	0.238	0.239	0.257	0.273	0.27	0.286	0.292	0.297	0.307	0.315	0.311	0.32	0.312	0.344	0.356	0.345	0.342	0.346
MgRat	0.29	0.31	0.31	0.32	0.33	0.33	0.33	0.36	0.34	0.34	0.34	0.34	0.34	0.33	0.34	0.34	0.34	0.34	0.34	0.34	0.34	0.34	0.34	0.34	0.31	0.34	0.34	0.34	0.32	0.35	0.35	0.35	0.35	0.35
Alm	0.68	0.66	0.65	0.64	0.64	0.63	0.63	0.61	0.62	0.62	0.61	0.61	0.61	0.61	0.61	0.60	0.60	0.60	0.59	0.59	0.60	0.59	0.59	0.59	0.61	0.58	0.58	0.58	0.60	0.57	0.57	0.57	0.57	0.57
Pyr	0.27	0.29	0.30	0.31	0.31	0.32	0.31	0.34	0.32	0.32	0.32	0.31	0.31	0.31	0.31	0.31	0.31	0.31	0.31	0.31	0.30	0.30	0.30	0.30	0.28	0.30	0.31	0.30	0.29	0.30	0.31	0.31	0.31	0.30
Sps	0.02	0.02	0.02	0.01	0.02	0.01	0.01	0.01	0.01	0.02	0.01	0.01	0.01	0.01	0.02	0.01	0.01	0.02	0.02	0.01	0.01	0.01	0.01	0.01	0.01	0.01	0.01	0.01	0.01	0.01	0.01	0.01	0.01	0.01
Grs	0.03	0.03	0.03	0.03	0.04	0.04	0.04	0.05	0.05	0.06	0.06	0.06	0.07	0.07	0.07	0.08	0.08	0.08	0.08	0.09	0.09	0.09	0.09	0.10	0.10	0.10	0.10	0.10	0.11	0.11	0.11	0.11	0.11	0.12

profil garnet C

Pt	1	2	3	4	5	6	9	10	11	12	13	14	15	16	17	18	19	20	21	22	23	24	25	26	27	28	29	30	33	34	35	36	38	40
Dist	0	21	41	62	82	103	165	186	206	227	247	268	289	309	330	350	371	392	412	433	454	474	495	516	536	557	577	598	1081	1102	1122	1143	1184	1225
SiO2	39.42	39.23	37.61	38.84	38.73	38.87	38.60	38.30	38.88	38.78	38.08	38.63	38.07	38.07	38.99	38.75	37.78	38.67	38.58	39.13	39.48	38.97	38.55	38.96	38.56	38.53	38.86	38.77	38.65	38.30	37.49	38.58	38.64	38.30
Al2O3	21.95	22.19	21.36	21.80	21.77	21.89	21.85	21.99	21.87	21.69	21.86	21.77	21.92	21.82	21.70	21.63	21.95	21.68	21.69	22.22	22,10	22.27	21.75	21.69	21.92	21.68	21.66	21.96	21.46	21.81	21.90	21.88	21.66	21.56
FeO	28.94	29,01	28.52	28.65	28.70	28.40	27.96	27.89	27.96	27.96	28,11	28.36	28.13	28,08	28,01	27.67	28.30	28,12	27.67	28,11	27.68	27.77	27.95	27.96	28.17	27.93	28.62	27.89	27.95	28,06	27.69	27.77	27.65	27.67
MgO	8,79	9,08	9,11	9,11	9,73	9,20	8,94	8,87	8,86	8,78	8,96	8,76	8,89	8,74	8,84	8,77	8,61	8,84	8,79	8,69	8,75	8,96	8,96	8,90	9,01	9,10	9,08	9,28	9,20	9,20	9,01	8,99	8,90	8,96
MnO	0.63	0.61	0.63	0.63	0.69	0.66	0.60	0.72	0.60	0.74	0.59	0.74	0.65	0.60	0.56	0.63	0.66	0.64	0.56	0.63	0.60	0.60	0.59	0.63	0.62	0.60	0.64	0.59	0.57	0.58	0.61	0.58	0.58	0.63
CaO	1,25	1,28	1,38	1,46	1,55	1,68	1,99	2,03	2,25	2,22	2,39	2,46	2,51	2,52	2,51	2,63	2,58	2,39	2,41	2,39	2,32	2,28	2,20	2,17	2,08	2,01	1,81	1,63	2,05	2,10	2,32	2,35	2,37	2,50
Total	100.98	101.41	98.62	100.49	101.16	100.71	99.94	99.80	100.41	100.16	99.99	100.72	100.17	99.83	100.61	100.08	99.88	100.35	99.69	101.16	100.94	100.85	100.01	100.31	100.36	99.85	100.67	100.12	99.89	100.04	99.02	100.15	99.80	99.61
Si	3,016	2,991	2,961	2,991	2,966	2,985	2,985	2,969	2,993	2,995	2,953	2,976	2,949	2,958	2,997	2,994	2,940	2,985	2,991	2,989	3,013	2,982	2,982	3,001	2,974	2,984	2,990	2,987	2,992	2,964	2,935	2,978	2,992	2,976
Al	1,979	1,994	1,982	1,978	1,965	1,981	1,991	2,009	1,983	1,974	1,998	1,976	2,001	1,998	1,966	1,970	2,013	1,972	1,982	2,001	1,988	2,008	1,983	1,969	1,992	1,978	1,964	1,994	1,958	1,989	2,020	1,990	1,976	1,975
Fe	1,852	1,850	1,878	1,845	1,838	1,824	1,808	1,808	1,799	1,806	1,823	1,827	1,822	1,825	1,801	1,788	1,842	1,815	1,794	1,796	1,767	1,777	1,808	1,801	1,817	1,809	1,841	1,797	1,810	1,816	1,813	1,792	1,790	1,798
Mg	1,003	1,032	1,069	1,046	1,110	1,053	1,031	1,025	1,016	1,010	1,035	1,006	1,027	1,012	1,013	1,010	0.999	1,017	1,015	0.989	0.996	1,022	1,033	1,022	1,035	1,051	1,041	1,065	1,062	1,061	1,051	1,034	1,027	1,037
Mn	0.041	0.04	0.042	0.041	0.045	0.043	0.039	0.047	0.039	0.048	0.039	0.048	0.042	0.039	0.037	0.041	0.043	0.042	0.037	0.041	0.039	0.039	0.039	0.041	0.04	0.039	0.042	0.038	0.038	0.038	0.04	0.038	0.038	0.042
Ca	0.103	0.105	0.116	0.12	0.127	0.139	0.165	0.169	0.185	0.184	0.199	0.203	0.208	0.21	0.207	0.218	0.215	0.198	0.2	0.195	0.19	0.187	0.182	0.179	0.172	0.166	0.149	0.135	0.17	0.174	0.195	0.195	0.196	0.208
MgRat	0.35	0.36	0.36	0.36	0.38	0.37	0.36	0.36	0.36	0.36	0.36	0.36	0.36	0.36	0.36	0.36	0.35	0.36	0.36	0.36	0.36	0.37	0.36	0.36	0.36	0.37	0.36	0.37	0.37	0.37	0.37	0.37	0.37	0.37
Alm	0.62	0.61	0.61	0.60	0.59	0.60	0.59	0.59	0.59	0.59	0.59	0.59	0.59	0.59	0.59	0.59	0.59	0.59	0.59	0.59	0.59	0.59	0.59	0.59	0.59	0.59	0.60	0.59	0.59	0.59	0.59	0.59	0.59	0.58
Pyr	0.33	0.34	0.34	0.34	0.36	0.34	0.34	0.34	0.33	0.33	0.33	0.33	0.33	0.33	0.33	0.33	0.32	0.33	0.33	0.33	0.33	0.34	0.34	0.34	0.34	0.34	0.34	0.35	0.35	0.34	0.34	0.34	0.34	0.34
Sps	0.01	0.01	0.01	0.01	0.01	0.01	0.01	0.02	0.01	0.02	0.01	0.02	0.01	0.01	0.01	0.01	0.01	0.01	0.01	0.01	0.01	0.01	0.01	0.01	0.01	0.01	0.01	0.01	0.01	0.01	0.01	0.01	0.01	0.01
Grs	0.03	0.04	0.04	0.04	0.04	0.05	0.05	0.06	0.06	0.06	0.06	0.07	0.07	0.07	0.07	0.07	0.07	0.06	0.07	0.07	0.06	0.06	0.06	0.06	0.06	0.05	0.05	0.04	0.06	0.06	0.06	0.06	0.06	0.07

profil garnet D

Pt	1	2	3	4	5	6	7	8	9	10	11	12	13	14	15	16	17	18	19	20	21	22	23	24	25	26	27	28	29	30	31	32	33	34
Dist	0	20	40	60	80	100	120	140	160	180	200	220	240	260	280	300	320	340	360	380	400	420	440	460	480	500	520	540	560	580	600	620	640	660
SiO2	38.58	37.97	38.08	38.87	38.64	38.86	38.10	38.53	37.96	38.12	38.45	38.25	38.00	38.65	38.67	38.92	38.07	38.02	39.02	38.83	38.11	38.70	38.58	38.43	38.58	38.15	38.02	38.47	37.45	39.28	38.01	38.20	38.61	39.02
Al2O3	21.90	21.95	21.89	21.96	21.75	21.64	21.83	21.89	21.78	22,12	21.80	21.73	21.81	21.87	21.79	21.71	21.78	21.81	21.82	21.55	21.75	21.72	21.74	21.81	21.84	21.80	21.77	21.80	21.30	21.77	21.81	22,05	21.87	22,08
FeO	27.73	27.20	27.60	27.71	27.28	27.56	27.58	27.36	26.75	27.50	27.64	26.76	27,01	27.14	27.15	26.98	27,08	26.51	26.81	26.83	26.43	26.54	26.46	26.31	26.19	26.78	26.23	26.82	26.69	26.55	27,02	26.65	27,05	26.92
MgO	10,16	10,27	10,17	10,11	9,95	10,11	10,04	9,93	9,81	9,85	9,75	9,53	9,51	9,53	9,51	9,51	9,35	9,27	9,13	9,29	9,10	9,25	9,20	9,14	9,34	9,28	9,27	9,46	9,32	9,49	9,60	9,70	9,75	9,81
MnO	0.61	0.61	0.73	0.65	0.58	0.64	0.70	0.64	0.66	0.69	0.68	0.66	0.60	0.56	0.56	0.64	0.65	0.69	0.53	0.65	0.62	0.61	0.59	0.64	0.52	0.57	0.71	0.56	0.57	0.59	0.58	0.58	0.61	0.59
CaO	1,14	1,12	1,20	1,29	1,29	1,40	1,51	1,65	1,73	1,84	2,06	2,25	2,28	2,53	2,62	2,70	2,84	2,98	2,99	3,11	3,13	3,12	3,24	3,29	3,19	3,02	3,07	2,97	2,86	2,77	2,73	2,50	2,37	2,24
Total	100.12	99.11	99.67	100.59	99.48	100.21	99.77	99.99	98.68	100.11	100.39	99.17	99.21	100.27	100.29	100.45	99.79	99.28	100.29	100.26	99.14	99.95	99.81	99.62	99.66	99.59	99.07	100.08	98.19	100.45	99.75	99.68	100.26	100.66
Si	2,968	2,949	2,948	2,976	2,987	2,987	2,949	2,969	2,961	2,940	2,960	2,972	2,956	2,972	2,974	2,986	2,950	2,956	2,996	2,988	2,965	2,984	2,979	2,973	2,978	2,958	2,959	2,966	2,950	3,005	2,945	2,952	2,968	2,980
Al	1,986	2,009	1,997	1,982	1,981	1,960	1,992	1,988	2,002	2,011	1,978	1,989	1,999	1,982	1,975	1,964	1,990	1,998	1,975	1,954	1,995	1,974	1,979	1,989	1,987	1,992	1,997	1,981	1,978	1,963	1,992	2,008	1,981	1,988
Fe	1,785	1,767	1,787	1,774	1,763	1,771	1,785	1,763	1,745	1,774	1,780	1,739	1,757	1,746	1,746	1,731	1,755	1,724	1,721	1,727	1,720	1,711	1,709	1,702	1,691	1,736	1,707	1,729	1,759	1,699	1,751	1,722	1,739	1,720
Mg	1,165	1,189	1,174	1,154	1,146	1,158	1,158	1,140	1,141	1,133	1,119	1,103	1,103	1,092	1,090	1,087	1,081	1,074	1,045	1,066	1,056	1,063	1,059	1,054	1,074	1,072	1,076	1,087	1,095	1,082	1,109	1,117	1,117	1,117
Mn	0.039	0.04	0.048	0.042	0.038	0.041	0.046	0.041	0.044	0.045	0.044	0.043	0.039	0.036	0.036	0.041	0.043	0.046	0.035	0.043	0.041	0.04	0.038	0.042	0.034	0.037	0.047	0.036	0.038	0.038	0.038	0.038	0.04	0.038
Ca	0.094	0.093	0.1	0.106	0.107	0.115	0.126	0.136	0.144	0.152	0.17	0.187	0.19	0.208	0.216	0.222	0.236	0.248	0.246	0.256	0.261	0.258	0.268	0.273	0.263	0.251	0.256	0.245	0.241	0.227	0.226	0.207	0.195	0.183
MgRat	0.40	0.40	0.40	0.39	0.39	0.40	0.39	0.39	0.40	0.39	0.39	0.39	0.39	0.39	0.38	0.39	0.38	0.38	0.38	0.38	0.38	0.38	0.38	0.38	0.39	0.38	0.39	0.39	0.38	0.39	0.39	0.39	0.39	0.39
Alm	0.58	0.57	0.58	0.58	0.58	0.57	0.57	0.57	0.57	0.57	0.57	0.57	0.57	0.57	0.57	0.56	0.56	0.56	0.57	0.56	0.56	0.56	0.56	0.55	0.55	0.56	0.55	0.56	0.56	0.56	0.56	0.56	0.56	0.56
Pyr	0.38	0.39	0.38	0.38	0.38	0.38	0.37	0.37	0.37	0.37	0.36	0.36	0.36	0.35	0.35	0.35	0.35	0.35	0.34	0.35	0.34	0.35	0.35	0.34	0.35	0.35	0.35	0.35	0.35	0.36	0.36	0.36	0.36	0.37
Sps	0.01	0.01	0.02	0.01	0.01	0.01	0.02	0.01	0.01	0.01	0.01	0.01	0.01	0.01	0.01	0.01	0.01	0.02	0.01	0.01	0.01	0.01	0.01	0.01	0.01	0.01	0.02	0.01	0.01	0.01	0.01	0.01	0.01	0.01
Grs	0.03	0.03	0.03	0.03	0.04	0.04	0.04	0.04	0.05	0.05	0.06	0.06	0.06	0.07	0.07	0.07	0.08	0.08	0.08	0.08	0.09	0.08	0.09	0.09	0.09	0.08	0.08	0.08	0.08	0.07	0.07	0.07	0.06	0.06

profil garnet E

Pt	1	2	3	4	5	7	8	9	10	11	12	13	15	16	17	18	19	20	21	22	23	24	26	27	28	29	30	31	32	33	34	36	37	39
Dist	0	26	51	77	102	153	178	204	229	254	280	306	357	382	407	433	458	484	509	534	560	585	636	661	686	712	737	762	788	813	839	889	915	966
SiO2	38.68	39.07	38.44	39.02	38.81	39.16	38.55	38.64	38.22	38.37	38.70	38.59	38.87	38.86	38.49	38.49	38.61	38.14	38.51	38.40	38.98	38.42	39.31	38.71	39.30	38.99	38.58	39.04	39.05	38.87	39.18	38.67	38.42	38.70
Al2O3	21.80	21.88	22,01	21.94	22,12	22.14	21.91	21.91	21.90	22,11	22,03	22.14	22,08	22.22	21.98	22.18	22.15	22.00	21.92	21.99	21.81	22,06	22,04	22,08	22,06	22.26	22,07	21.86	22,10	22,07	22.17	22.29	21.99	22,11
FeO	28.65	28,04	27.73	27.37	27.49	26.93	27,02	26.94	26.38	26.42	26.52	26.43	26.25	25.96	26.33	25.71	26.22	25.85	26.17	25.86	25.83	25.72	25.89	25.41	25.75	25.42	25.62	25.78	25.46	25.49	25.72	26.31	25.98	25.75
MgO	9,30	9,68	9,79	9,85	9,83	9,90	9,87	9,96	9,86	9,88	9,89	9,70	9,96	9,79	10,09	10,09	10,20	10,26	10,14	10,23	10,04	10,03	9,95	9,93	10,09	9,97	10,11	10,11	10,10	10,26	10,32	10,68	10,89	10,93
MnO	0.57	0.64	0.57	0.55	0.67	0.53	0.56	0.52	0.46	0.45	0.58	0.49	0.52	0.51	0.43	0.57	0.46	0.50	0.47	0.47	0.44	0.50	0.53	0.49	0.55	0.46	0.50	0.45	0.53	0.42	0.42	0.42	0.49	0.47
CaO	1,28	1,41	1,53	1,65	1,85	2,15	2,40	2,42	2,61	2,72	2,75	2,78	2,74	2,75	2,70	2,77	2,67	2,73	2,78	2,77	2,95	2,99	3,11	3,21	3,19	3,23	3,17	3,10	2,96	2,89	2,73	2,14	1,99	1,68
Total	100.27	100.72	100.07	100.38	100.77	100.80	100.30	100.41	99.44	99.95	100.47	100.12	100.42	100.09	100.01	99.81	100.31	99.49	99.99	99.72	100.04	99.72	100.83	99.83	100.92	100.33	100.05	100.34	100.20	100.01	100.54	100.52	99.76	99.63
Si	2,984	2,991	2,963	2,990	2,968	2,984	2,962	2,964	2,957	2,952	2,964	2,963	2,972	2,976	2,958	2,958	2,956	2,944	2,960	2,956	2,987	2,957	2,989	2,971	2,984	2,974	2,958	2,983	2,982	2,974	2,981	2,950	2,951	2,967
Al	1,982	1,974	2,000	1,981	1,993	1,988	1,984	1,981	1,997	2,005	1,988	2,004	1,989	2,006	1,991	2,008	1,998	2,002	1,985	1,995	1,970	2,001	1,975	1,997	1,974	2,002	1,995	1,968	1,989	1,990	1,988	2,004	1,991	1,998
Fe	1,848	1,795	1,787	1,753	1,758	1,716	1,736	1,728	1,707	1,700	1,698	1,697	1,678	1,663	1,693	1,652	1,679	1,669	1,682	1,664	1,655	1,655	1,646	1,631	1,635	1,622	1,643	1,647	1,626	1,631	1,636	1,678	1,669	1,652
Mg	1,069	1,104	1,124	1,125	1,120	1,125	1,130	1,139	1,137	1,134	1,128	1,110	1,136	1,118	1,155	1,156	1,164	1,181	1,161	1,174	1,146	1,151	1,128	1,136	1,142	1,134	1,156	1,151	1,150	1,170	1,171	1,214	1,247	1,249
Mn	0.037	0.041	0.037	0.036	0.043	0.034	0.036	0.034	0.03	0.029	0.038	0.032	0.034	0.033	0.028	0.037	0.03	0.033	0.03	0.03	0.028	0.032	0.034	0.032	0.035	0.03	0.033	0.029	0.034	0.027	0.027	0.027	0.032	0.03
Ca	0.106	0.115	0.126	0.136	0.152	0.175	0.197	0.199	0.217	0.224	0.226	0.228	0.224	0.226	0.222	0.228	0.219	0.226	0.229	0.228	0.242	0.247	0.253	0.264	0.259	0.264	0.26	0.254	0.242	0.237	0.222	0.175	0.164	0.138
MgRat	0.37	0.38	0.39	0.39	0.39	0.40	0.39	0.40	0.40	0.40	0.40	0.40	0.40	0.40	0.41	0.41	0.41	0.41	0.41	0.41	0.41	0.41	0.41	0.41	0.41	0.41	0.41	0.41	0.41	0.42	0.42	0.42	0.43	0.43
Alm	0.60	0.59	0.58	0.58	0.57	0.56	0.56	0.56	0.55	0.55	0.55	0.55	0.55	0.55	0.55	0.54	0.54	0.54	0.54	0.54	0.54	0.54	0.54	0.53	0.53	0.53	0.53	0.54	0.53	0.53	0.54	0.54	0.54	0.54
Pyr	0.35	0.36	0.37	0.37	0.37	0.37	0.37	0.37	0.37	0.37	0.37	0.36	0.37	0.37	0.37	0.38	0.38	0.38	0.37	0.38	0.37	0.37	0.37	0.37	0.37	0.37	0.37	0.37	0.38	0.38	0.38	0.39	0.40	0.41
Sps	0.01	0.01	0.01	0.01	0.01	0.01	0.01	0.01	0.01	0.01	0.01	0.01	0.01	0.01	0.01	0.01	0.01	0.01	0.01	0.01	0.01	0.01	0.01	0.01	0.01	0.01	0.01	0.01	0.01	0.01	0.01	0.01	0.01	0.01
Grs	0.04	0.04	0.04	0.04	0.05	0.06	0.06	0.06	0.07	0.07	0.07	0.07	0.07	0.07	0.07	0.07	0.07	0.07	0.07	0.07	0.08	0.08	0.08	0.09	0.08	0.09	0.08	0.08	0.08	0.08	0.07	0.06	0.05	0.05

profil garnet F

Pt	1	2	3	4	5	6	7	8	9	10	11	12	13	14	15	16	17	18	19	20	21	22	24	25	26	27	28	29	30	31	32	33	34	35
Dist	0	20	41	61	81	101	121	142	162	182	202	223	243	263	283	304	324	344	364	385	405	425	1221	1242	1263	1284	1305	1326	1347	1368	1389	1410	1430	1451
SiO2	38.69	38.58	38.90	38.52	38.53	38.37	38.58	38.60	38.37	38.55	38.89	38.54	38.13	38.42	37.98	38.61	38.66	38.48	38.36	38.53	38.36	38.56	38.62	38.66	38.90	38.80	38.65	38.63	38.76	39.11	39.09	38.75	38.93	39.10
Al2O3	22,04	22,10	22.21	22.25	21.85	22.23	22,07	21.99	22.31	22,03	21.96	22,04	21.90	21.94	22.30	21.95	22,03	21.92	22,10	21.96	21.92	21.99	22,10	22,06	22,10	21.89	22.22	21.94	22,04	22,02	21.94	21.78	21.84	22,01
FeO	28.93	29.38	28.86	28.97	28.78	28.78	29,10	28.74	28.86	28.78	28.78	29,04	29,06	28.97	29,05	29,01	29,06	28.83	29.45	29.24	29,12	29.13	28.84	28.57	28.92	28.76	29,10	28.99	28.87	29.02	28.97	29.13	29,04	29.02
MgO	8,98	9,10	9,16	9,19	9,00	9,13	9,24	9,00	9,03	8,92	8,98	9,05	9,04	9,14	9,09	8,92	9,18	9,07	8,95	9,10	9,04	9,06	9,23	9,21	9,07	9,14	9,16	9,05	9,17	9,06	9,21	9,13	9,15	9,18
MnO	0.65	0.64	0.64	0.72	0.69	0.66	0.69	0.68	0.61	0.66	0.64	0.65	0.59	0.61	0.68	0.66	0.67	0.70	0.69	0.62	0.69	0.67	0.75	0.69	0.64	0.71	0.61	0.65	0.69	0.69	0.65	0.69	0.71	0.75
CaO	1,11	1,33	1,35	1,44	1,41	1,48	1,56	1,63	1,64	1,65	1,68	1,65	1,70	1,61	1,61	1,58	1,50	1,51	1,46	1,44	1,37	1,48	1,48	1,46	1,50	1,47	1,49	1,46	1,47	1,48	1,49	1,43	1,48	1,50
Total	100.40	101.12	101.12	101.10	100.26	100.65	101.24	100.65	100.82	100.60	100.93	100.97	100.43	100.69	100.69	100.72	101.11	100.51	101.00	100.89	100.50	100.88	101.03	100.66	101.13	100.78	101.25	100.72	100.99	101.40	101.34	100.93	101.15	101.56
Si	2,983	2,962	2,976	2,954	2,978	2,954	2,957	2,972	2,950	2,970	2,984	2,962	2,951	2,961	2,930	2,973	2,966	2,968	2,953	2,965	2,963	2,966	2,963	2,972	2,978	2,982	2,959	2,974	2,973	2,987	2,987	2,979	2,983	2,983
Al	2,002	2,000	2,003	2,011	1,990	2,017	1,994	1,995	2,022	2,000	1,986	1,996	1,997	1,993	2,028	1,992	1,992	1,993	2,005	1,991	1,996	1,993	1,998	1,999	1,994	1,983	2,006	1,990	1,992	1,983	1,975	1,973	1,972	1,979
Fe	1,865	1,886	1,847	1,858	1,860	1,853	1,865	1,850	1,856	1,854	1,846	1,866	1,881	1,867	1,874	1,868	1,864	1,860	1,896	1,881	1,881	1,874	1,850	1,837	1,852	1,849	1,864	1,866	1,852	1,854	1,851	1,873	1,861	1,851
Mg	1,032	1,041	1,045	1,051	1,037	1,047	1,056	1,033	1,035	1,025	1,026	1,037	1,043	1,050	1,046	1,023	1,050	1,043	1,026	1,043	1,041	1,039	1,056	1,055	1,035	1,046	1,046	1,038	1,048	1,032	1,049	1,047	1,046	1,043
Mn	0.042	0.041	0.041	0.047	0.045	0.043	0.045	0.045	0.039	0.043	0.042	0.042	0.039	0.04	0.044	0.043	0.044	0.046	0.045	0.041	0.045	0.043	0.049	0.045	0.042	0.046	0.04	0.043	0.045	0.045	0.042	0.045	0.046	0.048
Ca	0.092	0.109	0.11	0.119	0.117	0.122	0.128	0.135	0.135	0.137	0.138	0.136	0.141	0.133	0.133	0.13	0.123	0.125	0.12	0.119	0.114	0.122	0.122	0.12	0.123	0.121	0.123	0.121	0.121	0.121	0.122	0.118	0.122	0.123
MgRat	0.36	0.36	0.36	0.36	0.36	0.36	0.36	0.36	0.36	0.36	0.36	0.36	0.36	0.36	0.36	0.35	0.36	0.36	0.35	0.36	0.36	0.36	0.36	0.37	0.36	0.36	0.36	0.36	0.36	0.36	0.36	0.36	0.36	0.36
Alm	0.62	0.61	0.61	0.60	0.61	0.60	0.60	0.60	0.61	0.61	0.61	0.61	0.61	0.60	0.61	0.61	0.61	0.61	0.61	0.61	0.61	0.61	0.60	0.60	0.61	0.60	0.61	0.61	0.60	0.61	0.60	0.61	0.61	0.60
Pyr	0.34	0.34	0.34	0.34	0.34	0.34	0.34	0.34	0.34	0.34	0.34	0.34	0.34	0.34	0.34	0.33	0.34	0.34	0.33	0.34	0.34	0.34	0.34	0.35	0.34	0.34	0.34	0.34	0.34	0.34	0.34	0.34	0.34	0.34
Sps	0.01	0.01	0.01	0.02	0.02	0.01	0.02	0.02	0.01	0.01	0.01	0.01	0.01	0.01	0.01	0.01	0.01	0.02	0.01	0.01	0.02	0.01	0.02	0.02	0.01	0.02	0.01	0.01	0.02	0.02	0.01	0.02	0.02	0.02
Grs	0.03	0.04	0.04	0.04	0.04	0.04	0.04	0.04	0.04	0.05	0.05	0.04	0.05	0.04	0.04	0.04	0.04	0.04	0.04	0.04	0.04	0.04	0.04	0.04	0.04	0.04	0.04	0.04	0.04	0.04	0.04	0.04	0.04	0.04

profil garnet G																																	
Pt	1	2	3	4	5	6	7	8	9	10	11	12	13	16	17	18	19	21	22	23	24	26	27	28	29	30	31	32	33	34	35	36	37	38
Dist	0	20	41	61	81	101	122	142	162	183	203	223	243	304	325	345	365	406	426	447	467	507	528	548	568	589	609	629	649	670	690	1094	1114	1133
SiO2	39.80	39.51	38.41	38.64	38.58	38.58	38.94	39.17	39.71	39.45	39.43	38.80	37.05	39.05	39.51	39.63	39.07	38.79	42.21	39.71	39.81	39.27	39.88	39.64	39.17	40.69	39.24	39.67	39.59	40.20	39.85	39.62	39.24	39.42
Al2O3	22.34	22.22	22.16	22.36	21.98	22.43	22.27	22.15	22.33	22.23	22.23	22.16	21.66	22.13	22,05	22.15	22.17	22.21	22.29	22.45	22.42	22.52	22.34	22.31	22.38	22.92	22.28	22.62	22.37	22.40	22.39	22.30	22.30	22,10
FeO	26.69	26.46	26.24	26.76	25.95	26.50	26.22	26.30	26.19	26,04	25.89	26,05	25.14	25.68	25.70	25.48	25.68	25.78	24.97	25.59	25.90	26.23	25.82	25.99	25.85	25.83	26.13	26.14	26.29	26,11	26,10	26.40	26.74	26.61
MgO	11,25	11,17	10,96	11,02	11,20	10,90	10,93	10,89	10,64	10,78	10,73	10,59	10,66	10,91	10,62	10,49	10,57	10,53	10,31	10,82	10,73	10,73	11,01	11,03	10,95	9,85	11,10	11,39	11,86	11,33	11,19	11,21	11,24	11,01
MnO	0.44	0.53	0.40	0.45	0.46	0.49	0.57	0.54	0.51	0.52	0.45	0.52	0.48	0.46	0.56	0.48	0.45	0.47	0.45	0.47	0.45	0.43	0.51	0.44	0.44	0.42	0.52	0.47	0.47	0.54	0.46	0.48	0.52	0.52
CaO	1,10	1,22	1,32	1,37	1,42	1,56	1,64	1,72	1,83	1,98	2,02	2,00	1,95	2,16	2,28	2,25	2,22	2,25	2,06	2,09	2,14	1,85	1,79	1,77	1,62	1,44	1,31	1,23	1,01	1,05	1,14	1,02	1,02	1,06
Total	101.62	101.11	99.49	100.61	99.58	100.47	100.57	100.76	101.21	101.01	100.76	100.11	96.95	100.38	100.71	100.48	100.15	100.03	102.28	101.14	101.45	101.02	101.36	101.18	100.41	101.15	100.58	101.51	101.60	101.63	101.13	101.04	101.07	100.72
Si	2,990	2,985	2,954	2,944	2,962	2,943	2,963	2,975	2,996	2,985	2,988	2,967	2,929	2,972	2,996	3,006	2,981	2,966	3,114	2,992	2,994	2,971	2,998	2,989	2,976	3,050	2,978	2,977	2,972	3,009	3,000	2,991	2,970	2,991
Al	1,978	1,978	2,009	2,008	1,989	2,017	1,997	1,982	1,986	1,982	1,985	1,997	2,018	1,985	1,971	1,980	1,993	2,002	1,938	1,993	1,987	2,008	1,980	1,982	2,004	2,025	1,993	2,001	1,979	1,976	1,987	1,984	1,989	1,976
Fe	1,677	1,672	1,687	1,705	1,666	1,691	1,668	1,671	1,653	1,647	1,641	1,666	1,662	1,634	1,630	1,617	1,638	1,649	1,540	1,612	1,629	1,659	1,623	1,639	1,642	1,620	1,659	1,641	1,650	1,635	1,643	1,666	1,693	1,689
Mg	1,259	1,258	1,256	1,252	1,281	1,240	1,240	1,232	1,196	1,216	1,212	1,207	1,256	1,238	1,200	1,187	1,201	1,200	1,134	1,215	1,202	1,210	1,234	1,239	1,240	1,100	1,256	1,274	1,327	1,265	1,255	1,261	1,268	1,245
Mn	0.028	0.034	0.026	0.029	0.03	0.032	0.037	0.035	0.033	0.033	0.029	0.033	0.032	0.03	0.036	0.031	0.029	0.031	0.028	0.03	0.029	0.027	0.032	0.028	0.028	0.027	0.033	0.03	0.03	0.034	0.029	0.031	0.033	0.033
Ca	0.088	0.099	0.109	0.112	0.116	0.128	0.133	0.14	0.148	0.161	0.164	0.164	0.165	0.176	0.185	0.183	0.181	0.184	0.163	0.169	0.172	0.15	0.144	0.143	0.132	0.115	0.107	0.099	0.081	0.084	0.092	0.083	0.083	0.086
MgRat	0.43	0.43	0.43	0.42	0.44	0.42	0.43	0.43	0.42	0.43	0.43	0.42	0.43	0.43	0.42	0.42	0.42	0.42	0.42	0.43	0.43	0.42	0.43	0.43	0.43	0.40	0.43	0.44	0.45	0.44	0.43	0.43	0.43	0.42
Alm	0.55	0.55	0.55	0.55	0.54	0.55	0.54	0.54	0.55	0.54	0.54	0.54	0.53	0.53	0.53	0.54	0.54	0.54	0.54	0.53	0.54	0.55	0.54	0.54	0.54	0.57	0.54	0.54	0.53	0.54	0.54	0.55	0.55	0.55
Pyr	0.41	0.41	0.41	0.40	0.41	0.40	0.40	0.40	0.40	0.40	0.40	0.39	0.40	0.40	0.39	0.39	0.39	0.39	0.40	0.40	0.40	0.40	0.41	0.41	0.41	0.38	0.41	0.42	0.43	0.42	0.42	0.42	0.41	0.41
Sps	0.01	0.01	0.01	0.01	0.01	0.01	0.01	0.01	0.01	0.01	0.01	0.01	0.01	0.01	0.01	0.01	0.01	0.01	0.01	0.01	0.01	0.01	0.01	0.01	0.01	0.01	0.01	0.01	0.01	0.01	0.01	0.01	0.01	0.01
Grs	0.03	0.03	0.04	0.04	0.04	0.04	0.04	0.05	0.05	0.05	0.05	0.05	0.05	0.06	0.06	0.06	0.06	0.06	0.06	0.06	0.06	0.05	0.05	0.05	0.04	0.04	0.04	0.03	0.03	0.03	0.03	0.03	0.03	0.03

37	38	39	40	41	42	43	44	45	46	47	48	49	50	51	52	53	56	58	59	60	61	64	65	66	67	68	69	70	72	73	74	75	76	77
931	956	982	1008	1034	1060	1086	1111	1137	1163	1189	1215	1241	1267	1292	1318	1344	1422	1473	1499	1525	1551	1629	1654	1680	1706	1732	1758	1783	1835	1861	1887	1913	1939	1965
38.64	38.88	38.87	38.21	38.65	38.83	38.60	38.70	38.74	38.44	39.58	38.69	38.87	38.51	38.48	38.57	38.87	39.21	38.85	38.54	38.47	38.67	38.66	38.47	38.51	38.39	38.40	38.40	38.44	38.25	38.68	39.98	38.62	38.50	38.81
21.85	21.86	21.66	21.78	21.87	21.81	21.99	21.84	22.14	21.76	22.22	22,05	21.63	21.70	21.68	21.74	21.55	21.92	21.56	21.67	21.53	21.74	21.70	21.85	21.73	21.59	21.76	21.61	21.79	21.45	21.53	22.76	21.64	21.49	21.55
26.72	26.99	26.70	26.72	26.52	26.78	27,06	26.77	26.87	26.80	26.68	27,01	26.98	26.96	26.58	26.59	26.82	27.20	26.75	26.97	26.66	27.13	27.39	27.21	27.33	27.59	27.50	27.51	27.59	27.42	27.57	27.35	27.44	27.57	27.94
7,90	7,94	8,02	8,07	8,02	8,06	7,93	8,09	7,99	7,98	8,17	7,89	7,99	7,93	8,10	7,88	7,91	7,74	8,04	7,88	7,90	7,89	7,74	7,78	7,82	7,77	7,78	7,83	7,93	7,86	7,94	7,26	7,82	7,94	7,97
0.74	0.66	0.71	0.73	0.66	0.73	0.70	0.63	0.65	0.71	0.68	0.62	0.64	0.69	0.60	0.64	0.74	0.69	0.75	0.69	0.65	0.70	0.78	0.74	0.75	0.76	0.68	0.72	0.73	0.64	0.73	0.76	0.74	0.71	0.71
4,33	4,29	4,34	4,36	4,24	4,25	4,27	4,37	4,21	4,36	4,42	4,29	4,24	4,37	4,30	4,37	4,33	4,18	4,15	4,14	4,19	4,20	4,18	4,11	4,03	3,95	3,98	3,85	3,90	3,84	3,70	3,43	3,60	3,58	3,50
100.19	100.62	100.30	99.87	99.95	100.45	100.54	100.41	100.60	100.05	101.74	100.55	100.35	100.16	99.74	99.79	100.22	100.95	100.11	99.90	99.39	100.35	100.46	100.16	100.17	100.04	100.10	99.92	100.39	99.46	100.15	101.55	99.85	99.80	100.48
2,986	2,991	2,999	2,966	2,989	2,991	2,975	2,983	2,978	2,977	3,001	2,979	2,999	2,981	2,985	2,990	3,003	3,006	3,002	2,989	2,996	2,988	2,988	2,979	2,983	2,982	2,979	2,984	2,974	2,986	2,997	3,032	2,998	2,994	2,999
1,990	1,982	1,969	1,992	1,993	1,980	1,997	1,984	2,007	1,986	1,986	2,001	1,966	1,980	1,982	1,986	1,962	1,981	1,964	1,981	1,976	1,980	1,977	1,994	1,984	1,977	1,989	1,979	1,987	1,974	1,966	2,035	1,980	1,969	1,962
1,727	1,736	1,723	1,735	1,715	1,725	1,745	1,726	1,728	1,736	1,692	1,739	1,741	1,746	1,724	1,724	1,733	1,744	1,729	1,749	1,736	1,753	1,770	1,763	1,771	1,793	1,784	1,788	1,785	1,790	1,786	1,735	1,781	1,793	1,805
0.91	0.911	0.922	0.934	0.924	0.925	0.911	0.93	0.916	0.921	0.923	0.906	0.919	0.915	0.937	0.911	0.91	0.885	0.927	0.911	0.917	0.908	0.891	0.898	0.903	0.899	0.899	0.907	0.915	0.915	0.917	0.821	0.905	0.921	0.918
0.048	0.043	0.047	0.048	0.043	0.048	0.045	0.041	0.042	0.047	0.044	0.04	0.042	0.045	0.039	0.042	0.049	0.045	0.049	0.045	0.043	0.046	0.051	0.048	0.049	0.05	0.045	0.048	0.048	0.042	0.048	0.049	0.048	0.047	0.047
0.359	0.354	0.359	0.363	0.351	0.351	0.353	0.361	0.347	0.362	0.359	0.354	0.351	0.362	0.357	0.363	0.358	0.343	0.344	0.344	0.349	0.348	0.346	0.341	0.334	0.329	0.331	0.321	0.324	0.322	0.307	0.279	0.299	0.298	0.29
0.35	0.34	0.35	0.35	0.35	0.35	0.34	0.35	0.35	0.35	0.35	0.34	0.35	0.34	0.35	0.35	0.34	0.34	0.35	0.34	0.35	0.34	0.34	0.34	0.34	0.33	0.34	0.34	0.34	0.34	0.34	0.32	0.34	0.34	0.34
0.57	0.57	0.57	0.56	0.57	0.57	0.57	0.56	0.57	0.57	0.56	0.57	0.57	0.57	0.56	0.57	0.57	0.58	0.57	0.57	0.57	0.57	0.58	0.58	0.58	0.58	0.58	0.58	0.58	0.58	0.58	0.60	0.59	0.59	0.59
0.30	0.30	0.30	0.30	0.31	0.30	0.30	0.30	0.30	0.30	0.31	0.30	0.30	0.30	0.31	0.30	0.30	0.29	0.30	0.30	0.30	0.30	0.29	0.29	0.30	0.29	0.29	0.30	0.30	0.30	0.30	0.29	0.30	0.30	0.30
0.02	0.01	0.02	0.02	0.01	0.02	0.02	0.01	0.01	0.02	0.02	0.01	0.01	0.02	0.01	0.01	0.02	0.02	0.02	0.02	0.01	0.02	0.02	0.02	0.02	0.02	0.02	0.02	0.02	0.01	0.02	0.02	0.02	0.02	0.02
0.12	0.12	0.12	0.12	0.12	0.12	0.12	0.12	0.11	0.12	0.12	0.12	0.12	0.12	0.12	0.12	0.12	0.11	0.11	0.11	0.12	0.11	0.11	0.11	0.11	0.11	0.11	0.11	0.11	0.11	0.10	0.10	0.10	0.10	0.10

44	45	46	47	48	50	51	52	53	54	56	57	59	60	61	62	64	65	66	68	70	71	72	73	74	76	77	79	80	81	82	83	84	85	86
1071	1096	1121	1145	1170	1220	1245	1269	1294	1319	1369	1393	1443	1468	1493	1517	1567	1592	1616	1666	2132	2158	2183	2208	2233	2283	2308	2359	2384	2409	2434	2459	2484	2509	2534
38.09	38.48	38.53	38.78	38.42	39.66	38.57	37.13	38.87	36.38	38.84	38.36	39.75	38.89	38.72	38.99	38.79	38.72	38.98	38.83	38.75	38.73	38.62	38.79	38.63	39.66	38.64	38.77	38.79	39.06	38.88	38.83	38.74	38.77	39.03
21.13	21.72	21.72	21.85	21.85	22.35	22.00	20.71	21.83	20.32	21.95	21.78	22,10	21.84	21.75	21.69	21.96	21.60	21.85	21.78	21.92	21.84	21.50	21.71	21.44	22.14	21.67	21.77	21.61	21.84	21.55	21.72	21.83	21.62	21.51
26.92	26.83	27,09	26.72	26.79	26.93	26.39	26.57	26.43	26.19	26.88	26.36	26.46	26.70	26.50	26.39	26.50	26.30	26.48	26.37	26.23	26.59	26.39	26.40	26.16	25.95	26.40	26.21	26.42	26.43	26.29	26.36	25.85	26.40	26.21
8,28	8,33	8,24	8,24	8,28	8,12	8,31	7,58	8,26	7,71	8,26	8,22	8,51	8,66	8,65	8,77	8,94	9,09	9,02	9,19	9,11	9,02	9,00	8,79	8,73	8,55	8,72	8,53	8,79	8,47	8,57	8,60	8,47	8,57	8,41
0.59	0.53	0.55	0.53	0.50	0.46	0.59	0.55	0.47	0.54	0.52	0.52	0.48	0.56	0.51	0.54	0.46	0.45	0.45	0.49	0.42	0.47	0.48	0.45	0.42	0.50	0.44	0.41	0.47	0.41	0.46	0.51	0.51	0.45	0.48
4,42	4,25	4,24	4,30	4,36	4,37	4,44	4,20	4,29	4,29	4,47	4,32	4,08	4,08	3,98	3,83	3,44	3,44	3,42	2,96	3,18	3,49	3,69	3,93	4,14	4,37	4,33	4,40	4,49	4,40	4,48	4,50	4,34	4,40	4,40
99.44	100.14	100.36	100.42	100.20	101.89	100.29	96.74	100.15	95.42	100.91	99.56	101.38	100.73	100.11	100.20	100.09	99.61	100.20	99.62	99.61	100.14	99.68	100.07	99.51	101.16	100.21	100.09	100.57	100.61	100.23	100.52	99.74	100.21	100.05
2,975	2,975	2,976	2,985	2,969	3,002	2,972	2,983	2,995	2,967	2,978	2,978	3,016	2,982	2,985	2,999	2,984	2,993	2,994	2,996	2,990	2,981	2,988	2,989	2,994	3,012	2,979	2,988	2,980	2,995	2,995	2,984	2,992	2,988	3,009
1,945	1,979	1,977	1,983	1,990	1,994	1,998	1,961	1,982	1,953	1,984	1,993	1,977	1,974	1,977	1,966	1,991	1,968	1,978	1,981	1,993	1,981	1,961	1,972	1,959	1,981	1,968	1,977	1,957	1,973	1,956	1,967	1,986	1,964	1,955
1,759	1,734	1,749	1,721	1,731	1,705	1,700	1,785	1,703	1,787	1,724	1,711	1,679	1,712	1,708	1,697	1,705	1,700	1,701	1,702	1,693	1,712	1,708	1,701	1,696	1,648	1,702	1,689	1,698	1,694	1,693	1,694	1,670	1,702	1,689
0.964	0.96	0.948	0.945	0.953	0.916	0.955	0.908	0.948	0.937	0.944	0.951	0.962	0.99	0.994	1,005	1,025	1,047	1,033	1,057	1,048	1,035	1,038	1,010	1,009	0.968	1,002	0.98	1,007	0.968	0.983	0.985	0.975	0.984	0.966
0.039	0.035	0.036	0.035	0.033	0.03	0.038	0.037	0.031	0.037	0.034	0.034	0.031	0.036	0.033	0.035	0.03	0.03	0.029	0.032	0.028	0.031	0.031	0.029	0.027	0.032	0.029	0.027	0.031	0.027	0.03	0.033	0.034	0.029	0.032
0.37	0.352	0.351	0.355	0.361	0.354	0.366	0.362	0.354	0.375	0.367	0.359	0.332	0.335	0.329	0.316	0.284	0.285	0.282	0.245	0.263	0.288	0.306	0.324	0.343	0.355	0.357	0.363	0.37	0.361	0.37	0.37	0.359	0.363	0.363
0.35	0.36	0.35	0.36	0.36	0.35	0.36	0.34	0.36	0.34	0.35	0.36	0.36	0.37	0.37	0.37	0.38	0.38	0.38	0.38	0.38	0.38	0.38	0.37	0.37	0.37	0.37	0.37	0.37	0.36	0.37	0.37	0.37	0.37	0.36
0.56	0.56	0.57	0.56	0.56	0.57	0.56	0.58	0.56	0.57	0.56	0.56	0.56	0.56	0.56	0.56	0.56	0.56	0.56	0.56	0.56	0.56	0.55	0.56	0.55	0.55	0.55	0.55	0.55	0.56	0.55	0.55	0.55	0.55	0.55
0.31	0.31	0.31	0.31	0.31	0.31	0.31	0.29	0.31	0.30	0.31	0.31	0.32	0.32	0.32	0.33	0.34	0.34	0.34	0.35	0.35	0.34	0.34	0.33	0.33	0.32	0.32	0.32	0.32	0.32	0.32	0.32	0.32	0.32	0.32
0.01	0.01	0.01	0.01	0.01	0.01	0.01	0.01	0.01	0.01	0.01	0.01	0.01	0.01	0.01	0.01	0.01	0.01	0.01	0.01	0.01	0.01	0.01	0.01	0.01	0.01	0.01	0.01	0.01	0.01	0.01	0.01	0.01	0.01	0.01
0.12	0.11	0.11	0.12	0.12	0.12	0.12	0.12	0.12	0.12	0.12	0.12	0.11	0.11	0.11	0.10	0.09	0.09	0.09	0.08	0.09	0.09	0.10	0.11	0.11	0.12	0.12	0.12	0.12	0.12	0.12	0.12	0.12	0.12	0.12

44	45	46	47	48	49	50	51	52	53	54	56	57	58	59	60	61	62	64	65	66	67	68	69	70	71	72
1307	1328	1349	1369	1390	1410	1431	1451	1472	1493	1513	1554	1575	1595	1616	1637	1657	1678	1719	1739	1760	1781	1801	1822	1842	1863	1883
38.68	38.15	38.59	38.53	38.55	38.10	38.28	38.41	37.59	38.39	38.21	38.45	38.45	36.73	38.43	38.57	38.72	38.06	38.32	38.29	39.36	38.72	38.83	38.58	38.56	38.53	37.92
21.81	21.82	21.46	21.64	21.84	21.72	21.92	21.78	21.34	21.53	21.47	21.32	21.54	20.87	21.61	21.42	21.60	21.38	21.63	21.57	22,07	21.73	21.77	21.75	21.80	21.77	21.64
27.22	27.32	27.38	26.84	27.57	27.35	27.34	27.56	27,08	27.64	27.00	27,12	27.53	27.25	27.24	27.42	27.44	27.67	27.65	27.76	27.69	28.19	28,05	27.99	27.97	28,08	28.32
8,82	8,85	8,86	8,74	8,79	8,73	8,93	8,65	9,05	8,76	8,88	8,72	8,83	7,68	8,75	8,81	8,46	9,01	9,05	9,12	9,08	9,21	9,24	9,31	9,22	9,39	9,45
0.62	0.66	0.60	0.62	0.64	0.62	0.66	0.60	0.56	0.71	0.62	0.64	0.58	0.66	0.60	0.71	0.56	0.68	0.53	0.59	0.69	0.64	0.66	0.69	0.61	0.61	0.67
2,98	2,94	3,08	3,10	3,14	3,28	3,30	3,21	3,19	3,26	3,20	3,19	3,10	3,00	3,01	2,86	2,73	2,81	2,41	2,38	2,27	2,15	2,08	1,93	1,84	1,67	1,48
100.13	99.73	99.97	99.48	100.52	99.80	100.44	100.21	98.81	100.29	99.38	99.43	100.03	96.19	99.63	99.78	99.51	99.61	99.59	99.70	101.15	100.64	100.63	100.26	100.01	100.05	99.48
2,984	2,961	2,987	2,990	2,970	2,959	2,952	2,969	2,949	2,970	2,974	2,992	2,977	2,971	2,983	2,991	3,006	2,965	2,976	2,973	3,000	2,978	2,984	2,976	2,980	2,976	2,955
1,983	1,996	1,958	1,979	1,983	1,988	1,993	1,985	1,974	1,963	1,970	1,955	1,966	1,990	1,976	1,958	1,976	1,963	1,979	1,973	1,982	1,970	1,971	1,978	1,986	1,982	1,987
1,756	1,773	1,772	1,742	1,776	1,777	1,763	1,782	1,777	1,788	1,758	1,765	1,783	1,843	1,768	1,778	1,781	1,802	1,796	1,802	1,765	1,813	1,803	1,806	1,807	1,814	1,845
1,014	1,024	1,023	1,011	1,009	1,011	1,026	0.997	1,058	1,010	1,031	1,011	1,019	0.926	1,012	1,018	0.979	1,045	1,048	1,055	1,032	1,056	1,059	1,071	1,063	1,081	1,097
0.04	0.044	0.039	0.041	0.041	0.041	0.043	0.039	0.037	0.047	0.041	0.042	0.038	0.045	0.039	0.047	0.037	0.045	0.035	0.039	0.045	0.042	0.043	0.045	0.04	0.04	0.044
0.246	0.244	0.256	0.258	0.259	0.273	0.273	0.266	0.268	0.27	0.267	0.266	0.257	0.26	0.25	0.237	0.227	0.234	0.2	0.198	0.185	0.177	0.171	0.16	0.152	0.139	0.124
0.37	0.37	0.37	0.37	0.36	0.36	0.37	0.36	0.37	0.36	0.37	0.36	0.36	0.33	0.36	0.36	0.36	0.37	0.37	0.37	0.37	0.37	0.37	0.37	0.37	0.37	0.37
0.58	0.58	0.57	0.57	0.58	0.57	0.57	0.58	0.57	0.57	0.57	0.57	0.58	0.60	0.58	0.58	0.59	0.58	0.58	0.58	0.58	0.59	0.59	0.59	0.59	0.59	0.59
0.33	0.33	0.33	0.33	0.33	0.33	0.33	0.32	0.34	0.32	0.33	0.33	0.33	0.30	0.33	0.33	0.32	0.33	0.34	0.34	0.34	0.34	0.34	0.35	0.35	0.35	0.35
0.01	0.01	0.01	0.01	0.01	0.01	0.01	0.01	0.01	0.02	0.01	0.01	0.01	0.02	0.01	0.02	0.01	0.01	0.01	0.01	0.02	0.01	0.01	0.02	0.01	0.01	0.01
0.08	0.08	0.08	0.09	0.08	0.09	0.09	0.09	0.09	0.09	0.09	0.09	0.08	0.09	0.08	0.08	0.08	0.08	0.07	0.06	0.06	0.06	0.06	0.05	0.05	0.05	0.04

35	36	37	38	39	40	41	42	43	44	45	46	47	48	49	51	52	53	54	55	56	57	58	59	60	61	62	63	64	65	66	67	68	69	70
680	700	720	740	760	780	1104	1123	1143	1162	1182	1201	1221	1240	1260	1637	1657	1678	1699	1719	1739	1760	1780	1801	1821	1842	1862	1883	1903	1924	1944	1965	1985	2006	2026
38.84	39.00	39.07	38.63	39.13	39.36	39.07	39.32	39.69	38.83	39.24	39.30	38.70	39.37	39.69	39.61	39.37	38.26	38.80	38.88	39.48	38.75	39.12	38.53	38.57	38.58	39.21	39.19	38.68	38.55	39.26	38.94	38.46	39.42	39.44
21.98	21.99	21.89	22,05	21.98	21.97	22,12	22,12	21.97	22.25	22,07	22.23	22.15	21.95	22,08	22.19	21.92	22.27	21.86	21.94	21.92	21.97	21.94	21.94	22.15	21.85	21.97	22,03	22,11	22.17	21.94	22,08	22.14	21.87	21.96
27,01	27,02	26.65	27.16	26.99	27,11	26.31	26.65	27,02	26.49	26.87	26.61	26.56	26.79	27,01	26.19	26.37	26.54	26.39	26.69	26.36	25.78	26.68	26.21	26.22	26.23	26.19	26,04	25.96	26.33	26.38	26.29	26.19	26,10	26.47
9,95	9,97	10,01	10,29	10,39	10,50	10,41	10,55	10,65	10,51	10,59	10,59	10,47	10,46	10,51	10,72	10,56	10,56	10,43	10,38	10,28	10,28	10,24	10,18	10,26	10,39	10,35	10,23	10,29	10,24	10,32	10,28	10,37	10,37	10,51
0.58	0.54	0.60	0.53	0.57	0.63	0.46	0.49	0.58	0.53	0.58	0.56	0.58	0.58	0.51	0.48	0.55	0.52	0.57	0.60	0.51	0.63	0.52	0.51	0.55	0.59	0.50	0.53	0.50	0.50	0.56	0.54	0.46	0.57	0.56
2,01	1,93	1,84	1,59	1,53	1,34	1,29	1,29	1,32	1,46	1,38	1,38	1,33	1,38	1,24	1,37	1,44	1,73	1,88	2,11	2,29	2,18	2,28	2,34	2,30	2,36	2,32	2,29	2,21	2,18	2,09	2,11	2,02	1,94	1,79
100.38	100.45	100.07	100.25	100.59	100.91	99.66	100.43	101.22	100.07	100.73	100.67	99.79	100.53	101.04	100.56	100.21	99.88	99.93	100.61	100.86	99.59	100.77	99.72	100.05	99.99	100.55	100.31	99.74	99.97	100.57	100.25	99.64	100.27	100.73
2,976	2,984	2,995	2,963	2,985	2,992	2,995	2,995	3,003	2,971	2,985	2,987	2,972	3,000	3,006	3,004	3,003	2,941	2,978	2,969	2,999	2,979	2,981	2,966	2,958	2,963	2,988	2,991	2,970	2,959	2,991	2,977	2,959	3,006	2,997
1,985	1,983	1,978	1,993	1,976	1,969	1,998	1,986	1,959	2,007	1,979	1,991	2,004	1,971	1,971	1,984	1,971	2,018	1,977	1,975	1,962	1,991	1,970	1,991	2,002	1,978	1,973	1,981	2,001	2,006	1,971	1,990	2,008	1,966	1,967
1,731	1,728	1,708	1,742	1,722	1,723	1,687	1,697	1,710	1,695	1,710	1,692	1,706	1,707	1,711	1,661	1,683	1,706	1,694	1,705	1,675	1,657	1,700	1,687	1,682	1,685	1,669	1,662	1,667	1,690	1,681	1,681	1,685	1,664	1,682
1,137	1,137	1,144	1,177	1,182	1,190	1,189	1,198	1,202	1,199	1,201	1,199	1,198	1,188	1,187	1,212	1,201	1,210	1,194	1,182	1,164	1,178	1,163	1,168	1,173	1,190	1,175	1,163	1,177	1,172	1,173	1,172	1,189	1,179	1,190
0.038	0.035	0.039	0.034	0.037	0.04	0.03	0.031	0.037	0.034	0.038	0.036	0.038	0.037	0.033	0.031	0.035	0.034	0.037	0.039	0.033	0.041	0.034	0.033	0.035	0.038	0.033	0.034	0.033	0.032	0.036	0.035	0.03	0.037	0.036
0.165	0.158	0.151	0.131	0.125	0.109	0.106	0.105	0.107	0.119	0.112	0.113	0.109	0.113	0.1	0.111	0.118	0.143	0.155	0.173	0.187	0.179	0.186	0.193	0.189	0.194	0.189	0.188	0.182	0.18	0.171	0.173	0.167	0.158	0.146
0.40	0.40	0.40	0.40	0.41	0.41	0.41	0.41	0.41	0.41	0.41	0.42	0.41	0.41	0.41	0.42	0.42	0.42	0.41	0.41	0.41	0.42	0.41	0.41	0.41	0.41	0.41	0.41	0.41	0.41	0.41	0.41	0.41	0.42	0.41
0.56	0.57	0.56	0.57	0.56	0.56	0.56	0.56	0.56	0.56	0.56	0.56	0.56	0.56	0.57	0.55	0.55	0.55	0.55	0.55	0.55	0.54	0.55	0.55	0.55	0.54	0.54	0.55	0.55	0.55	0.55	0.55	0.55	0.55	0.55
0.37	0.37	0.38	0.38	0.39	0.39	0.40	0.40	0.39	0.39	0.39	0.40	0.39	0.39	0.39	0.40	0.40	0.39	0.39	0.38	0.38	0.39	0.38	0.38	0.38	0.38	0.38	0.38	0.39	0.38	0.38	0.38	0.39	0.39	0.39
0.01	0.01	0.01	0.01	0.01	0.01	0.01	0.01	0.01	0.01	0.01	0.01	0.01	0.01	0.01	0.01	0.01	0.01	0.01	0.01	0.01	0.01	0.01	0.01	0.01	0.01	0.01	0.01	0.01	0.01	0.01	0.01	0.01	0.01	0.01
0.05	0.05	0.05	0.04	0.04	0.04	0.04	0.04	0.04	0.04	0.04	0.04	0.04	0.04	0.03	0.04	0.04	0.05	0.05	0.06	0.06	0.06	0.06	0.06	0.06	0.06	0.06	0.06	0.06	0.06	0.06	0.06	0.05	0.05	0.05

40	41	42	43	44	45	48	49	50	51	52	53	54	55	56	57	58	59	60	64	65	66	67	69	71	72	73	75	76	77	78	79	80	81	82
992	1017	1042	1068	1093	1118	1195	1220	1246	1409	1434	1459	1485	1510	1535	1560	1585	1610	1635	1736	1761	1787	1812	1862	1912	1937	1963	2013	2038	2063	2089	2114	2139	2164	2189
39.23	38.99	39.00	39.00	38.10	39.17	39.38	39.30	39.04	39.89	39.78	38.66	39.11	39.08	39.78	39.16	39.64	39.88	39.63	39.99	39.77	40.17	39.79	40.07	40.12	39.74	39.83	39.60	40.00	39.78	39.17	39.90	39.65	39.09	39.81
22,06	22.32	22,11	22.18	21.96	21.96	22.16	22.29	22,05	22.81	22.25	22.34	22.31	22.50	22.27	22.23	22.28	22.29	22.19	22.41	21.99	22.38	22.41	22.00	22.16	22.34	22.23	22.41	22.25	22,07	22.19	22.29	22.21	22.20	22,05
26.00	26.37	26.28	25.71	25.88	25.68	25.58	25.52	26,04	25.81	25.69	26.30	25.56	25.50	25.83	25.89	25.68	25.38	25.86	25.77	25.81	25.13	25.42	24.93	25.53	25,08	25.00	24.61	24.61	24.73	24.65	24.93	24.84	24.41	24.89
11,02	11,13	11,20	11,06	11,31	11,44	11,32	11,51	11,40	11,30	11,48	11,53	11,52	11,67	11,58	11,47	11,31	11,53	11,31	11,45	11,29	11,30	11,21	11,14	11,13	10,81	10,72	10,29	10,25	10,10	10,33	10,37	10,37	10,35	10,43
0.54	0.48	0.52	0.56	0.55	0.50	0.59	0.50	0.51	0.42	0.56	0.41	0.40	0.48	0.46	0.42	0.43	0.49	0.52	0.50	0.54	0.58	0.40	0.46	0.48	0.46	0.51	0.47	0.52	0.57	0.53	0.47	0.55	0.46	0.48
1,57	1,46	1,34	1,32	1,15	1,24	1,20	1,08	1,15	1,26	1,08	0.99	1,08	1,01	1,08	1,06	1,15	1,19	1,15	1,30	1,36	1,48	1,62	1,87	1,92	2,54	2,99	3,40	3,60	3,65	3,67	3,54	3,56	3,50	3,45
100.43	100.75	100.45	99.83	98.94	99.99	100.23	100.20	100.19	101.49	100.83	100.23	99.98	100.25	101.00	100.24	100.49	100.75	100.66	101.42	100.76	101.04	100.86	100.47	101.33	100.97	101.27	100.79	101.23	100.90	100.55	101.51	101.18	100.00	101.11
2,983	2,960	2,969	2,979	2,946	2,985	2,991	2,983	2,974	2,987	3,000	2,947	2,976	2,965	2,996	2,977	2,999	3,005	2,997	2,999	3,006	3,016	2,998	3,026	3,012	2,996	2,997	2,993	3,010	3,008	2,975	2,998	2,991	2,980	3,003
1,978	1,998	1,984	1,997	2,001	1,973	1,984	1,995	1,980	2,013	1,978	2,007	2,001	2,012	1,976	1,992	1,987	1,979	1,978	1,981	1,959	1,980	1,990	1,958	1,961	1,985	1,971	1,996	1,973	1,967	1,987	1,974	1,975	1,995	1,961
1,654	1,674	1,673	1,643	1,673	1,637	1,625	1,620	1,659	1,616	1,620	1,677	1,626	1,618	1,627	1,646	1,625	1,599	1,636	1,616	1,632	1,578	1,602	1,575	1,603	1,581	1,573	1,556	1,548	1,564	1,566	1,566	1,567	1,556	1,571
1,250	1,259	1,271	1,259	1,303	1,300	1,281	1,302	1,295	1,261	1,290	1,311	1,307	1,320	1,300	1,299	1,275	1,295	1,276	1,280	1,272	1,265	1,259	1,254	1,245	1,214	1,202	1,159	1,150	1,139	1,170	1,162	1,166	1,176	1,172
0.035	0.031	0.034	0.036	0.036	0.032	0.038	0.032	0.033	0.027	0.036	0.026	0.026	0.031	0.029	0.027	0.028	0.031	0.033	0.032	0.035	0.037	0.026	0.03	0.03	0.03	0.033	0.03	0.033	0.036	0.034	0.03	0.035	0.029	0.031
0.128	0.119	0.109	0.108	0.095	0.101	0.098	0.088	0.094	0.101	0.087	0.081	0.088	0.082	0.087	0.087	0.094	0.096	0.093	0.104	0.11	0.119	0.13	0.151	0.155	0.205	0.241	0.275	0.29	0.296	0.299	0.285	0.288	0.286	0.279
0.43	0.43	0.43	0.43	0.44	0.44	0.44	0.45	0.44	0.44	0.44	0.44	0.45	0.45	0.44	0.44	0.44	0.45	0.44	0.44	0.44	0.45	0.44	0.44	0.44	0.43	0.43	0.43	0.43	0.42	0.43	0.43	0.43	0.43	0.43
0.54	0.54	0.54	0.54	0.54	0.53	0.53	0.53	0.54	0.54	0.53	0.54	0.53	0.53	0.54	0.54	0.54	0.53	0.54	0.53	0.54	0.53	0.53	0.52	0.53	0.52	0.52	0.52	0.51	0.52	0.51	0.52	0.51	0.51	0.52
0.41	0.41	0.41	0.41	0.42	0.42	0.42	0.43	0.42	0.42	0.43	0.42	0.43	0.43	0.43	0.43	0.42	0.43	0.42	0.42	0.42	0.42	0.42	0.42	0.41	0.40	0.39	0.38	0.38	0.38	0.38	0.38	0.38	0.39	0.38
0.01	0.01	0.01	0.01	0.01	0.01	0.01	0.01	0.01	0.01	0.01	0.01	0.01	0.01	0.01	0.01	0.01	0.01	0.01	0.01	0.01	0.01	0.01	0.01	0.01	0.01	0.01	0.01	0.01	0.01	0.01	0.01	0.01	0.01	0.01
0.04	0.04	0.04	0.04	0.03	0.03	0.03	0.03	0.03	0.03	0.03	0.03	0.03	0.03	0.03	0.03	0.03	0.03	0.03	0.03	0.04	0.04	0.04	0.05	0.05	0.07	0.08	0.09	0.10	0.10	0.10	0.09	0.09	0.09	0.09

36	37	38	39	40	41	42	43	44
1472	1493	1514	1535	1556	1577	1598	1619	1640
38.69	38.88	38.88	37.52	38.86	38.92	38.83	38.84	39.30
21.93	21.76	21.84	21.67	21.94	22,02	21.91	22,02	21.66
28.86	28.78	28.70	26.61	28.37	29,12	28.79	29.38	28.92
9,22	9,22	9,13	9,50	9,10	9,19	9,08	9,24	9,08
0.74	0.66	0.65	0.50	0.62	0.62	0.65	0.65	0.65
1,38	1,36	1,38	1,27	1,27	1,34	1,33	1,34	1,19
100.82	100.66	100.59	97.07	100.17	101.21	100.59	101.47	100.80
2,974	2,990	2,991	2,971	2,995	2,979	2,987	2,970	3,015
1,987	1,972	1,979	2,023	1,993	1,987	1,986	1,984	1,958
1,855	1,851	1,846	1,762	1,829	1,864	1,852	1,879	1,855
1,056	1,057	1,047	1,121	1,046	1,049	1,041	1,053	1,038
0.048	0.043	0.043	0.033	0.04	0.04	0.042	0.042	0.042
0.114	0.112	0.114	0.108	0.105	0.11	0.11	0.11	0.098
0.36	0.36	0.36	0.39	0.36	0.36	0.36	0.36	0.36
0.60	0.60	0.61	0.58	0.61	0.61	0.61	0.61	0.61
0.34	0.35	0.34	0.37	0.35	0.34	0.34	0.34	0.34
0.02	0.01	0.01	0.01	0.01	0.01	0.01	0.01	0.01
0.04	0.04	0.04	0.04	0.04	0.04	0.04	0.04	0.03

39	41	42	43	44	45	46	47	48	49	50	51	52	53	54	55	56	57	58	59	60	61	63	64	65	66	67	68	69	70	71	72	73	74	75
1153	1193	1213	1232	1252	1272	1292	1311	1331	1351	1371	1390	1410	1430	1450	1469	1489	1509	1529	1548	1568	1588	1627	1647	1667	1687	1706	1726	1746	1766	1785	1805	1825	1845	1865
39.32	39.37	39.56	39.45	38.68	38.90	39.67	38.86	39.79	39.33	38.68	38.81	38.67	39.25	38.80	38.73	38.96	38.79	39.53	39.44	39.68	38.54	38.71	38.86	38.66	39.33	38.78	38.86	39.43	39.52	39.04	39.09	39.43	39.31	39.53
21.86	22,12	22,02	22,07	22.26	22.16	22.28	22.24	22.56	22.21	22.29	22.22	22.24	22.35	22.18	22.17	22.32	21.97	22.23	22.00	22.36	21.95	22,05	22.16	22.28	22.24	22.33	21.92	22.22	21.97	22.25	22.13	22.29	22,06	22,07
26.50	26.59	26.72	26.67	26.52	26.67	26.61	26.89	26.72	26.60	26.72	26.46	26.43	26.58	26.40	26.67	26.24	26.48	26.61	26.56	26.20	26.65	26.36	26.21	26.66	26.51	26.22	26.43	26.29	26.67	26.37	26.76	26.61	26.90	26.85
11,10	11,27	11,19	11,10	11,15	11,10	10,99	11,00	10,94	10,85	10,84	10,81	10,76	10,71	10,53	10,61	10,58	10,59	10,47	10,40	10,48	10,46	10,21	10,32	10,20	10,21	10,41	10,17	10,31	10,28	10,42	10,14	10,22	10,26	10,28
0.47	0.50	0.45	0.51	0.53	0.40	0.44	0.51	0.43	0.45	0.48	0.53	0.52	0.48	0.46	0.48	0.49	0.54	0.53	0.48	0.46	0.58	0.51	0.47	0.45	0.49	0.45	0.47	0.44	0.52	0.50	0.55	0.51	0.52	0.55
1,04	0.99	1,08	1,07	1,09	1,13	1,19	1,33	1,27	1,42	1,52	1,54	1,66	1,71	1,75	1,78	1,81	1,91	2,00	2,06	2,10	2,10	2,21	2,25	2,21	2,30	2,31	2,35	2,31	2,18	2,25	2,21	2,18	2,13	2,02
100.30	100.84	101.02	100.87	100.23	100.35	101.17	100.84	101.71	100.85	100.53	100.37	100.28	101.09	100.12	100.45	100.41	100.27	101.37	100.95	101.26	100.28	100.05	100.28	100.46	101.09	100.51	100.19	101.01	101.15	100.84	100.89	101.24	101.18	101.30
2,996	2,984	2,993	2,989	2,954	2,966	2,994	2,955	2,987	2,983	2,951	2,962	2,955	2,972	2,968	2,959	2,969	2,967	2,987	2,994	2,994	2,955	2,969	2,970	2,956	2,982	2,957	2,977	2,988	2,996	2,968	2,976	2,985	2,983	2,993
1,963	1,975	1,963	1,971	2,004	1,991	1,982	1,993	1,996	1,985	2,004	1,999	2,003	1,995	2,000	1,996	2,005	1,981	1,980	1,968	1,988	1,984	1,993	1,996	2,008	1,988	2,007	1,979	1,985	1,963	1,994	1,985	1,989	1,973	1,970
1,688	1,685	1,691	1,690	1,694	1,701	1,679	1,710	1,677	1,687	1,705	1,689	1,689	1,683	1,689	1,704	1,673	1,695	1,681	1,686	1,653	1,709	1,691	1,675	1,704	1,681	1,673	1,693	1,666	1,691	1,677	1,704	1,684	1,707	1,700
1,260	1,272	1,261	1,254	1,269	1,261	1,236	1,247	1,224	1,227	1,233	1,229	1,226	1,209	1,201	1,208	1,202	1,208	1,179	1,176	1,179	1,195	1,167	1,175	1,163	1,154	1,183	1,161	1,164	1,162	1,181	1,150	1,153	1,160	1,160
0.03	0.032	0.029	0.033	0.034	0.026	0.028	0.033	0.028	0.029	0.031	0.034	0.034	0.031	0.03	0.031	0.032	0.035	0.034	0.031	0.029	0.038	0.033	0.031	0.029	0.032	0.029	0.03	0.028	0.034	0.032	0.036	0.033	0.033	0.035
0.085	0.08	0.088	0.087	0.089	0.093	0.096	0.109	0.102	0.115	0.124	0.126	0.136	0.139	0.144	0.146	0.148	0.156	0.162	0.168	0.169	0.172	0.181	0.185	0.181	0.187	0.189	0.193	0.188	0.177	0.183	0.18	0.177	0.173	0.164
0.43	0.43	0.43	0.43	0.43	0.43	0.42	0.42	0.42	0.42	0.42	0.42	0.42	0.42	0.42	0.42	0.42	0.42	0.41	0.41	0.42	0.41	0.41	0.41	0.41	0.41	0.41	0.41	0.41	0.41	0.41	0.40	0.41	0.41	0.41
0.55	0.55	0.55	0.55	0.55	0.55	0.55	0.55	0.55	0.55	0.55	0.55	0.55	0.55	0.55	0.55	0.55	0.55	0.55	0.55	0.55	0.55	0.55	0.55	0.55	0.55	0.54	0.55	0.55	0.55	0.55	0.56	0.55	0.56	0.56
0.41	0.41	0.41	0.41	0.41	0.41	0.41	0.40	0.40	0.40	0.40	0.40	0.40	0.40	0.39	0.39	0.39	0.39	0.39	0.38	0.39	0.38	0.38	0.38	0.38	0.38	0.39	0.38	0.38	0.38	0.38	0.38	0.38	0.38	0.38
0.01	0.01	0.01	0.01	0.01	0.01	0.01	0.01	0.01	0.01	0.01	0.01	0.01	0.01	0.01	0.01	0.01	0.01	0.01	0.01	0.01	0.01	0.01	0.01	0.01	0.01	0.01	0.01	0.01	0.01	0.01	0.01	0.01	0.01	0.01
0.03	0.03	0.03	0.03	0.03	0.03	0.03	0.04	0.03	0.04	0.04	0.04	0.04	0.05	0.05	0.05	0.05	0.05	0.05	0.06	0.06	0.06	0.06	0.06	0.06	0.06	0.06	0.06	0.06	0.06	0.06	0.06	0.06	0.06	0.05

78	79	80	81	82	83	85	86	87	88	89	90	91	92	93	94	95	96	97	98	99	100
1990	2016	2042	2068	2094	2120	2171	2197	2223	2249	2275	2301	2326	2352	2378	2404	2430	2456	2481	2507	2533	2559
38.45	38.56	38.45	38.80	38.06	38.48	38.55	38.53	38.28	37.81	38.40	37.99	38.19	38.38	38.25	38.47	38.17	38.17	38.28	38.09	38.38	37.83
21.61	21.61	21.74	21.54	21.60	21.57	21.73	21.74	21.54	21.58	21.54	21.73	21.65	21.68	21.59	21.89	21.83	21.50	21.54	21.71	21.72	21.41
27.77	28.27	27.97	28.14	28,10	27.71	28.28	28.49	28.23	27.94	28.23	28.33	28.19	28.36	28.26	28.49	29,06	28.72	28.94	29.31	28.91	29.44
7,88	7,89	7,97	8,04	8,08	8,12	7,97	8,18	8,30	8,19	8,44	8,30	8,48	8,41	8,54	8,45	8,54	8,70	8,71	8,89	8,81	9,44
0.79	0.76	0.69	0.73	0.74	0.71	0.80	0.73	0.76	0.71	0.83	0.68	0.76	0.77	0.72	0.71	0.69	0.86	0.67	0.66	0.69	0.73
3,48	3,40	3,41	3,24	3,18	3,11	3,00	2,88	2,93	2,80	2,65	2,56	2,42	2,37	2,26	2,18	2,08	1,92	1,83	1,57	1,45	1,32
99.98	100.50	100.24	100.49	99.75	99.69	100.34	100.54	100.03	99.02	100.08	99.59	99.69	99.97	99.62	100.20	100.39	99.87	99.97	100.22	99.96	100.17
2,987	2,985	2,980	2,998	2,968	2,993	2,986	2,979	2,975	2,966	2,980	2,964	2,974	2,981	2,979	2,978	2,959	2,972	2,976	2,958	2,979	2,944
1,978	1,971	1,986	1,962	1,985	1,977	1,984	1,981	1,973	1,996	1,971	1,998	1,987	1,984	1,982	1,997	1,995	1,973	1,974	1,986	1,987	1,963
1,804	1,830	1,813	1,819	1,832	1,802	1,832	1,842	1,835	1,833	1,832	1,849	1,836	1,842	1,841	1,845	1,884	1,870	1,881	1,903	1,876	1,915
0.912	0.911	0.921	0.926	0.939	0.941	0.92	0.942	0.962	0.958	0.976	0.966	0.984	0.973	0.991	0.975	0.987	1,010	1,010	1,028	1,020	1,095
0.052	0.05	0.045	0.048	0.049	0.047	0.052	0.048	0.05	0.047	0.054	0.045	0.05	0.05	0.048	0.047	0.046	0.057	0.044	0.043	0.045	0.048
0.29	0.282	0.283	0.268	0.266	0.259	0.249	0.239	0.244	0.235	0.22	0.214	0.202	0.197	0.189	0.181	0.173	0.16	0.152	0.13	0.121	0.11
0.34	0.33	0.34	0.34	0.34	0.34	0.33	0.34	0.34	0.34	0.35	0.34	0.35	0.35	0.35	0.35	0.34	0.35	0.35	0.35	0.35	0.36
0.59	0.60	0.59	0.59	0.59	0.59	0.60	0.60	0.59	0.60	0.59	0.60	0.60	0.60	0.60	0.61	0.61	0.60	0.61	0.61	0.61	0.61
0.30	0.30	0.30	0.30	0.30	0.31	0.30	0.31	0.31	0.31	0.32	0.31	0.32	0.32	0.32	0.32	0.32	0.33	0.33	0.33	0.33	0.35
0.02	0.02	0.02	0.02	0.02	0.02	0.02	0.02	0.02	0.02	0.02	0.02	0.02	0.02	0.02	0.02	0.02	0.02	0.01	0.01	0.02	0.02
0.10	0.09	0.09	0.09	0.09	0.09	0.08	0.08	0.08	0.08	0.07	0.07	0.07	0.06	0.06	0.06	0.06	0.05	0.05	0.04	0.04	0.04

87	88	89	91	92	93	94	95	96	97	98	99	100	101	102	103	104	106	107	108	109	110	111	113	114	115	116	117	120	121	122	123	124	125	126
2559	2584	2609	2659	2684	2709	2734	2759	2784	2809	2834	2859	2884	2909	2934	2959	2984	3034	3059	3084	3109	3134	3159	3209	3234	3259	3284	3309	3385	3410	3435	3460	3485	3510	3535
38.58	38.66	38.51	38.42	38.64	38.95	38.41	38.99	40.14	37.30	38.17	38.12	38.74	38.83	38.74	38.84	39.08	39.26	39.11	38.81	38.99	38.59	38.59	38.83	38.77	38.56	38.86	38.01	38.69	38.58	38.49	31.57	38.32	38.85	38.56
21.73	21.55	21.69	21.53	21.97	21.80	21.59	21.61	22.30	20.75	21.79	21.35	21.58	21.45	21.66	21.61	21.70	21.62	21.79	21.75	21.61	21.78	21.72	21.56	21.78	21.89	21.62	21.38	21.84	22.00	21.73	17.73	21.75	22.15	21.85
26.19	25.91	26.35	26.00	26.33	26,11	26.36	26.45	26.45	26,04	25.95	26.75	26.89	26.77	26.97	27.15	26.96	26.66	27.44	26.86	27.23	27.71	27.15	27.66	27.43	27.50	28,03	27.97	28.23	28.27	28.51	28.41	28.65	29.02	28.79
8,58	8,42	8,44	8,55	8,45	8,35	8,36	8,24	8,18	8,82	7,56	8,63	8,40	8,38	8,36	8,37	8,08	8,24	8,24	8,43	8,43	8,42	8,47	8,67	8,43	8,53	8,50	8,78	8,52	8,75	8,82	8,32	9,02	8,77	8,85
0.52	0.40	0.47	0.54	0.51	0.56	0.56	0.55	0.54	0.48	0.45	0.48	0.52	0.47	0.46	0.53	0.49	0.52	0.48	0.52	0.63	0.56	0.53	0.60	0.60	0.55	0.55	0.59	0.59	0.55	0.53	0.55	0.56	0.60	0.68
4,61	4,52	4,49	4,47	4,39	4,35	4,35	4,36	4,36	4,34	4,26	4,16	4,23	4,17	4,06	4,07	4,04	3,87	3,86	3,76	3,48	3,65	3,30	3,26	3,21	3,04	2,97	2,79	2,30	2,09	1,87	1,59	1,43	1,36	1,29
100.22	99.47	99.95	99.51	100.29	100.11	99.63	100.19	101.97	97.74	98.17	99.49	100.37	100.07	100.24	100.57	100.34	100.17	100.92	100.14	100.37	100.70	99.76	100.59	100.23	100.06	100.52	99.52	100.16	100.23	99.96	88.16	99.73	100.76	100.03
2,974	2,996	2,977	2,982	2,975	2,999	2,981	3,005	3,027	2,959	2,998	2,968	2,987	3,000	2,989	2,990	3,009	3,022	2,998	2,994	3,003	2,972	2,990	2,990	2,992	2,981	2,995	2,966	2,990	2,978	2,983	2,853	2,976	2,985	2,986
1,975	1,969	1,977	1,969	1,993	1,978	1,974	1,963	1,982	1,940	2,017	1,960	1,961	1,953	1,970	1,961	1,969	1,961	1,969	1,977	1,962	1,978	1,983	1,957	1,981	1,994	1,964	1,967	1,989	2,002	1,985	1,888	1,991	2,006	1,994
1,688	1,680	1,704	1,687	1,695	1,681	1,711	1,705	1,668	1,728	1,705	1,742	1,734	1,730	1,740	1,748	1,736	1,716	1,759	1,733	1,754	1,785	1,759	1,781	1,770	1,777	1,807	1,825	1,825	1,825	1,848	2,147	1,861	1,865	1,865
0.986	0.973	0.973	0.989	0.97	0.958	0.967	0.947	0.919	1,043	0.885	1,002	0.966	0.964	0.961	0.96	0.927	0.946	0.942	0.969	0.968	0.966	0.978	0.995	0.97	0.983	0.976	1,022	0.981	1,006	1,019	1,120	1,044	1,005	1,021
0.034	0.026	0.031	0.035	0.033	0.036	0.037	0.036	0.034	0.033	0.03	0.032	0.034	0.031	0.03	0.034	0.032	0.034	0.031	0.034	0.041	0.037	0.035	0.039	0.039	0.036	0.036	0.039	0.038	0.036	0.035	0.042	0.037	0.039	0.045
0.381	0.375	0.372	0.372	0.362	0.359	0.362	0.36	0.353	0.369	0.358	0.347	0.35	0.345	0.335	0.336	0.333	0.319	0.317	0.31	0.287	0.301	0.274	0.269	0.266	0.252	0.245	0.233	0.19	0.173	0.155	0.154	0.119	0.112	0.107
0.37	0.37	0.36	0.37	0.36	0.36	0.36	0.36	0.36	0.38	0.34	0.37	0.36	0.36	0.36	0.36	0.35	0.36	0.35	0.36	0.36	0.35	0.36	0.36	0.35	0.36	0.35	0.36	0.35	0.36	0.36	0.34	0.36	0.35	0.35
0.55	0.55	0.55	0.55	0.55	0.55	0.56	0.56	0.56	0.55	0.57	0.56	0.56	0.56	0.57	0.57	0.57	0.57	0.58	0.57	0.58	0.58	0.58	0.58	0.58	0.58	0.59	0.59	0.60	0.60	0.60	0.62	0.61	0.62	0.61
0.32	0.32	0.32	0.32	0.32	0.32	0.31	0.31	0.31	0.33	0.30	0.32	0.31	0.31	0.31	0.31	0.31	0.31	0.31	0.32	0.32	0.31	0.32	0.32	0.32	0.32	0.32	0.33	0.32	0.33	0.33	0.32	0.34	0.33	0.34
0.01	0.01	0.01	0.01	0.01	0.01	0.01	0.01	0.01	0.01	0.01	0.01	0.01	0.01	0.01	0.01	0.01	0.01	0.01	0.01	0.01	0.01	0.01	0.01	0.01	0.01	0.01	0.01	0.01	0.01	0.01	0.01	0.01	0.01	0.02
0.12	0.12	0.12	0.12	0.12	0.12	0.12	0.12	0.12	0.12	0.12	0.11	0.11	0.11	0.11	0.11	0.11	0.11	0.10	0.10	0.09	0.10	0.09	0.09	0.09	0.08	0.08	0.08	0.06	0.06	0.05	0.04	0.04	0.04	0.04

71	72	73	74	75	76	77	78	79	80
2047	2067	2088	2108	2129	2149	2170	2190	2211	2231
38.56	39.54	39.40	38.82	39.29	38.72	39.64	39.70	39.25	39.40
22,12	22,06	21.94	21.98	21.89	22.28	22.35	21.88	22.00	21.98
26,08	26.51	26.21	26.18	26.48	26.70	26.56	26.35	26.59	26.31
10,38	10,54	10,64	10,73	10,81	10,77	10,80	10,79	10,87	10,94
0.50	0.58	0.59	0.56	0.57	0.50	0.48	0.55	0.61	0.60
1,80	1,69	1,63	1,48	1,42	1,36	1,23	1,10	1,16	1,14
99.44	100.93	100.41	99.75	100.46	100.32	101.07	100.37	100.47	100.36
2,969	2,998	3,000	2,978	2,993	2,958	2,995	3,018	2,989	2,998
2,007	1,971	1,969	1,987	1,965	2,006	1,990	1,960	1,974	1,971
1,679	1,681	1,669	1,679	1,687	1,706	1,678	1,675	1,694	1,674
1,192	1,191	1,208	1,227	1,227	1,226	1,216	1,222	1,233	1,240
0.033	0.038	0.038	0.036	0.037	0.032	0.031	0.035	0.039	0.038
0.148	0.138	0.133	0.121	0.116	0.111	0.1	0.09	0.095	0.093
0.42	0.42	0.42	0.42	0.42	0.42	0.42	0.42	0.42	0.43
0.55	0.55	0.55	0.55	0.55	0.56	0.56	0.55	0.55	0.55
0.39	0.39	0.40	0.40	0.40	0.40	0.40	0.40	0.40	0.41
0.01	0.01	0.01	0.01	0.01	0.01	0.01	0.01	0.01	0.01
0.05	0.05	0.04	0.04	0.04	0.04	0.03	0.03	0.03	0.03

83	84	85	86	87	88	89	90	91	92	93
2214	2239	2265	2290	2315	2340	2365	2391	2416	2441	2466
39.91	39.06	39.25	39.25	39.78	38.97	39.58	39.71	39.53	39.00	39.67
22.15	22.34	22.25	22,11	22.33	22,08	22.24	22.13	22.44	22.18	22.44
24.90	25,10	24.45	25.33	25.26	25.46	25.53	25.33	25.41	25.52	26,02
10,37	10,73	10,63	10,75	10,81	11,10	11,01	11,12	11,07	11,26	11,48
0.46	0.53	0.49	0.43	0.54	0.48	0.54	0.51	0.46	0.57	0.48
3,23	3,08	2,83	2,59	2,43	2,22	2,08	1,75	1,65	1,39	1,23
101.02	100.83	99.91	100.46	101.16	100.32	100.98	100.57	100.55	99.93	101.31
3,010	2,960	2,989	2,982	2,996	2,967	2,989	3,004	2,990	2,975	2,983
1,969	1,996	1,997	1,980	1,982	1,982	1,979	1,973	2,000	1,994	1,989
1,571	1,591	1,557	1,610	1,591	1,621	1,612	1,603	1,607	1,628	1,636
1,166	1,212	1,207	1,217	1,214	1,260	1,239	1,254	1,248	1,281	1,286
0.029	0.034	0.031	0.028	0.034	0.031	0.035	0.033	0.03	0.037	0.03
0.261	0.25	0.231	0.211	0.196	0.181	0.168	0.142	0.134	0.113	0.099
0.43	0.43	0.44	0.43	0.43	0.44	0.44	0.44	0.44	0.44	0.44
0.52	0.52	0.52	0.53	0.52	0.52	0.53	0.53	0.53	0.53	0.54
0.39	0.39	0.40	0.40	0.40	0.41	0.41	0.41	0.41	0.42	0.42
0.01	0.01	0.01	0.01	0.01	0.01	0.01	0.01	0.01	0.01	0.01
0.09	0.08	0.08	0.07	0.07	0.06	0.06	0.05	0.04	0.04	0.03

76	77	78	79	80	81	82	83	84	85
1884	1904	1924	1943	1963	1983	2003	2023	2042	2062
38.96	39.43	38.72	38.81	39.49	39.12	39.34	35.88	39.26	39.11
22.22	22,06	22,04	22.28	22.40	22.17	22.34	22.28	22.26	22,03
26.50	26.81	26.97	26.73	27,05	26.94	26.74	26.60	27,10	26.88
10,30	10,42	10,43	10,31	10,37	10,51	10,50	10,23	10,50	10,42
0.51	0.55	0.57	0.49	0.52	0.50	0.57	0.45	0.53	0.49
1,90	1,88	1,75	1,67	1,64	1,56	1,51	1,06	1,29	1,26
100.39	101.15	100.48	100.29	101.47	100.80	100.99	96.50	100.93	100.20
2,974	2,989	2,962	2,968	2,983	2,976	2,982	2,867	2,982	2,990
1,999	1,971	1,987	2,008	1,994	1,988	1,996	2,098	1,992	1,985
1,692	1,700	1,726	1,709	1,709	1,714	1,695	1,778	1,721	1,719
1,172	1,178	1,190	1,175	1,167	1,192	1,187	1,219	1,189	1,188
0.033	0.035	0.037	0.032	0.033	0.032	0.037	0.03	0.034	0.032
0.155	0.153	0.144	0.137	0.132	0.127	0.123	0.091	0.105	0.103
0.41	0.41	0.41	0.41	0.41	0.41	0.41	0.41	0.41	0.41
0.55	0.55	0.56	0.56	0.56	0.56	0.56	0.57	0.57	0.57
0.38	0.38	0.38	0.39	0.38	0.39	0.39	0.39	0.39	0.39
0.01	0.01	0.01	0.01	0.01	0.01	0.01	0.01	0.01	0.01
0.05	0.05	0.05	0.05	0.04	0.04	0.04	0.03	0.03	0.03

127	128
3561	3586
38.84	38.54
21.80	21.87
29.21	29.49
8,75	8,48
0.57	0.62
1,33	1,27
100.50	100.27
2,995	2,985
1,982	1,997
1,884	1,910
1,006	0.979
0.037	0.041
0.11	0.105
0.35	0.34
0.62	0.63
0.33	0.32
0.01	0.01
0.04	0.04

Garnet A

pt	Ce	Cr	Dy	Er	Eu	Gd	Ho	La	Li	Lu	Nd	Pr	Sc	Sm	Tb	Tm	Yb	Y	P
0	1.86		0.1519	0.0447		0.4531	0.038	2.772		0.02904	2.3333			0.29963	0.0509	0.00217	0.064	2.071	91.579
1	1.609		0.1821	0.0595		0.5502	0.0503	2.34		0.0296	1.9165			0.25297	0.08675	0.01049	0.1467	2.482	90.958
2	1.349		0.318	0.1018		0.6472	0.0624	1.903		0.03015	1.4997			0.20631	0.12261	0.0188	0.2294	2.893	89.444
3	1.088		0.4539	0.1441		1.0032	0.0745	1.466		0.03071	1.0829			0.15966	0.15846	0.02712	0.3121	3.304	87.931
4	1.018		0.5897	0.1864		1.3756	0.0867	1.224		0.03516	0.9919			0.17438	0.19828	0.04841	0.3389	5.28	99.82
5	1.063		0.9153	0.3476		1.7481	0.157	1.101		0.03985	0.9216			0.193	0.23835	0.07052	0.3622	7.355	119.863
6	1.109		1.253	0.5163		2.851	0.2309	0.978		0.04455	0.8514			0.21163	0.27841	0.09264	0.3855	9.43	139.907
7	1.432		1.5906	0.6851		4.3983	0.3048	0.918		0.24623	0.7896			0.3075	0.73199	0.35825	2.0338	29.519	155.326
8	2.393		4.8303	2.4033		5.9457	0.9318	1.002		0.56778	0.733			0.45038	1.43719	0.77204	4.6709	60.569	160.112
9	3.354		9.8359	5.0644		7.426	1.8952	1.085		0.88933	0.6764			0.59326	2.1424	1.18583	7.308	91.62	164.897
10	4.315		14.8415	7.7256		8.7522	2.8587	1.169		1.14552	0.696			0.82521	2.74887	1.52021	9.3927	118.124	169.682
11	5.565		19.4122	9.8832		10.0785	3.6852	1.536		1.25144	0.8906			1.26194	3.12831	1.672	10.2073	134.175	164.325
12	6.819		22.983	10.8829		11.4047	4.1971	1.907		1.35735	1.0851			1.69867	3.50775	1.8238	11.022	150.225	158.809
13	8.074		26.5537	11.8825		11.6134	4.709	2.279		1.46327	1.2797			2.13541	3.88718	1.97559	11.8366	166.276	153.292
14	10.063		30.1245	12.8822		11.8045	5.2209	2.665		1.33786	1.558			2.58691	3.54009	1.72663	10.1753	147.884	151.457
15	12.42		26.5121	11.4688		11.9956	4.7261	3.058		1.20881	1.8375			3.03864	3.18157	1.47137	8.4751	128.951	151.468
16	14.777		22.7866	10.0173		11.7002	4.2154	3.451		1.07975	2.1171			3.49037	2.82305	1.21612	6.7748	110.017	151.479
17	15.298		19.0612	8.5659		11.1607	3.7047	3.498		0.97423	2.4541			3.66089	2.62317	1.07616	5.93	97.494	146.5
18	12.368		16.9492	7.5958		10.6213	3.2682	2.894		0.88051	2.8198			3.69033	2.50287	0.99405	5.5144	88.187	132.145
19	9.439		15.6467	6.8672		10.0574	2.8689	2.29		0.78678	3.1856			3.71978	2.38257	0.91194	5.0987	78.879	117.789
20	6.556		14.3442	6.1386		9.4475	2.4696	1.697		0.70645	3.2478			3.69317	2.25589	0.8727	4.7983	72.322	109.672
21	5.262		13.3785	5.7714		8.8376	2.2471	1.467		0.65129	2.7395			3.56126	2.11721	0.914	4.7143	70.93	~~312.224~~
22	3.969		13.0456	6.0831		8.2574	2.3568	1.238		0.59613	2.2312			3.42934	1.97852	0.9553	4.6304	69.538	~~514.776~~
23	2.675		12.7127	6.3948		8.6784	2.4665	1.008		0.54378	1.7642			3.32224	1.84523	0.99346	4.5553	68.177	~~717.328~~
24	2.15		12.3826	6.6958		9.0995	2.5725	0.992		0.58638	2.6945			4.05312	1.89392	0.92537	4.779	67.866	~~638.859~~
25	1.94		12.1448	6.6346		9.5205	2.5542	1.063		0.62899	3.6248			4.784	1.94261	0.85729	5.0026	67.554	~~445.705~~
26	1.729		11.9069	6.5735		9.4839	2.5359	1.134		0.67159	4.555			5.51488	1.9913	0.78921	5.2263	67.243	~~252.551~~
27	1.557		11.6691	6.5123		9.2605	2.5176	1.155		0.69316	4.251			5.27463	1.97381	0.86347	5.4427	69.041	134.221
28	1.444		12.192	6.8351		9.0371	2.5429	1.097		0.70615	3.4433			4.63807	1.92931	0.99581	5.6562	71.699	132.141
29	1.331		13.0253	7.3145		9.0635	2.5861	1.04		0.71914	2.6356			4.0015	1.88482	1.12815	5.8697	74.357	130.062
30	1.228		13.8586	7.794		9.4782	2.6292	0.97		0.78574	2.1427			3.72349	1.88197	1.20442	6.2508	77.512	128.155
31	1.255		14.4692	8.3185		9.8928	2.8058	0.751		0.93564	2.1389			4.00254	1.94384	1.19356	6.8924	81.442	128.436
32	1.281		14.7336	8.9131		10.2874	3.1896	0.531		1.08554	2.1352			4.2816	2.00571	1.1827	7.534	85.371	128.717
33	1.308		14.9981	9.5078		10.427	3.5734	0.311		1.21826	2.1293			4.5367	2.06928	1.17899	8.1364	89.056	128.999
34	1.137		15.2975	10.0506		10.5667	3.9262	0.249		1.1329	2.0973			4.48767	2.15445	1.26602	8.2401	89.635	118.796
35	0.902		16.0408	9.9362		10.7063	3.8844	0.238		1.04755	2.0652			4.43863	2.23962	1.35305	8.3437	90.215	105.181
36	0.666		16.7841	9.8217		10.1987	3.8427	0.227		0.9622	2.0331			4.3896	2.32479	1.44008	8.4474	90.794	91.567
37	0.547		17.5274	9.7073		9.4804	3.801	0.225		1.06405	1.8197			4.40169	2.32347	1.47192	8.565	91.41	82.373
38	0.578		17.6393	9.8939		8.7621	3.8461	0.235		1.22683	1.5472			4.43369	2.294	1.4858	8.687	92.038	78.902
39	0.608		17.5458	10.1785		8.6386	3.9195	0.244		1.38962	1.2747			4.46569	2.26453	1.49968	8.8091	92.666	75.432
40	0.649		17.4522	10.4631		9.2851	3.9929	0.249		1.52567	1.2594			4.34443	2.29067	1.54262	9.0799	95.612	74.423
41	0.768		17.4154	11.0453		9.9316	4.0967	0.219		1.6271	1.5771			4.02478	2.3888	1.62316	9.5433	101.559	91.953
42	0.887		17.452	12.0127		10.4274	4.2398	0.189		1.72854	1.8947			3.70513	2.48693	1.70371	10.0067	107.505	109.482
43	1.006		17.4885	12.98		9.7878	4.3829	0.158		1.80574	2.2051			3.43836	2.57116	1.77768	10.4783	112.856	127.011
44	1.847		17.6022	13.8254		9.1483	4.5218	0.326		1.70054	2.4611			3.56967	2.55072	1.80207	11.0112	113.723	119.478
45	2.871		18.296	13.7518		8.5088	4.6286	0.543		1.59533	2.7171			3.70098	2.53029	1.82647	11.5441	114.589	105.627
46	3.896		18.9899	13.6781		8.7004	4.7354	0.761		1.49013	2.973			3.83229	2.50985	1.85087	12.077	115.456	91.776
47	4.507		19.6837	13.6045		9.1015	4.8421	0.906		1.55023	2.8157			4.0058	2.57753	1.88918	12.6137	118.4	83.744
48	4.671		20.5477	14.1437		9.5026	4.9528	0.972		1.65201	2.5541			4.18996	2.66742	1.93099	13.1514	121.868	82.013
49	4.836		21.4547	14.8374		9.6217	5.0644	1.038		1.75379	2.2926			4.37411	2.75731	1.97279	13.6891	125.335	80.282
50	4.861		22.3616	15.5311		9.4356	5.176	1.076		1.83379	2.5602			4.45731	2.73329	2.01011	13.9355	126.941	78.173
51	4.165		22.9533	15.8445		9.2495	5.2214	0.966		1.89021	3.4008			4.43118	2.58592	2.04256	13.8663	126.529	74.108
52	3.469		23.2036	15.7461		9.0241	5.1951	0.856		1.94662	4.2414			4.40504	2.43854	2.07501	13.7972	126.118	70.042
53	2.772		23.4539	15.6477		8.5952	5.1689	0.746		1.98719	4.8224			4.36017	2.30941	2.11059	13.7157	125.48	65.976
54	2.918		23.5455	15.5745		8.1663	5.1444	0.781		1.94552	4.0554			4.21799	2.27496	2.16245	13.5704	123.664	70.049
55	3.22		22.813	15.6327		7.7373	5.1295	0.844		1.90385	3.2884			4.07582	2.24052	2.21431	13.425	121.847	75.638
56	3.522		22.0806	15.6908		8.1397	5.1147	0.907		1.86218	2.5214			3.93365	2.20607	2.26617	13.2796	120.031	81.227
57	3.434		21.3481	15.7489		8.6971	5.0998	0.871		1.9769	2.7065			3.99963	2.23773	2.39647	13.7633	124.568	81.252
58	2.991		21.6095	16.3126		9.2544	5.3649	0.746		2.12076	3.0689			4.10441	2.28171	2.54139	14.3643	130.288	76.23
59	2.548		22.0561	16.9705		9.4398	5.6822	0.621		2.26462	3.4314			4.20918	2.32569	2.6863	14.9652	136.009	71.208
60	2.154		22.5027	17.6285		9.2876	5.9996	0.517		2.36095	3.5445			4.34581	2.40106	2.71737	15.5657	139.75	67.025
61	1.946		22.5992	18.1489		9.1355	6.1969	0.495		2.41417	3.4314			4.51133	2.50489	2.64516	16.1659	141.695	66.082
62	1.738		22.3782	18.5448		8.9514	6.2853	0.473		2.46738	3.3183			4.67686	2.60873	2.57294	16.766	143.639	65.139
63	1.531		22.1572	18.9406		8.6443	6.3738	0.452		2.51567	3.2011			4.78074	2.65917	2.52312	17.1981	144.656	64.195
64	1.519		22.0676	19.1901		8.3371	6.4349	0.404		2.54494	3.0683			4.64671	2.50352	2.55971	16.9815	142.092	66.733
65	1.533		22.4852	18.8748		8.0299	6.3902	0.353		2.57422	2.9354			4.51267	2.34786	2.5963	16.765	139.528	69.713
66	1.547		22.9028	18.5596		7.5365	6.3455	0.302		2.60349	2.8026			4.37863	2.1922	2.63289	16.5484	136.964	72.693
67	1.404		23.3204	18.2443		7.0194	6.3008	0.268		2.53808	2.9571			4.00292	2.22103	2.75555	17.2192	139.144	80.988
68	1.143		23.459	18.6565		6.5023	6.1274	0.248		2.46062	3.1482			3.59647	2.27331	2.88916	18.0029	141.927	93.315
69	0.881		23.5622	19.1613		6.6482	5.9375	0.228		2.38316	3.3393			3.19003	2.3256	3.02277	18.7867	144.71	105.642
70	0.676		23.6653	19.6661		7.2972	5.7477	0.239		2.4299	3.5237			3.18426	2.38793	3.0833	19.2082	147.768	111.24
71	0.638		23.6843	20.2382		7.9463	5.9685	0.342		2.57086	3.703			3.48253	2.45788	3.0884	19.3551	151.032	96.655
72	0.6		23.6394	20.8613		8.2637	6.5008	0.446		2.71183	3.8823			3.78079	2.52783	3.09349	19.5019	154.297	82.069
73	0.563		23.5945	21.4845		7.5865	7.0331	0.55		2.83858	4.0042			4.00627	2.54916	3.10521	19.6817	156.381	67.483
74	0.507		23.6082	21.6918		6.9092	7.3961	0.53		2.92269	3.9537			4.01341	2.42461	3.13677	19.9605	154.924	66.726
75	0.45		23.7978	20.6515		6.232	7.2512	0.502		3.0068	3.9033			4.02055	2.30007	3.16833	20.2393	153.466	66.988
76	0.393		23.9875	19.6112		6.5628	7.1064	0.473		3.09091	3.8529			4.02769	2.17552	3.1999	20.5181	152.009	67.249
77	0.46		24.1771	18.5709		6.9679	6.9615	0.452		3.16601	3.7232			3.84279	2.25385	3.1453	20.8389	155.156	66.028
78	0.604		24.5495	19.684		7.3729	7.014	0.436		3.24045	3.5878			3.64375	2.34712	3.08436	21.1628	158.642	63.869
79	0.749		24.9354	20.9556		7.6812	7.081	0.419		3.31489	3.4523			3.44472	2.44039	3.02342	21.4867	162.128	61.71
80	0.851		25.3213	22.2272		7.9284	7.1481	0.393		3.31575	3.5333			3.58594	2.39187	3.05864	21.7233	165.594	59.785
81	0.854		25.9433	22.7552		8.1756	7.2179	0.345		3.27014	3.751			3.94214	2.25378	3.15459	21.9046	169.046	58.42
82	0.856		26.7145	22.8134		8.3123	7.2894	0.297		3.22452	3.9686			4.29833	2.11569	3.25055	22.086	172.498	57.055
83	0.858		27.4856	22.8717		8.1842	7.3609	0.249		3.24024	4.132			4.4669	2.06746	3.36191	22.6914	176.46	55.69
84	1.158		28.1399	23.2784		8.0561	7.4131	0.422		3.40308	4.1652			4.18543	2.23478	3.51024	24.314	181.644	76.317
85	1.465		28.5138	24.5211		7.928	7.419	0.599		3.56592	4.1984			3.90397	2.40209	3.65856	25.9366	186.827	97.494
86	1.772		28.8877	25.7638		7.9795	7.4249	0.777		3.72875	4.2316			3.6225	2.56941	3.80688	27.5592	192.011	118.67
87	1.624		29.2615	27.0064		8.0354	7.4308	0.732		3.74929	4.9704			3.58948	2.63524	3.823	26.3606	191.959	111.462
88	1.239		29.1019	26.8396		8.0913	7.5477	0.572		3.76627	5.7267			3.56266	2.69854	3.83583	25.0916	191.777	89.44
89	0.853		28.929	26.6377		8.1017	7.6673	0.411		3.78325	6.483			3.53583	2.76185	3.84866	23.8226	191.595	67.418
90	0.605		28.756	26.4357		8.0883	7.7869	0.362		3.71948	6.4897			3.39189	2.77234	3.81572	23.3685	189.014	59.01
91	0.624		28.0781	25.3411		8.075	7.8313	0.529		3.61356	6.1052			3.18682	2.75527	3.75889	23.3396	185.181	77.207
92	0.643		27.1366	23.7806		8.0019	7.8364	0.695		3.50764	5.7207			2.98175	2.73819	3.70206	23.3108	181.348	95.405
93	0.66		26.1951	22.2201		7.8124	7.8415	0.854		3.52514	5.4962			2.82215	2.73829	3.67577	23.8068	180.107	113.128
94	0.624		25.7156	21.9679		7.6229	7.8536	0.613		3.78385	5.5843			2.75143	2.77194	3.70915	25.3285	183.929	107.5
95	0.588		26.1389	24.2724		7.4432	7.8794	0.372		4.04255	5.6724			2.68071	2.80559	3.74253	26.8502	187.752	101.871
96	0.552		26.5623	26.5769		7.7481	7.9052	0.131		4.30178	5.7608			2.61942	2.84067	3.77945	28.3604	191.674	96.243
97	0.515		27.0102	28.8575		8.053	7.9405	0.119		4.5873	5.8614			3.02263	2.94592	3.99079	29.3042	200.536	97.564
98	0.478		28.6645	29.9609		8.3579	8.4434	0.204		4.87282	5.962			3.42584	3.05116	4.20212	30.2479	209.398	101.844
99	0.441		30.3189	31.0642		8.364	8.9462	0.29		5.15834	6.0626			3.82905	3.15641	4.41346	31.1916	218.259	106.124
100	0.396		31.9732	32.1675		8.2427	9.4491	0.305		5.16958	5.7215			3.72266	3.11866	4.51356	32.0039	218.991	105.265
101	0.338		32.8157	32.1239		8.1214	9.5136	0.208		5.064	5.1924			3.39925	3.02002	4.56629	32.7602	216.261	96.119
102	0.281		33.3124	31.5919		8.1318	9.3915	0.111		4.95843	4.6632			3.07584	2.92138	4.61903	33.5165	213.53	86.972
103	0.229		33.8091	31.0599		8.3545	9.2693	0.02		4.885	4.4032			2.9529	2.86699	4.65035	33.5545	212.63	78.591
104	0.265		33.8174	30.6795		8.5772	9.2675	0.031		4.86342	4.5775			3.15324	2.88398	4.64715	32.434	214.68	81.389
105	0.301		33.0378	30.5437		8.802	9.4597	0.041		4.84183	4.7517			3.35359	2.90097	4.64395	31.3136	216.731	84.186
106	0.337		32.2582	30.4079		9.057	9.652	0.051		4.82726	4.917			3.54304	2.92296	4.65105	30.3593	219.066	86.984
107	0.352		31.5921	30.3616		9.3121	9.8434	0.069		4.91507	4.9524			3.57344	3.01789	4.80841	31.8296	225.549	73.836
108	0.358		32.5813	31.621		9.5671	10.0226	0.09		5.00287	4.9878			3.60385	3.11282	4.96578	33.2999	232.033	55.248
109	0.365		33.5706	32.8804		9.0383	10.2018	0.112		5.09068	5.0233			3.63426	3.20775	5.12314	34.7702	238.516	36.659
110	0.365		34.5598	34.1398		8.2421	10.381	0.122		5.27173	5.1513			4.07534	3.20807	5.32541	35.9313	245.508	26.524
111	0.358		34.9688	34.5671		7.4458	10.5309	0.118		5.48458	5.3111			4.65657	3.17612	5.54299	36.987	252.675	27.734
112	0.35		35.1797	34.7106		7.1279	10.6708	0.114		5.69744	5.4708			5.23779	3.14416	5.76058	38.0426	259.842	28.944
113	0.348		35.3907	34.854		7.4518	10.8107	0.114		5.8578	5.726			5.40762	3.14144	5.8528	39.0315	264.997	30.821
114	0.396		35.8871	35.123		7.7758	10.9684	0.154		5.94771	6.1095			5.02537	3.17796	5.77676	39.9307	267.454	38.192
115	0.443		36.7667	35.5604		8.0515	11.15	0.193		6.03761	6.493			4.64312	3.21447	5.70073	40.8299	269.911	45.564
116	0.49		37.6462	35.9978		7.9306	11.3316	0.233		6.10087	6.8051			4.25365	3.23542	5.60714	41.4944	270.9	52.935
117	0.809		38.2573	36.2643		7.8096	11.4476	0.349		5.945	6.5297			3.80491	3.12829	5.36912	40.2283	259.82	55.152
118	1.199		36.6597	35.1249		7.6886	11.0244	0.486		5.78912	6.2544			3.35617	3.02116	5.13111	38.9622	248.74	55.999
119	1.59		35.0622	33.9855		7.5768	10.6012	0.624		5.63324	5.9791			2.90742	2.91403	4.89309	37.6962	237.66	56.845
120	1.591		33.4647	32.8461		7.4674	10.1781	0.612		5.71773	6.5027			2.93034	2.89635	5.03335	37.8537	245.011	57.301
121	1.154		33.8459	33.1601		7.3581	10.1935	0.434		5.86619	7.2388			3.07877	2.90248	5.27428	38.39	257.266	57.321
122	0.717		34.7538	33.8608		7.466	10.3257	0.255		6.01465	7.9749			3.2272	2.90861	5.51521	38.9264	269.521	57.341
123	0.353		35.6616	34.5615		7.8178	10.4579	0.109		6.13994	7.9967			3.44767	2.96651	5.69762	39.8666	274.788	56.802
124	0.392		36.5607	35.1133		8.1696	10.6844	0.137		6.23925	7.2168			3.74895	3.08252	5.81438	41.2601	272.212	53.162
125	0.431		37.4498	35.4981		8.3916	11.0167	0.166		6.33855	6.437			4.05024	3.19853	5.93115	42.6535	269.636	49.522
126	0.47		38.3389	35.8829		7.8929	11.3491	0.194		6.41572	5.7731			4.24447	3.26136	5.98483	43.4188	266.696	45.883
127	0.581		38.9859	36.1369		7.3941	11.5509	0.222		6.36997	5.7522			3.84443	3.02899	5.68843	40.697	261.74	45.416
128	0.706		38.2894	35.6645		6.8954	11.0283	0.25		6.32423	5.7314			3.44439	2.79662	5.39203	37.9752	256.783	45.58
129	0.831		37.5928	35.1921		6.2855	10.5058	0.279		6.27849	5.7105			3.04435	2.56425	5.09563	35.2533	251.826	45.745
130	0.814		36.8962	34.7196		5.6535	9.9832	0.276		6.07346	5.4674			3.35534	2.48733	4.7737	33.5176	239.612	44.186
131	0.665		34.8359	32.5273		5.0216	9.32	0.246		5.83675	5.18			3.80778	2.44133	4.44669	31.978	225.955	41.008
132	0.516		32.5044	29.9929		4.9466	8.6289	0.215		5.60004	4.8926			4.26023	2.39534	4.11968	30.4385	212.298	37.83
133	0.387		30.1728	27.4584		5.3951	7.9377	0.188		5.49559	4.7412			4.25745	2.41619	4.01001	29.9334	207.467	36.958
134	0.34		29.036	26.6149		5.8435	7.8125	0.176		5.51547	4.7177			3.8268	2.49987	4.10463	30.4007	210.932	45.494
135	0.293		29.0221	27.3607		6.3363	8.2194	0.164		5.53534	4.6941			3.39615	2.58355	4.19925	30.868	214.397	54.029
136	0.246		29.0083	28.1066		7.0095	8.6263	0.152		5.61759	4.6954			3.11694	2.68661	4.38042	31.9221	221.904	62.565
137	0.213		29.9455	29.3805		7.6827	9.1111	0.135		5.95423	4.7978			3.4554	2.86871	4.91464	35.3693	245.896	58.014
138	0.182		34.762	32.8083		8.3559	9.9137	0.118		6.29088	4.9001			3.79385	3.0508	5.44885	38.8165	269.888	51.65
139	0.151		39.5785	36.2361		7.4982	10.7164	0.1		6.62752	5.0025			4.13231	3.2329	5.98307	42.2637	293.88	45.285
140	0.172		44.395	39.6639		6.4284	11.519	0.12		5.87822	4.3033			3.94069	2.85081	5.24152	36.9794	259.85	38.107
141	0.236		38.4457	34.7912		5.3586	10.314	0.168		4.97848	3.493			3.67564	2.39056	4.32324	30.4853	217.781	30.288
142	0.3		31.0048	28.7684		4.2258	8.8308	0.217		4.07874	2.6828			3.41058	1.93032	3.40495	23.9913	175.712	22.469
143	0.325		23.564	22.7457		3.0436	7.3477	0.238		3.15756	2.0184			2.81472	1.47177	2.58126	18.1106	134.023	15.74
144	0.23		17.2983	17.1702		1.8613	5.6894	0.167		2.21952	1.4687			1.95866	1.01456	1.83197	12.7123	92.632	12.442
145	0.135		11.957	11.9464		0.904	3.8935	0.097		1.28148	0.919			1.10259	0.55735	1.08268	7.314	51.24	9.144
146	0.041		6.6157	6.7226		0.6545	2.0975	0.026		0.53554	0.4851			0.42981	0.19863	0.48591	3.0304	18.771	5.846
147	0.027		2.433	2.6171		0.4051	0.6956	0.019		0.39413	0.4154			0.33378	0.14985	0.36905	2.2542	14.379	6.618
148	0.02		1.8964	2.0308		0.1557	0.5337	0.018		0.25272	0.3457			0.23775	0.10106	0.25219	1.478	9.986	7.73
149	0.013		1.3597	1.4445		0.1506	0.3718	0.017		0.11131	0.2761			0.14172	0.05228	0.13534	0.7019	5.593	8.843
150	48.036		0.8231	0.8582		0.1659	0.2098	26.634		0.11194	0.2671			0.15288	0.05762	0.1314	0.7507	5.827	25.83
151	127.551		0.8214	0.7968		0.1813	0.2127	70.704		0.12449	0.2633			0.17304	0.06751	0.13694	0.8688	6.448	53.226
152	207.066		0.8647	0.7795		0.7709	0.2294	114.774		0.13705	0.2594			0.1932	0.0774	0.14248	0.9869	7.069	80.622
153	241.356		0.9079	0.7622		1.7371	0.246	133.726		0.17937	16.7987			1.73172	0.12071	0.18326	1.2864	9.099	93.319
154	162.407		1.1339	0.9105		2.7032	0.3151	89.783		0.24122	44.185			4.2658	0.18594	0.24716	1.7048	12.052	69.213
155	83.459		1.4797	1.1673		3.1645	0.4186	45.84		0.30307	71.5713			6.79988	0.25117	0.31105	2.1232	15.005	45.106
156	4.511		1.8255	1.4242		2.3618	0.5221	1.897		0.3742	83.3873			7.91407	0.30754	0.38253	2.6371	18.753	21
157	2.095		2.261	1.8338		1.5591	0.656	0.669		0.46859	56.2173			5.47307	0.34173	0.473	3.39	24.49	23.23
158	2.307		2.9209	2.626		0.7564	0.8664	0.907		0.56297	29.0474			3.03207	0.37592	0.56347	4.1429	30.228	26.364

159	2.519	3.5809	3.4181	1.3552	1.0767	1.144	0.65736	1.8774	0.59107	0.4101	0.65394	4.8957	35.966	29.499
160	2.435	4.2408	4.2103	2.0021	1.287	1.161	0.96452	1.289	0.84048	0.62683	0.94732	6.8457	51.802	35.562
161	2.19	6.5052	6.2974	2.649	1.784	1.058	1.27897	1.6131	1.18223	0.84982	1.24767	8.8368	67.985	43.216
162	1.945	8.8246	8.4289	3.1697	2.2909	0.955	1.59343	1.9371	1.52398	1.0728	1.54801	10.8279	84.168	50.869
163	1.646	11.1441	10.5605	3.6218	2.7977	0.808	1.94489	1.983	1.71087	1.16039	1.79613	12.7226	93.4	55.016
164	1.239	12.6919	12.1337	4.0738	3.2921	0.573	2.31643	1.8779	1.81372	1.1745	2.0159	14.5649	98.859	52.033
165	0.831	13.8209	13.4039	4.4212	3.7798	0.338	2.68797	1.7728	1.91657	1.18861	2.23568	16.4073	104.319	49.05
166	0.428	14.95	14.6741	4.5557	4.2674	0.106	3.12895	1.9474	2.27832	1.33334	2.60492	19.0185	120.28	46.168
167	0.413	17.276	16.7356	4.6901	5.039	0.123	3.71115	2.691	3.16658	1.74372	3.27811	23.1932	157.597	52.323
168	0.397	22.0362	20.406	4.8397	6.3879	0.141	4.29335	3.4346	4.05483	2.1541	3.9513	27.3678	194.915	58.477
169	0.382	26.7963	24.0765	6.345	7.7369	0.158	4.87149	4.1813	4.92959	2.56222	4.62066	31.5207	231.984	64.631
170	0.353	31.5244	27.7313	7.8503	9.0768	0.148	5.08746	5.2066	4.59777	2.7682	4.94686	33.7366	246.828	76.554
171	0.317	33.3838	29.9913	9.3556	9.6063	0.126	5.30342	6.2319	4.26595	2.97417	5.27305	35.9524	261.672	91.038
172	0.281	35.2432	32.2513	9.4707	10.1359	0.103	5.51938	7.2572	3.93412	3.18015	5.59925	38.1682	276.517	105.523
173	0.244	37.1026	34.5112	8.9685	10.6654	0.083	5.70257	7.2024	3.99884	3.22717	5.62221	38.6719	283.523	106.29
174	0.206	37.6702	35.6074	8.4662	10.7535	0.064	5.8712	6.6679	4.23965	3.2036	5.51051	38.4152	287.049	84.087
175	0.167	37.6641	36.1868	8.1465	10.6456	0.046	6.03982	6.1334	4.48046	3.18003	5.39882	38.1586	290.575	61.884
176	0.14	37.658	36.7662	8.1324	10.5376	0.032	5.98365	5.7606	4.47782	3.13871	5.21654	37.3997	286.872	41.589
177	0.286	37.1464	36.2216	8.1182	10.3597	0.091	5.55101	5.6586	4.06749	3.06767	4.91606	35.7998	271.065	53.883
178	0.432	35.7883	33.795	8.0991	10.0646	0.151	5.11838	5.5566	3.65717	2.99664	4.61558	34.1999	255.258	66.177
179	0.579	34.4301	31.3684	7.994	9.7695	0.21	4.69814	5.4629	3.27255	2.92565	4.33517	32.6128	240.073	78.47
180	0.542	33.0899	29.0607	7.8889	9.4779	0.205	4.48958	5.5107	3.32696	2.85558	4.39755	31.2458	235.503	74.387
181	0.441	32.0573	28.7845	7.7839	9.2449	0.177	4.28103	5.5586	3.38136	2.7855	4.45992	29.8788	230.934	64.451
182	0.339	31.0246	28.5083	7.872	9.0119	0.149	4.07247	5.6064	3.43576	2.71542	4.5223	28.5117	226.364	54.516
183	0.271	29.9919	28.2322	8.0292	8.7789	0.132	4.12907	5.4291	3.85555	2.77124	4.49427	28.2899	224.325	49.303
184	0.251	30.4222	28.1313	8.1864	8.79	0.128	4.28042	5.1713	4.40591	2.87205	4.43394	28.4773	223.19	50.662
185	0.231	31.3753	28.0931	8.2531	8.8884	0.124	4.43178	4.9136	4.95626	2.97286	4.3736	28.6648	222.056	52.022
186	0.226	32.3283	28.055	8.1938	8.9867	0.127	4.53379	4.979	5.17207	3.07366	4.28699	28.505	222.643	53.993
187	0.361	32.5429	28.0652	8.1344	8.9792	0.186	4.56711	5.494	4.92233	3.17444	4.16379	27.862	225.628	61.502
188	0.497	31.7299	28.1429	8.1169	8.8242	0.245	4.60043	6.009	4.67258	3.27523	4.0406	27.219	228.612	69.01
189	0.632	30.9168	28.2206	8.4777	8.6693	0.304	4.60901	6.4943	4.44987	3.34642	3.93416	26.5645	230.18	76.518
190	0.59	30.152	28.2191	8.8384	8.5256	0.395	4.39379	6.7106	4.47161	3.15003	3.97918	25.8061	218.936	80.209
191	0.498	29.8227	27.5016	9.1992	8.483	0.496	4.17857	6.927	4.49335	2.95363	4.02419	25.0476	207.692	82.829
192	0.405	29.4935	26.7841	8.9165	8.4404	0.597	3.96335	7.1433	4.51509	2.75724	4.06921	24.2892	196.448	85.45
193	0.355	29.1643	26.0666	8.4533	8.3978	0.599	3.70556	6.7926	4.5214	2.6596	3.84428	23.5148	192.857	84.948
194	0.352	28.7075	24.9418	7.9902	8.3696	0.484	3.43585	6.2828	4.52339	2.58966	3.54364	22.7359	191.412	80.816
195	0.35	28.2149	23.7028	7.927	8.3455	0.37	3.16613	5.773	4.52537	2.51972	3.243	21.957	189.967	76.684
196	0.371	27.7223	22.4638	8.329	8.3213	0.266	3.02116	5.4182	4.52974	2.51967	3.1173	21.6492	187.533	74.528
197	0.535	27.4816	21.8418	8.731	8.2109	0.226	3.02125	5.2438	4.53687	2.60088	3.19499	21.8892	183.947	84.137
198	0.698	27.5337	21.9372	9.0576	8.0002	0.186	3.02134	5.0693	4.544	2.6821	3.27267	22.1292	180.362	93.747
199	0.862	27.5858	22.0325	8.9356	7.7894	0.145	3.02012	4.8763	4.54373	2.74452	3.31705	22.1611	177.067	103.357
200	0.808	27.5385	22.0849	8.8135	7.6028	0.124	3.01112	4.5727	4.49941	2.69502	3.16311	20.9545	175.501	95.627
201	0.708	26.8988	21.8812	8.6915	7.56	0.107	3.00212	4.2691	4.45509	2.64553	3.00917	19.7478	173.935	84.226
202	0.608	26.2591	21.6774	8.3948	7.5171	0.09	2.99311	3.9655	4.41077	2.59603	2.85524	18.5411	172.369	72.825
203	0.619	25.6193	21.4737	8.061	7.4743	0.152	2.86596	3.734	4.50403	2.59362	2.85156	17.9339	166.801	70.857
204	0.739	24.6881	20.4923	7.7272	7.2438	0.291	2.71378	3.5178	4.62642	2.60117	2.87971	17.4537	160.385	78.075
205	0.858	23.6952	19.3462	7.6719	6.9737	0.43	2.5616	3.3015	4.74882	2.60873	2.90786	16.9735	153.97	85.294
206	1.035	22.7023	18.2002	7.8878	6.7036	0.557	2.49443	3.3112	4.99519	2.5426	2.86372	16.4817	149.225	89.773
207	1.462	22.5117	17.6091	8.1037	6.4144	0.632	2.51004	3.541	5.3623	2.40472	2.74919	15.9786	146.106	82.422
208	1.889	23.1025	17.5584	8.3938	6.1067	0.707	2.52565	3.7708	5.72941	2.26684	2.63466	15.4755	142.987	75.072
209	2.316	23.6934	17.5078	9.0046	5.799	0.781	2.51079	3.9548	6.00585	2.17319	2.52948	15.0099	139.906	67.722
210	3.269	24.1221	17.4271	9.6154	5.5655	0.969	2.36438	3.9415	5.89086	2.27054	2.46469	14.7065	136.99	69.593
211	4.3	23.8511	17.2171	10.2262	5.6524	1.174	2.21796	3.9282	5.77586	2.36789	2.3999	14.403	134.073	72.85
212	5.331	23.5801	17.0071	9.5472	5.7393	1.378	2.07155	3.9149	5.66086	2.46524	2.33511	14.0996	131.157	76.106
213	5.067	23.3092	16.7971	8.6746	5.8262	1.309	1.97306	4.0319	5.23456	2.37138	2.30238	14.3438	129.566	75.887
214	3.748	22.3666	16.255	7.802	5.616	1.018	1.88176	4.1685	4.76153	2.24881	2.27446	14.6701	128.174	72.833
215	2.428	21.3232	15.663	7.4618	5.3612	0.726	1.79047	4.3051	4.2885	2.12624	2.24654	14.9965	126.782	69.78
216	1.367	20.2798	15.071	7.5557	5.1063	0.488	1.80212	4.0173	4.06407	2.04078	2.11382	14.5905	123.913	69.442
217	1.158	19.9272	14.7263	7.6495	4.9469	0.424	1.8977	3.3835	4.04231	1.98558	1.89566	13.5874	119.839	78.074
218	0.949	20.1379	14.5832	7.7138	4.8652	0.361	1.99328	2.7497	4.02055	1.93038	1.6775	12.5842	115.765	86.705
219	0.741	20.3485	14.4401	7.6806	4.7835	0.297	2.02054	2.283	4.02111	1.88218	1.53463	11.7032	111.686	95.337
220	0.825	20.1749	14.1625	7.6474	4.6875	0.333	1.82204	2.3685	4.09541	1.85712	1.64059	11.2259	107.593	101.599
221	0.938	18.7313	13.4403	7.6142	4.544	0.377	1.62355	2.454	4.16971	1.83206	1.74655	10.7486	103.5	107.637
222	1.05	17.2877	12.7182	7.8863	4.4006	0.422	1.42505	2.5395	4.24401	1.80699	1.85251	10.2712	99.406	113.675
223	2.344	15.8441	11.996	8.1872	4.2571	1.072	1.3369	2.598	3.99483	1.8213	1.74073	10.2571	98.23	129.991
224	4.442	16.0052	11.3742	8.4882	4.1406	2.134	1.25916	2.654	3.71512	1.83932	1.60839	10.2868	97.329	153.298
225	6.539	16.3178	10.7619	8.5724	4.0267	3.196	1.18142	2.7099	3.4354	1.85734	1.47604	10.3165	96.429	176.605
226	7.721	16.6305	10.1496	8.5092	3.9127	3.704	1.15005	3.3974	3.29117	1.91125	1.38733	10.0834	95.514	194.881
227	6.507	16.3993	9.8694	8.446	3.8942	2.765	1.15021	4.5144	3.23911	1.98957	1.3283	9.6716	94.591	199.995
228	5.292	15.7982	9.8151	8.6614	3.9406	1.825	1.15037	5.6315	3.18705	2.0679	1.26927	9.2598	93.667	205.109
229	4.078	15.1971	9.7609	9.6055	3.987	0.886	1.16117	6.124	3.2976	2.13839	1.23751	9.033	93.419	210.223
230	3.3	14.7414	9.7377	10.5495	4.0016	0.723	1.19982	4.983	3.83352	2.18841	1.27709	9.29	94.938	209.333
231	2.541	14.6663	9.7957	11.4936	3.9333	0.594	1.23847	3.8419	4.36944	2.23843	1.31668	9.547	96.457	208.179
232	1.782	14.5911	9.8537	10.9513	3.8649	0.465	1.27712	2.7008	4.90536	2.28845	1.35626	9.8041	97.976	207.025
233	1.394	14.5159	9.9118	10.3437	3.7966	0.362	1.30507	2.2729	4.76947	2.25133	1.32858	9.2901	96.67	202.909
234	1.215	14.4422	9.839	9.7362	3.5325	0.274	1.33255	1.8763	4.6041	2.21039	1.29796	8.7424	95.24	197.122
235	1.037	14.3684	9.7604	9.6159	3.2598	0.185	1.36003	1.4796	4.43873	2.16945	1.26733	8.1946	93.81	191.335
236	0.917	14.2947	9.6819	9.7705	2.9871	0.141	1.28238	1.3877	4.20384	2.13631	1.20655	7.9763	92.418	188.659
237	0.92	14.463	9.3271	9.925	2.8831	0.191	1.14544	1.4678	3.92975	2.10758	1.12877	7.9438	91.048	192.568
238	0.923	14.7679	8.8166	10.3417	2.8742	0.241	1.0085	1.5478	3.65565	2.07884	1.05099	7.9113	89.678	196.478
239	0.925	15.0727	8.3061	11.3133	2.8654	0.291	0.95689	1.5888	3.53755	2.12909	1.03807	8.0875	92.217	200.39
240	0.826	15.5678	8.224	12.2848	2.9515	0.287	1.08591	1.547	3.74973	2.34657	1.16247	8.7054	103.031	205.335
241	0.728	16.4654	9.0491	13.2537	3.2389	0.284	1.21494	1.5053	3.96192	2.56405	1.28688	9.3232	113.845	210.281
242	0.629	17.3631	9.8742	13.0131	3.5263	0.281	1.34433	1.4633	4.17238	2.78165	1.41188	9.9446	124.687	215.227
243	0.769	18.2662	10.7016	12.7725	3.815	0.515	1.63531	1.2886	3.60762	3.05373	1.80631	12.11	148.067	199.726
244	1.019	21.6367	12.6037	12.5319	4.7047	0.86	1.92628	1.074	3.04286	3.32581	2.20074	14.2754	171.446	174.763
245	1.269	25.0071	14.5058	10.5637	5.5944	1.204	2.21726	0.8793	2.47809	3.59788	2.59518	16.4408	194.825	149.8
246	1.462	28.3775	16.408	7.7959	6.4842	1.543	1.99668	0.7361	2.00831	3.20893	2.38537	15.0311	176.618	155.352
247	1.553	25.5871	14.8361	5.0281	5.9506	1.874	1.53936	0.6168	1.58248	2.51406	1.89592	11.9671	139.164	213.979
248	1.645	19.9457	11.6564	2.9797	4.7584	2.204	1.08203	0.4974	1.15666	1.8192	1.40648	8.903	101.71	272.607
249	1.854	14.3043	8.4768	2.1827	3.5662	2.603	0.71326	0.4919	0.83044	1.2414	0.98588	6.2635	70.302	328.131
250	4.475	9.6664	5.8119	1.3857	2.5278	4.409	0.49851	0.6845	0.67749	0.86724	0.68502	4.3626	49.407	319.942
251	7.095	6.774	4.0426	0.6249	1.7571	6.215	0.28375	0.8771	0.52454	0.49308	0.38417	2.4618	28.512	311.754
252	9.716	3.8816	2.2732	0.6061	0.9863	8.021	0.07787	1.0723	0.37709	0.13588	0.0961	0.6433	8.503	303.565
253		1.113	0.5788	0.6061	0.2487		0.05408	1.3197	0.34253	0.12676	0.07041	0.5167	6.667	

Garnet B

pt	Ca	Mn	Li	Sc	V	Cr	La	Ce	P	Pr	Nd	Sm	Eu	Gd	Tb	Dy	Ho	Er	Tm	Yb	Lu	Y
23	7524.413	3213.894	2.254	0.37601	72.417	190.166	2.254	8.85	129.338	0.37601	1.1507	2.1022	0.55832	12.1767	3.11485	22.3504	3.8645	9.783	1.4112	8.272	1.1703	124.557
24	8271.812	3323.514	1.9653	0.32547	80.962	172.696	1.9653	7.499	126.242	0.32547	1.1029	2.55553	0.48555	12.5418	2.99099	20.4834	3.5425	9.0794	1.2611	7.655	1.0005	113.919
25	8824.056	3288.979	1.8183	0.31759	87.627	142.55	1.8183	6.278	130.305	0.31759	1.169	3.02029	0.38636	12.3108	2.6637	16.9532	2.9464	7.6642	0.9993	6.437	0.7315	94.061
26	9376.301	3254.445	1.6714	0.30971	94.292	112.405	1.6714	5.058	134.368	0.30971	1.2352	3.48505	0.28717	12.0799	2.33641	13.4229	2.3503	6.249	0.7375	5.219	0.4625	74.204
27	9569.799	3235.44	1.3626	0.25242	97.829	106.281	1.3626	4.416	126.739	0.25242	1.1253	3.48261	0.32035	11.5297	2.15783	12.8839	2.2994	5.9727	0.697	4.987	0.4662	70.837
28	9643.715	3221.613	1	0.17865	100.324	108.164	1	3.966	115.212	0.17865	0.9567	3.32444	0.39767	10.8731	2.02882	13.3421	2.4302	6.0759	0.7302	5.084	0.5607	72.967
29	9717.631	3207.786	0.6373	0.10489	102.82	110.048	0.6373	3.516	103.686	0.10489	0.7881	3.16627	0.47498	10.2166	1.89981	13.8002	2.5611	6.1792	0.7635	5.181	0.6552	75.096
30	10989.935	3284.842	0.564	0.095	113.119	115.145	0.564	2.946	97.075	0.095	0.889	3.34402	0.59633	10.3621	2.01386	14.3898	2.7535	6.5524	0.8366	5.347	0.7173	79.272
31	12877.313	3408.543	0.6393	0.11791	127.424	121.892	0.6393	2.313	92.988	0.11791	1.128	3.69419	0.7403	10.9193	2.25265	15.047	2.9773	7.0642	0.9302	5.55	0.7628	84.498
32	14764.692	3532.245	0.7145	0.14081	141.728	128.639	0.7145	1.68	88.9	0.14081	1.3671	4.04436	0.88427	11.4765	2.49145	15.7042	3.2012	7.5759	1.0238	5.752	0.8084	89.724
33	15210.223	3649.883	0.8459	0.17759	146.688	128.356	0.8459	1.646	87.117	0.17759	1.7934	4.48153	0.93663	11.839	2.64485	16.5603	3.3401	8.0606	1.086	6.105	0.8656	94.418
34	14575.369	3762.978	1.0193	0.22477	144.646	122.805	1.0193	2.059	87.062	0.22477	2.3599	4.98388	0.92035	12.0555	2.73425	17.5654	3.4152	8.5251	1.1247	6.569	0.9316	98.714
35	13940.517	3876.072	1.1927	0.27195	142.603	117.255	1.1927	2.473	87.006	0.27195	2.9263	5.48623	0.90407	12.2721	2.82366	18.5705	3.4903	8.9895	1.1634	7.034	0.9976	103.009
36	14037.092	3899.723	2.0446	0.36981	140.802	113.424	2.0446	3.505	82.902	0.36981	3.536	5.99418	0.87625	12.4332	2.88429	19.6505	3.6422	9.1807	1.1577	7.323	1.0115	104.461
37	14918.201	3827.435	3.6242	0.52204	139.26	111.438	3.6242	5.199	74.455	0.52204	4.192	6.50813	0.83606	12.5349	2.91404	20.8108	3.8766	9.0788	1.1044	7.424	0.9695	102.863
38	15799.312	3755.148	5.2038	0.67426	137.718	109.451	5.2038	6.893	66.008	0.67426	4.848	7.02207	0.79586	12.6365	2.9438	21.9712	4.111	8.9769	1.0511	7.526	0.9275	101.265
39	16762.52	3754.229	6.0687	0.75279	139.108	111.924	6.0687	8.046	60.801	0.75279	5.277	7.51026	0.76182	12.755	2.91559	22.8745	4.2579	9.2564	1.1002	7.681	0.9464	104.191
40	17852.365	3863.398	5.8314	0.71765	145.02	121.273	5.8314	8.365	60.591	0.71765	5.3557	7.95873	0.73725	12.8996	2.79799	23.3813	4.2699	10.1241	1.3075	7.919	1.059	114.093
41	18942.211	3972.568	5.594	0.6825	150.933	130.623	5.594	8.684	60.382	0.6825	5.4344	8.40721	0.71268	13.0441	2.68039	23.8881	4.2819	10.9919	1.5147	8.158	1.1716	123.995
42	19403.957	4054.315	5.1275	0.6258	153.337	133.998	5.1275	8.445	63.288	0.6258	5.3934	8.47151	0.70146	12.8954	2.65837	24.3724	4.4051	11.8998	1.7731	9.292	1.5009	132.02
43	18428.637	4073.323	4.1369	0.51979	147.711	123.703	4.1369	6.927	73.323	0.51979	5.0787	7.65685	0.72079	12.0759	2.85505	24.805	4.7829	12.8997	2.1486	12.475	2.3262	135.749
44	17453.316	4092.332	3.1462	0.41377	142.086	113.407	3.1462	5.409	83.358	0.41377	4.7639	6.84218	0.74012	11.2564	3.05172	25.2377	5.1607	13.8997	2.5242	15.658	3.1515	139.477
45	16858.561	4084.125	2.2413	0.31648	138.819	106.259	2.2413	4.033	91.3	0.31648	4.4155	6.18136	0.76366	10.487	3.1962	25.499	5.4178	14.6572	2.7187	17.488	3.6361	142.331
46	17653.57	3976.535	1.6491	0.25105	144.165	110.605	1.6491	3.177	91.599	0.25105	3.9443	6.08233	0.80259	9.9006	3.15013	25.1347	5.2345	14.5298	2.2524	14.378	2.8765	141.988
47	18448.58	3868.945	1.057	0.18562	149.511	114.95	1.057	2.321	91.899	0.18562	3.4731	5.9833	0.84153	9.3142	3.10406	24.7703	5.0511	14.4023	1.7861	11.267	2.1168	141.646
48	19346.602	3783.322	0.5252	0.12769	154.883	118.661	0.5252	1.535	90.758	0.12769	3.0452	5.92784	0.87374	9.0068	3.09169	24.6785	4.9523	14.3023	1.3972	8.701	1.4614	142.217
49	20960.486	3850.359	0.4129	0.12185	160.44	117.961	0.4129	1.236	79.604	0.12185	2.9179	6.17509	0.85921	10.6387	3.31359	26.4805	5.441	14.3929	1.5463	9.914	1.5308	149.14
50	22574.371	3917.396	0.3006	0.11601	165.996	117.261	0.3006	0.937	68.451	0.11601	2.7905	6.42235	0.84469	12.2706	3.53548	28.2825	5.9297	14.4834	1.6954	11.127	1.6002	156.062
51	24102.385	3979.013	0.2049	0.11374	171.317	116.506	0.2049	0.697	57.773	0.11374	2.7016	6.64717	0.82922	13.8024	3.74567	29.9605	6.3948	14.5769	1.8421	12.279	1.6636	162.736
52	23371.604	3898.088	0.5451	0.20535	170.456	114.306	0.5451	1.981	59.603	0.20535	3.6232	6.28198	0.78907	12.7025	3.64773	28.3771	6.2382	14.7469	1.9264	11.829	1.5706	162.865
53	22640.822	3817.163	0.8852	0.29697	169.595	112.106	0.8852	3.266	61.433	0.29697	4.5447	5.91679	0.74891	11.6025	3.5498	26.7937	6.0816	14.917	2.0107	11.378	1.4777	162.995
54	21910.041	3736.238	1.2253	0.38858	168.734	109.906	1.2253	4.551	63.264	0.38858	5.4663	5.55161	0.70875	10.5026	3.45187	25.2103	5.925	15.087	2.095	10.928	1.3847	163.124
55	22751.037	3795.782	1.0115	0.37528	165.53	112.236	1.0115	4.367	55.549	0.37528	5.7348	5.12156	0.76762	11.94	3.65179	27.59	6.1649	16.365	2.1963	12.095	1.4842	168.768
56	23679.209	3863.117	0.7669	0.35617	162.195	114.816	0.7669	4.102	47.304	0.35617	5.967	4.68791	0.83198	13.5182	3.86824	30.1895	6.4268	17.7045	2.2985	13.351	1.5945	174.718
57	24607.379	3930.452	0.5223	0.33705	158.861	117.397	0.5223	3.837	39.059	0.33705	6.1993	4.25427	0.89634	15.0964	4.08468	32.789	6.6887	19.0439	2.4008	14.608	1.7047	180.667
58	23731.287	3902.086	0.4263	0.30949	161.594	117.153	0.4263	3.006	40.39	0.30949	6.0483	4.28554	0.9097	14.9138	3.98001	32.9678	6.9746	19.2501	2.4129	14.812	1.7966	183.566
59	22557.273	3857.918	0.3548	0.28054	165.329	116.443	0.3548	2.08	43.302	0.28054	5.834	4.39358	0.91464	14.4405	3.82231	32.7468	7.2645	19.269	2.41	14.843	1.8855	185.96
60	21383.26	3813.75	0.2833	0.25158	169.064	115.733	0.2833	1.155	46.214	0.25158	5.6197	4.50161	0.91958	13.9672	3.66462	32.5259	7.5543	19.288	2.4072	14.874	1.9743	188.354
61	22431.023	3903.807	0.2044	0.21566	169.976	114.905	0.2044	0.803	47.607	0.21566	5.4244	4.54688	0.99472	13.2939	3.73903	33.6759	7.8385	19.4284	2.5094	14.684	2.0066	193.84
62	24145.781	4034.16	0.1234	0.17765	170.04	114.041	0.1234	0.623	48.545	0.17765	5.2348	4.57331	1.09092	12.5605	3.88313	35.2374	8.1209	19.6052	2.6431	14.428	2.022	200.254
63	25860.539	4164.512	0.0423	0.13964	170.104	113.178	0.0423	0.442	49.482	0.13964	5.0452	4.59973	1.18713	11.8271	4.02723	36.7989	8.4033	19.7821	2.7769	14.173	2.0374	206.667
64	26434.588	4256.472	0.0439	0.15286	170.536	113.5	0.0439	0.419	53.941	0.15286	5.4374	4.41715	1.16126	11.7063	4.11858	36.7593	8.801	20.4792	2.9059	14.543	2.16	210.375
65	26471.676	4330.359	0.0844	0.19019	171.14	114.379	0.0844	0.47	60.058	0.19019	6.1035	4.13618	1.07794	11.8737	4.18509	35.9662	9.253	21.4213	3.0327	15.208	2.333	212.808
66	26508.762	4404.247	0.1249	0.22752	171.744	115.259	0.1249	0.52	66.175	0.22752	6.7696	3.85522	0.99461	12.0412	4.2516	35.173	9.705	22.3634	3.1595	15.873	2.506	215.241
67	26766.443	4401.223	0.1421	0.25563	171	114.169	0.1421	0.513	65.796	0.25563	6.6488	3.92962	0.99842	12.1777	4.34935	36.12	9.5837	22.9015	3.1546	16.986	2.6617	217.459
68	27176.936	4344.921	0.1432	0.27736	169.322	111.714	0.1432	0.465	60.918	0.27736	5.9828	4.25019	1.06261	12.2927	4.46873	38.2724	9.0653	23.1597	3.0584	18.411	2.8053	219.526
69	27587.428	4288.619	0.1442	0.29909	167.644	109.26	0.1442	0.418	56.041	0.29909	5.3169	4.57077	1.1268	12.4077	4.58812	40.4249	8.547	23.418	2.9622	19.836	2.949	221.594
70	27323.375	4257.078	0.1352	0.29335	168.303	110.115	0.1352	0.377	52.455	0.29335	5.0811	4.81969	1.16937	12.1386	4.62457	42.3181	8.582	24.2563	2.9657	20.204	2.9048	223.993
71	26389.059	4250.14	0.1162	0.26032	171.283	114.258	0.1162	0.343	50.155	0.26032	5.2727	4.99742	1.19046	11.4878	4.57861	43.9537	9.1669	25.671	3.0681	19.524	2.6741	226.721
72	25454.744	4243.203	0.0972	0.22728	174.263	118.402	0.0972	0.31	47.854	0.22728	5.4643	5.17515	1.21155	10.8369	4.53266	45.5893	9.7518	27.0857	3.1705	18.844	2.4433	229.449
73	24928.482	4202.969	0.0877	0.18949	174.431	120.776	0.0877	0.286	45.794	0.18949	5.705	5.40812	1.13355	10.2251	4.42835	45.7783	10.025	27.1743	3.179	18.374	2.3737	230.571
74	24983.578	4115.298	0.0917	0.14491	170.593	120.629	0.0917	0.278	44.077	0.14491	6.0155	5.71981	0.91438	9.6688	4.24091	43.9063	9.8539	25.3734	3.0536	18.204	2.5338	229.404
75	25038.674	4027.627	0.0957	0.10034	166.756	120.482	0.0957	0.269	42.36	0.10034	6.326	6.03149	0.69521	9.1126	4.05347	42.0342	9.6829	23.5726	2.9282	18.034	2.694	228.237
76	25674.121	3974.013	0.0928	0.08092	166.228	120.924	0.0928	0.247	43.749	0.08092	6.5816	6.34447	0.63347	8.916	3.98647	41.1383	9.5494	22.7109	2.9117	18.358	2.8234	230.55
77	27524.592	3991.701	0.0755	0.1142	172.631	122.595	0.0755	0.197	51.639	0.1142	6.722	6.66019	0.9013	9.4723	4.17163	42.2861	9.4947	23.8153	3.123	19.717	2.8887	240.146
78	29375.062	4009.388	0.0582	0.14747	179.033	124.267	0.0582	0.147	59.529	0.14747	6.8624	6.97591	1.16914	10.0287	4.35679	43.4339	9.4399	24.9197	3.3344	21.077	2.954	249.743
79	30590.568	4002.325	0.0497	0.18095	181.967	124.709	0.0497	0.11	66.293	0.18095	6.785	7.06296	1.32784	10.4254	4.40626	43.9482	9.4684	25.8006	3.4828	22.1	2.9721	255.555
80	29728.404	3914.277	0.0699	0.21513	173.552	121.125	0.0699	0.114	69.369	0.21513	5.9949	6.40179	1.12943	10.3001	4.01173	42.3897	9.7697	25.9499	3.425	22.022	2.8355	248.98
81	28866.242	3826.229	0.0901	0.2493	165.137	117.54	0.0901	0.119	72.446	0.2493	5.2047	5.74062	0.93103	10.1748	3.61721	40.8313	10.071	26.0993	3.3673	21.945	2.699	242.406
82	28174.775	3765.353	0.1023	0.2759	158.024	114.956	0.1023	0.125	74.63	0.2759	4.6574	5.13818	0.79296	10.1259	3.31769	39.9399	10.3903	26.4004	3.3294	21.935	2.6388	238.176
83	28490.607	3864.824	0.0676	0.25774	158.59	118.271	0.0676	0.145	71.545	0.25774	5.5426	4.88235	1.01102	10.5283	3.57884	42.9855	10.8156	27.5969	3.4091	22.322	3.0289	247.779
84	28806.439	3964.295	0.0328	0.23958	159.156	121.587	0.0328	0.166	68.46	0.23958	6.4279	4.62652	1.22907	10.9307	3.83998	46.031	11.241	28.7935	3.4887	22.71	3.4191	257.382
85	29055.43	4054.007	-4.801E-06	0.22209	160.095	124.679	-4.801E-06	0.184	65.607	0.22209	7.2468	4.3964	1.42592	11.3364	4.09135	48.8449	11.6322	29.8982	3.5759	23.115	3.7936	266.371
86	28171.908	3978.357	-3.218E-06	0.21587	167.359	123.99	-3.218E-06	0.173	66.677	0.21587	6.9405	4.60192	1.26342	11.7979	4.17699	47.7342	11.4457	29.4466	3.7916	23.806	3.9039	264.944
87	27288.387	3902.707	-1.636E-06	0.20965	174.622	123.3	-1.636E-06	0.163	67.747	0.20965	6.6342	4.80744	1.10093	12.2595	4.26263	46.6235	11.2592	28.995	4.0074	24.497	4.0143	263.517
88	26404.865	3827.058	-5.291E-08	0.20344	181.886	122.611	-5.291E-08	0.152	68.818	0.20344	6.3279	5.01296	0.93843	12.721	4.34827	45.5129	11.0727	28.5433	4.2231	25.188	4.1246	262.089
95	27885.283	3897.73	0.0641	0.31362	172.855	129.635	0.0641	0.516	53.49	0.31362	5.4994	3.94465	0.70325	9.0714	4.44407	44.313	11.5195	34.9989	4.7448	28.067	4.4646	280.56
96	28241.52	3950.592	0.0673	0.30384	175.184	129.479	0.0673	0.441	59.083	0.30384	6.1024	4.16874	0.88714	9.2701	4.44352	46.929	11.7909	35.1564	5.0869	27.936	4.2986	287.883
97	28597.758	4003.454	0.0705	0.29406	177.514	129.324	0.0705	0.366	64.677	0.29406	6.7055	4.39282	1.07103	9.4688	4.44296	49.5451	12.0623	35.314	5.429	27.804	4.1327	295.205
98	28518.311	4008.163	0.0606	0.28898	179.748	127.725	0.0606	0.32	59.847	0.28898	6.8082	4.3465	1.07901	9.3664	4.36545	49.593	12.0083	35.4856	5.4087	28.17	4.204	296.276
99	28251.291	3992.14	0.0451	0.28592	181.941	125.505	0.0451	0.287	50.53	0.28592	6.6956	4.18376	1.01125	9.1342	4.2548	48.5353	11.8142	35.6633	5.2324	28.751	4.3774	294.656
100	27984.271	3976.118	0.0295	0.28286	184.134	123.285	0.0295	0.254	41.214	0.28286	6.583	4.02103	0.9435	8.9021	4.14416	47.4776	11.62	35.841	5.0562	29.331	4.5508	293.035
101	27560.262	3954.175	0.0188	0.26995	182.067	122.53	0.0188	0.207	39.468	0.26995	6.1481	3.86374	0.96874	8.961	4.19542	46.9384	11.6068	35.9446	5.059	31.102	4.7018	293.685
102	27035.826	3928.445	0.0112	0.25075	177.275	122.712	0.0112	0.152	42.565	0.25075	5.507	3.70994	1.05346	9.2062	4.35024	46.7308	11.7092	36.0007	5.1763	33.635	4.8385	295.786
103	26511.391	3902.714	0.0036	0.23154	172.484	122.894	0.0036	0.097	45.661	0.23154	4.866	3.55614	1.13819	9.4514	4.50506	46.5233	11.8116	36.0568	5.2937	36.168	4.9752	297.888
104	26910.117	3930.189	0.0028	0.25117	170.729	124.243	0.0028	0.082	47.077	0.25117	4.7062	3.68336	1.16891	9.763	4.60871	46.7858	12.0412	36.1677	5.5171	37.895	5.1558	302.443
105	28158.605	4006.639	0.0083	0.30653	171.771	126.667	0.0083	0.103	46.945	0.30653	4.9895	4.06925	1.14991	10.1358	4.66527	47.481	12.3878	36.3291	5.8383	38.88	5.3768	309.257
106	29407.092	4083.089	0.0138	0.36189	172.813	129.09	0.0138	0.125	46.813	0.36189	5.2728	4.45514	1.13091	10.5086	4.72183	48.1761	12.7344	36.4904	6.1595	39.865	5.5978	316.071
107	29760.117	4102.773	0.0167	0.37704	174.312	129.782	0.0167	0.148	46.271	0.37704	5.7466	4.59906	1.12885	10.8638	4.81975	48.5044	13.0206	37.0834	6.3284	40.175	5.8416	320.736
108	28933.514	4047.679	0.0162	0.33922	176.416	128.191	0.0162	0.174	45.188	0.33922	6.4712	4.42421	1.14911	11.1957	4.97218	48.3494	13.2273	38.2451	6.2966	39.597	6.1155	322.569
109	28106.91	3992.584	0.0157	0.3014	178.52	126.601	0.0157	0.199	44.106	0.3014	7.1959	4.24937	1.16936	11.5276	5.1246	48.1944	13.4339	39.4068	6.2648	39.019	6.3895	324.402
110	27806.951	3921.305	0.0137	0.27045	179.415	125.07	0.0137	0.214	44.644	0.27045	7.8378	4.14587	1.15134	11.468	5.12961	48.1146	13.4216	40.1343	6.1954	39.178	6.5947	325.454
111	28518.637	3818.935	0.0087	0.25271	177.988	123.654	0.0087	0.206	48.293	0.25271	8.3206	4.17942	1.05981	10.6564	4.85146	48.1793	12.9886	40.0278	6.0537	40.752	6.668	325.007
112	29230.322	3716.565	0.0038	0.23497	176.562	122.238	0.0038	0.199	51.943	0.23497	8.8035	4.21297	0.96829	9.8448	4.57331	48.2439	12.5557	39.9213	5.9121	42.325	6.7413	324.56
113	29720.336	3650.177	0.002	0.23153	175.462	122.019	0.002	0.193	56.027	0.23153	8.8368	4.27574	0.9086	9.314	4.37221	48.3283	12.2672	39.8906	5.8585	43.622	6.8046	325.729
114	29556.49	3689.924	0.0097	0.27027	175.326	125.328	0.0097	0.194	61.389	0.27027	7.5437	4.42474	0.94285	9.6117	4.39841	48.4709	12.4046	40.0835	6.0647	44.101	6.8382	331.666
115	29392.645	3729.671	0.0173	0.30901	175.191	128.637	0.0173	0.195	66.751	0.30901	6.2506	4.57373	0.97709	9.9094	4.42461	48.6135	12.5421	40.2764	6.2709	44.58	6.8718	337.603
116	29012.215	3749.596	0.0306	0.32794	174.287	130.444	0.0306	0.284	69.481	0.32794	5.2257	4.62435	1.00313	10.1716	4.39601	48.5896	12.6499	40.3513	6.4292	44.802	6.8922	340.201
117	27527.854	3668.489	0.0728	0.24587	169.463	124.596	0.0728	0.825	58.8	0.24587	5.5679	4.17352	0.98734	10.2531	4.08814	47.7172	12.6065	39.8253	6.3441	43.713	6.8457	325.781
118	26043.492	3587.381	0.115	0.16381	164.639	118.748	0.115	1.366	48.119	0.16381	5.9102	3.7227	0.97156	10.3345	3.78027	46.8448	12.563	39.2992	6.2589	42.625	6.7991	311.362
119	24725.045	3515.915	0.1513	0.09553	160.46	113.393	0.1513	1.835	38.141	0.09553	6.2795	3.31726	0.95267	10.3587	3.50723	46.0658	12.5326	38.8804	6.1759	41.808	6.7813	298.21
120	25457.611	3563.629	0.1144	0.19775	164.258	114.126	0.1144	1.426	36.869	0.19775	6.9843	3.47277	0.89547	9.6741	3.66479	46.4422	12.6628	39.7878	6.1205	44.353	7.1198	300.715
121	26190.176	3611.343	0.0776	0.29997	168.056	114.86	0.0776	1.016	35.596	0.29997	7.689	3.62827	0.83827	8.9895	3.82235	46.8185	12.7929	40.6953	6.065	46.898	7.4584	303.22
122	26922.742	3659.057	0.0407	0.40218	171.853	115.593	0.0407	0.607	34.324	0.40218	8.3938	3.78378	0.78107	8.3049	3.9799	47.1949	12.9231	41.6027	6.0096	49.443	7.7969	305.725
123	28112.029	3710.466	0.0384	0.42784	176.836	122.227	0.0384	0.526	46.582	0.42784	7.5975	3.57285	0.97334	8.8056	4.13051	48.5414	13.2414	42.8055	6.5284	50.383	7.9807	322.031
124	29307.959	3761.929	0.0366	0.45238	181.835	128.946	0.0366	0.45	59.036	0.45238	6.7794	3.3566	1.16923	9.3234	4.28102	49.902	13.5625	44.0127	7.0555	51.3	8.1622	338.537
125	30503.889	3813.392	0.0347	0.47692	186.835	135.665	0.0347	0.374	71.49	0.47692	5.9613	3.14034	1.36513	9.8413	4.43153	51.2626	13.8835	45.2198	7.5827	52.217	8.3438	355.044
126	29855.264	3815.022	0.0652	0.43399	184.362	133.095	0.0652	0.463	67.439	0.43399	6.6123	2.78504	1.42185	9.5195	4.32757	49.5664	13.1454	44.2854	7.5486	52.026	8.2933	346.844
127	28993.68	3810.9	0.0994	0.38327	181.027	129.452	0.0994	0.571	61.482	0.38327	7.4329	2.41368	1.4625	9.1008	4.19423	47.5173	12.285	43.1038	7.4497	51.708	8.2162	335.791
128	28132.096	3806.778	0.1335	0.33255	177.692	125.81	0.1335	0.678	55.526	0.33255	8.2534	2.04232	1.50315	8.682	4.0609	45.4682	11.4246	41.9222	7.3509	51.39	8.139	324.738
129	28210.396	3806.712	0.4968	0.34011	178.854	125.306	0.4968	1.128	49.41	0.34011	8.088	2.45555	1.37704	8.6994	4.06772	44.8806	11.7318	42.9949	7.3116	53.018	8.453	327.904
130	28513.008	3807.614	0.9387	0.36157	181.09	125.551	0.9387	1.66	43.257	0.36157	7.6873	3.05603	1.21112	8.8207	4.108	44.6418	12.3177	44.6057	7.2866	55.112	8.8604	334.462
131	28815.619	3808.516	1.3805	0.38304	183.325	125.796	1.3805	2.192	37.104	0.38304	7.2865	3.65651	1.0452	8.9421	4.14828	44.403	12.9036	46.2164	7.2615	57.206	9.2679	341.021
132	28041.898	3790.876	1.2873	0.48099	180.34	126.703	1.2873	2.546	59.221	0.48099	7.5313	3.86783	1.08656	9.2456	4.12738	44.2102	13.1447	46.6404	7.3458	57.697	9.4611	342.199
133	26845.76	3765.959	0.984	0.60897	175.305	127.869	0.984	2.83	92.434	0.60897	8.0293	3.92642	1.20927	9.6206	4.08247	44.0354	13.2506	46.5985	7.473	57.559	9.5703	341.266
134	25649.621	3741.042	0.6808	0.73695	170.27	129.036	0.6808	3.114	125.646	0.73695	8.5274	3.98501	1.33198	9.9955	4.03757	43.8606	13.3565	46.5566	7.6001	57.422	9.6794	340.333
135	26075.01	3683.217	0.5423	0.69661	166.555	125.622	0.5423	2.795	117.55	0.69661	8.3615	3.69398	1.38716	9.8367	3.92717	43.3342	13.3145	46.4187	7.4464	57.017	9.6136	337.742
136	27456.895	3605.979	0.501	0.55699	163.618	119.507	0.501	2.12	85.087	0.55699	7.8038	3.19671	1.4025	9.3629	3.77814	42.6003	13.1853	46.2243	7.1268	56.455	9.4445	334.174
137	28838.779	3528.742	0.4596	0.41737	160.682	113.392	0.4596	1.446	52.624	0.41737	7.2462	2.69944	1.41783	8.8892	3.62911	41.8663	13.056	46.0298	6.8073	55.893	9.2754	330.606
138	28972.564	3494.064	0.3989	0.35028	162.456	112.412	0.3989	1.024	41.637	0.35028	6.8487	2.78889	1.3994	8.773	3.67096	42.0433	13.0761	46.9138	6.9938	57.378	9.5941	334.315
139	28042.334	3495.668	0.3216	0.34502	168.247	115.81	0.3216	0.818	48.958	0.34502	6.5878	3.37852	1.35216	8.9616	3.87554	42.9969	13.2234	48.7172	7.6117	60.606	10.3288	344.23
140	27112.104	3497.272	0.2443	0.33975	174.038	119.207	0.2443	0.611	56.278	0.33975	6.3269	3.96815	1.30492	9.1501	4.08012	43.9504	13.3707	50.5207	8.2296	63.835	11.0634	354.144
141	26158.018	3492.694	0.1802	0.31147	177.326	119.765	0.1802	0.479	55.705	0.31147	5.8512	4.11559	1.24014	8.8973	4.11735	43.8441	13.1502	50.253	8.3751	64.054	11.3533	352.32
142	25174.848	3480.58	0.132	0.25511	177.565	116.859	0.132	0.438	45.508	0.25511	5.1137	3.72396	1.15396	8.1062	3.95056	42.4457	12.4815	47.4604	7.9449	60.605	11.1011	336.185
143	24191.678	3468.465	0.0838	0.19876	177.803	113.954	0.0838	0.396	35.311	0.19876	4.3762	3.33232	1.06778	7.3151	3.78377	41.0473	11.8128	44.6678	7.5147	57.155	10.8488	320.05
144	23510.408	3492.002	0.0558	0.17533	176.125	113.385	0.0558	0.408	30.912	0.17533	4.0709	3.06986	1.0536	7.2629	3.73883	40.6509	11.5814	43.3867	7.3542	56.353	10.8125	311.538
145	23362.449	3578.515	0.0635	0.21006	171.06	116.943	0.0635	0.514	36.757	0.21006	4.5291	3.0356	1.16658	8.5159	3.90914	42.0244	12.1224	44.7756	7.6704	60.226	11.1576	316.493
146	23214.49	3665.029	0.0712	0.24479	165.995	120.501	0.0712	0.62	42.601	0.24479	4.9872	3.00133	1.27957	9.769	4.07945	43.3979	12.6634	46.1645	7.9865	64.099	11.5028	321.449
147	23290.227	3718.06	0.0885	0.26472	163.009	124.483	0.0885	0.725	47.564	0.26472	5.4135	3.02957	1.32485	10.4949	4.17701	44.4037	13.0612	47.2722	8.2646	66.879	11.8385	328.592
148	23963.789	3681.606	0.1317	0.24507	165.575	129.597	0.1317	0.823	50.171	0.24507	5.7548	3.22483	1.18916	9.8121	4.08017	44.4268	13.0764	47.6284	8.4407	66.736	12.1493	341.585
149	24637.352	3645.153	0.1748	0.22543	168.142	134.71	0.1748	0.922	52.778	0.22543	6.096	3.42008	1.05347	9.1293	3.98333	44.4498	13.0916	47.9845	8.6169	66.594	12.46	354.577
150	24820.516	3587.913	0.251	0.2288	169.344	138.914	0.251	1.104	53.432	0.2288	6.3353	3.55217	0.94373	8.4757	3.85315	44.0008	13.0841	48.0846	8.7176	66.607	12.6681	362.948
151	22816.078	3437.947	0.4743	0.33483	164.455	139.057	0.4743	1.657	45.371	0.33483	6.12	3.40247	0.9498	7.952	3.57426	41.446	12.975	47.0425	8.4822	67.318	12.4187	350.704
152	20811.643	3287.98	0.6976	0.44087	159.566	139.201	0.6976	2.21	37.31	0.44087	5.9047	3.25276	0.95587	7.4283	3.29537	38.8913	12.8659	46.0004	8.2467	68.028	12.1692	338.459
153	19017.162	3145.327	0.8905	0.52865	154.758	138.636	0.8905	2.682	30.439	0.52865	5.6476	3.13191	0.96571	6.9073	3.04574	36.6243	12.7579	45.1318	8.051	68.802	11.9727	327.542
154	19247.525	3073.208	0.7901	0.44033	150.726	131.241	0.7901	2.361	35.04	0.44033	4.9876	3.28941	1.0119	6.4123	3.07823	37.1322	12.66	45.9355	8.2385	70.192	12.2865	329.429
155	19477.887	3001.087	0.6897	0.352	146.695	123.846	0.6897	2.04	39.642	0.352	4.3277	3.4469	1.05809	5.9173	3.11073	37.6402	12.5621	46.7392	8.426	71.582	12.6003	331.316
156	19713.875	2931.006	0.5893	0.26387	142.731	116.517	0.5893	1.719	44.232	0.26387	3.6704	3.60538	1.10447	5.4316	3.14409	38.1634	12.4703	47.5631	8.6183	73.013	12.9207	333.355
210	22748.381	3386.201	4.7244	1.28529	148.857	81.916	4.7244	23.777	80.551	1.28529	6.3564	2.86416	0.94974	7.9113	3.45703	37.2494	11.898	48.6262	9.4196	77.764	14.856	352.159
211	24319.08	3546.166	7.215	1.95025	161.396	82.115	7.215	35.805	88.028	1.95025	8.1598	3.60983	1.05051	7.5917	3.50864	38.8557	12.2777	49.1487	9.502	80.902	15.3085	365.584
212	24591.334	3580.469	9.9554	2.49605	165.612	81.312	9.9554	43.971	91.463	2.49605	9.636	3.97982	1.09001	7.3048	3.48032	39.231	12.2929	48.2663	9.3237	80.733	15.2119	367.964
213	22913.334	3426.031	13.071	2.86285	157.328	79.004	13.071	46.338	88.827	2.86285	10.6208	3.78554	1.03747	7.067	3.33193	37.7577	11.7608	45.2736	8.7541	75.597	14.2906	353.756
214	21235.334	3271.591	16.1867	3.22966	149.044	76.696	16.1867	48.706	86.191	3.22966	11.6056	3.59127	0.98493	6.8293	3.18354	36.2844	11.2286	42.2809	8.1844	70.461	13.3693	339.549
215	20718.621	3220.17	17.0204	3.24366	144.83	76.664	17.0204	47.197	81.126	3.24366	11.8664	3.42786	0.9453	7.0851	3.13132	36.0305	10.9652	40.9087	7.8761	67.639	12.9456	333.631
216	22780.555	3397.5	12.7873	2.47428	149.652	81.683	12.7873	37.083	70.663	2.47428	10.5196	3.33298	0.93435	8.4368	3.29265	38.4843	11.2986	43.1351	8.1481	69.953	13.6268	346.122
217	24842.488	3574.831	8.5542	1.70489	154.475	86.703	8.5542	26.969	60.201	1.70489	9.1728	3.23811	0.9234	9.7885	3.45397	40.938	11.6321	45.3614	8.4201	72.267	14.3079	358.613
218	26079.785	3698.826	5.2031	1.11555	157.41	90.54	5.2031	18.773	51.769	1.11555	8.1396	3.18612	0.92312	10.6081	3.54652	42.3901	11.8471	46.6154	8.6007	73.802	14.7109	364.914

219	24416.02	3635.192	4.9552	1.15965	153.704	90.217	4.9552	17.326	50.476	1.15965	8.2099	3.28502	0.9604	9.5555	3.39712	40.318	11.6459	44.4489	8.4598	72.596	14.1352	349.44
220	22752.254	3571.558	4.7073	1.20374	149.998	89.894	4.7073	15.88	49.183	1.20374	8.2801	3.38392	0.99768	8.5029	3.24772	38.246	11.4447	42.2824	8.3188	71.39	13.5596	333.967
221	21457.992	3511.157	4.4491	1.21875	146.909	90.144	4.4491	14.42	48.875	1.21875	8.2937	3.41903	1.02332	7.5465	3.11765	36.375	11.2499	40.5092	8.1735	70.006	13.0319	320.514
222	22589.998	3471.984	4.1236	1.04286	147.868	94.148	4.1236	12.875	55.038	1.04286	7.9355	3.03526	0.97251	7.2213	3.11456	35.8242	11.0977	41.3189	7.9999	67.458	12.8194	320.329
223	23722.004	3432.812	3.7982	0.86697	148.826	98.152	3.7982	11.329	61.201	0.86697	7.5772	2.6515	0.9217	6.8961	3.11146	35.2734	10.9454	42.1285	7.8262	64.909	12.6069	320.144
224	24826.316	3402.911	3.4779	0.70628	150	102.159	3.4779	9.847	66.76	0.70628	7.2739	2.28936	0.87869	6.6052	3.11003	34.802	10.8256	42.925	7.6644	62.543	12.4108	320.422
225	25314.229	3579.387	3.2717	0.88381	155.97	106.237	3.2717	9.794	58.869	0.88381	8.1936	2.40857	1.00905	7.0766	3.14556	36.0984	11.4281	43.4286	7.7677	64.236	12.5812	331.006
226	25802.139	3755.864	3.0656	1.06134	161.94	110.315	3.0656	9.741	50.977	1.06134	9.1133	2.52779	1.13942	7.548	3.18109	37.3947	12.0306	43.9322	7.871	65.929	12.7517	341.589
227	26290.049	3932.34	2.8594	1.23887	167.91	114.392	2.8594	9.689	43.086	1.23887	10.033	2.64701	1.26978	8.0194	3.21661	38.691	12.6331	44.4358	7.9742	67.622	12.9221	352.172
228	26643.256	3886.35	2.2668	1.22069	165.563	109.288	2.2668	8.184	52.448	1.22069	9.8523	2.83042	1.24106	7.7104	3.19634	38.6977	12.4874	44.3138	7.8061	65.968	12.5008	344.436
229	26989.941	3829.589	1.6554	1.19305	162.813	103.739	1.6554	6.61	62.646	1.19305	9.6184	3.01694	1.20464	7.3636	3.17337	38.642	12.3054	44.1615	7.6248	64.152	12.0509	335.814
230	27336.627	3772.829	1.044	1.1654	160.064	98.19	1.044	5.035	72.843	1.1654	9.3844	3.20346	1.16822	7.0168	3.15039	38.5863	12.1234	44.0093	7.4435	62.336	11.6009	327.192
231	27377.266	3743.392	0.8414	0.92736	167.585	101.297	0.8414	3.826	64.837	0.92736	8.7777	3.3406	1.18183	6.9699	3.12249	38.0305	11.9851	44.202	7.5741	64.016	11.6939	327.071
232	27369.998	3718.233	0.7028	0.65639	176.714	105.76	0.7028	2.675	53.981	0.65639	8.1126	3.47	1.20328	6.97	3.09382	37.3965	11.8535	44.4488	7.7534	66.243	11.872	328.282
233	27362.732	3693.074	0.5643	0.38542	185.842	110.223	0.5643	1.524	43.126	0.38542	7.4474	3.5994	1.22472	6.9701	3.06515	36.7624	11.7219	44.6955	7.9327	68.471	12.05	329.493
234	26364.424	3645.223	0.4134	0.30712	172.135	106.711	0.4134	1.192	37.023	0.30712	7.003	3.61103	1.18774	7.0448	3.07229	35.3432	11.2367	43.2995	7.5944	65.401	11.2718	313.998
235	25079.184	3590.803	0.259	0.28461	151.816	100.891	0.259	1.097	32.296	0.28461	6.6225	3.58856	1.13383	7.1411	3.08981	33.6968	10.649	41.4279	7.1063	60.797	10.2166	293.667
236	23793.943	3536.383	0.1046	0.2621	131.497	95.071	0.1046	1.002	27.569	0.2621	6.242	3.56609	1.07993	7.2374	3.10733	32.0503	10.0613	39.5563	6.6181	56.194	9.1615	273.337
237	24012.475	3573.729	0.0756	0.25579	133.818	96.464	0.0756	0.895	29.401	0.25579	6.2245	3.39526	1.01634	7.2145	3.07159	33.4242	10.1522	39.7821	6.7066	55.129	9.2887	274.687
238	24918.344	3653.018	0.1039	0.25688	146.487	101.154	0.1039	0.782	34.231	0.25688	6.3729	3.15662	0.94833	7.1371	3.0115	36.1787	10.5533	40.9667	7.0587	55.682	9.9563	285.948
239	25824.215	3732.307	0.1322	0.25798	159.156	105.845	0.1322	0.669	39.062	0.25798	6.5213	2.91799	0.88031	7.0598	2.95142	38.9331	10.9544	42.1512	7.4108	56.235	10.6239	297.209
240	26420.816	3768.017	0.2167	0.31132	167.07	109.215	0.2167	0.832	38.078	0.31132	6.6952	2.99634	0.9193	7.1402	3.10048	39.8876	11.2714	43.4309	7.5874	57.381	10.7443	306.596
241	26808.766	3774.324	0.3391	0.39991	171.777	111.696	0.3391	1.182	33.173	0.39991	6.8862	3.28855	1.03049	7.3271	3.39065	39.6277	11.5317	44.7748	7.6457	58.928	10.4955	314.718
242	27196.715	3780.632	0.4615	0.4885	176.483	114.177	0.4615	1.533	28.268	0.4885	7.0772	3.58075	1.14167	7.514	3.68083	39.3678	11.7921	46.1187	7.704	60.474	10.2468	322.84
243	27427.969	3886.362	0.5275	0.58447	180.92	115.838	0.5275	1.727	29.073	0.58447	7.0967	3.76891	1.12096	7.7299	3.73287	39.3813	12.1904	46.6801	7.8717	60.599	10.1949	327.184
244	27507.443	4088.397	0.5388	0.6876	185.096	116.704	0.5388	1.77	35.411	0.6876	6.9503	3.85627	0.97248	7.974	3.55426	39.6595	12.7222	46.4835	8.1455	59.349	10.3336	327.867
245	27586.918	4290.432	0.5501	0.79072	189.273	117.571	0.5501	1.812	41.748	0.79072	6.8038	3.94362	0.82401	8.218	3.37565	39.9376	13.2541	46.2869	8.4192	58.098	10.4722	328.55
246	27659.135	4338.372	0.5519	0.79416	191.484	118.193	0.5519	1.784	46.381	0.79416	7.1635	3.88021	0.77892	8.1515	3.2626	40.1096	13.5682	45.9995	8.3673	57.118	10.3939	327.82
247	27721.277	4172.454	0.5405	0.65923	190.969	118.476	0.5405	1.657	48.649	0.65923	8.2256	3.60754	0.87732	7.6539	3.24056	40.1343	13.5801	45.5862	7.8634	56.514	10.0142	325.128
248	27783.42	4006.536	0.5291	0.5243	190.453	118.759	0.5291	1.529	50.917	0.5243	9.2878	3.33488	0.97573	7.1564	3.21852	40.1589	13.592	45.1728	7.3596	55.909	9.6345	322.437
249	27763.684	3871.894	0.4888	0.44004	189.261	118.608	0.4888	1.375	52.442	0.44004	9.5784	3.12754	1.02078	7.0273	3.22211	40.2418	13.5079	44.6386	7.0767	55.192	9.3003	320.119
250	27577.42	3800.86	0.3898	0.45881	186.693	117.574	0.3898	1.167	52.459	0.45881	8.2999	3.0531	0.95734	7.6477	3.27782	40.4433	13.2284	43.8585	7.2432	54.246	9.0585	318.562
251	27391.156	3729.825	0.2908	0.47759	184.125	116.54	0.2908	0.959	52.475	0.47759	7.0214	2.97865	0.8939	8.2681	3.33354	40.6448	12.9489	43.0785	7.4098	53.299	8.8167	317.006
252	27355.502	3692.46	0.2088	0.48253	182.334	116.901	0.2088	0.815	51.806	0.48253	6.2005	2.91032	0.86318	8.6003	3.37941	40.9138	12.6838	42.478	7.4614	52.356	8.5724	314.991
253	27795.609	3761.454	0.1808	0.44375	183	121.663	0.1808	0.87	48.968	0.44375	6.8249	2.86134	0.93585	8.0219	3.39421	41.3956	12.4639	42.445	7.1501	51.422	8.3202	311.528
254	28235.719	3830.447	0.1527	0.40496	183.666	126.426	0.1527	0.926	46.131	0.40496	7.4494	2.81235	1.00852	7.4435	3.40902	41.8775	12.244	42.4119	6.8387	50.489	8.0681	308.066
255	28568.775	3887.388	0.1265	0.36895	184.402	130.165	0.1265	0.952	44.47	0.36895	7.9287	2.73802	1.06103	7.0375	3.40808	42.105	12.08	42.4175	6.6109	49.786	7.8512	304.852
256	28301.219	3876.706	0.1105	0.34847	185.532	128.158	0.1105	0.817	49.402	0.34847	7.5935	2.52149	1.00041	7.5984	3.31881	40.9053	12.2299	42.6404	6.8518	50.376	7.8319	303.032
257	28033.66	3866.023	0.0946	0.32799	186.661	126.15	0.0946	0.681	54.334	0.32799	7.2584	2.30495	0.93979	8.1593	3.22955	39.7057	12.3798	42.8632	7.0928	50.965	7.8126	301.213
258	27787.588	3858.269	0.0801	0.30694	187.551	124.189	0.0801	0.549	58.322	0.30694	6.9444	2.11753	0.8841	8.6565	3.15454	38.6414	12.5071	43.031	7.308	51.342	7.7826	299.381
259	27865.979	3894.735	0.0871	0.27735	184.825	122.936	0.0871	0.471	48.037	0.27735	6.9499	2.36993	0.90284	8.1911	3.29476	39.6209	12.2931	42.3675	7.1335	48.505	7.5901	297.368
260	27944.369	3931.202	0.094	0.24776	182.098	121.682	0.094	0.392	37.753	0.24776	6.9555	2.62232	0.92158	7.7258	3.43497	40.6005	12.079	41.7039	6.9589	45.667	7.3977	295.354
261	28022.758	3967.669	0.1009	0.21816	179.371	120.428	0.1009	0.313	27.468	0.21816	6.961	2.87471	0.94032	7.2604	3.57519	41.58	11.865	41.0403	6.7843	42.83	7.2052	293.34
262	26863.846	3791.99	0.1657	0.248	176.442	120.181	0.1657	0.417	37.691	0.248	6.8364	3.12131	0.96847	6.9989	3.54284	40.7318	11.9022	40.1681	6.3509	42.903	6.802	289.027
263	25670.506	3610.408	0.2322	0.27949	173.507	119.961	0.2322	0.526	48.485	0.27949	6.708	3.36774	0.99688	6.743	3.50569	39.8328	11.9463	39.2901	5.9102	43.058	6.3929	284.65
264	24477.166	3428.826	0.2986	0.31098	170.573	119.742	0.2986	0.635	59.279	0.31098	6.5797	3.61417	1.02529	6.4872	3.46853	38.9338	11.9905	38.4121	5.4695	43.212	5.9838	280.273
265	23480.66	3312.829	0.4917	0.31027	165.376	112.597	0.4917	1.038	63.798	0.31027	5.9509	3.29087	0.92004	5.9859	3.18579	36.5144	10.9636	35.5377	5.0842	39.924	5.5197	255.572
266	22510.045	3205.459	0.7015	0.30533	159.881	104.54	0.7015	1.48	67.492	0.30533	5.2562	2.89263	0.7972	5.4524	2.87075	33.8951	9.7958	32.4006	4.7062	36.184	5.0483	228.197
267	21539.428	3098.088	0.9113	0.30038	154.387	96.484	0.9113	1.921	71.186	0.30038	4.5615	2.49438	0.67437	4.9188	2.55571	31.2757	8.628	29.2636	4.3282	32.444	4.577	200.822
268	21992.322	3378.429	0.816	0.29271	162.618	99.415	0.816	1.855	65.054	0.29271	4.8567	2.80418	0.72939	5.5929	2.79517	32.6993	8.924	30.63	4.4683	33.701	4.7574	216.433
269	22813.219	3759	0.6418	0.28434	174.398	105.186	0.6418	1.657	56.382	0.28434	5.4077	3.29703	0.83039	6.5792	3.17797	35.168	9.5984	33.1607	4.7425	36.251	5.1063	243.157
270	23634.115	4139.57	0.4677	0.27596	186.178	110.957	0.4677	1.459	47.711	0.27596	5.9588	3.78987	0.93139	7.5655	3.56077	37.6367	10.2729	35.6913	5.0166	38.8	5.4552	269.881
271	24389.281	4190.138	0.341	0.25691	188.485	113.222	0.341	1.285	42.23	0.25691	6.0231	3.59568	0.99623	8.2461	3.71109	38.2491	10.5994	36.8173	5.1273	38.989	5.6074	279.193
272	25116.996	4102.893	0.2341	0.23341	186.836	114.023	0.2341	1.121	38.081	0.23341	5.8842	3.11458	1.04596	8.7989	3.76433	38.0862	10.7806	37.3566	5.1696	38.192	5.6774	281.233
273	25844.713	4015.649	0.1272	0.2099	185.186	114.823	0.1272	0.957	33.933	0.2099	5.7453	2.63347	1.09569	9.3518	3.81757	37.9233	10.9618	37.8959	5.212	37.395	5.7474	283.274
274	26028.086	3891.397	0.1175	0.23176	180.906	114.47	0.1175	0.906	35.803	0.23176	5.5605	2.82375	1.05127	9.4515	3.74515	37.7726	11.0725	36.9045	5.1087	36.76	5.7191	279.146
275	25872.475	3744.101	0.1682	0.28186	174.986	113.398	0.1682	0.924	41.421	0.28186	5.347	3.43213	0.94822	9.2689	3.59448	37.6293	11.1392	34.9598	4.9145	36.224	5.6296	271.177
276	25716.863	3596.804	0.2189	0.33196	169.067	112.326	0.2189	0.942	47.039	0.33196	5.1336	4.0405	0.84517	9.0863	3.44381	37.4861	11.206	33.0152	4.7204	35.689	5.5401	263.208
277	25382.668	3613.262	0.2181	0.36934	169.137	115.121	0.2181	0.905	48.656	0.36934	5.1445	4.29374	0.77935	8.6377	3.41994	38.0192	11.2762	32.5816	4.5655	34.55	5.4006	261.326
278	24888.23	3776.654	0.1712	0.39531	174.581	121.385	0.1712	0.819	46.682	0.39531	5.3568	4.22834	0.74693	7.9502	3.50982	39.1592	11.3496	33.5039	4.4458	32.869	5.2164	264.905
279	24393.793	3940.045	0.1242	0.42127	180.025	127.65	0.1242	0.732	44.708	0.42127	5.5691	4.16294	0.71451	7.2628	3.59971	40.2992	11.4229	34.4263	4.3261	31.187	5.0321	268.484
280	24546.113	4075.104	0.1135	0.40329	187.939	131.531	0.1135	0.682	44.918	0.40329	5.4783	4.2033	0.72376	7.2101	3.64603	41.0017	11.5232	34.8954	4.387	30.417	4.9092	272.233
281	25528.633	4173.794	0.1494	0.32889	199.024	132.354	0.1494	0.679	47.929	0.32889	4.9985	4.37943	0.78651	7.972	3.63643	41.1427	11.6579	34.783	4.6799	30.816	4.8649	276.2
282	26511.15	4272.484	0.1854	0.25448	210.109	133.177	0.1854	0.676	50.94	0.25448	4.5188	4.55556	0.84926	8.734	3.62682	41.2838	11.7926	34.6705	4.9728	31.215	4.8207	280.167
283	26792.635	4353.276	0.1989	0.23135	213.073	132.859	0.1989	0.661	51.577	0.23135	4.3789	4.45958	0.89138	9.2209	3.70364	41.161	11.7122	34.1086	5.0614	31.402	4.7254	278.722
284	25764.881	4400.643	0.1706	0.30396	200.867	130.41	0.1706	0.622	47.779	0.30396	4.8739	3.85541	0.89496	9.194	3.94186	40.5456	11.2301	32.7074	4.7682	31.193	4.5346	267.172
285	24737.127	4448.009	0.1423	0.37656	188.661	127.961	0.1423	0.584	43.982	0.37656	5.3688	3.25125	0.89853	9.1672	4.18009	39.9302	10.7479	31.3062	4.4751	30.983	4.3438	255.621
286	23803.635	4431.919	0.1294	0.41456	179.342	124.762	0.1294	0.558	41.562	0.41456	5.7027	2.82731	0.92331	9.0778	4.27403	39.2016	10.3212	29.9959	4.1939	30.573	4.1924	245.62
287	23139.053	4234.805	0.1601	0.35382	178.258	119.423	0.1601	0.569	43.071	0.35382	5.5768	2.9175	1.00856	8.8098	3.95637	38.1503	10.053	28.9451	3.9465	29.59	4.1537	240.038
288	22474.471	4037.69	0.1909	0.29308	177.173	114.085	0.1909	0.58	44.58	0.29308	5.451	3.00768	1.09381	8.5418	3.63872	37.099	9.7848	27.8943	3.6992	28.606	4.1149	234.455
289	21997.842	3867.338	0.2141	0.2401	176.781	110.199	0.2141	0.587	45.18	0.2401	5.328	3.11472	1.1606	8.2686	3.35972	36.2285	9.5414	26.9752	3.4806	27.636	4.0374	229.195
290	22436.396	3827.292	0.2008	0.22492	179.756	113.385	0.2008	0.58	41.358	0.22492	5.2186	3.30384	1.1375	7.9701	3.26893	36.2383	9.4189	26.6976	3.4022	26.732	3.7716	225.506
291	22874.951	3787.246	0.1876	0.20975	182.731	116.57	0.1876	0.572	37.536	0.20975	5.1093	3.49296	1.1144	7.6717	3.17815	36.2482	9.2964	26.4201	3.3238	25.829	3.5057	221.817
292	23252.057	3753.734	0.2096	0.20193	185.317	119.122	0.2096	0.627	34.484	0.20193	5.0261	3.66272	1.08415	7.3919	3.09854	36.1645	9.2053	26.1237	3.2464	24.907	3.2553	218.227
293	22933.959	3794.153	0.6314	0.27733	183.504	114.504	0.6314	1.378	40.133	0.27733	5.2394	3.61355	0.97307	7.3245	3.14545	35.0232	9.4701	25.6139	3.181	23.789	3.1785	215.758
294	22615.861	3834.572	1.0532	0.35272	181.692	109.887	1.0532	2.13	45.783	0.35272	5.4527	3.56437	0.86199	7.2572	3.19235	33.8819	9.7348	25.104	3.1155	22.671	3.1017	213.288
295	22297.764	3874.99	1.475	0.42812	179.879	105.27	1.475	2.882	51.433	0.42812	5.666	3.51519	0.75091	7.1898	3.23925	32.7406	9.9995	24.5942	3.05	21.553	3.0249	210.819
296	23364.363	3972.767	1.082	0.42984	205.367	113.28	1.082	2.36	57.8	0.42984	5.4889	3.71129	0.78567	8.8014	3.35567	35.9846	9.6729	24.8475	3.2027	22.297	2.8623	218.966
297	24442.074	4071.005	0.6825	0.43097	231.074	121.391	0.6825	1.827	64.173	0.43097	5.3087	3.90937	0.82161	10.4265	3.47266	39.2637	9.3416	25.107	3.3571	23.057	2.699	227.197
298	25519.787	4169.242	0.2829	0.4321	256.78	129.503	0.2829	1.294	70.547	0.4321	5.1285	4.10744	0.85754	12.0516	3.58965	42.5429	9.0103	25.3665	3.5116	23.816	2.5356	235.429
299	25184.045	4178.621	0.2577	0.39693	233.581	128.21	0.2577	1.171	59.746	0.39693	5.5571	4.21068	0.92184	11.4228	3.62196	41.1763	8.7307	24.8963	3.4077	22.354	2.6198	225.012
300	24696.238	4178.44	0.2728	0.35785	205.12	125.906	0.2728	1.092	47.099	0.35785	6.0512	4.30371	0.98918	10.5516	3.64517	39.31	8.4567	24.3476	3.2761	20.653	2.7306	212.589
301	24208.432	4178.26	0.2879	0.31877	176.659	123.602	0.2879	1.013	34.451	0.31877	6.5452	4.39674	1.05653	9.6803	3.66838	37.4436	8.1827	23.7989	3.1444	18.952	2.8414	200.166
302	24632.605	4396.322	0.3779	0.39488	183.235	128.085	0.3779	1.256	38.727	0.39488	6.9906	4.4699	1.21022	9.7179	3.7099	37.9271	8.6303	24.3745	3.2955	19.412	2.854	206.918
303	25265.592	4664.354	0.4851	0.49736	197.834	134.123	0.4851	1.573	46.878	0.49736	7.4248	4.53851	1.38368	9.9636	3.75562	38.9486	9.2431	25.2077	3.5114	20.368	2.8441	218.06
304	25898.576	4932.385	0.5923	0.59983	212.433	140.16	0.5923	1.891	55.029	0.59983	7.859	4.60712	1.55715	10.2094	3.80134	39.9701	9.856	26.0408	3.7272	21.323	2.8342	229.203
305	25719.867	4894.469	0.4981	0.55219	212.853	135.447	0.4981	1.598	54.073	0.55219	7.4204	4.8645	1.49262	9.8731	3.80878	38.8535	9.4715	25.0545	3.6978	20.044	2.8083	226.155
306	25232.537	4740.224	0.3275	0.44747	207.884	126.645	0.3275	1.073	49.654	0.44747	6.6501	5.19365	1.33761	9.3156	3.80167	36.924	8.7078	23.3763	3.5752	17.914	2.7763	217.713
307	24745.205	4585.98	0.1568	0.34274	202.914	117.843	0.1568	0.548	45.235	0.34274	5.8798	5.5228	1.18259	8.7581	3.79456	34.9945	7.9441	21.6982	3.4526	15.785	2.7443	209.271
308	25584.021	4587.247	0.0883	0.29357	204.36	115.341	0.0883	0.354	50.184	0.29357	5.9468	5.21719	1.16552	8.8522	3.86298	34.6057	7.9695	21.8682	3.3931	16.431	2.7319	205.36
309	27183.963	4677.768	0.0784	0.27629	209.489	116.454	0.0784	0.351	60.51	0.27629	6.4944	4.54726	1.22763	9.3203	3.97475	35.1011	8.4477	23.0989	3.3699	18.67	2.7307	204.049
310	28783.902	4768.288	0.0685	0.259	214.617	117.567	0.0685	0.348	70.835	0.259	7.0419	3.87734	1.28973	9.7884	4.08652	35.5965	8.9259	24.3296	3.3467	20.909	2.7294	202.739
311	28333.326	4781.188	0.0594	0.22424	210.704	118.614	0.0594	0.312	70.731	0.22424	6.7568	3.61111	1.23341	9.9739	3.9879	34.6067	8.8439	23.7953	3.1783	20.906	2.611	196.579
312	26178.969	4729.593	0.0509	0.17495	199.277	119.606	0.0509	0.25	61.961	0.17495	5.7797	3.68033	1.07867	9.9245	3.71446	32.3828	8.2964	21.7944	2.8893	19.04	2.3952	186.389
313	24024.613	4677.998	0.0424	0.12566	187.851	120.598	0.0424	0.188	53.191	0.12566	4.8025	3.74954	0.92394	9.875	3.44102	30.159	7.7489	19.7935	2.6003	17.174	2.1793	176.199
314	22385.168	4618.37	0.0347	0.10164	183.447	122.096	0.0347	0.169	53.062	0.10164	4.4743	4.01666	0.91196	9.9752	3.3453	28.9505	7.3135	18.351	2.3934	15.973	2.0798	170.604
315	21357.516	4549.198	0.0281	0.10765	187.387	124.195	0.0281	0.2	63.2	0.10765	4.9169	4.51892	1.06958	10.253	3.46074	28.9486	7.0112	17.5721	2.2841	15.563	2.1184	170.469
316	20329.865	4480.027	0.0215	0.11365	191.327	126.293	0.0215	0.232	73.339	0.11365	5.3595	5.02118	1.2272	10.5308	3.57619	28.9467	6.7089	16.7932	2.1747	15.153	2.1571	170.334
317	20406.18	4461.429	0.0182	0.11116	193.071	125.112	0.0182	0.232	75.974	0.11116	5.4663	5.37206	1.30468	10.7714	3.58395	28.8818	6.515	16.2784	2.1652	15.191	2.0709	169.148
318	22379.787	4529.749	0.0204	0.09409	191.04	118.296	0.0204	0.178	65.713	0.09409	4.9959	5.46279	1.24443	10.9479	3.40664	28.7086	6.5073	16.2174	2.3272	15.999	1.7701	166.156
319	24353.393	4598.069	0.0226	0.07702	189.009	111.48	0.0226	0.124	55.453	0.07702	4.5255	5.55351	1.18419	11.1244	3.22933	28.5354	6.4997	16.1565	2.4892	16.807	1.4694	163.164
320	25382.883	4682.97	0.0241	0.06869	189.753	106.304	0.0241	0.11	49.618	0.06869	4.2829	5.62419	1.12849	11.2891	3.14463	28.5046	6.505	16.0532	2.5426	16.74	1.2784	161.18
321	23968.455	4810.792	0.0236	0.08299	197.68	105.375	0.0236	0.199	55.241	0.08299	4.6301	5.64301	1.08457	11.4235	3.29963	28.8423	6.5439	15.8401	2.3147	14.408	1.3715	161.808
322	22554.027	4938.613	0.0232	0.09729	205.606	104.445	0.0232	0.288	60.864	0.09729	4.9772	5.66183	1.04064	11.5579	3.45463	29.1799	6.5828	15.627	2.0869	12.076	1.4647	162.436
323	21356.559	4997.537	0.0265	0.1135	210.426	104.024	0.0265	0.389	63.727	0.1135	5.1596	5.57366	1.0088	11.6528	3.54717	29.0622	6.5295	15.4221	1.91	10.272	1.5375	161.047
324	21087.088	4761.759	0.0458	0.13787	201.958	105.784	0.0458	0.546	54.781	0.13787	4.637	5.0279	1.02862	11.5786	3.37253	26.9967	6.082	15.2522	1.9512	10.725	1.5232	151.033
325	20817.617	4525.982	0.0651	0.16224	193.491	107.543	0.0651	0.703	45.835	0.16224	4.1144	4.48213	1.04844	11.5044	3.19788	24.9312	5.6345	15.0822	1.9923	11.179	1.509	141.019
326	20516.475	4297.061	0.0863	0.1851	185.052	109.137	0.0863	0.846	37.731	0.1851	3.6043	4.0473	1.05226	11.3997	3.01769	22.9469	5.1937	14.7771	2.0145	11.471	1.48	131.432
327	19931.281	4129.626	0.124	0.19443	176.872	109.249	0.124	0.87	37.173	0.19443	3.2056	4.60734	0.91256	11.0209	2.78777	21.6909	4.8139	13.2597	1.8664	10.322	1.3185	125.673
328	19346.09	3962.191	0.1617	0.20377	168.692	109.361	0.1617	0.894	36.614	0.20377	2.8069	5.16737	0.77285	10.6421	2.55786	20.4348	4.434	11.7423	1.7184	9.173	1.1571	119.915
329	18772.771	3798.749	0.1991	0.21243	160.749	109.44	0.1991	0.917	36.232	0.21243	2.4135	5.71656	0.63491	10.2732	2.33102	19.1954	4.0596	10.2461	1.5706	8.039	0.9984	114.211
330	19252.875	3989.593	0.2068	0.16085	173.81	106.586	0.2068	0.833	51.499	0.16085	2.4842	5.30325	0.65394	10.7866	2.37738	19.4338	4.1737	10.6303	1.4556	8.255	1.0866	113.28
331	19732.977	4180.436	0.2144	0.10927	186.87	103.732	0.2144	0.749	66.765	0.10927	2.5549	4.88995	0.67297	11.3	2.42374	19.6722	4.2879	11.0146	1.3405	8.472	1.1749	112.349
332	20213.08	4371.279	0.222	0.0577	199.93	100.878	0.222	0.665	82.032	0.0577	2.6256	4.47664	0.692	11.8134	2.4701	19.9106	4.402	11.3989	1.2254	8.688	1.2631	111.419
333	19503.473	4317.324	0.1608	0.04312	192.545	105.192	0.1608	0.587	75.092	0.04312	2.3861	4.33399	0.73886	11.6845	2.51378	20.0331	4.2114	10.8204	1.2296	8.501	1.2705	110.327
334	18693.18	4242.652	0.0938	0.03167	183.429	110.113	0.0938	0.511	66.274	0.03167	2.1204	4.21424	0.78806	11.5011	2.55723	20.1457	3.995	10.1604	1.244	8.279	1.2711	109.222
335	17882.889	4167.98	0.0267	0.02022	174.314	115.034	0.0267	0.434	57.455	0.02022	1.8547	4.09448	0.83727	11.3178	2.60068	20.2584	3.7787	9.5004	1.2583	8.058	1.2717	108.117
336	17086.113	4211.1	0.0708	0.02678	178.217	117.054	0.0708	0.419	54.999	0.02678	1.6922	4.02497	0.74831	11.9612	2.78689	22.5646	4.1229	10.5947	1.4505	9.292	1.2893	123.578
337	16292.053	4277.869	0.1372	0.03696	184.735	118.491	0.1372	0.418	53.821	0.03696	1.5504	3.96554	0.63161	12.7707	3.00176	25.3113	4.5796	12.0411	1.6784	10.819	1.3104	142.365
338	15497.992	4344.638	0.2036	0.04714	191.252	119.929	0.2036	0.416	52.642	0.04714	1.4085	3.9061	0.51491	13.5801	3.21663	28.058	5.0363	13.4876	1.9063	12.346	1.3315	161.152
339	13886.296	4325.562	0.3832	0.06595	179.868	170.559	0.3832	0.978	56.561	0.06595	1.147	3.28767	0.48517	13.6759	3.50496	30.458	5.8409	15.7887	2.1924	14.558	1.7792	185.479
340	11992.717	4276.891	0.6019	0.08773	162.312	238.147	0.6019	1.734	62.237	0.08773	0.8443	2.47653	0.4854	13.5257	3.81863	32.7386	6.7656	18.3844	2.4986	17.007	2.3741	211.716
341	10099.137	4228.22	0.8206	0.10951	144.757	305.736	0.8206	2.49	67.913	0.10951	0.5415	1.66538	0.48563	13.3755	4.13229	35.0192	7.6902	20.9802	2.8048	19.455	2.9689	237.954

Garnet G pt	Ce	Dy	Er	Eu	Gd	Ho	La	Lu	Nd	P	Pr	Sc	Sm	Tb	Tm	Yb	Y
4	10.0969	9.9112	4.1445	0.57405	10.4275	1.77898	9.2552	0.53324		213.374			1.978	1.65736	0.48825	3.646	46.057
5	7.3364	10.2024	4.3347	0.51364	10.6797	1.79195	6.0045	0.49354		203.916			2.377	1.78648	0.46899	3.5059	47.833
6	4.576	10.4936	4.5249	0.45323	10.9318	1.80492	2.7538	0.45384		194.458			2.508	1.91559	0.44973	3.3659	49.609
7	2.9148	10.7584	4.5047	0.43373	11.1274	1.80992	1.0691	0.45591		194.87			2.306	1.9579	0.48054	3.3738	50.604
8	2.2872	10.9983	4.2867	0.45269	11.2697	1.80744	0.8564	0.49724		204.56			1.996	1.9186	0.55841	3.5208	50.867
9	1.6595	11.2382	4.0687	0.47166	11.412	1.80495	0.6438	0.53857		214.25			2.066	1.87929	0.63628	3.6679	51.129
10	1.4964	11.0473	4.2221	0.4858	11.4496	1.82514	0.533	0.56416		211.557			2.458	1.892	0.68448	3.7785	52.334
11	1.5959	10.6128	4.5854	0.49723	11.4281	1.85815	0.4797	0.58085		201.865			2.863	1.9341	0.7159	3.8686	54.072
12	1.6954	10.1783	4.9487	0.50866	11.4066	1.89116	0.4265	0.59753		192.172			3.195	1.9762	0.74733	3.9586	55.81
13	1.5521	11.0282	5.158	0.52395	11.7237	2.02701	0.4561	0.61801		181.794			3.562	2.04099	0.74478	4.1706	57.202
14	1.3331	12.2785	5.3193	0.54044	12.1464	2.19492	0.5115	0.63967		171.202			3.86	2.11286	0.73164	4.4205	58.486
15	1.1141	13.5288	5.4806	0.55693	12.5691	2.36283	0.5669	0.66133		160.61			3.952	2.18473	0.7185	4.6705	59.771
16	1.2976	13.8309	5.6379	0.615	12.9605	2.39944	0.5398	0.68899		148.083			4.057	2.2684	0.79662	5.0288	61.688
17	1.533	14.0107	5.7947	0.67842	13.348	2.41913	0.5021	0.71743		135.306			4.317	2.35359	0.8865	5.4011	63.686
18	1.7655	14.1802	5.9482	0.74093	13.7221	2.43806	0.4645	0.7453		122.523			4.67	2.43716	0.97499	5.7674	65.651
19	1.683	13.2439	5.7465	0.70467	12.6746	2.37491	0.4308	0.71332		109.034			4.833	2.34676	0.91389	5.4914	64.069
20	1.6006	12.3076	5.5449	0.66842	11.6271	2.31177	0.3972	0.68134		95.545			4.799	2.25635	0.85279	5.2154	62.487
29	0.761	12.8623	5.9448	0.49392	10.827	2.30669	0.1943	0.72475		68.717			7.041	2.25646	0.70388	4.2592	62.278
30	0.6708	14.2536	6.4765	0.5874	12.2554	2.57489	0.1934	0.81018		73.855			7.27	2.49627	0.78682	4.9102	69.17
31	0.6112	14.4445	6.3801	0.67909	13.3024	2.65226	0.2049	0.80518		73.381			7.233	2.47907	0.84441	5.4234	70.67
32	0.5516	14.6355	6.2837	0.77079	14.3493	2.72963	0.2164	0.80018		72.907			7.185	2.46187	0.90199	5.9367	72.17
33	0.4994	14.5998	6.0503	0.76705	14.4072	2.71419	0.2122	0.81231		71.877			6.889	2.41582	0.90521	6.0667	71.432
34	0.4515	14.4289	5.7353	0.70643	13.8754	2.64343	0.1985	0.83466		70.516			6.47	2.35258	0.87602	5.9684	69.36
35	0.4037	14.2581	5.4202	0.64582	13.3437	2.57267	0.1848	0.85701		69.155			6.338	2.28934	0.84682	5.87	67.288
40	0.5192	11.6819	6.5455	0.51475	10.1303	2.32653	0.224	0.97535		68.677			6.693	2.09754	0.83936	6.1005	64.811
41	0.5421	13.2222	7.5199	0.58915	10.8516	2.63106	0.2186	1.11208		77.03			6.856	2.36686	0.98565	6.9325	74.598
42	0.4778	14.1379	7.8837	0.5205	12.1357	2.77964	0.1863	1.1205		84.405			6.55	2.40522	1.11118	7.0075	79.442
43	0.4131	15.0518	8.2455	0.4514	13.4216	2.92773	0.154	1.12853		91.776			5.831	2.44288	1.23664	7.0801	84.271
44	0.9592	15.8624	8.5105	0.39686	14.547	3.05064	0.3461	1.13065		96.866			5.176	2.4907	1.33459	7.1404	88.323
53	2.4051	14.5006	8.7345	0.51618	10.9627	3.1246	0.7543	1.24405		77.612			6.327	2.14783	1.13888	8.7833	81.121
54	3.4253	15.7246	8.7356	0.53427	10.9388	3.24549	1.3612	1.22173		86.828			5.225	2.22855	1.32306	9.2996	83.676
55	4.4455	16.9485	8.7366	0.55235	10.9149	3.36638	1.9682	1.19941		96.044			4.619	2.30926	1.50724	9.8158	86.232
101	6.228	23.3416	14.9516	0.59589	12.8811	5.09359	2.0196	2.66524		72.061			3.848	3.01049	2.40383	17.9873	128.007
102	4.4077	24.0394	15.3543	0.5442	13.3739	5.18031	1.2329	2.75025		71.287			3.961	3.05974	2.42664	18.2693	130.596
103	4.5881	21.0243	13.5513	0.57512	12.2115	4.4321	1.4528	2.43386		74.881			3.946	2.61847	2.05696	15.574	112.768
104	4.7685	18.0092	11.7482	0.60603	11.049	3.68389	1.6727	2.11748		78.475			4.065	2.17719	1.68728	12.8787	94.939
113	3.2421	19.8861	13.3828	0.22096	13.4212	4.26324	0.815	1.97351		112.602			2.503	3.12121	1.70559	12.3865	116.751
114	2.4029	20.7583	13.7371	0.28263	13.5825	4.30407	0.6255	1.91423		102.683			3.281	2.98005	1.76173	12.2784	113.958
115	1.5636	21.6304	14.0913	0.34429	13.7437	4.3449	0.4359	1.85494		92.764			3.717	2.83888	1.81788	12.1703	111.164
116	0.8924	22.1678	14.1358	0.39505	13.8765	4.39941	0.2801	1.78959		84.748			3.692	2.74448	1.85143	12.0277	108.932
117	0.8659	21.4213	12.9921	0.40396	13.9004	4.50642	0.2539	1.70093		84.032			3.58	2.82942	1.79836	11.7529	108.858
118	0.8395	20.6748	11.8484	0.41287	13.9242	4.61342	0.2277	1.61227		83.316			3.919	2.91437	1.74528	11.4781	108.784
119	0.8035	20.0682	11.124	0.40647	13.874	4.63123	0.2227	1.5798		83.815			4.755	2.95548	1.6875	11.2302	108.416
120	0.7482	19.7453	11.2498	0.36901	13.6737	4.46813	0.2604	1.66128		86.774			5.562	2.90768	1.62017	11.0369	107.451
121	0.6929	19.4225	11.3756	0.33154	13.4733	4.30503	0.2982	1.74275		89.734			5.775	2.85989	1.55284	10.8436	106.487
122	0.7851	18.6491	11.117	0.32831	13.3371	4.05656	0.3055	1.68943		93.178			5.381	2.79691	1.50236	10.3261	102.818
123	1.055	17.333	10.3954	0.36629	13.2781	3.7053	0.2761	1.47379		97.206			4.793	2.71567	1.47218	9.4181	95.893
124	1.3249	16.017	9.6739	0.40427	13.2192	3.35405	0.2467	1.25815		101.234			4.583	2.63442	1.442	8.5101	88.968
125	1.418	15.6913	9.3097	0.45058	12.9185	3.18947	0.2915	1.20334		97.649			4.903	2.54763	1.38758	8.1081	86.17
126	1.3815	16.0911	9.2072	0.50297	12.4407	3.16165	0.3908	1.26635		88.486			5.317	2.45677	1.3154	8.0768	86.396
127	1.3451	16.491	9.1047	0.55537	11.963	3.13383	0.4901	1.32936		79.324			5.387	2.36591	1.24323	8.0455	86.623
128	1.1985	17.0484	9.2195	0.54739	12.5869	3.23067	0.4064	1.31403		72.547			5.084	2.47592	1.26338	7.9409	88.908
129	1.0048	17.6732	9.4272	0.51362	13.6815	3.38077	0.2446	1.26521		66.79			4.701	2.67176	1.32298	7.805	92.073
130	0.8111	18.298	9.635	0.47985	14.7762	3.53087	0.0827	1.2164		61.034			4.483	2.86761	1.38258	7.669	95.238
131	0.8178	18.966	9.776	0.51478	15.24	3.54635	0.0948	1.24075		63.038			4.548	2.96649	1.41834	8.353	97.912
132	0.8673	19.6433	9.9027	0.56437	15.5691	3.5331	0.144	1.28072		66.7			4.938	3.04467	1.44901	9.2121	100.48
133	0.9167	20.3206	10.0295	0.61397	15.8982	3.51985	0.1932	1.32069		70.361			5.548	3.12284	1.47968	10.0712	103.048
134	0.7664	19.2875	9.4835	0.58848	14.7868	3.52727	0.1457	1.28996		70.633			6.185	3.01519	1.3775	9.4556	98.007
135	0.6049	18.1597	8.9002	0.55883	13.5956	3.53584	0.0928	1.25531		70.716			6.503	2.89724	1.26796	8.7584	92.545
136	0.4497	17.0264	8.3183	0.52768	12.431	3.52418	0.0448	1.21695		70.646			6.411	2.7699	1.15925	8.0931	86.949
137	0.3749	15.8204	7.7546	0.47681	11.6143	3.24785	0.06	1.13		68.558			6.108	2.51965	1.06129	7.8466	79.603
138	0.3001	14.6145	7.1909	0.42595	10.7976	2.97151	0.0751	1.04305		66.47			5.87	2.26939	0.96333	7.6001	72.258
142	0.4197	13.1693	6.4642	0.58715	9.9512	2.80578	0.2815	1.03404		60.736			6.03	1.9524	1.00539	6.1392	70.997
143	0.5121	13.5136	6.5556	0.56854	10.4218	3.00894	0.219	1.03845		89.06			6.409	2.0307	0.93023	6.4077	71.511
144	0.6045	13.8579	6.647	0.54993	10.8925	3.2121	0.1565	1.04286		117.384			6.976	2.10899	0.85506	6.6761	72.025
145	1.0506	13.8402	6.6128	0.53118	11.0064	3.15822	0.2426	1.00538		153.165			7.242	2.13788	0.83104	6.6445	70.898
149	3.4692	14.0459	7.1017	0.61448	11.7503	2.70941	0.8306	0.98068		285.69			7.787	2.50641	1.05865	6.5742	74.135
150	3.624	14.9175	7.7149	0.69716	12.7512	3.01273	0.7797	1.10572		300.011			7.197	2.7943	1.14076	7.1698	81.187
151	3.1082	15.2905	8.009	0.72942	12.8038	3.15309	0.6828	1.14566		269.748			8.388	2.84849	1.10735	7.286	82.54
152	2.2888	15.4376	8.1585	0.73885	12.4269	3.21965	0.565	1.14707		219.292			16.459	2.79685	1.02161	7.1852	81.313
153	1.4693	15.5848	8.308	0.74828	12.05	3.28621	0.4473	1.14847		168.837			45.597	2.7452	0.93587	7.0844	80.085
154	1.1878	15.569	8.0818	0.82081	11.9016	3.12081	0.3883	1.10019		134.511			104.953	2.5548	0.94384	6.7543	76.664
155	1.0312	15.5155	7.7685	0.90798	11.8063	2.90163	0.3428	1.04038		103.926			174.236	2.33222	0.97356	6.3709	72.734
156	0.8745	15.4619	7.4552	0.99515	11.7109	2.68244	0.2974	0.98058		73.341			193.879	2.10964	1.00328	5.9876	68.805
157	1.1154	15.3308	7.2426	0.99655	11.5874	2.67391	0.3031	0.95934		74.083			147.414	2.17315	0.99853	6.169	69.246
158	1.3839	15.1942	7.037	0.99201	11.4619	2.67998	0.3123	0.94079		76.995			76.52	2.25648	0.9914	6.3896	69.99
159	1.6213	14.9764	6.8156	0.97977	11.3051	2.67909	0.3173	0.91901		79.409			30.7	2.33125	0.98133	6.5643	70.435
160	1.3597	13.4533	6.3425	0.84377	10.646	2.56656	0.2533	0.84561		73.822			13.844	2.26852	0.92422	6.0019	66.067
164	0.9624	13.7623	6.581	0.76901	12.2356	2.75107	0.25	0.91617		69.894			8.485	2.49275	0.81424	6.4594	68.815
165	0.9678	14.8971	6.9872	0.81361	13.3352	2.86327	0.2836	0.98968		75.239			8.645	2.587	0.83011	6.9713	73.165
166	0.9037	15.4051	7.1725	0.77992	14.0302	2.82523	0.276	1.01779		86.244			8.272	2.54312	0.88844	7.1052	76.271
167	0.8397	15.9132	7.3577	0.74623	14.7253	2.78719	0.2685	1.04589		97.25			7.719	2.49925	0.94676	7.2391	79.377
168	0.9065	15.8266	7.2141	0.7155	14.8322	2.71933	0.2881	1.06006		110.124			7.557	2.42897	0.96356	7.2167	79.199
169	1.1474	14.9487	6.6327	0.68872	14.1563	2.61177	0.3437	1.05568		125.487			7.452	2.32353	0.92508	6.9863	74.65
170	1.3883	14.0707	6.0513	0.66193	13.4804	2.50422	0.3994	1.0513		140.849			7.001	2.2181	0.88659	6.7559	70.101
171	1.4135	13.1458	5.7149	0.6568	12.5324	2.32559	0.3998	0.96942		162.759			6.336	2.13381	0.83177	6.3636	66.671
172	1.264	12.1829	5.577	0.6692	11.364	2.08939	0.3555	0.82477		189.973			5.903	2.06664	0.7637	5.8402	64.147
173	1.1144	11.2201	5.4391	0.68161	10.1955	1.85318	0.3112	0.68012		217.187			5.742	1.99947	0.69564	5.3169	61.623
174	1.0629	11.0138	5.1647	0.64217	9.6986	1.79006	0.2693	0.62416		240.926			5.765	1.96879	0.65913	5.0787	59.506
175	1.0585	11.1703	4.8248	0.57788	9.5236	1.80993	0.2286	0.61072		262.999			5.71	1.95561	0.63774	4.9772	57.585
176	1.054	11.3268	4.4849	0.51359	9.3485	1.8298	0.188	0.59728		285.071			5.557	1.94243	0.61635	4.8757	55.664
177	1.2321	11.5037	4.2843	0.49186	9.1195	1.83749	0.2589	0.65579		287.121			5.265	1.94236	0.61309	4.9098	55.239
178	1.456	11.6858	4.1186	0.48081	8.8768	1.84213	0.3578	0.73236		284.145			4.898	1.94557	0.61437	4.9779	55.19
179	1.68	11.8678	3.953	0.46977	8.6342	1.84676	0.4567	0.80893		281.17			4.724	1.94878	0.61565	5.046	55.141
180	1.8071	11.4722	4.1879	0.44271	9.5515	1.87339	0.4889	0.74562		275.18			4.581	1.9791	0.61786	4.7242	56.845
181	1.9262	11.0284	4.4562	0.41432	10.5658	1.90186	0.5154	0.67062		268.938			4.066	2.01168	0.62014	4.3697	58.696
182	2.0204	10.6207	4.7179	0.38935	11.4958	1.93348	0.54	0.59939		262.623			3.127	2.04386	0.6232	4.0318	60.441
183	1.6007	10.9583	4.841	0.43485	10.689	2.03004	0.5251	0.60596		254.786			1.962	2.0677	0.64218	4.033	60.015
184	1.1811	11.2959	4.9641	0.48035	9.8821	2.1266	0.5101	0.61253		246.949			1.029	2.09155	0.66116	4.0342	59.588
185	3.6946	11.8906	5.201	0.68403	9.7527	2.26364	2.6344	0.63431		239.199			0.485	2.16755	0.70517	4.1702	60.624
186	20.5534	13.7426	5.9943	1.66132	12.9366	2.59866	15.2215	0.73054		231.875			0.222	2.49862	0.87161	4.9659	68.816
187	37.4123	15.5946	6.7875	2.63861	16.1205	2.93367	27.8086	0.82676		224.55			0.143	2.82969	1.03804	5.7616	77.008

Dataset S3

Monazite	Location	Analysis	Pb ppm	Th ppm	U ppm	Th/U	Measured ratios $^{206}Pb/^{238}U$	2σ error	$^{207}Pb/^{235}U$	2σ error	$^{208}Pb/^{232}Th$	2σ error	Error correlation ($^{206}Pb/^{238}U$)/($^{207}Pb/^{235}U$)	Ages (Ma) $^{207}Pb/^{206}Pb$	2σ error	Ages (Ma) $^{206}Pb/^{238}U$	2σ error	Ages (Ma) $^{207}Pb/^{235}U$	2σ error	Ages (Ma) $^{208}Pb/^{232}Th$	2σ error
M3	garnet corona	07220410a	4833	46728	655	71.4	0.37671	0.00970	6.24289	0.16316	0.10860	0.00256	0.99	1959	39	2061	45	2011	23	2084	47
		08220410a	4344	39967	1042	38.4	0.38194	0.00980	6.27779	0.16158	0.10996	0.00260	1.00	1945	38	2085	46	2015	23	2109	47
		09220410a	4161	37465	1172	32.0	0.38172	0.00980	6.32455	0.16238	0.11067	0.00262	1.00	1959	38	2084	46	2022	23	2122	48
		10220410a*	4016	35987	1141	31.6	0.38382	0.00986	6.41352	0.16532	0.11107	0.00262	1.00	1974	38	2094	46	2034	23	2129	48
		11220410a	3926	37703	685	55.0	0.37378	0.00962	6.16346	0.16048	0.10803	0.00256	0.99	1951	39	2047	45	1999	23	2073	47
		12220410a	4124	38152	1113	34.3	0.37153	0.00954	6.12666	0.15802	0.10854	0.00258	1.00	1951	38	2037	45	1994	23	2083	47
		13220410a	4015	37077	1133	32.7	0.36773	0.00944	5.97349	0.15428	0.10842	0.00256	0.99	1924	38	2019	44	1972	22	2081	47
		14220410a	3877	37583	630	59.6	0.37587	0.00968	5.96853	0.15712	0.10752	0.00254	0.98	1883	40	2057	45	1971	23	2064	47
		17220410a	1485	60815	1145	53.1	0.37460	0.00966	6.20153	0.16430	0.10731	0.00254	0.97	1958	40	2051	45	2005	23	2060	46
M1	matrix	19220410a	4190	40269	614	65.5	0.38301	0.00992	6.68575	0.17976	0.10918	0.00260	0.96	2052	40	2090	46	2071	24	2094	47
		20220410a	3243	30781	422	72.9	0.38657	0.01004	6.63376	0.18068	0.10911	0.00258	0.95	2021	41	2107	47	2064	24	2093	47
		21220410a	3512	33630	373	90.1	0.37961	0.00996	6.50656	0.18426	0.10740	0.00254	0.93	2019	44	2075	47	2047	25	2062	47
		22220410a	3392	33417	242	137.9	0.37192	0.00966	6.31423	0.17258	0.10686	0.00254	0.95	2002	42	2038	45	2020	24	2052	46
		25220410a	2645	25527	396	64.5	0.37782	0.00990	6.32737	0.18052	0.10825	0.00258	0.92	1978	44	2066	46	2022	25	2078	47
		26220410a	2514	24739	288	85.9	0.37138	0.00972	6.20212	0.17560	0.10655	0.00254	0.92	1973	44	2036	46	2005	25	2046	46
		28220410a	2666	25695	381	67.5	0.37365	0.00970	6.18806	0.17102	0.10776	0.00256	0.94	1958	42	2047	46	2003	24	2069	47
M13	garnet corona	29220410a*	2540	25792	317	81.3	0.36243	0.00946	5.86449	0.16538	0.10310	0.00246	0.93	1917	44	1994	45	1956	24	1983	45
		30220410a	2554	25329	278	91.2	0.37082	0.00970	6.05440	0.17250	0.10600	0.00252	0.92	1933	45	2033	46	1984	25	2036	46
		33220410a	2989	29611	301	98.5	0.37283	0.00976	6.30146	0.18120	0.10695	0.00254	0.91	1995	45	2043	46	2019	25	2054	46
		36220410a	2072	20720	170	121.7	0.37748	0.01000	6.70199	0.20022	0.10664	0.00254	0.89	2082	47	2065	47	2073	26	2048	46
M12	cordierite	42220410a	3019	30710	319	96.3	0.36237	0.00950	5.96332	0.17478	0.10359	0.00248	0.89	1947	46	1993	45	1971	25	1992	45
		43220410a	3504	34976	290	120.4	0.38431	0.01006	6.38088	0.18676	0.10619	0.00254	0.89	1963	46	2096	47	2030	26	2040	46
M7	inclusion in	07220410b	3436	29255	1805	16.2	0.38007	0.00978	6.48405	0.17972	0.10598	0.00256	0.93	2011	42	2077	46	2044	24	2036	47
	garnet	08220410b	3488	28368	1978	14.3	0.38398	0.00988	6.53893	0.18158	0.10883	0.00264	0.93	2008	42	2095	46	2051	24	2088	48
		09220410b	10440	79551	3740	21.3	0.38353	0.00986	6.53198	0.18114	0.10899	0.00264	0.93	2008	42	2093	46	2050	24	2091	48
		10220410b	11282	84742	4281	19.8	0.38280	0.00984	6.50028	0.18084	0.10919	0.00264	0.92	2003	42	2089	46	2046	24	2095	48
M6	garnet corona	11220410b*	8361	67660	3148	21.5	0.36139	0.00932	6.06015	0.17016	0.10287	0.00248	0.92	1980	43	1989	44	1985	24	1979	46
		15220410b*	3654	31896	1926	16.6	0.36765	0.00948	6.25963	0.17874	0.10388	0.00252	0.90	1995	55	1954	46	1974	29	1998	46
		16220410b	4026	35564	1642	21.7	0.37599	0.00970	6.31429	0.18170	0.10700	0.00258	0.90	2007	44	2058	45	2020	25	2055	47
M8	garnet corona	17220410b*	23039	42916	5258	8.2	0.35764	0.00924	5.89449	0.17014	0.10261	0.00248	0.90	1983	44	1971	44	1960	25	1974	46
		18220410b*	23781	44063	5234	8.4	0.36269	0.00938	6.02281	0.17498	0.10366	0.00250	0.89	1963	45	1995	44	1979	25	1994	46
		19220410b	29453	52048	7093	7.3	0.36922	0.00954	6.19700	0.18046	0.10588	0.00256	0.89	1982	45	2026	45	2004	25	2034	47
M4	garnet corona	20220410b	26864	56458	1094	51.6	0.37686	0.00986	6.42208	0.19650	0.10781	0.00260	0.86	2009	48	2062	46	2035	27	2069	48
M11	garnet corona	23220410b	4197	36576	1946	18.8	0.36793	0.00954	6.28375	0.18906	0.10644	0.00258	0.86	2013	47	2020	45	2016	26	2044	47
		24220410b	3815	33360	1753	19.0	0.36885	0.00958	6.29805	0.19142	0.10618	0.00256	0.85	2012	48	2024	45	2018	27	2040	47
		25220410b	69383	31589	1255	25.2	0.38074	0.00990	6.44913	0.19800	0.10862	0.00262	0.85	1998	48	2080	46	2039	27	2084	48
		26220410b	68800	32354	981	33.0	0.38095	0.00994	6.48009	0.20158	0.10798	0.00262	0.84	2006	49	2081	46	2043	27	2073	48
M2	matrix	27220410b	119897	60223	618	97.4	0.36992	0.00972	6.19893	0.19768	0.10755	0.00260	0.82	1979	51	2029	46	2004	28	2065	47
		28220410b	104613	51524	708	72.7	0.37416	0.00980	6.32158	0.20144	0.10851	0.00262	0.82	1994	51	2049	46	2022	28	2082	48

Zircon	Analysis	Pb ppm	Th ppm	U ppm	Th/U	Measured ratios $^{207}Pb/^{206}Pb$	2σ	$^{206}Pb/^{238}U$	2σ	$^{207}Pb/^{235}U$	2σ	Error correlation ($^{206}Pb/^{238}U$)/($^{207}Pb/^{235}U$)	Ages (Ma) $^{207}Pb/^{206}Pb$	2σ error $^{207}Pb/^{206}Pb$	Ages (Ma) $^{206}Pb/^{238}U$	2σ error 2σ	Ages (Ma) $^{207}Pb/^{235}U$	2σ error 2σ
	05150311b	105	38	274	0.1	0.12805	0.00274	0.37178	0.00782	6.56623	0.1456	0.95	2071	38	2038	37	2055	20
	06150311b	59	22	147	0.1	0.12887	0.00284	0.38044	0.00794	6.76245	0.15232	0.93	2083	39	2078	37	2081	20
	07150311b	51	11	118	0.1	0.13706	0.0031	0.40551	0.0084	7.66637	0.17426	0.91	2190	39	2194	39	2193	20
	09150311b	73	28	209	0.1	0.13477	0.00306	0.35447	0.00716	6.58908	0.14736	0.90	2161	39	1956	34	2058	20
	05150311c	111	123	239	0.5	0.14136	0.00312	0.40488	0.00864	7.89667	0.1802	0.94	2244	38	2192	40	2219	21
	06150311c	49	29	139	0.2	0.1281	0.0034	0.32557	0.00706	5.75444	0.15276	0.82	2072	46	1817	34	1940	23
	07150311c	18	21	45	0.5	0.12554	0.00314	0.35073	0.00738	6.07523	0.15118	0.85	2036	44	1938	35	1987	22
	08150311c	57	28	154	0.2	0.12777	0.00302	0.37744	0.00772	6.65346	0.1548	0.88	2068	41	2064	36	2067	21
	09150311c	135	123	301	0.4	0.14845	0.0035	0.41452	0.00832	8.48907	0.19336	0.88	2328	40	2236	38	2285	21
	10150311c	91	40	239	0.2	0.12904	0.00312	0.38156	0.00756	6.79173	0.15614	0.86	2085	42	2084	35	2085	20
	03150311d	320	344	813	0.4	0.12775	0.0028	0.35262	0.00772	6.21268	0.14532	0.94	2067	38	1947	37	2006	20
	04150311d	229	182	549	0.3	0.12836	0.00288	0.37412	0.00808	6.62303	0.1552	0.92	2076	39	2049	38	2062	21
	05150311d	151	80	363	0.2	0.12791	0.00294	0.37889	0.00806	6.68385	0.15756	0.90	2069	40	2071	38	2071	21
	06150311d	170	153	391	0.4	0.12838	0.00316	0.37536	0.00794	6.64614	0.16414	0.86	2076	43	2055	37	2066	22

APPENDIX S1 : Trace element LA-ICP-MS analytical procedure

LA-ICP-MS trace element maps were acquired using a Resonetics M-50-LR 193 nm excimer laser coupled to an Agilent 7700x Quadrupole ICP-MS housed at Adelaide Microscopy, University of Adelaide. Instrument conditions and mapping protocols similar to that employed in this study are outlined by (Raimondo et al., 2017). Mapping was performed on standard 30 μm-thick polished thin sections by ablating a series of parallel rasters across the sample surface to form a square or rectangular grid. A beam diameter of 16 μm coupled with a laser repetition rate of 10 Hz produced an energy density of ~3.5 J/cm^2 at the target, and a scan speed of 22 μm/s and line spacing of 16 μm were used.

Data acquisition was performed in time-resolved analysis mode as a single continuous experiment. Each analysis comprised a suite of 39 elements (Figures S4-S6 and Datasets S1 and S2); dwell times for major elements were 0.005 s (to reduce excessive count rates) and all other masses were 0.008 s, giving a total sweep time of 0.31 s. Standards were analysed in duplicate at the start and end of each mapping run, and included reference glasses NIST 610 and 612 (Jochum et al., 2011; Pearce et al., 1997) and garnet standard MON-GT (C. Harris & Vogeli, 2010; Chris Harris et al., 2000). Data reduction was performed using the software *Iolite* (Hellstrom et al., 2008; Paton et al., 2011; Woodhead et al., 2007), with quantification via the Trace Elements DRS applied using ^{29}Si for internal calibration, applicable to garnet pixels only. Finally, image and data processing was completed using *XMapTools* 2.3.4 (Lanari et al., 2014; Raimondo et al., 2017) and *ImageJ* (Abramoff, Magalhães & Ram, 2004).

REFERENCES

Harris, C., & Vogeli, J. (2010). OXYGEN ISOTOPE COMPOSITION OF GARNET IN THE PENINSULA GRANITE, CAPE GRANITE SUITE, SOUTH AFRICA: CONSTRAINTS ON MELTING AND EMPLACEMENT MECHANISMS. *South African Journal of Geology*, *113*(4), 401-412. https://doi.org/10.2113/gssajg.113.4.401

Harris, Chris, Smith, H. S., & le Roex, A. P. (2000). Oxygen isotope composition of phenocrysts from Tristan da Cunha and Gough Island lavas : Variation with fractional crystallization and evidence for assimilation. *Contributions to Mineralogy and Petrology*, *138*(2), 164-175. https://doi.org/10.1007/s004100050015

Hellstrom, J., Paton, C., Woodhead, J., & Hergt, J. (2008). Iolite : Software for spatially resolved LA-(quad and MC) ICPMS analysis. *Mineralogical Association of Canada short course series*, *40*, 343–348.

Jochum, K. P., Weis, U., Stoll, B., Kuzmin, D., Yang, Q., Raczek, I., Jacob, D. E., Stracke, A., Birbaum, K., Frick, D. A., Günther, D., & Enzweiler, J. (2011). Determination of Reference Values for NIST SRM 610–617 Glasses Following ISO Guidelines. *Geostandards and Geoanalytical Research*, *35*(4), 397-429. https://doi.org/10.1111/j.1751-908X.2011.00120.x

Lanari, P., Vidal, O., De Andrade, V., Dubacq, B., Lewin, E., Grosch, E. G., & Schwartz, S. (2014). XMapTools : A MATLAB©-based program for electron microprobe X-ray image processing and geothermobarometry. *Computers & Geosciences*, *62*, 227-240. https://doi.org/10.1016/j.cageo.2013.08.010

Paton, C., Hellstrom, J., Paul, B., Woodhead, J., & Hergt, J. (2011). Iolite : Freeware for the Visualisation and Processing of Mass Spectrometric Data. *J. Anal. At. Spectrom. VL - IS -*, *online*. https://doi.org/10.1039/C1JA10172B

Pearce, N. J. G., Perkins, W. T., Westgate, J. A., Gorton, M. P., Jackson, S. E., Neal, C. R., & Chenery, S. P. (1997). A Compilation of New and Published Major and Trace Element Data for NIST SRM 610 and NIST SRM 612 Glass Reference Materials. *Geostandards Newsletter*, *21*(1), 115-144. https://doi.org/10.1111/j.1751-908X.1997.tb00538.x

Raimondo, T., Payne, J., Wade, B., Lanari, P., Clark, C., & Hand, M. (2017). Trace element mapping by LA-ICP-MS : Assessing geochemical mobility in garnet. *Contributions to Mineralogy and Petrology*, *172*(4), 17. https://doi.org/10.1007/s00410-017-1339-z

Woodhead, J. D., Hellstrom, J., Hergt, J. M., Greig, A., & Maas, R. (2007). Isotopic and Elemental Imaging of Geological Materials by Laser Ablation Inductively Coupled Plasma-Mass Spectrometry. *Geostandards and Geoanalytical Research*, *31*(4), 331-343. https://doi.org/10.1111/j.1751-908X.2007.00104.x

Appendix S2 : U-Th-Pb monazite and zircon geochronology analytical procedures

The identification, distribution and characterization of chemical zoning of monazite was performed in-situ, following the approach of Williams, Jercinovic, Goncalves & Mahan (2006), on a Cameca SX100 ® electron microprobe at the Laboratoire Magmas et Volcans in Clermont-Ferrand (France). All monazite grains were identified through full-thin-section X-ray mapping for Ce Lα, P Kα along with Al Kα, Mg Kα to obtain a mineralogically and texturally map in order to reveal the monazite distribution with respect to the leucosome, quartz saturated and undersaturated domains (Figure 18). Analytical conditions were a 15 keV accelerating voltage with a 200 nA beam current, a defocussed beam at 35 µm, and a counting time of 9 ms per pixel with a 35 µm pixel setp size. High resolution compositional maps were performed on all the selected grains for Y Lα, Ca Kα, Th Mα and U Mß. Analytical conditions were 15 kV, 200 Na with a rastering focussed beam. Counting time varies from 100 to 150 ms, with a step size ranging from 0.4 to 1 µm. Intensities of all raw compositional were normalized in counts per second and processed all together so that gray levels (i.e. composition) and zoning features can be compared from grain to grain. Zircon were identified via a conventional optical microscope.

U-Th-Pb geochronology of zircon and monazite was conducted by laser ablation inductively coupled plasma spectrometry (LA-ICPMS) at the Laboratoire Magmas et Volcans, Clermont-Ferrand (France). The analyses involve the ablation of minerals with a Resonetics Resolution M-50 powered by an ultra short pulse ATL Atlex Excimer laser system operating at a wavelength of 193 nm (detailed description in Müller, Shelley, Miller & Broude (2009). Spot diameters of 20-26 µm and 7 µm associated to repetition rates of 3 Hz and 1 Hz were used for zircon and monazite respectively. The ablated material is carried into helium, and then mixed with nitrogen and argon, before injection into a plasma source of an Agilent 7500 cs ICP-MS equipped with a dual pumping system to enhance the sensitivity.

The alignment of the instrument and mass calibration was performed before every analytical session using the NIST SRM 612 reference glass, by inspecting the signal of 238U and by minimising the ThO+/Th+ ratio (<< 1%). The mean sensitivity on ^{238}U at the instrumental conditions reported in Table 1 and using a spot size of 44 µm is about 15-20,000 cps/ppm. The analytical method for isotope dating of monazite with laser ablation ICPMS is basically similar to that developed for zircon and monazite and reported in Paquette & Tiepolo (2007) and Tiepolo, Bottazzi, Palenzona & Vannucci (2003). The signal of ^{204}(Pb+Hg), ^{206}Pb, ^{207}Pb, ^{208}Pb, ^{232}Th and ^{238}U

masses are acquired. The occurrence of common Pb in the sample can be monitored by the evolution of the ^{204}(Pb+Hg) signal intensity, but no common Pb correction was applied owing to the large isobaric interference from Hg. The ^{235}U signal is calculated from ^{238}U on the basis of the ratio ^{238}U/^{235}U= 137.88. Single analyses consisted of 20 seconds of background integration with laser off followed by 1 minute integration with the laser firing and a 20 seconds delay to wash out the previous sample (approximatively 10 seconds for 6 orders of magnitude) and prepare the next analysis.

Data are corrected for U-Pb and Th-Pb fractionation occurring during laser sampling and for instrumental mass discrimination (mass bias) by standard bracketing with repeated measurements of GJ-1 zircon (Jackson, Pearson, Griffin & Belousova, 2004) or Moacyr monazite (Gasquet, Bertrand, Paquette, Lehmann & Ratzov, 2010) standard. Data reduction was carried out with the software package GLITTER® (Macquarie Research Ltd, 2001; Jackson et al. (2004); Van Achterbergh, Ryan, Jackson & Griffin (2001). For each analysis, the time resolved signal of single isotopes and isotope ratios was monitored and carefully inspected to verify the presence of perturbations related to inclusions, fractures, mixing of different age domains or common Pb. Calculated ratios were exported and Concordia ages and diagrams were generated using Isoplot/Ex v. 2.49 software package by Ludwig (2001). The concentrations in U-Th-Pb were calibrated relative to the certified contents of 91500 zircon standard (Wiedenbeck, Allé, Corfu, Griffin & Meier, 1995) and Moacyr monazite (Seydoux-Guillaume, Wirth, Deutsch & Schärer, 2004).

REFERENCES

Gasquet, D., Bertrand, J.-M., Paquette, J.-L., Lehmann, J., Ratzov, G., Guedes, R. D. A., Tiepolo, M., Boullier, A.-M., Scaillet, S., & Nomade, S. (2010). Miocene to Messinian deformation and hydrothermal activity in a pre-Alpine basement massif of the French western Alps : New U-Th-Pb and argon ages from the Lauzière massif. *Bulletin de La Societe Geologique de France*, *181*(3), 227-241. https://doi.org/10.2113/gssgfbull.181.3.227

Jackson, S. E., Pearson, N. J., Griffin, W. L., & Belousova, E. A. (2004). The application of laser ablation-inductively coupled plasma-mass spectrometry to in situ U–Pb zircon geochronology. *Chemical Geology*, *211*(1), 47-69. https://doi.org/10.1016/j.chemgeo.2004.06.017

Ludwig, K. (2001). Users manual for Isoplot/Ex Version 2.49 : A geochronological toolkit for Microsoft Excel. *Berkeley Geochronology Center Spec. Publ.*, *1a*, 55.

Müller, W., Shelley, M., Miller, P., & Broude, S. (2009). Initial performance metrics of a new custom-designed ArF excimer LA-ICPMS system coupled to a two-volume laser-ablation cell. *Journal of Analytical Atomic Spectrometry*, *24*(2), 209-214. https://doi.org/10.1039/B805995K

Paquette, J. L., & Tiepolo, M. (2007). High resolution (5 µm) U–Th–Pb isotope dating of monazite with excimer laser ablation (ELA)-ICPMS. *Chemical Geology*, *240*(3), 222-237. https://doi.org/10.1016/j.chemgeo.2007.02.014

Seydoux-Guillaume, A.-M., Wirth, R., Deutsch, A., & Schärer, U. (2004). Microstructure of 24-1928 Ma concordant monazites; implications for geochronology and nuclear waste deposits. *Geochimica et Cosmochimica Acta*, *68*(11), 2517-2527. https://doi.org/10.1016/j.gca.2003.10.042

Tiepolo, M., Bottazzi, P., Palenzona, M., & Vannucci, R. (2003). A laser probe coupled with ICP - Double-focusing sector-field mass spectrometer for in situ analysis of geological samples and U-Pb dating of zircon. *The Canadian Mineralogist*, *41*, 259-272. https://doi.org/10.2113/gscanmin.41.2.259

Van Achterbergh, E., Ryan, C. G., Jackson, S. E., & Griffin, W. L. (2001). Data reduction software for LA-ICP-MS. In *Laser ablation-ICPMS in the earth science* (Sylvester P., Vol. 29, p. 239-243). Mineralogical Association of Canada.

Wiedenbeck, M., Allé, P., Corfu, F., Griffin, W. L., Meier, M., Oberli, F., Quadt, A. V., Roddick, J. C., & Spiegel, W. (1995). Three Natural Zircon Standards for U-Th-Pb, Lu-Hf, Trace Element and Ree Analyses. *Geostandards Newsletter*, *19*(1), 1-23. https://doi.org/10.1111/j.1751-908X.1995.tb00147.x

Williams, M. L., Jercinovic, M. J., Goncalves, P., & Mahan, K. (2006). Format and philosophy for collecting, compiling, and reporting microprobe monazite ages. *Chemical Geology*, *225*(1-2), 1-15.